INFORMATION TO USERS

This manuscript has been reproduced from the microfilm master. UMI films the text directly from the original or copy submitted. Thus, some thesis and dissertation copies are in typewriter face, while others may be from any type of computer printer.

The quality of this reproduction is dependent upon the quality of the copy submitted. Broken or indistinct print, colored or poor quality illustrations and photographs, print bleedthrough, substandard margins, and improper alignment can adversely affect reproduction.

In the unlikely event that the author did not send UMI a complete manuscript and there are missing pages, these will be noted. Also, if unauthorized copyright material had to be removed, a note will indicate the deletion.

Oversize materials (e.g., maps, drawings, charts) are reproduced by sectioning the original, beginning at the upper left-hand corner and continuing from left to right in equal sections with small overlaps.

Photographs included in the original manuscript have been reproduced xerographically in this copy. Higher quality 6" x 9" black and white photographic prints are available for any photographs or illustrations appearing in this copy for an additional charge. Contact UMI directly to order.

UMI®

UNIVERSITY OF ALBERTA

ANGULAR DEPENDENCE OF RESISTIVITY AND INTRINSIC PROPERTIES OF YBCO THIN FILMS

By

©

MAHER ABDELHADI

A thesis submitted to the Faculty of Graduate Studies and Research in partial fulfillment of the requirements for the degree of Doctor of Philosophy

Department of Physics

Edmonton, Alberta

Spring 2002

Canadä

UNIVERSITY OF ALBERTA

LIBRARY RELEASE FORM

NAME OF AUTHOR:	Maher Abdelhadi
TITLE OF THESIS:	Angular dependence of resistivity and intrinsic properties of YBCO thin films
DEGREE:	Doctor of Philosophy
YEAR THE DEGREE GRANTED:	2002

Permission is hereby granted to the University of Alberta Library to reproduce single copies of this thesis and to lend or sell such copies for private, scholarly or scientific research purposes only.

The author reserves all other publication and other rights in association with the copyright in the thesis, and except as hereinbefore provided, neither the thesis nor any substantial portion thereof may be printed or otherwise reproduced in any material form whatever without the author's prior written permission.

Maher Abdelhadi

412 Avadh Bhatia Physics Lab

Department of Physics

University of Alberta

Edmonton, Alberta T6G 2J1

Date: Dec. 21, 2001

UNIVERSITY OF ALBERTA

FACULTY OF GRADUATE STUDIES AND RESEARCH

The undersigned certify that they have read, and recommend to the Faculty of Graduate Studies and Research for acceptance, a thesis entitled "Angular dependence of resistivity and intrinsic properties of $YBa_2Cu_3O_{7-\delta}$ thin films" submitted by Maher Abdelhadi in partial fulfilment of the requirements for the degree of Doctor of Philosophy in   Physics.

Dr. Jan A. Jung (*Supervisor*)

Dr. Jurgen P. Franck (*Committee Chair*)

Dr. Mark Freeman

Dr. Frank Marsiglio

Dr. Arthur Mar
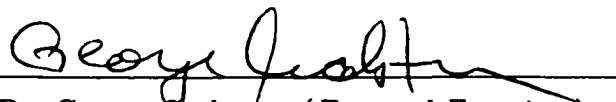
Dr. George Crabtree (*External Examiner*)
Argonne National Laboratory,

Argonne, IL 60439, USA

Date: *Oct. 13/01*

To

My Wife,

and

My Sons,
Osama and Basel

Abstract

We have investigated systematically the angular dependence of resistivity $\rho(\theta)$, where θ is the angle between the magnetic field and the ab-planes, and the temperature dependence of resistivity $\rho(T)$ over a temperature range between T_{c0} and T_c-onset within the superconducting transition in an applied magnetic field $\mathbf{B}$ up to 1 T in a series of $YBa_2Cu_3O_{7-\delta}$ (YBCO) thin films both optimally doped and underdoped of different T_c, critical current density J_c, film thickness, and preparation techniques. The angular dependence of ρ was measured using a high resolution angle-control system with the angular position of the sample accurately monitored by an optical encoder. Our studies were concentrated on four different important properties of $\rho(\theta)$ and $\rho(T)$: T_c dependence of the normal state resistivity, pinning by planar defects (twin boundaries) close to T_c, variation of anisotropy factor γ, and phase-slip resistivity.

1. The studies of the normal state resistivity revealed an upward deviation in $\rho(T)$ from the high temperature T-linear dependence below a certain characteristic temperature T^*. This upward deviation increases with an increasing oxygen content (optimally doped films show the largest upward deviation and the highest T^*).

2. For a few YBCO films, investigation of $\rho(\theta)$ for the angular range $0 - 180^o$ revealed a minimum in $\rho(\theta)$ near $\theta = 90^o$ ($\mathbf{B} \parallel$ c-axis) which was attributed to magnetic pinning by twin boundaries (TB's). However, the majority of the films display a broad maximum around $\theta = 90^o$ similar to that observed in untwinned YBCO single crystals. The presence of a minimum in $\rho(\theta)$ for $\mathbf{B} \parallel$ c-axis is not related to the magnitude of J_c. This minimum is present only in films that were deposited very slowly, thus allowing the growth of crystallographically well-defined and sharp TB's.

3. $\rho(\theta)$ measured for $\mathbf{B}$ close to $\theta = 0^o$ ($\mathbf{B} \parallel$ ab-planes) for both $\mathbf{B} \parallel \mathbf{J}$ and $\mathbf{B} \perp \mathbf{J}$ (where $\mathbf{J}$ is the current density) revealed a sample dependent variations in the

shape and width of the minimum at $\theta = 0°$, from a flat to a very sharp behavior. The results of scaling of $\rho(\theta)$ with the reduced field $B(\gamma^{-2}\cos^2\theta + \sin^2\theta)^{1/2}$ allowed a quantitative determination of the value of the intrinsic anisotropy factor γ which varies between 7 and 400, and is independent of T_c, film thickness, or J_c. The sharper the minimum in $\rho(\theta)$ at $\theta = 0°$ the larger is the anisotropy. For highly anisotropic film ($\gamma \sim 400$), $\rho(\theta)$ showed an identical behavior for **B** $\parallel$ **J** and **B** $\perp$ **J**. The large variation in γ could be attributed to the "buckling" of the CuO_2 planes.

4. For a 2D-like highly anisotropic ($\gamma \sim 400$) film, the measurements of ρ revealed a resistive maximum in $\rho(\theta)$ at $\theta = 0°$ over a narrow temperature range below T_c-onset. The width of this maximum decreases with an increasing **B**. A corresponding maximum has been observed in $\rho(T)$ at temperatures just below T_c onset. The resistivity of the maximum is higher than the normal state resistivity at T_c onset. The maximum in $\rho(T)$ is almost independent of the magnitude of magnetic field applied along the ab-planes. However, the resistivity at the maximum is dramatically reduced when **B** is rotated from the ab-planes towards the c-axis. The maxima in $\rho(T)$ and $\rho(\theta)$ at $\theta = 0°$ also decrease with an increasing applied current density. The data imply that the resistive peaks in $\rho(T)$ and $\rho(\theta)$ originate from the thermally activated phase-slip voltage according to theories of Langer-Ambegaokar and McCumber-Halperin.

ACKNOWLEDGEMENT

I would like to express my deep thanks and appreciation to my supervisor Dr. Jan Jung for his great continuous support and guidance during the course of the research and preparation of this manuscript. I am really impressed by his deep insight and great ambition in the field of superconductivity. Moreover, the amount of time and effort that he devoted to help me in my research were indispensable. I am indebted to him for many new things that I learned in the field of superconductivity.

I would like to express my thanks to the members of my committee Professors J. P. Frank, Mark Freeman, Frank Marsiglio, Arthur Mar, from University of Alberta and Prof. George Crabtree from Argonne National Laboratory for their comments and suggestions on my research and thesis.

The experimental part of this research required the assistance of several people, I would like to thank Mr. T. Walford for his valuable technical support in building many parts of the experimental setup. Special thanks to Mr. D. Mullin for his indefinite help with the sputtering system in particular and for his help in the thin film laboratory in general, and to Mr. B. Burris for his assistance in interfacing and computer programming. My deep thanks are due to Ms. L. Chandler, our graduate secretary, for her administrative help, encouragement, and moral support during my Ph.D. studies.

I would like to acknowledge many fruitful discussions with Drs. S. B. Woods regarding the experimental measurements and setup, and Wai Kwok from Argonne National Laboratory. I wish to express special thanks to Dr. H. Darhmaoui for his assistance before and after I came to University of Alberta.

I am also grateful to Drs R. Hughes and J. Preston of McMaster University, and to Dr. M. Denhoff of the National Research Council of Canada for providing us with YBCO thin films.

I am also grateful to all Physics department staff, faculty, and students who have helped me directly and indirectly to complete my thesis.

Contents

List of Tables

List of Figures

Chapter 1

Introduction and Theoretical Background

Many of the unusual properties of high temperature superconductors (HTSC) stem from large anisotropy caused by the layered structure, and from extremely short coherence length and prominent fluctuation effects associated with the high transition temperature of cuprates. Large anisotropy reveals itself in resistivity, upper critical field H_{c2}, and critical current density measurements. Moreover, it has been recognized both experimentally and theoretically that the normal state of HTSC exhibits an extraordinary behavior above T_c, due to the nature of the characteristic excitations in the normal state, which however still remains unresolved. Therefore, proper understanding of the normal state is an essential first step towards the explanation of the fundamentals of the mechanism of high temperature superconductivity. Investigations of the normal state have involved so far a wide variety of electrical, magnetic and optical studies.

We have focused our attention on a few important aspects related to the intrinsic anisotropy obtained from scaling rules, superconducting fluctuation effects at temperatures between $T_c(\rho = 0)$ and the onset T_c, and on the normal state resistivity in YBCO thin films. These are described in detail in the next section.

1

1.1 Motivation and goals

There has been a huge amount of published data related to the measurement of the angular dependence of the in-plane resistivity in a magnetic field on HTSC. The purpose of most of these measurements was to investigate the dissipation mechanism in these materials. Many groups have reported that when both the magnetic field **B** and the current density **J** are oriented along the CuO_2 planes, the resistivity ρ of some samples either does not change with the variation of an angle ϕ between **B** and **J** or changes only very slightly. An important question that has been raised: is this a Lorentz-force free dissipation? Normally in order to extract contributions from the Lorentz-force-driven dissipation for an applied current and field in the ab-planes, the resistivity measurements have to be performed for two configurations, **B** $\parallel$ **J** and **B** $\perp$ **J**, and the results have to be compared. When the flux lines are drifting with velocity $\mathbf{v}_L$, due to the macroscopic Lorentz force (**J** $\times$ **B**), flux-line motion generates an electric field $\mathbf{E} = \mathbf{B} \times \mathbf{v}_L$ along the direction of the current **J**. In an ideal flux-flow, the flux line velocity $\mathbf{v}_L$ is determined by the balance between the Lorentz force and the viscous drag force, $\mathbf{J} \times \Phi = \eta \mathbf{v}_L$, where Φ is the total magnetic flux and η is the viscosity coefficient. Then $v_L = (J\Phi/\eta) \sin \phi$ and the corresponding angular dependence of resistivity is $\rho(\phi) = (B\Phi/\eta) \sin^2 \phi$.

Although, in principle the angular dependence of resistivity $\rho(\phi)$ should follow this simple formula for the Lorentz-force-driven dissipation, many experimental findings appear to contradict it. For the case of YBCO, this could be due to an additional twin boundary contribution to the resistivity [1, 2], which superimposes on the intrinsic resistivity. As a result, an angular dependence of resistivity with additional terms, $\rho = \rho_0 + \rho_1 \sin^2 \phi + \rho_2 \sin^2 2\phi$, has been proposed, where ρ_0, ρ_1, and ρ_2 are constants [1, 3]. A sharp minimum in the resistivity due to twin boundary pinning has been observed, when the magnetic field is oriented close to the twin plane [1, 2]. Such a sharp minimum was observed only in high quality twinned single crystals but has not been seen in impure single crystals or in as-grown thin films. [3, 5]. Moreover, the simple Lorentz-force dependent dissipation mechanism does not apply to the case of

2

BSCCO whose resistivity $\rho(\theta)$, where θ is the angle between the field direction **B** and the ab-planes, shows an extremely sharp angular dependence when **B** is very close to the ab-planes. Iye et. al [3], using a high resolution angular system to measure the in-plane resistivity $\rho(\theta)$ for BSCCO confirmed that for rotation of **B** off c-axis, $\rho(\theta)$ is independent of the plane of rotation with respect to the current. However for YBCO, the same group observed the dependence of $\rho(\theta)$ on the relative angle between the applied current and field. Kwok et. al [4] performed a measurement of the angular dependence of resistivity very close to the ab-planes on YBCO single crystals. A sharp minimum in $\rho(\theta)$ was observed when the field was rotated in a plane perpendicular to the current whereas a flat minimum of $\rho(\theta)$ was detected when the field was rotated in a plane parallel to the current direction.

If one compares the experimental results for $\rho(\theta)$ in YBCO (small anisotropy) with that for BSCCO (very highly anisotropic and approaching the 2D-limit), one could notice that the contributions of the non-Lorentz-force mechanism to the resistivity become more significant in systems with higher anisotropy. In addition, the presence of a sharp minimum in $\rho(\theta)$ for YBCO could also suggest that in some cases the anisotropy of this compound is much higher than previously assumed value (typical value of $\gamma \approx 7$ for optimally doped YBCO). These experimental results could also imply that the angular dependence of resistivity may partially originate from the Lorentz-force-free dissipation mechanism.

These experimental findings and ideas have motivated us to carry out the systematic studies of the angular dependence of resistivity in YBCO thin films with a focus on the following experiments:

1. Investigation of the intrinsic anisotropy in YBCO thin films. Is a value of $\gamma \approx 7$ a universal one in optimally doped YBCO films or is it much higher in some cases?

2. Investigation of the difference between the angular dependence of resistivity measured for two different orientations of **B** versus **J**, i.e **B** $\perp$ **J** (where the field is rotated in a plane perpendicular to the current) and **B** $\parallel$ **J** (where the

3

field is rotated in a plane parallel to the current). Is this difference related to the anisotropy or not? These ideas originated from the fact that for highly anisotropic HTSC like BSCCO, $\rho(\theta)$ for $\mathbf{B} \perp \mathbf{J}$ and $\mathbf{B} \parallel \mathbf{J}$ is identical [3].

3. Investigation of how effective is the twin boundary pinning in YBCO thin films. Motivation for these studies stemmed from the experimental fact that a sharp minimum in $\rho(\theta)$ (which was attributed to twin boundary pinning) has been observed only in high quality twinned YBCO single crystals but not in thin films [3, 5].

An unusual behavior of $\rho(T)$ and $\rho(\theta)$ has been observed close to the T_c onset in highly anisotropic HTSC. Remarkable sharp peaks have been seen in the temperature dependence of resistivity just below T_c onset and in $\rho(\theta)$ for magnetic field rotations very close to the ab-planes in BSCCO [6, 7, 8], LCCO [9], TBCCO and organic superconductors [7]. These resistive peaks are much larger than the normal state resistivity at T_c onset and they decrease with an increasing applied magnetic field and (or) an applied current. The presence of such peaks has been interpreted as due to a quasireentrant superconductivity resulting from an intrinsic granularity of the HTSC. In thin wires of conventional superconductors like aluminium (Al) [10, 11, 12], the temperature dependence of resistivity has also been found to exhibit a similar peak below T_c onset, whose magnitude decreases with an increasing applied current. The peak in $\rho(T)$ of Al wires has been attributed to the phase-slip induced resistivity.

It has been argued [7] that in HTSC the presence of such peaks in $\rho(\theta)$ close to T_c is a result of quasi-2D nature and very high anisotropy of these materials and therefore this could explain why such peaks have never been reported in moderately anisotropic superconductors like YBCO [7]. Motivated by these experimental observations we have decided to investigate the temperature and angular dependence of resistivity very close to T_c in YBCO thin films in order to:

1. Verify the existence of these resistive peaks in $\rho(T)$, at different magnitudes and directions of the applied field, and in $\rho(\theta)$ for angles θ very close to the

4

ab-planes.

2. Find the relationship between the resistive peaks and the intrinsic anisotropy of YBCO thin films. Are these peaks associated only with high anisotropy as it was suggested [7]?

3. Investigate the origin of this dissipation, which is much larger than the normal state resistivity.

Another important experimental observation that has attracted our attention is related to the peculiar properties of the normal state of HTSC. For many HTSC, the temperature dependence of resistivity $\rho(T)$ exhibits a deviation from the T-linear dependence at temperatures $T^* \gg T_c$. For most underdoped cuprates, a *downward* deviation of $\rho(T)$ from its high temperature T-linear behavior has been observed at temperatures $T^* < 200K$. The downward deviation increases with a decreasing oxygen content. This phenomenon was attributed to a spin-gap opening [13, 14]. On the other hand, an unusual *upward* deviation from the T-linear dependence has been reported in BSCCO (2212), BSCCO (2223) [15], and in Nd doped $La_{2-x}Sr_xCuO_4$ [16] at temperatures well above T_c. The upward deviation was attributed to a structural transformation and a charge ordering in the stripe phase [15]. Observations of an upward deviation in $\rho(T)$ in some HTSC, stimulated our investigations of this phenomena in YBCO thin films both optimally doped and underdoped. We have focused on the following experiments:

1. Investigation of the presence of the upward deviation in YBCO thin films. How is it related to the oxygen content, T_c, thickness, and other properties of YBCO thin films?

2. Investigation of the origin of this unusual behavior. Is it an intrinsic property of the temperature dependence of the normal state resistivity? How is it related to the sample disorder?

5
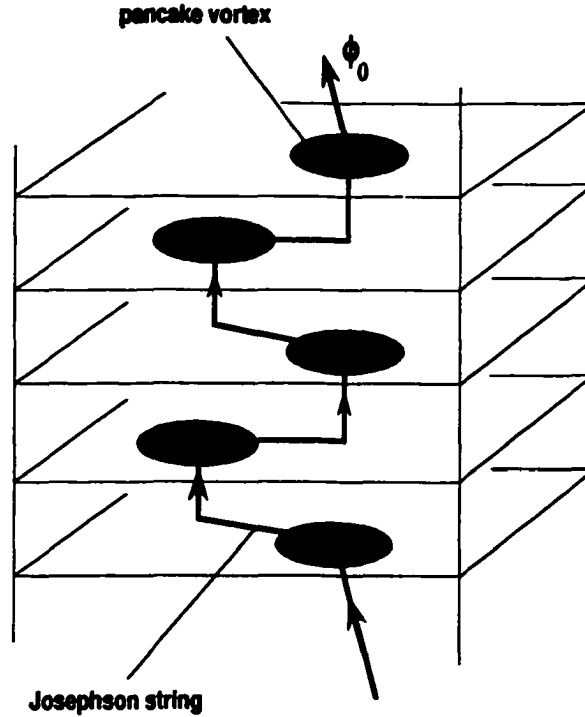
Figure 1.1: Schematic diagram of the structure of a single flux line in a strongly anisotropic superconductor. The vortex line can be viewed as an array of pancake vortices located in the superconducting CuO_2 layers connected by Josephson strings (located between the layers).

We studied the anisotropy in YBCO thin films with the help of the scaling laws for $\rho(\theta)$ in different magnetic fields. Kes et al. [17] proposed a model which can be applied to highly anisotropic 2D HTSC like BSCCO. In this model, the flux line is no longer a straight line in the sample, but instead it transforms to vortex pancakes in the superconducting CuO_2 planes connected by Josephson strings located between the CuO_2 planes (see Fig.1.1). The essential driving force originates from the perpendicular component of the applied field acting on the pancakes only, whatever the field direction may be. According to this model, the angular dependence of resistivity should follow the scaling behavior $B\sin\theta$ (vertical component of the field) [17]. The scaling behavior can be extended to 3D anisotropy (less anisotropic materials) by including the anisotropy parameter γ and using the 3D GL-effective mass model $B_{reduced} = B(\gamma^{-2}\cos^2\theta + \sin^2\theta)^{1/2}$.

6

Our experimental results and discussions are presented in the next few Chapters with the following sequence: In Chapter 2, the experimental setup, experimental procedure, sample preparation and sample characterization are discussed. Our experimental results regarding an upward deviation from the T-linear dependence in normal state resistivity are presented in Chapter 3. Studies of twin boundary pinning effects in YBCO films using the angular dependence of resistivity are presented in Chapter 4. Important results of ours regarding the anisotropy in YBCO films using the scaling rules and the "lock-in transition" are discussed in Chapter 5. Finally, our major results which shows the presence of sharp resistivity peaks just below the T_c-onset and our interpretation using the phase-slip model are presented in Chapter 5. The material of this thesis is presented in a scientific paper format, where each chapter includes its own introduction, experimental results, discussion, followed by a summary, conclusions, and references.

In the following sections of this Chapter we present theoretical models related to the above issues. In the next section, the issue of layered structure of the HTSC cuprates and the corresponding anisotropy is discussed from the point of view of the 2D Lawrence-Doniach and the 3D Ginzburg-Landau models with emphasis on a 2D-3D crossover. Then, anomalous normal state properties of HTSC are discussed. In the last section, we present some theoretical models which describe the superconducting fluctuation effects.

1.2   Layered superconductors and anisotropy

1.2.1   The Lawrence-Doniach model

In this model [18], layered superconductors are treated as a stacked array of two dimensional (2D) superconductors (within each the GL order parameter $\psi_n(x,y)$ is a 2D function), coupled together by Josephson tunnelling between adjacent layers. This model reduces to the anisotropic 3D GL theory for long-wavelength phenomena which dominate near T_c, but it can give rise to different results for short-wavelength

7

phenomena at lower temperatures after effectively crossing over to 2D behavior.

Following the conventional GL theory notations, the model can be defined in terms of a free-energy expression for the stack of layers. The layers define the ab-planes and the c-axis is normal to them. One could take z as the coordinate along c-axis, with s as the interlayer distance, and x, y as coordinates in the planes. Then omitting the vector potential for simplicity, the free energy can be written as

$$F = \sum_n \int \alpha |\psi_n|^2 + \frac{1}{2}\beta |\psi_n|^4 + \frac{\hbar^2}{2m_{ab}} \left(\left| \frac{\partial \psi_n}{\partial x} \right|^2 + \left| \frac{\partial \psi_n}{\partial y} \right|^2 \right) + \frac{\hbar^2}{2m_c s^2} |\psi_n - \psi_{n-1}|^2 \quad (1.1)$$

where the sum runs over the layers and the integral is over the area of each layer, α and β are constants introduced by the GL theory, and m_{ab} and m_c are the effective charge carrier masses along the ab-planes and c-axis, respectively (for simplicity, the relatively small anisotropy in the ab-planes has been ignored). The z-derivative has been replaced by the finite difference form which is appropriate to a discrete system. Minimizing Eq.1.1 with respect to a variation in ψ_n^*, one obtains the LD equation for ψ_n:

$$\alpha \psi_n + \beta |\psi_n|^2 \psi_n - \frac{\hbar^2}{2m_{ab}} \left(\frac{\partial^2}{\partial x^2} + \frac{\partial^2}{\partial y^2} \right) \psi_n - \frac{\hbar^2}{2m_c s^2} (\psi_{n+1} - 2\psi_n + \psi_{n-1}) = 0 \quad (1.2)$$

Note that the last term is the discrete form of the second derivative.

1.2.2   The anisotropic Ginzburg-Landau limit

The free energy expression of Eq.1.1 can be reduced directly to a GL form in the long-wavelength limit where the variation along the z is smooth enough to replace $(\psi_n - \psi_{n-1})/s$ by $\partial \psi / \partial z$. In this limit Eq.1.2 reduces to

$$\alpha \psi + \beta |\psi|^2 \psi - \frac{\hbar^2}{2} \left(\nabla - i\frac{2e}{\hbar c}\mathbf{A} \right) \cdot \left(\frac{1}{m} \right) \cdot \left(\nabla - i\frac{2e}{\hbar c}\mathbf{A} \right) \psi = 0 \quad (1.3)$$

where the vector potential term was inserted and now both ∇ and $\mathbf{A}$ are 3D quantities and m is the mass tensor with principal values (m_{ab}, m_{ab}, m_c). If the interlayer coupling is weak, then $m_c \gg m_{ab}$.

8

The mass anisotropy causes the coherence length ξ to be anisotropic. The GL coherence length can be generalized to include the effect of anisotropy as:

$$\xi_i^2(T) = \frac{\hbar^2}{2m_i|\alpha(T)|} \tag{1.4}$$

where the subscript i refers to a particular principal axis. According to the GL theory $\alpha(T)$ is isotropic and proportional to $(T - T_c)$, which implies that ξ diverges like $|T - T_c|^{-1/2}$. Hence, sufficiently close to T_c, ψ will vary smoothly to justify this continuum GL approximation.

The mass anisotropy affects the shape of the vortex line in a superconductor. For example, consider an Abrikosov vortex in a sample with the magnetic field along the a-axis. In an isotropic superconductor, this vortex would have a circular symmetry. In an anisotropic superconductor, however, the core radius along the plane direction will be ξ_{ab}, whereas the core radius in the c direction will be $\xi_c \ll \xi_{ab}$. On the other hand, the flux-penetration radius will be λ_c along the plane direction, whereas it will have a smaller value λ_{ab} in the c direction. Thus, both the core and the current streamlines confining the flux are flattened into ellipses with long axes parallel to the planes (b axis), as shown in Fig.1.2.

The anisotropy of the upper critical field in this GL regime can be worked out. Since $H_{c2} = \phi_0/2\pi\xi^2$ (where $\phi_0 = h/2e$ is the flux quantum) is determined by vortices of current flowing in a plane perpendicular to the field, the relevant values of ξ_i are those for the two axes perpendicular to the field direction. For field along the two distinct principal axes, we have

$$H_{c2\|c} = \phi_0/2\pi\xi_{ab}^2 \tag{1.5}$$

$$H_{c2\|ab} = \phi_0/2\pi\xi_{ab}\xi_c \tag{1.6}$$

so that $H_{c2\|ab} \gg H_{c2\|c}$ since $\xi_{ab} \gg \xi_c$. But because $H_{c1} \sim 1/\lambda^2$, which is inversely related to $1/\xi^2$, the anisotropy in H_{c1} will be inverse to that for H_{c2}; i.e., $H_{c1\|ab} \ll H_{c1\|c}$. Based on the above equations and relations one could define the conventional

9
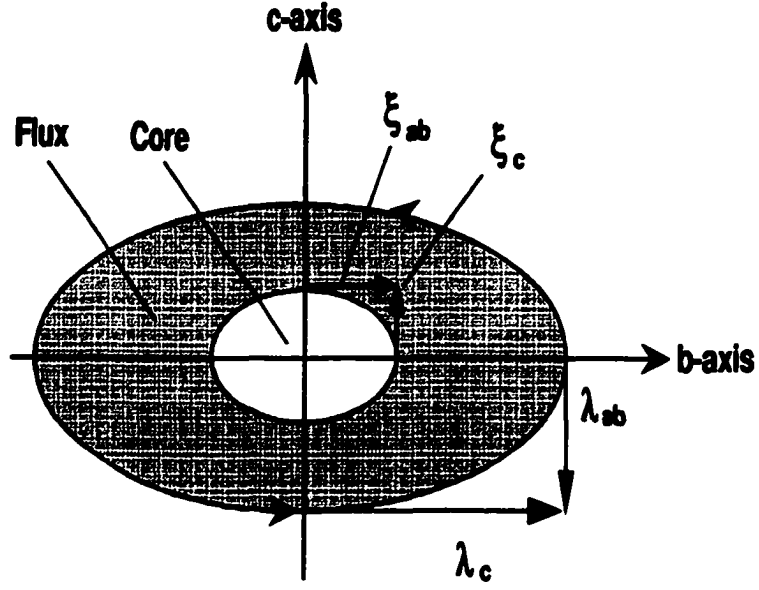
Figure 1.2: Schematic diagram of the cross-section of a vortex along the a-axis in an anisotropic superconductor. The anisotropy parameter is expressed as $\gamma \equiv \left(\frac{m_c}{m_{ab}}\right)^{1/2} = \frac{\lambda_c}{\lambda_{ab}} = \frac{\xi_{ab}}{\xi_c}$.

dimensionless anisotropy parameter γ as

$$\gamma \equiv \left(\frac{m_c}{m_{ab}}\right)^{1/2} = \frac{\lambda_c}{\lambda_{ab}} = \frac{\xi_{ab}}{\xi_c} = \left(\frac{H_{c2\|ab}}{H_{c2\|c}}\right) = \left(\frac{H_{c1\|c}}{H_{c1\|ab}}\right) \tag{1.7}$$

The anisotropy parameter γ is approximately 7 for YBCO and $\geq$ 150 for BSCCO. This anisotropy is one of the decisive factors in making the HTSC act differently from the conventional superconductors.

Within the anisotropic GL approximation, the angular dependence of H_{c2} can be written as

$$H_{c2}(\theta) = \frac{H_{c2\|ab}}{(\cos^2\theta + \gamma^2\sin^2\theta)^{1/2}} \tag{1.8}$$

where θ is the angle between the magnetic field and the ab-planes.

1.2.3 Crossover to two-dimensional behavior

Very close to T_c, $\xi_c(T) \approx \xi_c(0)(1 - T/T_c)^{-1/2}$ will always be large enough to justify the GL approximation discussed in the previous section. But as the temperature

10

decreases, $\xi_c(T)$ decreases until it becomes smaller than the interlayer distance s. Below this distance the smooth variation assumption used to obtain the GL limit (Eq.1.3) will break down at some temperature T^*.

This leads to a criterion usually adopted to go from a continuous anisotropic to a discrete layered description. This criterion is related to the magnitude of the coherence length along the c-axis ξ_c with respect to the interlayer separation s which can be expressed by the dimensionless ratio $\tau = 2\xi_c^2(0)/s^2$. The ratio τ characterizes the crossover from a quasi-2D layered to a continuous 3D anisotropic behavior. For a large coherence length $\xi_c(0)$, $\tau \gg 1$, the continuous description is always appropriate. On the other hand, for a small $\tau \ll 1$, a crossover will take place at a temperature $T^* = (1 - \tau)T_c < T_c$, where the system behaves in a quasi-2D manner at low temperatures below T^* and exhibits 3D anisotropic behavior above T^* [20]. In a field strictly parallel to the layers and at $T < T^*$ the vortex cores lie between the layers, and each layer, treated as a 2D superconductor of zero thickness, has an infinite critical field. This unphysical infinity is eliminated by taking into account the finite layer thickness, pair breaking due to Pauli paramagnetism, and spin-orbit coupling effects [19]. In general, a continuous anisotropic description is appropriate to YBCO over a wide temperature range, whereas the more strongly anisotropic Bi and Tl compounds belong to the class of materials with $\tau \ll 1$, and therefore the LD model applies. In fact, BSCCO crosses over to 2D behavior at a temperature approximately 0.1 K below T_c in fields exactly parallel to the ab-planes.

1.3   Intrinsic pinning

Intrinsic pinning in oxide superconductors is a consequence of the layered structure of these materials, with strong superconductivity present in the metallic CuO_2 planes and only weak or vanishing superconductivity in the intermediate buffer layers. Therefore the superconducting order parameter and, the condensation energy are expected to exhibit strong oscillations with period s, the interlayer distance. If the magnetic

11

field **B** is aligned parallel to the ab-planes (y-axis), the vortex lattice tries to accommodate itself to the layer structure so that the vortex cores come to lie in between the strongly superconducting CuO_2 planes. A current density **J** (applied parallel to the x-axis) flowing along the planes will exert a Lorentz force on the vortices which point along the c-axis (z-axis). In order to move, the vortices have to cross the strongly superconducting layers, which involves a large expenditure of condensation energy, thus creating the *intrinsic* pinning barriers. Note that a current density running along the c-axis will push the vortices to move along the planes (x-axis) where no barriers are inhibiting the flow. In this case, point defects are essential for producing a finite critical current density [20].

The first quantitative analysis of intrinsic pinning in layered superconductors was introduced by Tachiki and Takahashi [21]. In their model the modulus of the order parameter $\Psi = f \exp(i\phi)$ is assumed to exhibit a periodic spatial variation of the form

$$f(z) = f_0 + f_1 \cos 2\pi \frac{z}{s}, \quad 0 < f_1 < f_0 \tag{1.9}$$

The strength of the coupling between the layers is parameterized by the ratio $\delta = f_1/f_0$. A vortex running parallel to the planes (y-axis) and located at a height $z = z_0$ will modify the order parameter according to

$$f_v(r, z_0) = f(z) \tanh \left[\left(\frac{x}{\xi}\right)^2 + \left(\frac{z - z_0}{\varepsilon \xi}\right)^2 \right]^{1/2} \tag{1.10}$$

where $\varepsilon = \gamma^2$ is the anisotropy of the system. This modification leads to a periodically changing cost in the condensation energy density $(H_c^2/8\pi)\{1 - [f_v(r, z_0)/f(z)]^2\}$. A simple integration in the xz-plane provides the intrinsic pinning potential u_{in}.

1.4 Twin boundary pinning

Since YBCO has an orthorhombic crystal structure, in which the a and b directions in the plane are not exactly equivalent, twin planes are a prominent form of defect in this material. Twin planes are parallel to the (110) and (1$\bar{1}$0) lattice planes and

and they form separate domains in which the *a* and *b* directions interchange roles. Because point defects and impurities accumulate along a twin boundary and weaken the superconductivity there, it will attract vortices. Moreover, because of its extended planar structure, the pinning acts in a coherent rather than a random way on a flux line lying in the plane, making the pinning unusually effective. In this case, the Larkin-Ovchinnikov collective pinning model [22] is not appropriate.

The first observations about the effect of twin boundaries on pinning of vortices in YBCO were made by Vinnikov et al. [23] and by Dolan et al. [24]. In their decoration analysis of the low-field vortex structure, the attraction of the vortices to the twinning planes manifests itself directly in a higher concentration of flux lines within the twin planes in comparison to that in the bulk. The attraction of the vortices to the twin boundaries produces a variety of interesting effects, such as vortex trapping and locking when the field is rotated towards the direction of the twin boundary planes, and an enhanced pinning for vortex motion orthogonal to the twin planes.

Not only are the vortices attracted to the twin boundaries; their motion along the twin planes seems to be influenced by the twin boundaries as well. In particular, for both the field and the current density directed along the ab-planes (i.e., the Lorentz force and hence the vortex motion directed along the c-axis) the motion of the flux lines appears to be more strongly hindered than in the bulk, an effect which was attributed to the presence of enhanced pinning within the twin planes. This conclusion can be drawn from the experiments of Kwok et al. [4], who observed a sharp ($\sim 5^{o}$ wide) drop in resistivity close to T_c when the magnetic field is aligned with the twin boundaries. The same conclusion can be obtained from the torque experiments of Gyorgy et al. [25] and from the magnetization experiments of Liu et al. [26] who observed an increase in the critical current density within the glass regime whenever the field is directed along the twinning planes. On the other hand, for a magnetic field directed along the c-axis, experiments of Duran et al. [27] suggested that the pinning along twin boundaries is reduced. This conclusion was based on the analysis of real-time imaging experiments of flux profiles, which suggest that the twinning planes

13

provide favorable channels for flux penetration into the sample. However, magneto-optical experiments by Vlasko-Vlasov et al. [28] show that the twin boundaries act as obstacles to the flux entering the sample, leading to an accumulation of vortices along one side of the twinning planes and a depletion on the other. Whereas some flux enters the sample through a narrow channel along the twin boundary potential well, their main effect is to guide the vortices on one side of the twin planes into the sample.

Thus it appears that vortices trapped in the potential well of a twin boundary and moving along the twin planes experience an enhanced pinning in some cases, but a reduced pinning in others. Due to the reduction of the order parameter in the twin plane (which follows from the observed attraction of the vortices to the plane), the vortex core is elongated along the plane [29], and hence the pinning is reduced. On the other hand, thermal fluctuations (which are particularly important in HTSC) leading to a smearing of the pinning potential at high temperatures, are reduced when the vortex is trapped in the potential well of the twin boundary, causing an enhanced pinning force in the planes. Whereas the thermal effect should be dominant at high temperatures, reduced pinning may be more relevant at low temperatures. The direction of motion (along or perpendicular to the c-axis) may influence the result as well, since in one direction (along the c-axis) the intrinsic pinning potential of the layered structure is relevant.

Enhanced pinning by twin boundary can be understood as a two-step process: Consider a magnetic field directed along the ab-planes. As the vortices are turned toward the twin planes, the attractive interaction between the vortices and the twin boundaries leads to a deformation of the vortices, with increasingly large segments of the vortices trapped in the potential wells of the twin boundaries. Under the action of a driving current $J \parallel$ ab-planes, the vortices are forced to move along the c-axis, with the trapped segments moving within the twin boundary potential well. Due to the partial trapping of the vortex in the potential well, transverse thermal fluctuations of the vortex line are suppressed (dimensional reduction of the fluctuations) [20], leading

14

to an enhanced pinning for those vortex segments trapped by the twin boundaries.

1.5 The normal state of high-T_c superconductors

One of the important issues which remains unresolved in the physics of the high temperature superconductors is the nature of the excitations in the normal state $(T > T_c)$. Many normal state properties have been found to behave anomalously compared to a simple metallic or Fermi liquid behavior [30, 31], possibly indicating the existence of quite exotic elementary excitations typical for strongly correlated electron systems. A deep insight in the normal state may provide a way to the understanding of the superconductivity mechanism itself. Experimentally, the investigations of the normal state involve a wide variety of electrical, magnetic, and optical studies.

Many models have been constructed to deal with the normal state behavior, which can be roughly classified into Fermi- and non-Fermi-liquid scenarios. They either assume preformed pairing leading to the superconducting gap (of the same d-wave symmetry) or treat the pseudogap separately from the superconducting gap. These models include spin-fluctuations [37], stripe phase [38], bipolaronic conduction [39], and interlayer tunnelling [40].

This section outlines the most important normal state anomalies. Our experimental results related to the normal state resistivity, which reveal an unusual behavior above T_c, will be discussed in Chapter 3.

1.5.1 Anomalous normal state properties

Compared with metals, the high-T_c cuprates exhibit a few anomalous properties in the normal state such as anisotropy, pseudogap, and non-Fermi-liquid behavior. Accordingly, many models have been proposed to interpret these anomalies. Below, we summarize the major properties of the normal state.

15

Anisotropy

As we discussed in the previous section HTSC have a highly anisotropic layered structure composed of CuO_2 planes separated by buffer layers. The electrical conductivity within the planes is much higher than that in the perpendicular direction. While the resistivity anisotropy ρ_c/ρ_{ab} can reach as high as 10^5 in strongly anisotropic BSCCO materials, it is only between 30-70 and roughly temperature independent for fully oxygenated YBCO. This large anisotropy had led to the interlayer tunnelling theory of high-T_c superconductivity [32], which assumes that the blocking of the c-axis conduction in the normal state provides the energy of superconducting condensation. The resistivity anisotropy ratios ρ_c/ρ_{ab} are consistent with the effective mass anisotropy γ estimated from the anisotropy of the magnetic properties of superconductivity (such as ξ, λ etc.) [31].

Temperature dependence of resistivity

For homogeneous single-phase superconducting samples, the in-plane resistivity ρ_{ab} is metallic with temperature [30]. The T-linear dependence of resistivity is quite ubiquitous for the HTSC in their optimal doping (maximum T_c) regime. This linear dependence have been observed over a wide temperature range from T_c up to 1000 K [34], where a T^2 temperature dependence is expected (according to Fermi-liquid, if no other scattering exists, electron-electron scattering gives a T^2 dependence of resistivity [31]). It was noted by many workers that for the "best" samples of YBCO, the linear $\rho(T)$ extrapolates to zero as $T \to 0$ (vanishingly small residual resistivity) [31]. For the overdoped samples, resistivity takes the form

$$\rho = \rho_0 + a\,T^n\,, \qquad 1 < n \leq 2\,, \qquad (1.11)$$

while in the underdoped regime, ρ is linear in T at high temperature but starts to deviate downward below a certain characteristic temperature $T^* \sim 200K$. The downward resistivity deviation from T-linear dependence is believed to be a manifestation of a spin-gap opening [34, 13], and has been normally observed in underdoped cuprates.

16

As the hole doping level is decreased further by decreasing the oxygen content, the resistivity increases rapidly (upward bending in $\rho(T)$) at lower temperatures, indicating the onset of localization effects (carrier localization) [14].

Spin gap (pseudogap)

Recently, there has been an interest in underdoped cuprates because these materials display unusual normal state properties that suggest the opening of a pseudogap in the spin or charge excitation spectrum well above T_c. Although there is an ample evidence for the existence of a pseudogap in underdoped cuprates, no one has established a direct correlation between the pseudogap and the superconductivity. Furthermore, it is not known whether a superconducting gap opens at T_c.

Spin gap refers to a reduction in the density of states in the spin excitation spectrum. The phenomenon is found to be universal for at least the underdoped cuprates. Many experimental techniques were employed to probe spin gap in YBCO such as resistivity [14, 13], NMR [35], and neutron scattering [36]. The spin gap is closely related to the individual CuO_2 planes, and it is unlikely to depend on the interlayer coupling.

Currently, the major controversial issues related to pseudogap in the normal state are:

- The relationship between the pseudogap and superconducting gap. There is still debate on whether or not the pseudogap is a precursor of the superconducting gap.

- Dependence of T^*, where T^* is the temperature at which the pseudogap opens, on doping level. T^* is generally believed to be linearly dependent on the doping level, i.e. T^* drops with an increasing hole density. It could reach T_c at optimal doping, where the pseudogap develops into the superconducting gap. On the underdoped side, T^* may be saturated instead of extrapolating to a lower doping region.

17

- Spin-charge separation. This scenario assumes that the pseudogap is associated with the pairing of spinons, which are hypothetically charge-neutral fermions with the electron's spin, whereas the charge is carried by a spinless boson called holon.

- Existence of pseudogap in the overdoped regime.

1.5.2 Carrier doping

The doping of charge carriers (holes or electrons) in cuprates is crucial for many aspects of material properties. The parent compounds are antiferromagnetic insulators. Upon addition of charge carriers, they become superconducting at low temperatures. Carrier doping can be achieved by two ways: changing oxygen stoichiometry or adding metals (such as Pb or Y). The chemical composition of high-T_c cuprates can be represented by a general formula, $(Ln_{1-x}M_x)_{n+1}Cu_nO_{3n+1-m}$, where Ln is a trivalent rare-earth ion, e.g. Y, and M is a divalent alkaline ion such as Ba, Sr, or Ca, n is the number of CuO_2 planes and m denotes the number of oxygen vacancies. Since copper can have 4 to 6 oxygen coordinations to form CuO_4 squares, CuO_5 pyramids and CuO_6 octahedra, a large number of perovskite-like structures with oxygen deficiency can be synthesized from these "building blocks". In these compounds, the copper is usually oxidized in a state of Cu^{p+} with $0 < p < 0.4$, the value of m is thus related to the concentration x of divalent ions M. According to the doping status, a cuprate can achieve three doping regimes: optimal, under- and over-doping. The superconducting transition temperature reaches the maximum value in the optimal doping state, which has 0.2 holes per Cu site. The most significant macroscopic effects of doping on superconducting properties of cuprates include dependence of transition temperature T_c upon the doping level and pseudogap behavior in underdoped samples. The experimental studies on the former had successfully led to a reliable empirical relations. A consistent $T_c - p$ (hole concentration) relation had been established

$$\frac{T_c}{T_{cmax}} \propto 1 - a(p - b)^2 , \qquad (1.12)$$

18

where T_{cmax} is the maximum T_c at optimal doping level, a and b are experimental parameters related to cuprate type [41]. One difficulty involved in applying this elegant relation is the precise determination of oxygen concentration and T_c.

1.6 Superconducting fluctuation effects

It has been shown experimentally that superconducting fluctuations below and above T_c play an important role in various physical properties of HTSC. In conventional superconductors the superconducting fluctuations in a thin one-dimensional wire leads to the appearance of a finite resistance below T_c. The dissipation originates from superconducting fluctuations of the order parameter ψ. In particular, the fluctuations of the phase of the order parameter mainly contribute to the resistive dissipation. Above T_c, thermodynamical fluctuations toward the superconducting state lead to the appearance of excess conductivity, diamagnetism, specific heat, and tunnelling currents. In conventional superconductors these effects are generally small, but they can be measured experimentally, particularly in superconducting samples of reduced dimensionality (on the scale of GL coherence length), such as thin wires and films, and whisker-shaped crystals [42]. In HTSC the fluctuation effects are expected to be more pronounced because of the high operating temperatures which enhances the fluctuation effects.

1.6.1 2D superconducting fluctuations:
the Kosterlitz-Thouless transition

As it was mentioned earlier, superconducting fluctuations can cause resistance to appear in a thin 1D superconducting wire below T_c. These fluctuations reduce the order parameter ψ to zero at some point along the wire, thus momentarily disconnecting the phase at one end of the wire from the other. This allows the phase to slip by 2π before ψ recovers its usual finite value. This idea of superconducting fluctuations inducing phase slip events was first introduced by Langer and Ambegaokar [43] and

19

was later used to explain the appearance of a finite resistance in 1D Al wires below T_c by Moshchalkov [12]. The phase slip model is described in detail in Chapter 6.

In the case of 2D superconductors, the fluctuation effects lead to the onset of resistance at Kosterlitz-Thouless transition temperature $T_{KT} < T_c$. The appearance of a finite resistivity above T_{KT} is due to the creation of thermally-excited vortices. Below T_{KT}, thermal energy is insufficient to allow the vortices to unbind. Above T_{KT} they can unbind because the free energy $U - TS$ (where U is the internal energy and S is the entropy) is lowered sufficiently by the gain in entropy that is associated with two independently moving vortices relative to a single bound pair. In a 2D film the phase slip by 2π can occur continuously by the motion of a vortex from one edge of the film to the other. However, a more typical process would be the creation of a vortex-anti-vortex pair in the interior of the film, followed by their motion in opposite directions driven by the current, until both disappear at opposite edges. Either process leads to a 2π phase slip between the ends of the film.

The behavior of the resistivity as a function of temperature is schematically shown in Fig.1.3. The superconducting transition takes place at the mean-field supercon-ducting transition temperature T_{c0}, which indicates a large drop of resistivity and a loss of entropy accompanied by the growth of amplitude of the order parameter. The resistivity, however, does remain finite due to fluctuations of the phase of the order parameter until T_{KT} is reached, below which the resistivity becomes zero due to the freezing of the phase. In this case the resistivity, $\rho(T)$, is expected to follow a temperature dependence of the form:

$$\rho(T)/\rho_n = a \exp\left[-2\left(\frac{b(T_c/T_{KT} - 1)}{T/T_{KT} - 1}\right)^{1/2}\right] \quad (1.13)$$

where a and b are the dimensionless constants of the order of unity. Such a resistivity behavior has been reported in thin films in conventional superconductors [44] and in HTSC in both single crystals and thin films of YBCO [45], and BSCCO [46]. In some cases the magnetoresistivity is found to follow a power law [47], which is a further evidence for the existence of the Kosterlitz-Thouless transition. This is expected in

20

1

no long range correlation
in phase of the order parameter

Fluctuations of ψ

ρ/ρ_n

Free vortices

bound pairs
of vortices

0   T_{KT} T_{c0} T
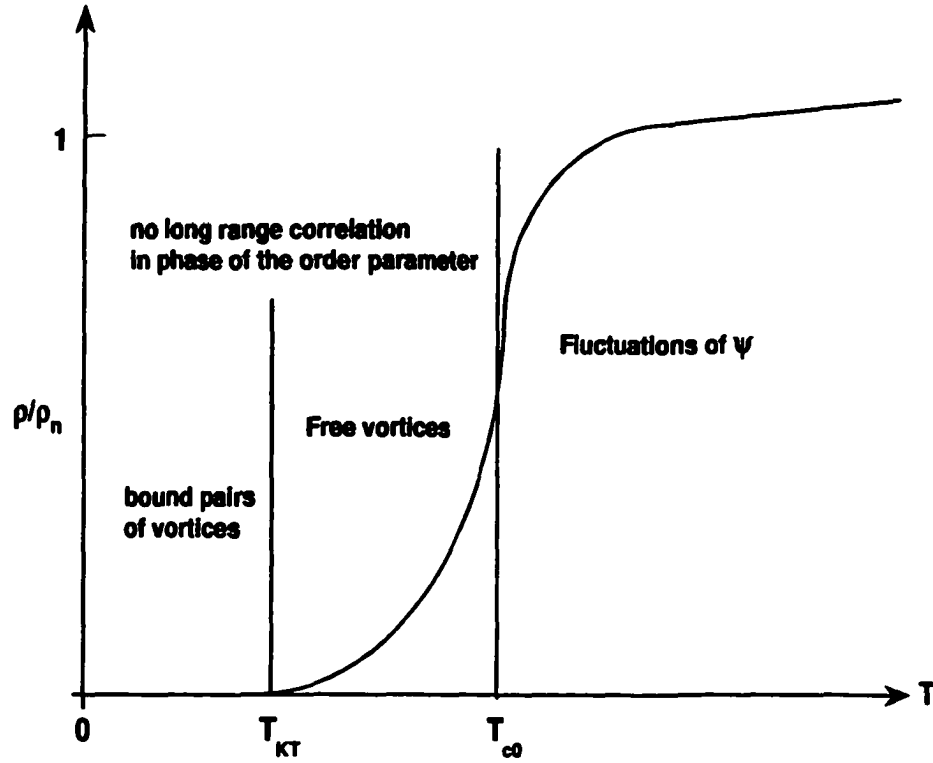
Figure 1.3: Schematic diagram of the normalized resistivity in a Kosterlitz-Thouless transition in two dimensions. The resistivity drops sharply at the mean-field superconducting transition temperature T_{c0} with tail that goes to zero at Kosterlitz-Thouless transition temperature T_{KT}.

the case of infinitesimally small currents only, because a larger current would destroy the bound vortex-antivortex pairs around and below T_{KT}, resulting in a nonlinear current-voltage relation.

1.6.2   Superconducting Fluctuations in HTSC

HTSC are characterized by a short coherence length. For highly anisotropic materials like $Bi_2Sr_2CaCu_2O_{8+x}$, $\xi_{ab} \approx 10 - 30\mathring{A}$ and $\xi_c \approx 0.2 - 3\mathring{A}$ represent the coherence lengths in the ab-plane and along the c-axis, respectively. Such a 2D anisotropy enhances significantly the superconducting fluctuation effects. There has been theoretical and experimental work in conventional thin-film superconductors, which may

21

provide a unique model for this specific issue in the study of the superconducting fluctuation effects within the framework of the Gaussian fluctuation theory [19, 42]. The critical fluctuation region, where the superconducting fluctuation effect is significant, can be understood using the Ginzburg criterion in a zero magnetic field as

$$\frac{T}{T_{c0}} - 1 \leq \frac{1}{32\pi^2} \left(\frac{k_B}{\Delta C(T_c)\xi_{ab}(0)\xi_c(0)} \right)^2 \qquad (1.14)$$

When the magnetic field is applied, this critical fluctuation region extends greatly because of the reduction of the effective dimensionality of the system from two to zero dimensions due to the orbital quantization, and it is expected to be

$$\frac{T}{T_{cB}} - 1 \leq \left(\frac{k_B B}{\Delta C(T_c)\phi_0\xi_c(0)} \right)^{2/3} \qquad (1.15)$$

where T_{cB} and T_{c0} represent the superconducting transition temperature in a magnetic field B and in a zero field, respectively, and $\Delta C(T_c)$ represents the jump in the specific heat at T_c. For example, the estimated critical fluctuation regions for YBCO in a zero field and in a 5 T field parallel to the c-axis using equations 1.14 and 1.15 are $T \sim 0.2$ K and $T \sim 2.2$ K, respectively. Similarly, for single crystal BSCCO, they are estimated to be about $T \sim 6$ K in a zero field and $T \sim 15$ K in a 5 T field. Fisher et al. [48] considered the effect of higher order terms to the GL free energy and found these terms to become significant while the leading Gaussian term is still quite small relative to the mean-field jump. Therefore it is important to include a $|\psi|^4$ term in the GL free energy beyond the Gaussian term. Following this concept, Tsuneto and his collaborators [49] developed a renormalized superconducting fluctuation theory, which explicitly considered higher-order contributions from the GL free energy expansion. As a result, they have shown that many features such as resistivity, its angular dependence, magnetization, specific heat, and their scaling behaviors, have successfully been calculated with reasonable agreements, at least near the mean-field transition temperature, T_c.

22

1.6.3 A phenomenological superconducting fluctuation theory

As we described earlier, the dissipation stems from superconducting fluctuations of the order parameter. It is natural to expect that this may be a good approximation as a mechanism of the resistivity at least at low temperatures. In order to describe this effect a new phenomenological theory of dissipation has been developed by taking into account only the broken phase relation between pancake vortices in the superconducting fluctuation regime, and by assuming that the layer structure in HTSC forms intrinsic Josephson junctions. In the following, the essence of this approach, is described.

The resistive dissipation in the broken phase coherence was discussed by Ambegaokar and Halperin [50] for the case of a conventional Josephson junction. According to their calculations the resistivity is written as

$$\rho(T)/\rho_n = (I_0[E_J/2k_B(T - T_{irr})])^{-2} \tag{1.16}$$

where ρ_n is the normal-slate resistivity, $I_o(x)$ is the modified Bessel function, E_J is the Josephson coupling energy and T_{irr} is the irreversibility temperature. Note that the thermal energy $k_B T$ is replaced by $k_B(T - T_{irr})$. Although this shift in temperature has brought controversy regarding whether or not the cause of superconducting fluctuations is thermal fluctuations, this is phenomenologically introduced into the expression in order to produce better agreement with the experimental results. This temperature modification has also an important implication on the issue of the vortex phases. Because of this shift in temperature, zero resistivity is reached at a finite temperature, T_{irr}, which may separate the phase diagram into two distinct regions governed by different vortex dynamics. In fact, the resistivity observed experimentally in both $La_{2-x}Sr_xCuO_{4-\delta}$ and BSCCO (YBCO is exceptional on this point) has a clear tendency to diverge in the logarithmic plot towards T_{irr}, at least within the experimental sensitivity. This fact provides direct information on the occurrence of

23

long-range order of the phase in the superconducting order parameter at T_{irr}.

According to the Lawrence-Doniach model [18], the maximum Josephson current density, perpendicular to the layers, is given by $J_{max} = \phi_0/2\pi\mu_0 s\lambda_c^2$ for 3D anisotropic superconductors, where s is the interlayer distance and λ_c is the penetration depth along the c-axis. Then, the maximum Josephson current, I_{max}, flowing along the c-axis can be written by introducing the effective Josephson junction area, A(H,T), as

$$I_{max} = A(B,T)J_{max} = \frac{A(B,T)\phi_0}{2\pi\mu_0 s\lambda_c^2} \tag{1.17}$$

Therefore, the corresponding Josephson coupling energy, $E_J = I_{max}\hbar/e$, is given by

$$E_J = \frac{A(B,T)\phi_0^2}{2\pi^2\mu_0 s\lambda_c^2} \tag{1.18}$$

By applying a magnetic field perpendicular to the superconducting layers, a straight stack of pancakes is formed at sufficiently low temperatures. This straight stack is disturbed by the thermal motion of pancakes at high temperatures, resulting in the formation of Josephson strings in between the superconducting layers. As a result, a phase change associated with the Josephson current between the adjacent junction layers is created within the effective junction area A(B,T), which can be approximated to be proportional to $r_s\Delta r$, where $r_s = s\gamma$ is the Josephson penetration depth and characterizes the Josephson interaction range, γ is the anisotropy ratio and Δr is the relative displacement between the pancakes in the adjacent layers induced by thermal fluctuations. Following this, one can separate the thermal effect and the field effect in the effective junction area as $A(B,T) = a(B)[\Delta T/T_c]^\alpha$, where a(B) depends only on magnetic field and decreases with an increasing B, and $\Delta T = T - T_{irr}$. The parameter α is introduced to absorb all corrections from the ideal picture and in fact reflects the extent of the Josephson coupling area between the layers.

By substituting the new form of A(B,T) into Eq.1.18, one can describe the Josephson coupling energy as

$$E_J = \left[\frac{a(B,T)\phi_0^2}{2\pi^2\mu_0 s\lambda_c^2}\right]\left(\frac{\Delta T}{T_c}\right)^\alpha \tag{1.19}$$

24

Consequently, using Eq.1.16 and by introducing $\lambda_c(T) = \lambda_c(0)[1 - T/T_c]^{-1/2}$, one can obtain the final expression for the resistivity for $\mathbf{B} \parallel$ c-axis as

$$\rho/\rho_n = \left(I_0 \left[\frac{C(B)(1 - T/T_c)}{\Delta T/T_c)^{1-\alpha}} \right] \right)^{-2} , \qquad (1.20)$$

where $C(B) = a(B)\phi_0^2/4\pi^2\mu_0 sk_B T_c \lambda_c(0)^2$, which depends only on the magnetic field.

25

Bibliography

[1] W. K. Kwok,U. Welp, G. W. Crabtree, K. G. Vandervoort, R. Hulscher, J. Z. Liu, *Phys. Rev. Lett.*, **64**, 966 (1990).

[2] S. Fleshler, Wai-Kwong Kwok, U. Welp, V. M. Vinokur, M. K. Smith, J. Downey, G. W. Crabtree, *Phys. Rev. B* **47**, 14448 (1993).

[3] Y. Iye, S. Nakamura, T. Tamegai, T. Terashima, K. Yamamoto, Y. Bando, *Physica C* **166**, 62 (1990).

[4] W. K. Kwok, U. Welp, V. M. Vinokur, S. Fleshler, J. Downey, G. W. Crabtree, *Phys. Rev. Lett.* **67**, 390 (1991).

[5] Y. Iye, A. Watanabe, S. Nakamura, T. Tamegai, T. Terashima, K. Yamamoto, Y. Bando, *Physica C* **167**, 278 (1990).

[6] S. Aukkaravittayapun, P. J. King, Yu. I. Latyshev, R. M. Bowley, *Physica C* **277**, 196 (1997).

[7] M. Chaparala, O. H. Chung, Z. F. Ren, M. While, P. Coppens, J. H. Wang, A. P. Hope, M. J. Naughton, *Phys. Rev. B* **53**, 5818 (1996).

[8] S. H. Han, Y. Zhao, G. D. Gu, G. J. Russell, N. Koshizuka, *Advances in Super-conductivity*,**8** , (1996), 109-112, (Proc. of the 8th International Symposium on Superconductivity (ISS '95),Oct.30-Nov.2, 1995, Hamamatsu.

[9] M. A. Crusellas, J. Fontcuberta and S. Pinol, *Phys. Rev. B* **46**, 14089 (1992).

[10] M. Park, M.S. Isaacson, J.M. Parpia, *Phys. Rev. Lett.* **75**, 3740 (1995).

[11] Y.K. Kwong, K. Lin, P.J. Hakonen, M.S. Issacson, J. M. Parpia, *Phys. Rev. B* **44**, 462 (1991).

[12] V. V. Moshchalkov, L. Gielen, G. Neuttiens, C. Van Haesendonck, Y. Bruynser-aede , *Phys. Rev. B* **49**, 15412 (1994).

[13] T. Ito, K. Takenaka, and S. Uchida , *Phys. Rev. Lett.* **70**, 3995 (1993).

[14] B. Wuyts, V. V. Moshchalkov, and Y. Bruynseraede, *Phys. Rev. B* **53**, 9418 (1996).

[15] Weimin Chen, J. P. Franck, and J. Jung, *Phys. Rev. B* **60**, 3527 (1999).

[16] Y. Nakamura and S. Uchida, *Phys. Rev. B* **46**, 5841 (1992).

[17] P. H. Kes, J. Aarts, V. M. Vinokur, and C. J. van der Beek , *Phys. Rev. Lett.* **64**, 1063 (1990).

[18] W. E. Lawrence and S. Doniach, in E. Kanda (ed.) *Proc. 12th Int. Conf. Low Temp. Phys.* (Kyoto, 1970; Keigatu, Tokyo, 1971), p.361.

[19] M. Tinkham,*Introduction to Superconductivity*, second edition, McGraw-Hill, New York,(1996).

[20] G. Blatter, M. V. Feigel'man, V. B. Geshkenbein, A. I. Larkin, V. M. Vinokur, *Rev. Mod. Phys.* **66**, 1125 (1994).

[21] M. Tachiki and S. Takahashi, *Solid State Commun.* **70**, 291 (1989).

[22] A. I. Larkin and Yu. V. Ovchinnikov, *J. low Temp. Phys.* **34**, 409 (1979).

[23] L. Ya. Vinnikov, L. A.Gurevich, G. A. Yemelchenko, Yu. A. Ossipyan , *Solid State Commun.* **67**, 421 (1988).

[24] G.J. Dolan, G.V. Chandrashekhar, T.R. Dinger, C. Feild, F. Holtzberg, *Phys. Rev. Lett.* **62**, 827 (1989).

[25] E. M. Gyorgy, R. B. van Dover, K. A. Jackson, L. F. Schneemeyer, J. V. Waszczak, *Appl. Phys. Lett.* **55**, 283 (1989).

[26] J. Z. Liu, Y. X. Jia, R. N. Shelton, M. J. Fluss, *Phys. Rev. Lett.* **66**, 1354 (1991).

[27] C. A. Duran, P.L. Gammel, R. Wolfe, V. J. Fratello, D. J. Bishop, J. P. Rice, D. M. Ginsberg, *Nature* **357**, 474 (1991).

[28] V. K. Vlasko-Vlasov, L. A. Dorosinskii, A. A. Polyanskii, V. I. Nikitenko, U. Welp, B. W. Veal, G. W. Crabtree, *Phys. Rev. Lett.* **72**, 3246 (1994).

[29] A. Gurevich, *Phys. Rev. B* **46**, 3187 (1992).

[30] P. B. Allan, Z. Fisk, and A. Migliori, *Physical properties of high temperature superconductors* I, ed. by D. M. Ginsberg, World Scientific, Singapore 1989, P. 213.

[31] Y. Iye, *Physical properties of high temperature superconductors* III, ed. by D. M. Ginsberg, World Scientific, Singapore 1992, P. 285.

[32] S. Chakravarty, A. Sudbo, P. W. Anderson, S. Strong, Science, **261**, 337 (1993).

[33] N. P. Ong, *Physical properties of high temperature superconductors* II, ed. by D. M. Ginsberg, World Scientific, Singapore 1994, P. 459.

[34] M. Gurvitch, and A. T. Fiory, *Phys. Rev. Lett.* **59**, 1337 (1987).

[35] M. Takigawa, W. L. Hults, J. L. Smith , *Phys. Rev. Lett.* **71**, 2650 (1993).

[36] P. Dai, M. Yethiraj, H. A. Mook, T. B. Lindemer, and F. Dogan, *Phys. Rev. Lett.* **77**, 5425 (1987).

[37] D. Pines, *Z. Phys. B* **103**, 129 (1997).

[38] V. J. Emery and S. A. Kivelson, *Nature* **374**, 434 (1995).

[39] A. S. Alexandrov, A. M. Bratkovsky, N. F. Mott, *Phys. Rev. Lett.* **72**, 1734 (1994).

[40] P. W. Anderson, Science **268**, 1154 (1995); ibid **82**, 2620 (1999); A. J. Leggett, *Science* **274**, 587 (1996).

[41] M. R. Presland, J. L. Tallon, R. G. Bukley, R. S. Liu, N. E. Flower, *Physica C* **176**, 95 (1991).

[42] W. J. Skocpol and M. Tinkham, *Rept. Prog. Phys.* **20**, 1049 (1975).

[43] J.S. Langer and V. Ambegaokar, *Phys. Rev.* **164**, 498 (1967).

[44] M. R. Beasley, J. E. Mooij, T. P. Orlando, *Phys. Rev. Lett.* **42**, 1165 (1979).

[45] Q. Y. Ying and H. S. Kwok, *Phys. Rev. B* **42**, 2242 (1990).

[46] P. C. Stamp, *Phys. Rev. Lett.* **63**, 582 (1989).

[47] M. Ban, T. Ichiguchi, T. Onogi , *Phys. Rev. B* **40**, 4419 (1989).

[48] D. S. Fisher, M. P. A. Fisher,D. A. Huse, *Phys. Rev. B* **43**, 130 (1991).

[49] T. Tsuneto, *J. Phys. Soc. Japan* **57**, 3499 (1988).

[50] V. Ambegaokar and B. Halperin, *Phys. Rev. Lett.* **22**, 1364 (1969).

Chapter 2

Experimental Procedure and Sample Characterization

2.1 Introduction

The study of the anisotropy of the high temperature superconductors (HTSC) requires a particularly high degree of precision in the angular control for the measurements of an angle-dependent physical property (resistivity, torque etc.). Especially, the measurement of the angular dependence of resistivity $\rho(\theta)$ in a magnetic field **B** requires a careful control of θ when measuring $\rho(\theta)$ very close to the ab-planes for both single crystals and films.

For highly anisotropic HTSC like BSCCO for example, the angular dependence of $\rho(\theta)$ is very steep when **B** is very close to and through the ab-planes (for rotations off the c-axis) and requires an angular resolution much better than 1° in order to detect fine details of the resistivity $\rho(\theta)$. A poor angular resolution leads sometimes to underestimating the intrinsic anisotropy factor $\gamma = \sqrt{m_c/m_{ab}}$. Moreover, precise angular alignment of **B** parallel to the ab-planes is an essential experimental requirement for the measurement of $\rho(\theta)$ within the ab-planes or for the measurements that require the field to be parallel to the applied current **J**. For magnetic field rotations in the ab-planes, even small misalignment between the c-axis and the normal to the

30

plane in which the field is rotated, could lead to an additional contribution of the c-axis resistivity which may actually dominate the angular dependence of $\rho(\phi)$ (where ϕ is the angle of rotation of the field in the ab-planes) [1].

The use of the normal stepping motors or the commercial micro-stepping systems to obtain high angular resolution (less than 0.1°) without using a sensor (optical encoder), which allows one to read the exact angular position of the sample, may lead to a substantial ambiguity in the angular position especially if one adds to that the error due to a backlash of the stepping motor. Stepping motor backlashes can be minimized or eliminated by using a high ratio gear reducer between the sample and the stepping motor.

The other important issue, which also requires a special attention in the measurement of $\rho(\theta)$, is the precise control of the sample temperature. When a sample is rotated in a magnetic field, this produces an induced emf in the heater circuit and in the leads of the thermometers attached to the sample holder. If the rotation speed is large, this will disturb the heater current and consequently cause large temperature fluctuations during the measurement. In order to reduce these effects very slow rotation speed is essential.

In the design of the experimental setup used to measure the angular dependence of resistivity, we have used a combination of a stepping motor and a 100-1 planetary gear reducer to eliminate the backlash and to provide reliable fine rotations. We have used an optical encoder attached directly to the sample to read accurately the angular position of the sample. The sample was rotated with very low speed to minimize the temperature fluctuations.

In the following sections experimental setup, sample preparation, measurement procedure and sample characterization are described in detail.

31

2.2 Experimental setup

The setup that was used to perform the resistive measurements consists of four major parts: cryostat, non-superconducting magnet, sample holder and the angle-control system. LN_2 cryostat, capable of holding LN_2 for a period between 48 to 72 hours, was equipped with a narrow tube. This allowed the magnet pole separation to be as small as 10 cm in order to achieve greater magnetic fields in the sample region. The cryostat consists of a two vacuum-can system. The outer can was evacuated down to a pressure of about 5×10^{-7} torr and the inner one was filled with low pressure helium gas.

The magnetic field was generated using a horizontal copper-wound water-cooled magnet which was powered by two HP Harrison 6260A DC power supplies connected in parallel. The magnet had an iron core that yielded a large field strength. The magnet provided a maximum field of 1 T at 110 A and 10 V. The magnetic field at the sample was monitored using a Hall probe located directly behind the sample. This consistently showed that the applied field did not change by more than 0.1%.

The sample holder was attached to a stainless steel hollow tube of 10 mm outer diameter and about 1 m long. The upper end of the tube hosted all the electrical connections and was connected to the angle-control system through a flexible coupling. The lower end was attached to a V-shape copper block with a carbon-glass resistance thermometer, an inductionless heater and a Hall probe (to monitor the field at the sample position) embedded inside it. The sample was placed on the flat side of the V-shape copper block. Good thermal contact between the sample and the copper block holder was achieved using a thin layer of Apiezon grease.

Computer-controlled angle-control system was built using a 200-step stepping motor, an IMS Micro-LYNX-4 integrated micro-stepping controller, a 100-1 CGI Paragon Planetary Gear-head reducer and a US Digital 3-channel (index) 2000-line optical encoder. The Micro-LYNX-4 has a programmable integrated micro-stepping motor drive and high-performance controller which provided microstep resolution up to 51200 steps per revolution. This could allow one to obtain an angular resolution of

32

0.007°. However, in general the microstepping devices do not have a linear response which results in a nonuniform microsteps. In order to eliminate this nonuniform microstepping, we have used a backlash-free 100-1 gear reducer. The optical encoder was attached directly to the sample holder by means of flexible coupling from one side, and the other side was connected to the gear head. We used a three-channel 2000-line optical encoder which imposed an upper limit on the angular resolution that can be accurately monitored. Although the microstepping device could reach an angular resolution as high as 0.007°, the minimum angular step the encoder could read was $360^\circ/8000(lines) = 0.045^\circ$.

We also performed critical current versus temperature measurements using a scanning Hall probe system which consists of a cryogenic refrigerator and a copper-block sample holder. The Hall probe is kept at room temperature and in air in order to avoid any offsets in the magnetic field reading. This system was built and tested earlier for this purpose by Darhmaoui and Jung [2, 3, 4].

2.3 Sample Preparation

Since the discovery of the HTSC, several methods have been employed to prepare high-T_c thin films. Most YBCO films were deposited onto heated substrates of $SrTiO_3$, $LaAlO_3$, MgO or sapphire using laser ablation from stoichiometric ceramic targets, rf and dc sputtering from ceramic targets, and reactive coevaporation technique. Among these methods, off-axis rf sputtering was considered to be the most successful one because it allowed a slow growth of films and a large area deposition [5].

In this work, we have used rf magnetron sputtering technique to prepare c-axis oriented YBCO thin films on (100) oriented $SrTiO_3$ and $LaAlO_3$ substrates. This method allowed us to grow films with different thicknesses and transition temperatures through changing the sputtering conditions.

The sputtering deposition system that was used to prepare YBCO thin films

33

consists of a vacuum chamber with a base pressure of 1×10^{-7} torr produced by a cryopump, an rf magnetron gun and a heater with a nickel plate and a chromel-alumel thermocouple. A temperature controller was used to control the substrate temperature with a stability of $\pm 1^\circ C$.

It is known that the growth of epitaxial thin films depends on the deposition conditions and the substrates. For a sputtering deposition technique, these conditions include: the substrate temperature, the O_2/Ar gas pressure ratio, the total gas pressure, the substrate-target distance, the sputtering configuration (on-axis or off-axis) and the sputtering power which controls the deposition rate. YBCO thin films were deposited on (100) oriented $SrTiO_3$ and $LaAlO_3$ substrates (of dimensions $10 \times 10 \times 0.5\,mm^3$ and $10 \times 14 \times 0.5\,mm^3$) using the off-axis configuration. The substrates were attached to the heater plate using a silver paste in order to achieve uniform heating. A 2-inch diameter commercial stoichiometric $Y_1Ba_2Cu_3O_{7-\delta}$ target of 99.999% purity was used during the deposition. The sputtering was performed using an rf power between 20 to 50 W at a total pressure of 110 - 125 mtorr in 5:1 oxygen-argon gas mixtures. During sputtering the substrates temperatures were kept at $750^\circ C$ for both kind of substrates. The deposition time ranged between 10 to 20 hours. After deposition, the chamber was filled with oxygen at a pressure slightly less than 1 atmosphere and the films were subsequently cooled down to $500^\circ C$ for 15 - 30 minutes annealing and then slowly down to room temperature.

We have also investigated YBCO thin films that were deposited in different laboratories using laser ablation technique (McMaster University, and National Research Council of Canada NRC) and dc sputtering technique (St. Petersburg Electrotechnical University, Saint Petersburg, Russia) [6, 7] (see Table 2.1).

Initially the films were patterned with a metal mask, using the conventional photolithography technique and wet etched with a diluted phosphoric acid, into rings of outer and inner dimensions of 8.5 and 5.0 mm or into disks of 8.5 mm in diameter. After the measurement of the temperature dependence of the critical current density (J_c), the films were patterned into a form of a 30 to 100μm wide (see Table 2.1) and

34

Table 2.1: Samples characteristics: substrate type, deposition method, thickness of films and the width of the bridges.

Film No.	Film ID	Substrate type	Deposition Method	Thickness (nm)	Bridge Width (μm)
1	MID053	$SrTiO_3$	Laser ablation	210	60
2	MAH2	$LaAlO_3$	rf-magnetron	310	40
3	BT6004	$SrTiO_3$	Laser ablation	230	60
4	NRC-L96-08	Sapphire/CeO_2	Laser ablation	140	60
5	MAH16	$SrTiO_3$	rf-magnetron	210	30
6	YR117	Al_2O_3/CeO_2	dc-magnetron	330	60
7	YR118	Al_2O_3/CeO_2	dc-magnetron	610	100
8	MAH17	$LaAlO_3$	rf-magnetron	100	60
9	NRC-L96-11	Sapphire/CeO_2	Laser ablation	110	60
10	NRC-L96-20	$LaAlO_3$	Laser ablation	340	60
11	MID049	$LaAlO_3$	Laser ablation	130	60
12	NRC-L96-12	Sapphire/CeO_2	Laser ablation	190	60
13	MAH18	$SrTiO_3$	rf-magnetron	420	60

6.4 mm long strip with six measurements probes Fig.2.1(a) . Large area contacts on the film were deposited by silver-sputtering in order to minimize Joule heating effects. The silver-sputtering was performed using an rf power between 30 to 40 W at an Ar pressure of 15 mtorr for about 15-20 minutes. Copper leads were attached to silver contacts using mechanically pressed indium. A typical distance between voltage probes was 0.4 mm.

35
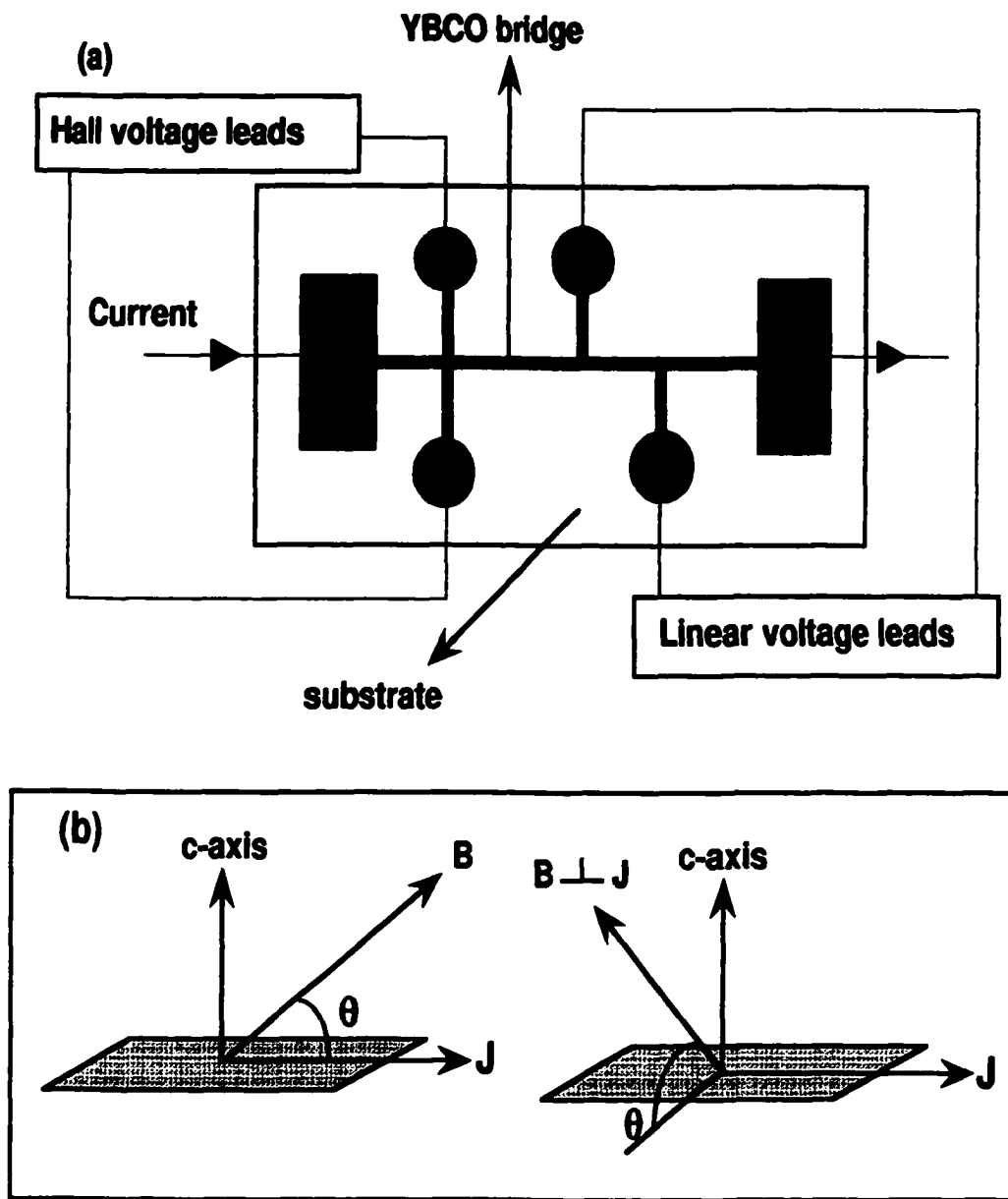
Figure 2.1: (a) schematic illustration of the bridge which was etched from a disk-
or a ring-shaped samples, showing the voltage and current leads. (b) Two configura-
tions of **B** with respect to **J** that were used during the measurements of the angular
dependence of resistivity $\rho(\theta)$ in a magnetic field: **B** is rotated in a plane parallel to
both **J** and the c-axis (left side), or **B** is rotated in a plane parallel to the c-axis but
perpendicular to **J** (right side).

36

2.4 Measurement Procedure

2.4.1 Resistivity measurement

We have performed the measurements of the resistivity as a function of temperature $\rho(T)$ between T_c and 300 K in zero magnetic field, and between T_c and 100 K in a constant magnetic field. The measurement of the temperature dependence of resistivity in a constant magnetic field was carried out for three different orientations of the field $\mathbf{B}$ relative to the current $\mathbf{J}$: (1) $\mathbf{B} \parallel \mathbf{J}$ (with $\mathbf{B} \parallel$ ab-planes, i.e $\theta = 0^{\circ}$); (2) $\mathbf{B} \perp \mathbf{J}$ (with $\mathbf{B} \parallel$ ab-planes, i.e $\theta = 0^{\circ}$); and (3) $\mathbf{B} \parallel$ c-axis (with $\mathbf{B} \perp \mathbf{J}$, i.e $\theta = 90^{\circ}$), where θ is the angle between the ab-planes and the direction of the magnetic field $\mathbf{B}$. $\rho(T)$ measurements for the range of temperatures between T_c and 300 K were performed twice, during cooling from room temperature down to T_c and during heating from T_c up to room temperature. No temperature hysteresis in $\rho(T)$ was observed.

We have also measured the resistivity as a function of the angle θ between the ab-plane of the film and the direction of the magnetic field $\mathbf{B}$. These measurements were done over a temperature range within the superconducting transition, as a function of the magnitude of the magnetic field and the applied current density. The angle θ was changed by rotating the copper sample holder about its vertical axis in a horizontal magnetic field up to 1 Tesla. Films were mounted on the sample holder with the c-axis perpendicular to the sample holder's vertical rotating axis, which allowed us to change the magnetic field direction in a plane parallel to the c-axis.

Resistivity was measured using a standard DC four-probe method. The current was applied to the sample in the form of short pulses (of duration less than 200 ms) in both directions, in order to eliminate the background noise and charge accumulation, as well as to reduce Joule heating. The voltage was measured using a Keithley 2182 nanovoltmeter in synchronization with a Keithley 236 current source, where the nanovoltmeter was used as the triggering unit. The nanovoltmeter was operated in a "delta" mode. This mode allowed the measurement and the calculation of the voltage using a DC current-reversal technique to eliminate the effects of thermal emf's in the

37

leads. Each "delta" reading was calculated from two voltage measurements for two opposite directions of the current. In this mode, the basic "delta" voltage calculation is given by:

$$V_{delta} = \frac{V_1 - V_2}{2} \qquad (2.1)$$

where V_1 and V_2 are the voltages corresponding to the positive and negative directions of the current. The 2182 nanovoltmeter is optimized to provide low-noise readings when the measurement speed (the applied current reversal speed) is set between 100 msec and 333 msec. Each "delta" mode measurement was repeated ten times and subsequently stored in the buffer of the nanovoltmeter. The average value of these ten measurements, the maximum and the minimum values were transferred to the computer. The difference between the average and the corresponding maximum or minimum value was less than 0.1%.

Most of the measurements were done at temperatures within the superconducting transition region where the change in resistivity with temperature was most steep, and for magnetic fields applied very close to the ab-planes, where the variation of $\rho(\theta)$ is large. Large changes in $d\rho/dT$ essentially require precise temperature control. Therefore, temperature, which was monitored by a carbon-glass resistance thermometer, was controlled using an inductionless heater to better than $\pm 10mK$ for each single angular sweep. This was achieved by rotating the sample very slowly in a magnetic field in order to eliminate emf in the heater and thermometer leads which could otherwise disturb the temperature stability.

Term "resistivity" was used in this work to denote the quantity E/J (where E is the electric field and J is the transport current density), and it does not imply an ohmic response.

Before each $\rho(\theta)$ measurement in a magnetic field, the field was first aligned parallel to the ab-planes using the Hall probe located behind the sample and the angle-control system. This position was marked as a reference point using the index channel of the optical encoder.

All angular measurements were carried out with the transport current J parallel to

38

the ab-planes. However, each angular measurement was performed for two different orientations of the magnetic field with respect to the current. In the first one the field was rotated in a plane perpendicular to the current direction, while in the other one the field was rotated in a plane parallel to the current and the c-axis directions [see Fig.2.1(b)]. All measurements were done in the field cooling (FC) regime, with the magnetic field applied to the sample at a temperature above the T_c(onset), followed by slow cooling down to the required temperature of measurement. A typical angular sweep ranges between $\theta = -90^o$ and $\theta = +90^o$ with an angular step between $3^o - 5^o$. For θ close to the ab-planes, the angular step was smaller (between $0.05^o - 0.3^o$) in order to detect very sharp dependence of resistivity on the angle θ (shown by some YBCO films with high intrinsic anisotropy).

The measurements of $\rho(\theta)$ and $\rho(T)$ were computerized using a GBIB IEEE-488 interface card for all electronics except the Micro-LYNX angle-controller which was remotely controlled by an RS-232 interface port. The program code was written in Microsoft Visual Basic language. The experimental setup with the remote control was capable of performing automatic measurement of the voltage (1nV-100V) as a function of the current (10 pA-100 mA), the temperature (65-300 K), and the angle ($0.045^o - 360^o$).

2.4.2 Critical current measurements

The magnitude of the critical current in the ab-planes of YBCO films was obtained from the magnitude of the axial component of the magnetic field generated by a maximum self-supporting supercurrent circulating in a ring- or disk-shaped sample. For YBCO thin films, persistent current was induced in a ring- or disk-shaped sample by applying and subsequently switching off the external magnetic field generated by a solenoid along the c-axis of the film. The profile of the current's self-magnetic field was recorded with a scanning Hall probe at a constant distance from the surface of the film. The external magnetic field was increased in steps until the self-field of the persistent current reached the saturation level (for more details about the $J_c(T)$

39

measurement procedure see [2, 4]).

2.5 Sample Characterization

2.5.1 Temperature dependence of resistivity

Measurements of the temperature dependence of resistivity over a temperature range between T_c and 300 K in a zero magnetic field were performed on thirteen YBCO thin films of different thickness and preparation techniques, both optimally doped and underdoped. Using the resistivity versus temperature curve, the zero resistance transition temperature T_{c0}, mid-point transition temperature T_{cm}, onset transition temperature T_c (onset), superconducting transition width ΔT_c, and resistivities at 100 K $\rho(100K)$ and at 300 K $\rho(300K)$ were calculated for all films and tabulated in Table 2.2. The zero resistance transition temperature T_{c0} is defined as the temperature at which the resistive voltage drops below 10-15 nV in a zero magnetic field. The mid-point transition temperature T_{cm} is the temperature at which the temperature derivative of resistivity $d\rho/dT$ has a maximum, T_c onset is the largest temperature at which $d\rho/dT$ reaches 5% of its maximum value. The transition width ΔT_c is the difference between the two temperatures at which $d\rho/dT$ reaches 10% of its maximum value (this is in fact equivalent to the standard 10%-90% criteria of $\rho(T)$). Fig.2.2 shows a typical resistivity curve and its temperature derivative $d\rho/dT$ measured for temperatures between 84K and 92K. The graph illustrates different definitions of T_c and ΔT_c described above.

Films with the highest T_c (i.e films 1, 3 and 11) are characterized by a sharp transition width $\Delta T_c \simeq 1\,K$. The resistivity $\rho(T)$ of most of YBCO films investigated in this work exhibited a linear temperature dependence only at high temperatures (between 220 K and 300 K), but at lower temperatures down to onset T_c they showed an upward deviation from this linear dependence (see the next Chapter).

Table 2.2:   Normal and superconducting properties of YBCO films. ρ is the in-plane resistivity, T_{c0} is the transition temperature at $\rho = 0$ and B=0, T_{cm} is the mid-point transition temperature taken as the temperature at which $d\rho/dT$ is maximum, ΔT_c is the transition width and t is the thickness of the film. Films are sorted according to their T_{c0}.

Film No.	substrate type	t (nm)	T_{c0} (K)	T_{cm} (K)	ΔT_c (K)	$\rho(100K)$ ($\mu\Omega cm$)	$\rho(300K)$ ($\mu\Omega cm$)	$\frac{\rho(300K)}{\rho(100K)}$
1	$SrTiO_3$	210	90.0	90.5	1.0	8.03	27.32	3.40
11	$LaAlO_3$	130	89.9	90.6	1.0	38.37	133.71	3.49
3	$SrTiO_3$	230	89.5	90.3	1.2	74.89	265.82	3.55
9	Sapphire/CeO_2	110	86.2	86.8	0.9	33.48	98.09	2.93
10	$LaAlO_3$	340	85.8	86.6	1.2	54.10	126.85	2.34
12	Sapphire/CeO_2	190	85.4	87.1	1.6	100.20	297.21	2.97
13	$SrTiO_3$	420	85.4	86.1	1.2	67.57	208.24	3.08
7	Al_2O_3/CeO_2	610	85.0	85.9	2.0	389.41	1119.23	2.87
8	$LaAlO_3$	100	84.6	86.1	3.0	41.22	127.15	3.08
6	Al_2O_3/CeO_2	330	84.6	86.2	2.5	259.39	741.16	2.86
5	$SrTiO_3$	210	84.5	86.4	1.9	113.42	315.39	3.78
4	Sapphire/CeO_2	140	81.7	82.6	3.7	14.21	34.16	2.40
2	$LaAlO_3$	310	80.3	81.0	2.3	169.69	450.14	2.65

2.5.2   Temperature dependence of the critical current

The temperature dependence of the critical current in the ab-planes has been measured over a temperature range between 10K to T_c in a zero magnetic field for about fifteen YBCO films of various thickness, T_c, and preparation techniques, using the scanning Hall probe device described earlier.

The experimental data for four selected YBCO thin films, which exhibit typical temperature dependence of $I_c(T)$, are shown in Fig.2.3(a). Critical currents in each sample were normalized to their values at 10K. All films in Fig.2.3(a) are characterized
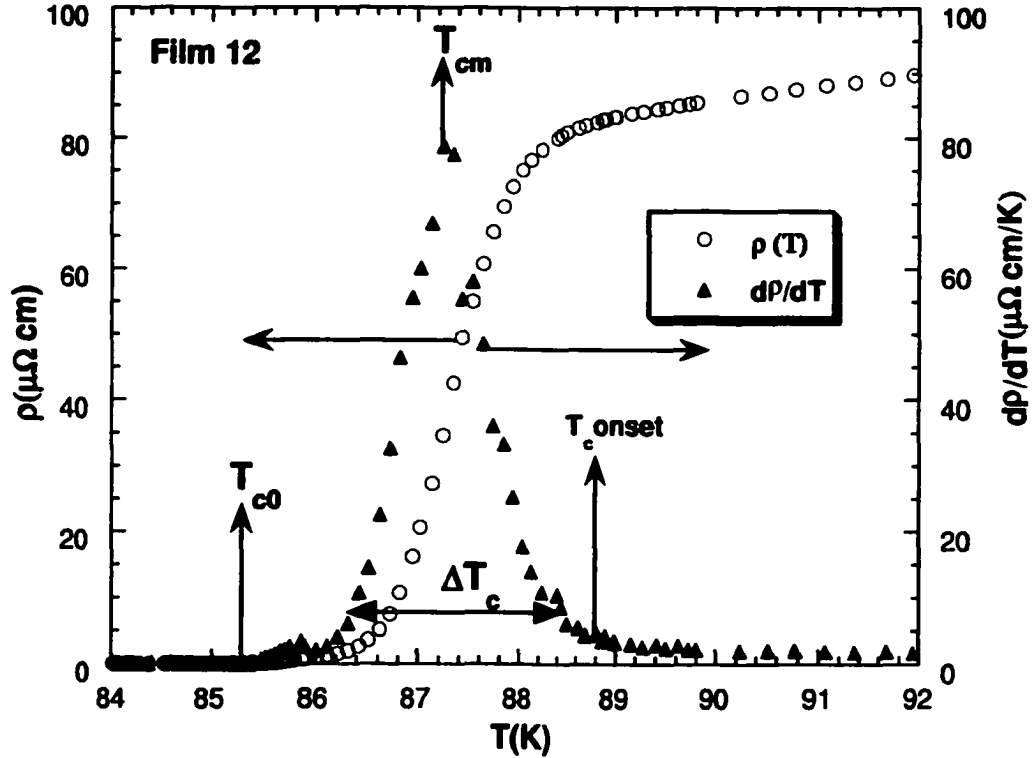
Figure 2.2: The resistivity $\rho(T)$ curve and its temperature derivative $d\rho/dT$ versus temperature between 84K to 92K measured in a zero magnetic field of a typical YBCO film. The zero resistance transition temperature T_{c0}, the mid-point transition temperature T_{cm}, the onset transition temperature T_c-onset, and the superconducting transition width ΔT_c are marked on the graph.

by a Ginzburg-Landau-like (GL) concave temperature dependence $(T_c - T)^{3/2}$ close to T_c which extends to lower temperatures for films with low T_c. A Ginzburg-Landau-like temperature dependence $(T_c - T)^{3/2}$ over a full temperature range (10 - 90K) was observed by Darhmaoui and Jung in most thin films of T_c below approximately 60K [4, 8]. The magnitude of the critical current density at 10K in various films investigated was between 1.6×10^6 and $3.0 \times 10^7 A/cm^2$ (see Table 2.3).

In order to identify more clearly a GL-like temperature dependence $(T_c - T)^{3/2}$ portion of I_c (as it was done in Ref. [2]), the data of Fig.2.3(a) were replotted as $[I_c(T)/I_c(10K)]^{2/3}$ versus temperature in Fig.2.3(b). The results revealed the presence of a Ginzburg-Landau-like (GL) temperature dependence of the critical current $I_c(T)$ close to T_c. For film 1, with the highest $T_c \approx 90.5$, $[I_c(T)/I_c(10K)]^{2/3}$ versus

42
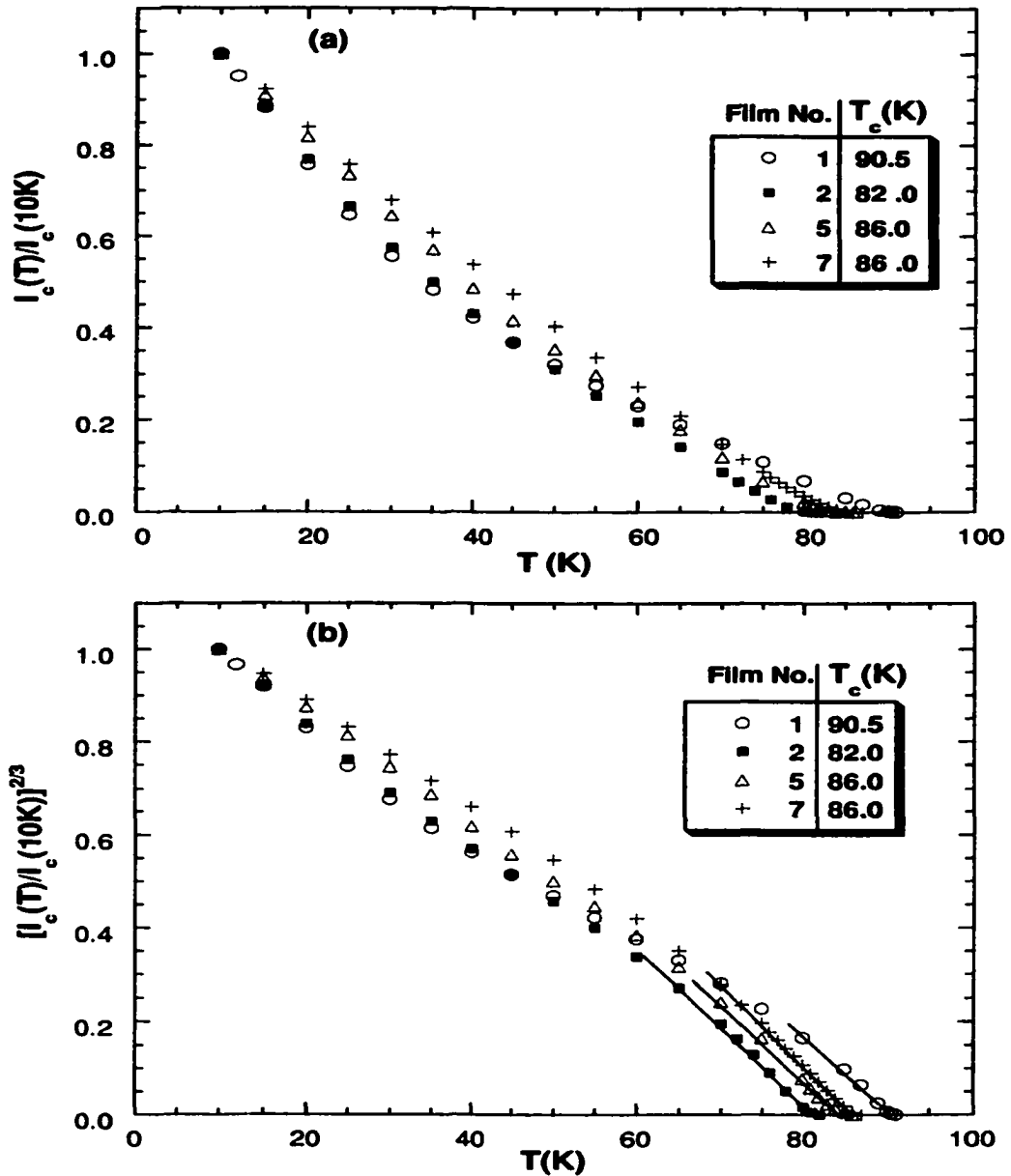
Figure 2.3: (a) Temperature dependence of the critical current in selected c-axis oriented YBCO thin films with T_c that ranges between 82 K and 90.5 K. The critical current is normalized to its value at 10K. (b) Plot of the results shown in (a) as $[I_c(T)/I_c(10K)]^{2/3}$ versus temperature. This allows one to identify the Ginzburg-Landau portions of $I_c(T)$ (solid lines) close to T_c. A gradual expansion of the Ginzburg-Landau $(T_c - T)^{3/2}$ tail to low temperatures can be seen upon reduction of T_c.

43

temperature shows a linear dependence (GL-like temperature dependence) approximately between T_c and 82 K. The GL-like temperature dependence extends down to about 68 K for films 5 and 7 and down to about 62 K for film 2 ($T_c \approx 82K$).

According to Darhmaoui and Jung [2, 4] by plotting $I_c^{2/3}(T)$ versus temperature, it is possible to separate a GL-like dependence of $I_c(T)$ at low temperature from an Ambegaokar-Baratoff (AB)-like behavior. Theoretical fits to the experimental data of Fig.2.3(b) were performed assuming a superposition of these two dependencies of the critical current on temperature [see Figures 2.4 and 2.5]. An AB-like dependence was calculated from Clem's model of an Ambegaokar-Baratoff to a Ginzburg-Landau crossover in $J_c(T)$ of granular superconductors [9] using the coupling constant ϵ_0 between the grains as a fitting parameter.

$I_c(T)$ of oxygen deficient YBCO thin films of T_c as low as 50K is characterized by a pure GL-like $(T_c - T)^{3/2}$ dependence [2, 4]. Optimally doped YBCO thin films exhibit an AB-like $I_c(T)$ [2, 4]. Therefore, the superposition of a GL-like and an AB-like dependence in $I_c(T)$ indicate that YBCO films could be modelled as a mixture of two phases of low and high oxygen deficiency. At low temperatures, the AB-like part of $I_c(T)$ is weakly temperature dependent, and $I_c(T)$ is dominated by the GL-like dependence. Theoretical fits to the experimental data were performed using superposition of the GL-like and the AB-like dependencies [see Figures 2.4 and 2.5], with the ratio of the AB component of $I_c(T)$ to the total critical current $I_c(T)$ at 10 K taken as a fitting parameter [10]. This ratio (fraction) is sample-dependent. For our YBCO films, the fraction changes between 0.48 and 0.68 and is T_c-independent. Table 2.3 shows some of the critical current-related parameters: T_c obtained from the measurement of J_c (taken as the temperature at which the field signal drops below the sensitivity of the Hall probe: $\pm 2mG$), T_{c0} obtained from the resistivity measurement, critical current densities at 10K and 77K, and the fraction (ratio) of the AB-component in $I_c(T)$ to the total value of I_c at 10K.

44
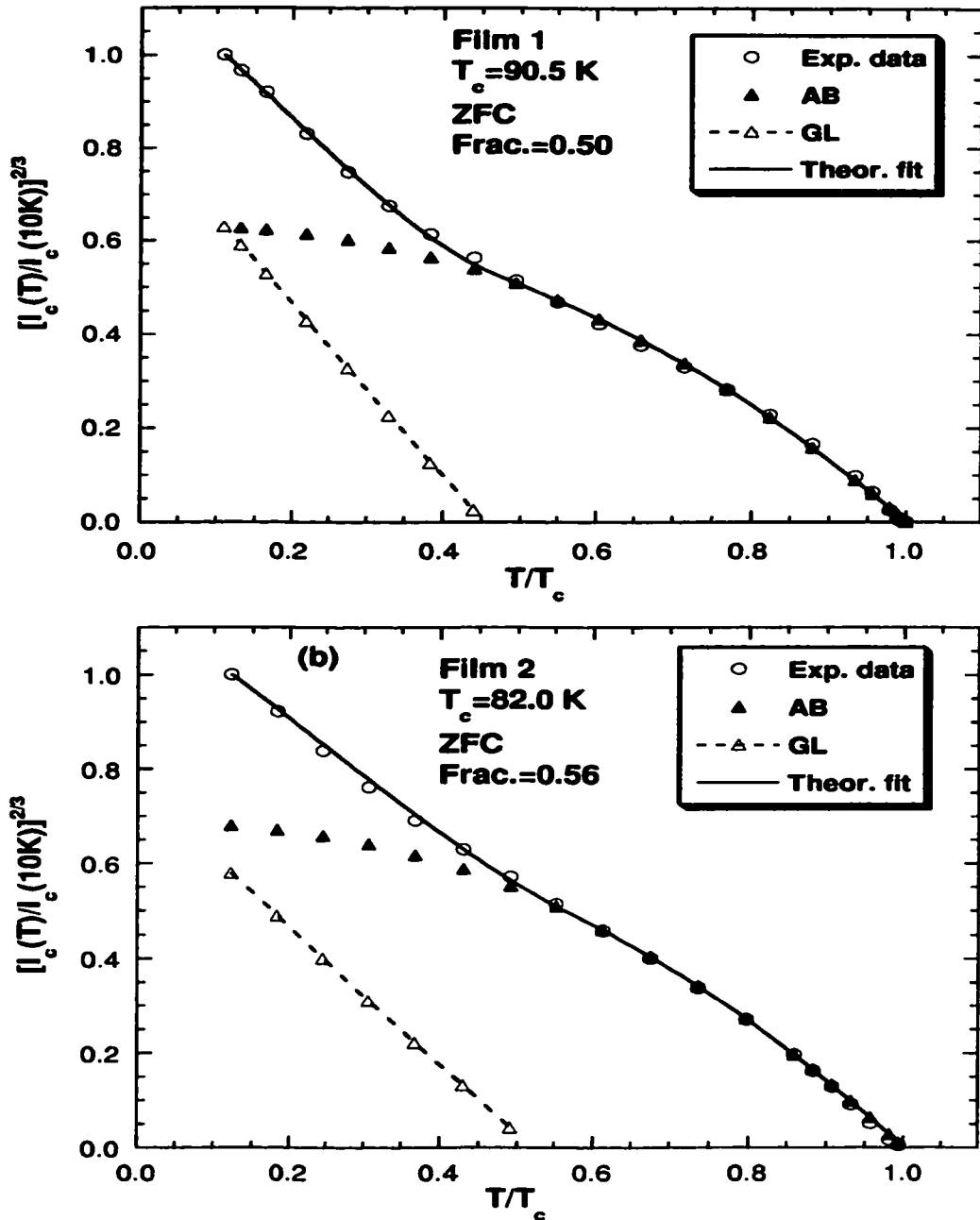
Figure 2.4: The dependence of the critical current on the normalized temperature (plotted as $[I_c(T)/I_c(10K)]^{2/3}$ versus T/T_c for two selected YBCO disk-shaped films 1 (a) and 2 (b). The open circles mark the experimental data for $I_c(T)$. The solid lines represent theoretical fits to the experimental data: they are the superposition of the GL-like dependence (open triangles) at low temperature and the AB-like dependence [Clem's model (solid triangles) with the coupling constant $\epsilon_0 = 100$]. Frac. represents the fraction (ratio) of the AB-component of $I_c(T)$ to the total critical current at 10K.

45
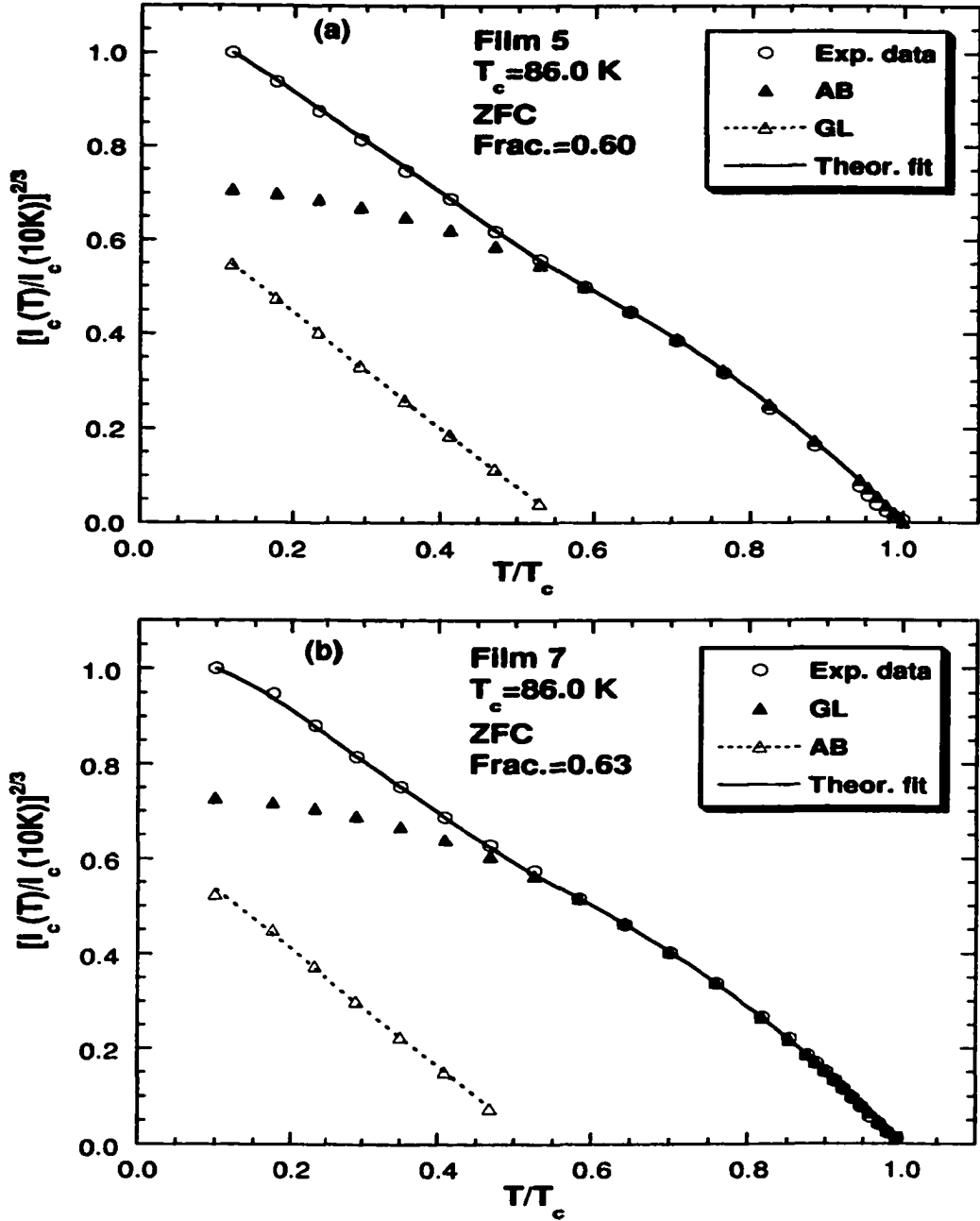
Figure 2.5: The dependence of the critical current on the normalized temperature (plotted as $[I_c(T)/I_c(10K)]^{2/3}$ versus T/T_c for two selected YBCO disk-shaped films 5 (a) and 7 (b) with a larger fraction (Frac.) of the AB-like $I_c(T)$ to the total $I_c(T)$ at 10 K. The open circles mark the experimental data for $I_c(T)$. The solid lines represent theoretical fits to the experimental data: they are the superposition of the GL-like dependence (open triangles) at low temperature and the AB-like dependence [Clem's model (solid triangles) with the coupling constant $\epsilon_0 = 100$].

46

Table 2.3: Critical current-related parameters: $T_c(J_c = 0)$ is the transition temperature obtained from the measurement of $J_c(T)$ (taken as the temperature at which the field signal drops below the sensitivity of the Hall probe: $\pm 2mG$), T_{c0} is the corresponding transition temperature obtained from the resistivity measurement (taken as the temperature at which the nanovoltmeter signal drops below $10 - 15nV$), $J_c(10K)$ and $J_c(77K)$ are the critical current densities at 10 K and 77 K, respectively, and the Frac. is the ratio of the AB-component in $I_c(T)$ to the total value of I_c at 10K. The data is sorted according to T_{c0}

Film No.	T_{c0} (K)	$T_c(J_c = 0)$ (K)	$J_c(10K)$ $(A/cm^2) \times 10^6$	$J_c(77K)$ $(A/cm^2) \times 10^5$	Frac.
1	90.0	90.5	24.0	22.1	0.50
11	89.9	90.5	19.1	17.4	0.54
3	89.5	90.5	24.1	23.6	0.52
9	86.2	86	30.5	18.9	0.51
10	85.8	87.5	14.3	10.5	0.48
12	85.4	86	19.6	11.1	0.52
13	85.4	86	N/A	25.2	N/A
7	85.0	86	1.6	1.0	0.63
6	84.6	85	2.0	1.1	0.62
8	84.6	85	9.2	3.9	0.68
5	84.5	86	22.0	10.8	0.60
4	81.7	82	5.2	0.8	0.66
2	80.3	82	10.5	2.0	0.56
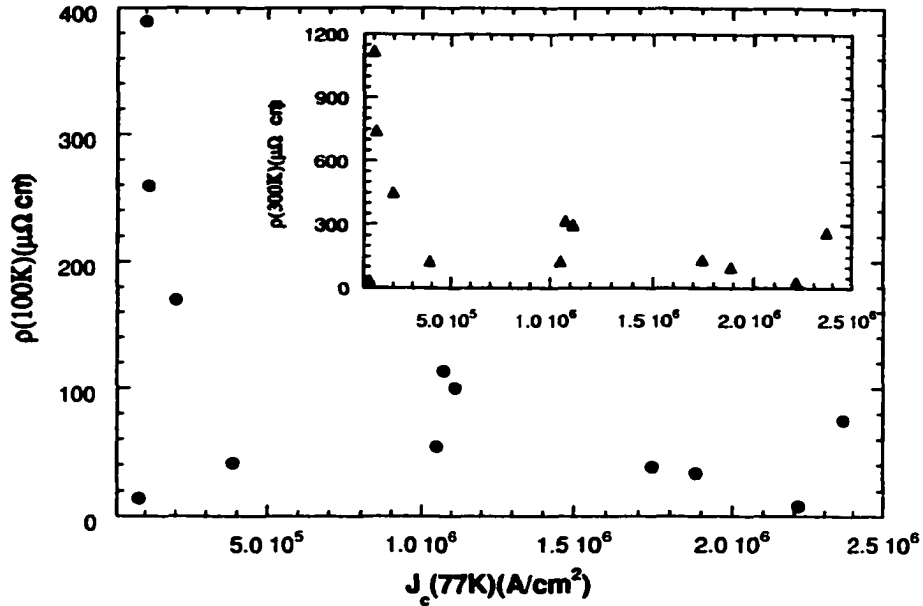
Figure 2.6: The resistivity measured at 100K $\rho(100K)$ for thirteen YBCO films plotted as a function of the magnitude of the critical current density measured at 77K $J_c(77K)$. The inset shows the results for $\rho(300K)$ plotted as a function of $J_c(77K)$.

2.5.3 Relation between J_c and the normal state properties

We have investigated a possible relationship between the magnitude of J_c at different temperatures and the normal state properties obtained from resistivity measurements for YBCO films. No correlation has been found between the magnitude of $J_c(T)$ and T_c. However, in general the normal state resistivity decreases with an increasing critical current density. Fig.2.6 shows a plot of the resistivity at 100 K as a function of J_c at 77 K for all thirteen YBCO films studied. For films with small J_c (below $5 \times 10^5 A/cm^2$) the resistivity at 100 K and at 300 K (see the inset of Fig.2.6) decreases very fast with an increasing J_c, and appears to saturate for films with higher J_c.

Another J_c related quantity that shows an unusual behavior as a function of the normal state resistivity is the fraction (ratio) of the magnitude of the AB-component of $J_c(T)$ to the total magnitude of J_c measured at 10 K. Fig.2.7 presents a plot of the resistivity at 100 K and 300 K as a function of the fraction for all thirteen YBCO films. The resistivity at 100 K and 300 K follows a variable amplitude sinusoidal-
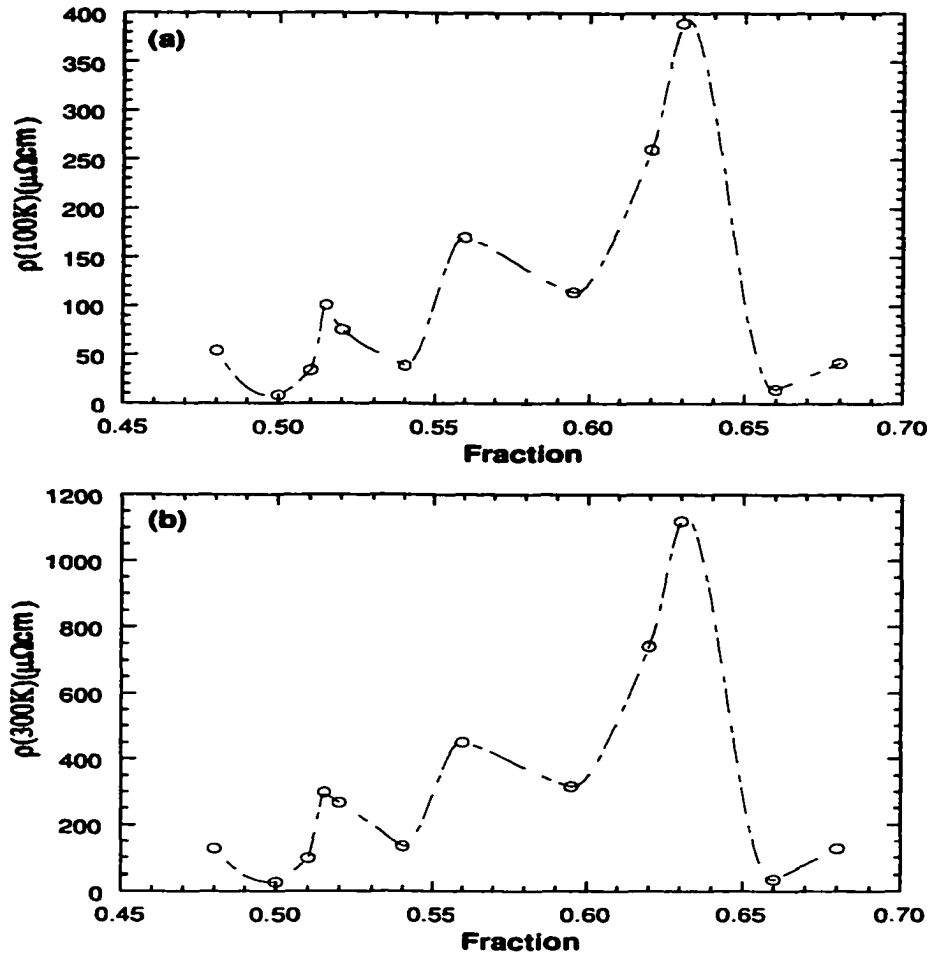
Figure 2.7: (a) The resistivity measured at 100 K $\rho(100K)$ for thirteen YBCO films plotted as a function of the fraction. (b) $\rho(300K)$ plotted as a function of the fraction. The fraction is the ratio of the AB-component in $I_c(T)$ to the total value of I_c at 10K. The dashed line is a guide for the eye.

like behavior with an increasing fraction, where it shows many cusps with different amplitudes. The fraction (ratio) is not related to the magnitude of J_c at 10 K or 77 K. At this time we are unable to explain the unusual behavior of ρ versus fraction. One could speculate that the cusps of ρ versus fraction are related to the percolation thresholds as the amount of AB-like optimally doped phase increases relative to the underdoped GL-like one in YBCO.

49

Bibliography

[1] Y. Iye, T. Terashima and Y. Bando, *Physica C* **184**, 362 (1991).

[2] H. Darhmaoui, *Critical currents and intrinsic properties in YBCO thin films*, Ph.D. thesis, University of Alberta 1997.

[3] H. Darhmaoui, J. Jung, J. Talvacchio, M. A.-K. Mohamed, L. Friedrich, *Phys. Rev. B* **53**, 12330 (1996).

[4] H. Darhmaoui, J. Jung, Phys. Rev. B **53**, 14621 (1996).

[5] T. R. Lamberger, *Physical properties of high temperature superconductors* **III**, ed. by D. M. Ginsberg, World Scientific, Singapore 1992, P. 471.

[6] E.K. Hollmann, S.V. Razumov, A.V. Tumarkin, *Physica C* **338**, 246 (2000).

[7] E.K. Hollmann, D.A. Plotkin , S.V. Razumov, A.V. Tumarkin , *Physica C* **296**, 37 (1998).

[8] H. Darhmaoui, J. Jung, *Phys. Rev. B* **57**, 8009 (1998).

[9] J. R. Clem, B. Bumble, S. I. Raider, W. J. Gallagher, and Y. C. Shih , *Phys. Rev. B* **35**, 6637 (1987).

[10] J. Jung, H. Yan, H. Darhmaoui, M. Abdelhadi, B. Boyce, T. Lemberger, *Supercond. Sci. Technol.* **12**, 1086 (1999).

Chapter 3

Upward Deviation from T-Linear Dependence in the Normal State Resistivity of YBCO Thin Films

3.1 Introduction

One of the most striking features of the high-T_c superconductors (HTCS) is the extraordinary transport properties of the normal state because they are inconsistent with the conventional electron-phonon scattering mechanism [1]. These properties have been extensively investigated, since the excitation which interacts with carriers in the normal state might play an important role in understanding the mechanism of superconductivity [2]. Many normal-state properties, like resistivity and Hall coefficient, have been found to behave anomalously with respect to a simple metallic or Fermi liquid behavior. This possibly indicates the existence of quite unusual elementary excitations which are typical for strongly correlated electron systems [3]. Therefore this non-Fermi liquid character has been emphasized as a key to understanding the physics of the HTSC [4].

Among the normal-state properties investigated experimentally, resistivity measurements displayed many interesting features. At the hole concentration for optimum

51

T_c, the in-plane resistivity $\rho_{ab}(T)$ is linear in temperature over a wide temperature range that extends from above T_c onset to nearly 1000 K [5, 6]. Martin et al. [6] reported a T-linear resistivity down to 10 K in $Bi_2Sr_2CuO_6$. For underdoped cuprates, the in-plane resistivity $\rho_{ab}(T)$ exhibits a well-known downturn from the T-linear relation at a temperature $T^* \gg T_c$ which is normally considered as a signature of spin gap opening [7, 8]. For YBCO, it is well established by now that the reduction of the oxygen content (x) leads to a decrease in T_c and a corresponding marked increase in the absolute resistivity for single crystals and thin films. However, reducing x below its optimum doping value (x=6.95) produces a clear change in the temperature dependence of $\rho_{ab}(T)$. The temperature range over which $\rho_{ab}(T)$ is linear systematically shifts to higher temperature and becomes narrower, and a downward bending develops at lower temperatures, eventually followed by an upward bending which becomes more pronounced as x decreases [3]. For $x \leq 6.3$, the YBCO material becomes non-superconducting and only an upward curvature can be observed [3].

Recently, some unusual features in the normal state resistivity have been reported by a few groups. Nakamura and Uchida [9] have reported a resistivity jump from the high temperature linear behavior both in $\rho_{ab}(T)$ and $\rho_c(T)$ at $T > T_c$ in Nd doped $La_{2-x}Sr_xCuO_4$. They attributed this jump to a structural phase transition together with stripe correlations [9, 10]. More recently Chen et al. [7] observed an upward resistivity deviation from the T-linear dependence in Bi-2223 whiskers at a temperature $T^* \sim 250K$. The authors explained the resistivity anomalies using the scenario of the structural transformation and charge ordering in the stripe phase within the CuO_2 planes.

In this Chapter, we report similar upward deviations in the normal state resistivity of YBCO thin films of various T_c, critical current density J_c, thickness and preparation techniques. For all thirteen films studied except one, $\rho(T)$ measurements showed an upward deviation from the high temperature T-linear behavior below a temperature $T^* \sim 265\,K$ for optimally doped films ($T_c \sim 90\,K$) and below $T^* \sim 210 - 240K$ for underdoped ones ($T_c \sim 80 - 86.5\,K$). While $\rho(T)$ continues to decrease with a

decreasing T as usual, the upward deviation continues to increase with a decreasing temperature down to another characteristic temperature T_1 close to T_c onset. Below T_1 the upward deviation seizes and $\rho(T)$ decreases rapidly to zero. For one film $(T_c \sim 85.8\,K)$, $\rho(T)$ exhibits a downturn below $T^* \sim 237K$ similar to that observed usually in underdoped single crystals and films. For this film, the y-intercept, at T=0 K, of the line fitted to the high temperature data has a *large positive* value compared to a *large negative* values for the films that showed a large upward deviation. We found that in general the "excess resistivity" caused by the upward deviation, increases with an increasing oxygen content for YBCO films.

3.2 Experimental results

Temperature dependence of resistivity $\rho(T)$ has been measured in a zero magnetic field over a temperature range between $T_{c_0}(\rho = 0, \mathbf{B} = 0)$ and 300 K for thirteen YBCO thin films of various T_c, J_c, thickness and preparation techniques both optimally doped and underdoped. The zero resistance transition temperature $T_{c_0}(\rho = 0, \mathbf{B} = 0)$, mid-point transition temperature T_{cm} (taken as the temperature at which $d\rho/dT$ is maximum), superconducting transition width ΔT_c, resistivity at 100 K $\rho(100)$ and at 300 K $\rho(300)$, and the ratio of $\rho(300)/\rho(100)$ for all films are listed in Table 3.1.

Fig.3.1 shows the temperature dependence of the in-plane resistivity $\rho(T)$ in a zero magnetic field between T_{c_0} and 300 K for two selected YBCO films 3 (close to an optimum doping) and 4 (an underdoped film). The transition width is about 1.2 K for film 3 and 3.7 K for film 4 (see Table 3.1). Both films did not exhibit any foot or a step in $\rho(T)$ at the zero resistance temperature T_{c0}, which usually exists in samples mixed with other phases of lower transition temperature. For both films, $\rho(T)$ at high temperatures follows the usual linear behavior. The linear relation is indicated by the solid line in Fig.3.1. The fit to $\rho(T)$ data in the high temperature region was performed using a linear function with two parameters of the form: $\rho(T) = a + bT$. The solid straight line for film 3 has a *large negative* y-intercept, but a *small positive*

one for film 4 (see Table 3.2). An unusual feature in $\rho(T)$ can be observed below a certain temperature T^* which is about 265 K and 220 K for films 3 and 4, respectively. Below T^*, $\rho(T)$ starts to deviate upward from the linear relation represented by the solid line (in Fig.3.1) with a decreasing temperature, rather than following the well-known downturn observed in some underdoped HTSC.

This upward deviation increases as T decreases, eventually reaches a maximum at another characteristic temperature T_1 which is about 100 K for both films (see Table 3.2). In order to see the upward deviation more clearly the "excess resistivity", defined as: $\Delta\rho(T) = \rho(T) - (a + bT)$, which is the difference between $\rho(T)$ data and the linear relation fitted to the high temperature data, has been plotted as a function of temperature. Although the choice of the fitting range for the linear relation $\rho(T) = a + bT$ could slightly affect the deviation temperature, the two major features; the deviation of ρ from T-linear dependence at T^* and the maximum at a temperature T_1 are clearly identifiable regardless of this choice. The range over which $\rho(T)$ shows an upward deviation from the linear dependence is wide ($> 100K$) for all films studied. This deviation has been observed in almost all of the YBCO films studied which implies that this behavior could be related to the intrinsic properties of YBCO thin films. The fractional deviation defined as: $\Delta\rho(T_1)/\rho(T_1) = [\rho(T_1) - (a + bT_1)]/\rho(T_1)$ is about 29% for film 3 and about 10% for film 4 (see Table 3.2).

Fig.3.2 shows $\rho(T)$ and $\Delta\rho(T)$ for two slightly underdoped films 7 and 9 with T_c of 85.0 K and 86.2 K respectively. The transition width is about 0.9 K for film 9 and about 2.0 K for film 7 . Both films did not exhibit any foot or a step in $\rho(T)$ at the zero resistance temperature T_{c0}. For both films, the linear behavior of $\rho(T)$ extends over a wider range of temperatures than that for film 3 [see Fig.3.1(a)]. The upward deviation from the linear behavior is much smaller than that displayed in Fig.3.1 for films 3 and 4. The fractional deviation $\Delta\rho(T_1)/\rho(T_1)$ is about 5% for film 7 and only 3% for film 9 (see Table 3.2). The solid line fitted to the high temperature data for both films has a very small (close to zero) y-intercept (see Table 3.2).

Fig.3.3 displays $\rho(T)$ for the underdoped film 10 with $T_c = 85.8K$ and a transition

54
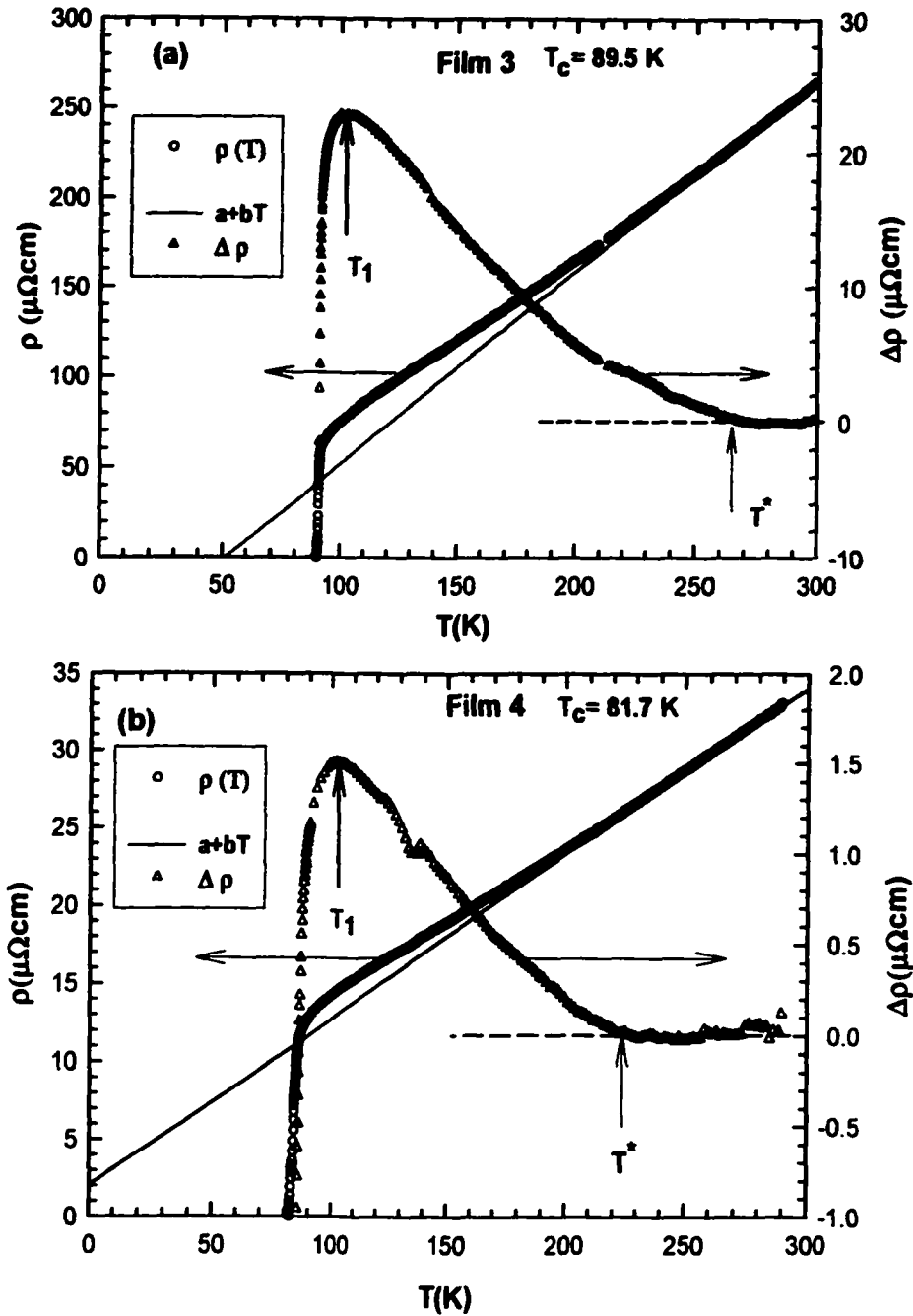
Figure 3.1: Temperature dependence of the in-plane resistivity $\rho(T)$ measured in a zero magnetic field between T_{c0} and 300 K for YBCO films 3 (close to optimum doping)(a) and 4 (underdoped) (b). $\Delta\rho = \rho(T) - (a + bT)$ (open triangles) is the upward deviation from the solid line fitted to the high temperature data between 265 and 300 K for film 3 and between 225 and 300 K for film 4. T_1 is the temperature at which $\Delta\rho$ reaches its maximum value. Note the difference in $\Delta\rho$, y-intercept $(\rho(0))$ and T^* between these films.
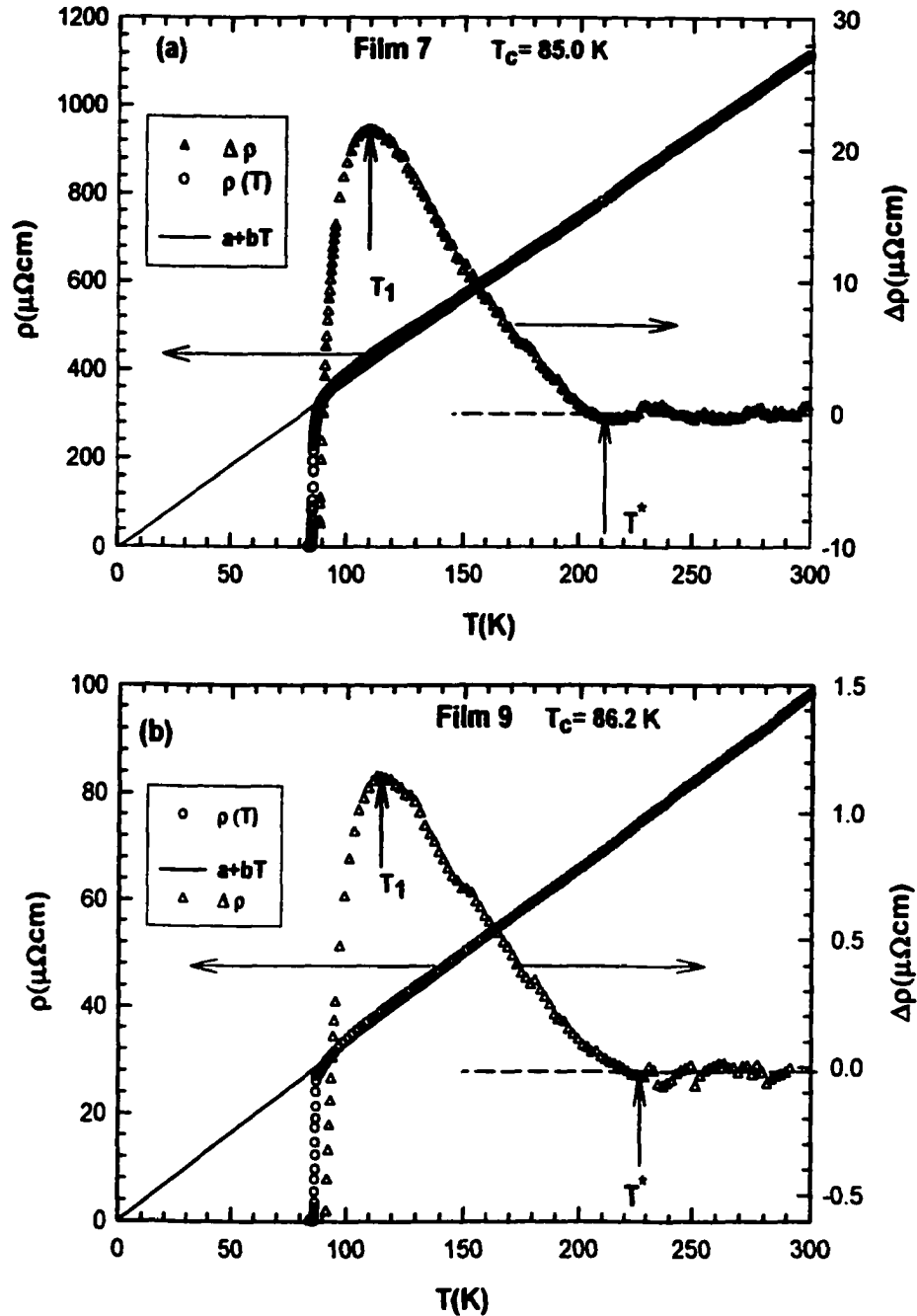
Figure 3.2: Temperature dependence of the in-plane resistivity $\rho(T)$ measured in a zero magnetic field between T_{c0} and 300 K for two underdoped YBCO films 7 (a) and 9 (b). $\Delta\rho = \rho(T) - (a + bT)$ (open triangles) is the upward deviation from the solid line fitted to the high temperature data between 210 and 300 K for film 7 and between 225 and 300 K for film 9. T_1 is the temperature at which $\Delta\rho$ reaches its maximum value. Note that both films show a small fractional upward deviation $\Delta\rho/\rho(T_1)$ and an almost zero y-intercept $(\rho(0))$ in comparison to those of Fig.3.1 which show a large fractional $\Delta\rho/\rho(T_1)$ associated with a large y-intercept (see Table 3.2).

56

Table 3.1: Normal and superconducting properties of YBCO films. ρ is the in-plane resistivity, T_{c0} is the transition temperature at $\rho = 0$ and B=0, T_{cm} is the mid-point transition temperature taken as the temperature at which $d\rho/dT$ is maximum, ΔT_c is the transition width and t is the thickness of the film. Films are sorted in an order of decreasing T_{c0}.

Film No.	substrate type	t (nm)	T_{c0} (K)	T_{cm} (K)	ΔT_c (K)	$\rho(100K)$ ($\mu\Omega cm$)	$\rho(300K)$ ($\mu\Omega cm$)	$\frac{\rho(300K)}{\rho(100K)}$
1	$SrTiO_3$	210	90.0	90.5	1.0	8.03	27.32	3.40
11	$LaAlO_3$	130	89.9	90.6	1.0	38.37	133.71	3.49
3	$SrTiO_3$	230	89.5	90.3	1.2	74.89	265.82	3.55
9	Sapphire/CeO_2	110	86.2	86.8	0.9	33.48	98.09	2.93
10	$LaAlO_3$	340	85.8	86.6	1.2	54.10	126.85	2.34
12	Sapphire/CeO_2	190	85.4	87.05	1.6	100.20	297.21	2.97
13	$SrTiO_3$	420	85.4	86.1	1.2	67.57	208.24	3.08
7	Al_2O_3/CeO_2	610	85.0	85.92	2.0	389.41	1119.23	2.87
8	$LaAlO_3$	100	84.6	86.1	3.0	41.22	127.15	3.08
6	Al_2O_3/CeO_2	330	84.6	86.2	2.5	259.39	741.16	2.86
5	$SrTiO_3$	210	84.5	86.4	1.9	113.42	315.39	3.78
4	Sapphire/CeO_2	140	81.7	82.6	3.7	14.21	34.16	2.40
2	$LaAlO_3$	310	80.3	81.0	2.3	169.69	450.14	2.65

width of about 1.2 K. Deviation from the T-linear dependence is very small especially at high temperatures. In order to see this deviation clearly we have plotted the excess resistivity $\Delta\rho(T) = \rho(T) - (a + bT)$ as a function of temperature on the same graph. This film did not show any noticeable upward deviation like other films but shows a downturn deviation from the T-linear relation fitted to the high temperature data. $\rho(T)$ starts to deviate from the linear relation (solid line in Fig.3.3) at $T^* = 230K$. Below T^*, $\Delta\rho(T)$ is negative (indicating a downward deviation) and decreases faster as T approaches the onset T_c. Note that the solid line (fitted to the high temperature

Film 10   T$_c$ = 85.8 K

o ρ (T)

— a+bT

Δ Δρ

ρ(μΩcm)

Δρ(μΩcm)

T*

T (K)
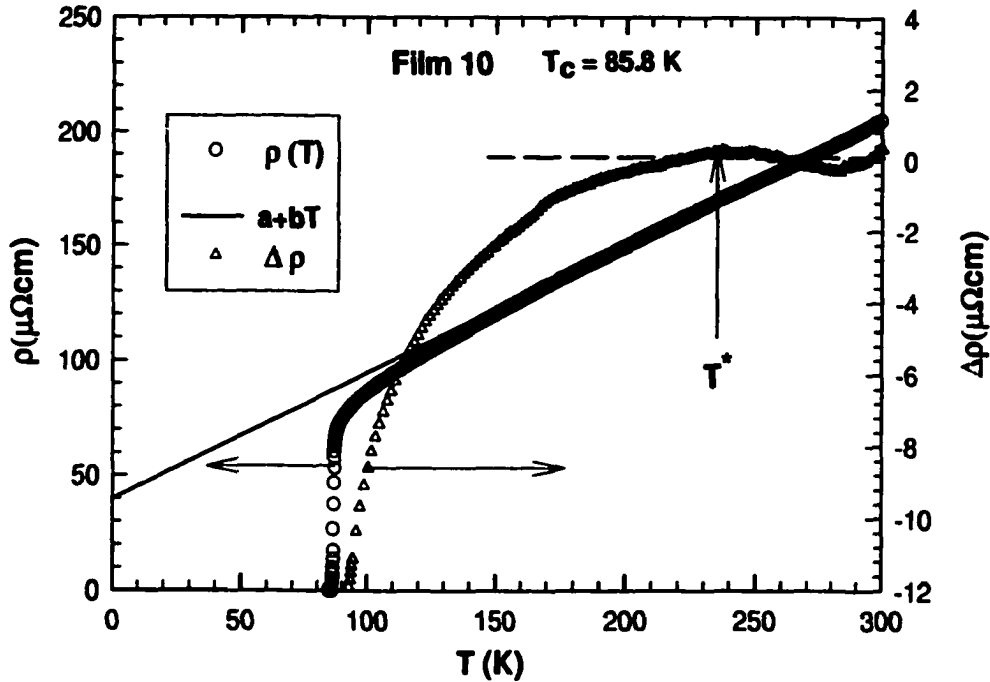
Figure 3.3:   Temperature dependence of the in-plane resistivity $\rho(T)$ measured in a zero magnetic field between T_{c0} and 300 K for the underdoped YBCO film 10. $\Delta\rho = \rho(T) - (a + bT)$ (open triangles) is the downward deviation from the solid line fitted to the high temperature data between 230 and 300 K. Note the *downward deviation* at $T^* = 230K$ and the *large positive* y-intercept $(\rho(0))$ of the solid line. The measurement of $\rho(T)$ performed two months earlier showed a very small upward deviation $\Delta\rho/\rho(T_1) \sim 1.3\%$ which has disappeared in the present measurement.

data) for this film shows a *large positive* y-intercept. In fact this film exhibits the largest positive y-intercept among all films investigated and it is the only film that displayed a downturn deviation too.

Deviation of $\rho(T)$ data from the T-linear dependence observed at high temperatures ($T^* > 200\,K$), has been investigated for all thirteen films. The deviation-related characteristic parameters: T^*, T_1, maximum fractional deviation at T_1: $\Delta\rho(T_1)/\rho(T_1)$ together with the parameters a and b for the linear function (fitted to the high temperature data) are listed for all samples in Table 3.2.

58

Table 3.2: Upward deviation-related characteristic parameters of YBCO films, T_{c0} is the transition temperature at $\rho = 0$ and B=0, T^* and T_1 are the temperatures at which the deviation from the linear dependence starts and becomes maximum, respectively. $\Delta\rho(T_1)/\rho(T_1)$ is the maximum fractional deviation calculated at T_1 and a and b are the y-intercept and the slope of the linear function $\rho(T) = a + bT$ fitted to the high temperature data. Films are sorted in an order of decreasing T_{c0}.

Film No.	T_{c0} (K)	T^* (K)	T_1 (K)	$\Delta\rho(T_1)/\rho(T_1)$ %	a $(\mu\Omega cm)$	b $(\mu\Omega cm/K)$
1	90.0	266	115	17	-5.04	0.11
11	89.9	265	104	31	-27.70	0.54
3	89.5	266	102	29	-53.25	1.07
9	86.2	225	114	3	-0.08	0.33
10	85.8	237	N/A	0	39.39	0.55
12	85.4	230	106	8	-8.19	1.02
13	85.4	240	97	18	-19.93	0.76
7	85.0	220	110	5	-4.74	3.75
8	84.6	223	103	10	-8.25	0.45
6	84.6	220	110	11	-7.81	2.50
5	84.5	236	112	4	3.79	1.04
4	81.7	221	102	10	2.04	0.11
2	80.3	210	106	3	22.72	1.43

3.3 Discussion

3.3.1 T_c-dependence of the upward deviation in $\rho(T)$

The temperature T^* at which $\rho(T)$ deviates from the T-linear dependence is T_c and sample dependent. Fig.3.4(a) shows temperatures T^* at which the deviation starts and T_1 at which this deviation has a maximum as a function of T_c for all films that showed upward deviation. The upward deviation from T-linear dependence occurs at high temperatures ($T^* \sim 265K$) for films close to an optimum doping, and at lower temperatures ($T^* \sim 210 - 240K$) for underdoped films. In general T^* increases with an increasing T_c for YBCO films. This is in contrast to the observation that the temperature T^* at which the downward deviation of $\rho(T)$ from the T-linear dependence occurs, has been shown to decrease with an increasing oxygen concentration and to approach T_c for optimally doped YBCO crystals ($T_c \sim 90$ K) [2].

This downward deviation was found to coincide with the development of a gap in the spin excitation [2] (known as pseudo-gap opening seen in the neutron and NMR studies [11, 12]), since the temperature at which the spin gap becomes apparent decreases with an increasing oxygen concentration and becomes indistinguishable from the superconducting gap in optimally doped YBCO.

The temperature T_1 at which the upward deviation reaches a maximum is almost sample independent [see Fig.3.4(a)]. The plot in Fig.3.4(a) of T_1 versus T_c for different films does not reveal any systematic variation of T_1 with T_c. It is almost constant with small fluctuations about an average value of 107 K.

Ito el al. [2] studied the deviation from the T-linear behavior in the in-plane resistivity of YBCO single crystals with various oxygen concentration (x). They observed a perfect linear behavior for $T_c = 90K$ crystals ($x = 6.90$ very close to the optimum doping $x = 6.95$). This is in contrast to our films where we observed the largest upward deviation from the T-linear for films with $T_c \sim 90K$. Although $\rho(T)$ for slightly oxygen deficient YBCO single crystals shows linear dependence over a wide range of temperatures and deviates downward from T-linear at low T^*, in

60
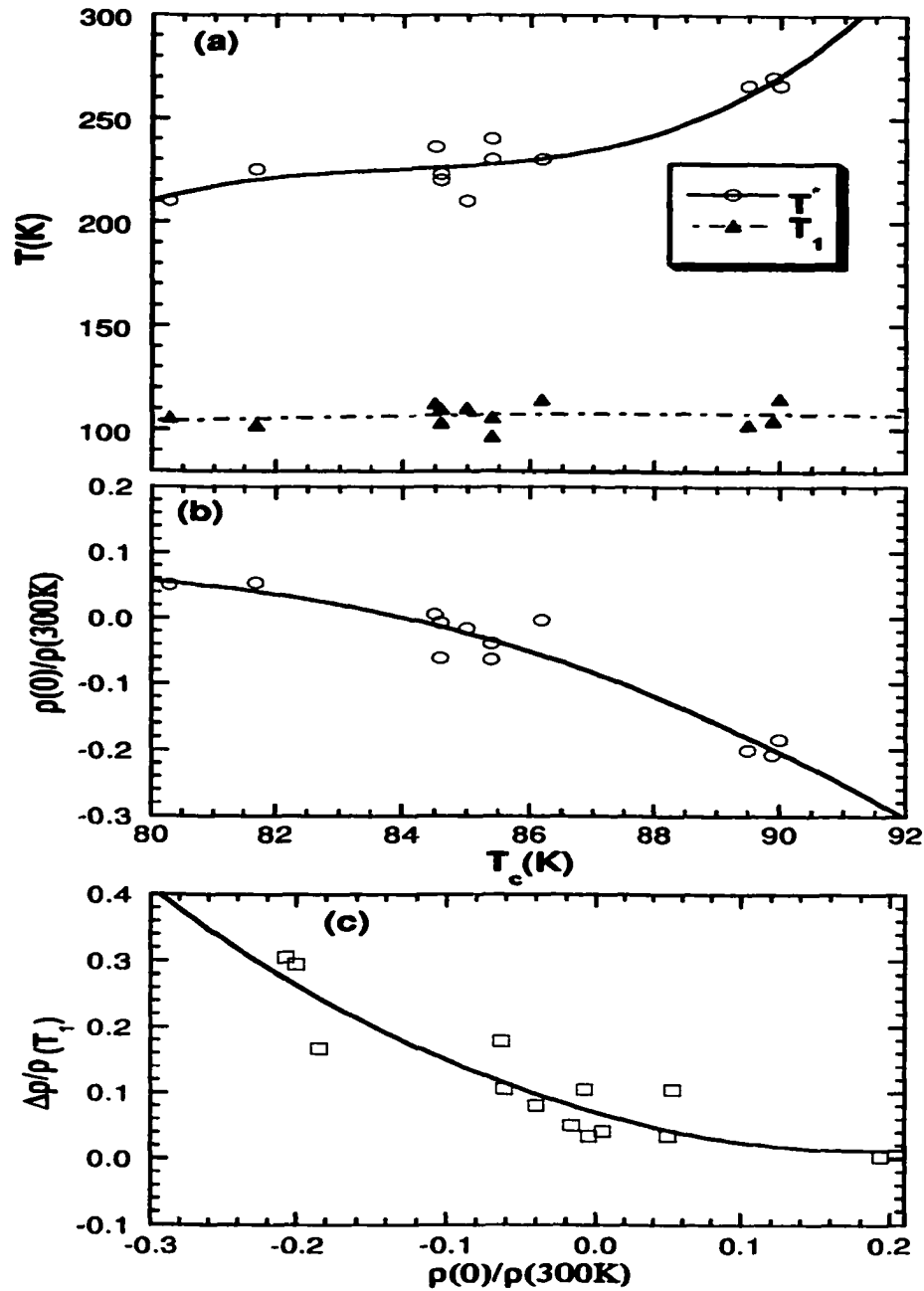
Figure 3.4: (a) Temperatures T^* (at which the upward deviation of $\rho(T)$ starts) and T_1 (at which the deviation has a maximum) plotted as a function of T_c for all films that exhibit an upward deviation. Note that T_1 is almost T_c-independent, but T^* increases with an increasing T_c for YBCO films. (b) Normalized residual resistivity: $\rho(0)/\rho(300)$ plotted as a function of T_c for all YBCO films with an upward deviation. For each film, $\rho(0)$ was taken as the y-intercept of the line fitted to the high temperature data between T^* and 300 K. (c) Fractional deviation from the linear dependence fitted to the high temperature data: $\Delta\rho(T_1)/\rho(T_1)$ plotted as a function of the corresponding y-intercept. The solid lines are guides for the eye.

61

highly oxygen deficient crystals it starts to deviate rapidly downward from the T-linear dependence at higher T^*. The deviation temperature T^* is 180 K and 220 K for $x = 6.85$ and 6.78, respectively [2].

Whyts et. al. [3] investigated systematically the normal state resistivity in a series of oxygen-deficient c-axis oriented YBCO thin films. An *upward* deviation of $\rho(T)$ from the T-linear dependence near $T^* \sim 265K$ was observed in an underdoped film with $x = 6.85$ while for films with $x < 6.85$, $\rho(T)$ displayed the usual *downward* deviation. Similar upward deviation has also been observed in other HTSC's. Chen et al. [7] have seen an upward deviation of $\rho(T)$ from the linear dependence at $T^* \sim 250K$ in Bi-2223 ($T_c \sim 110K$) and Bi-2212 ($T_c \sim 87K$) whiskers. The upward deviation increases with a decreasing temperature over a range of about 50 K. The upward deviation observed in Bi-2212 whiskers is similar to the one observed in our YBCO films, where in both compounds the excess resistivity $\Delta\rho$ above T^* keeps increasing smoothly until it reaches a maximum before going down rapidly below T_1. However, for Bi-2212, the deviation $\Delta\rho$ extends over a narrow temperature range of about 30 K, while for YBCO films it extends over a much wider range of temperature $[(T^* - T_1) \sim 100 - 150K]$. Chen et. al [7] attributed this effect to a structural transformation or lattice distortion followed by charge or spin excitations as established by neutron scattering studies.

3.3.2 Relation between the upward deviation in $\rho(T)$ and the y-intercept $\rho(0K)$

The residual resistivity $\rho(0K)$, both its magnitude and sign, is believed to be related to the carrier density in the normal state [4]. To verify this we have studied the relationship between the y-intercept of the linear part of $\rho(T)$ and the corresponding upward deviation (which is related to the oxygen deficiency). For each film, $\rho(0)$ was taken as the y-intercept, at T=0 K, of the line fitted to the high temperature data between T^* and 300 K after extrapolation to T=0 K. Variation of both magnitude and sign of the y-intercept in our YBCO thin films (see Table 3.2) appear to be related to the oxygen deficiency of the films. Films with the largest deviation $\Delta\rho(T_1)/\rho(T_1)$ are characterized in general by a large negative y-intercept (for example films 3 and 11 with y-intercepts of -53 and -28 $\mu\Omega cm$ have a deviation $\Delta\rho(T_1)/\rho(T_1)$ of about 29% and 31%, respectively). On the other hand, films with a small upward deviation $\Delta\rho(T_1)/\rho(T_1) < 5\%$ are characterized by either a very small (approaching zero) negative or positive y-intercept. For example films 5 and 9 have y-intercepts of 3.8 and -0.1 $\mu\Omega cm$ respectively and a deviation $\Delta\rho(T_1)/\rho(T_1)$ of about 4% and 3%, respectively. Fig.3.4(b) shows the normalized residual resistivity $\rho(0)/\rho(300)$ divided by the resistivity at 300 K as a function of T_c for all YBCO films with an upward deviation. In general the normalized residual resistivity $\rho(0)$ decreases with an increasing T_c for different films. Films that are close to an optimum doping $(T_c \sim 90\,K)$ have large negative values of $\rho(0)/\rho(300)$ while underdoped films have either small negative values (very close to zero) or positive values.

It is interesting to investigate the correlation between the y-intercept of the linear high temperature part of $\rho(T)$ and the deviation $\Delta\rho$, and whether they are related to the oxygen concentration. This could enable us to correlate these quantities to the hole concentration as it is known that the hole concentration increases with an increasing oxygen content [4, 7]. Fig.3.4(c) shows the fractional deviation $\Delta\rho(T_1)/\rho(T_1)$ from T-linear dependence plotted as a function of the normalized y-intercept $\rho(0)/\rho(300K)$ for all YBCO films (see Table 3.2). In general $\Delta\rho(T_1)/\rho(T_1)$ decreases with an in-

creasing y-intercept reaching almost zero (no upward deviation) at y-intercept of +40 $\mu\Omega cm$ for film 10 which did not show any upward deviation. $\Delta\rho(T_1)/\rho(T_1)$ reaches a large values up to 30% (for film 3, which is close to an optimum doping with $T_c \sim 90K$), with a negative y-intercept of -53 $\mu\Omega cm$.

3.3.3 Dependence of the upward deviation on the O_2 content

Chen el al. [7] found that annealing of Bi-2223 whiskers in O_2 shifts the y-intercept to negative values while annealing in N_2 (removing oxygen) shifts it up to positive values. In addition, samples that were annealed in O_2 revealed a corresponding increase in the excess resistivity $\Delta\rho$ with decreasing T, while those annealed in N_2 displayed a smaller $\Delta\rho$ that is almost temperature independent. They attributed the increase in $\Delta\rho$ at low temperature to an increase in hole concentration [7]. Our results shown in Fig.3.4(c) and Table 3.2 agree with these findings. One could therefore interpret the upward resistivity deviation from the linear dependence in YBCO thin films in a similar manner. Further support for this view came from the following experiment that we performed on films 4 and 10. For both films the resistivity measurement has been repeated under the same conditions and the same applied current (5 μA) approximately two months after the first measurement (see Table 3.2). Fig.3.5 shows the old and new $\rho(T)$ data together with the corresponding deviation $\Delta\rho$ from the T-linear dependence. There are four main features that can be seen clearly from this graph for both films: (1) the new measurement revealed a drop in T_{c0} by about 1.1 K for film 4 and about 0.7 K for film 10 [see the insets in Fig.3.5]; (2) a significant increase in the resistivity was observed especially for film 10; (3) the y-intercept increased to larger positive values; and (4) the upward deviation $\Delta\rho$ decreased in the new measurement compared to the old one while T^* did not show any significant change [see Fig.3.5 and Table 3.3]. The drop in T_c and the corresponding increase in the resistivity imply that both films have lost oxygen. This loss has resulted in a small decrease in the upward deviation $\Delta\rho$ and a corresponding increase in the y-intercept for both films. Film 10 has shown an interesting feature. While the old measurement

64

Table 3.3: Comparison between the old and new upward-related properties for YBCO films 4 and 10. The Table lists the transition temperature T_{c0}, maximum fractional upward deviation $\Delta\rho(T_1)/\rho(T_1)$ and the y-intercept of the linear function $\rho(T) = a + bT$ fitted to the high temperature data. The new measurements were carried out approximately two months after the first one.

Film No.	T_{c0} old (K)	T_{c0} new (K)	$\frac{\Delta\rho(T_1)}{\rho(T_1)}$ old %	$\frac{\Delta\rho(T_1)}{\rho(T_1)}$ new %	y-intercept old ($\mu\Omega cm$)	y-intercept new old ($\mu\Omega cm$)
4	81.7	80.6	10.3	8.7	2.04	5.26
10	86.5	85.8	1.3	0.3	23.45	39.39

has shown a small upward normalized deviation from the T-linear dependence with a maximum $\Delta\rho(T_1)/\rho(T_1) \sim 1.3\%$, the new one exhibited an almost negligible upward deviation $(\Delta\rho(T_1)/\rho(T_1) \sim 0.3\%$. The new measurement for film 10 has shown instead a downward deviation at a high temperature $T^* = 230K$ compared to 175 K for the old one. This could imply that below a certain oxygen concentration $\rho(T)$ switches its deviation (from the T-linear dependence) from an upward one to a downward one.

We have repeated the measurement of $\rho(T)$ for a second time for all films listed in Table 3.2 after a period between two to three months from the first one. Except for films 4 and 10 discussed above, the drop in T_c for the other films was very small and not associated with any increase in the resistivity as that shown by films 4 and 10. The changes in the upward deviation from the T-linear was also very small for these films. However, we have noticed that a decrease in y-intercept (if any) is always associated by a corresponding increase in the upward deviation.

The discussion above could imply that the increase in the upward deviation is caused by an increased hole concentration as a result of high oxygen content (as in the case of 90 K films). According to Chen et al. [7] this leads to a continuous charge localization due to sufficient holes. On the other hand, an increase in $\Delta\rho$ with a decreasing temperature is small in underdoped films, because the reduced hole concentration may prevent charge segregation from occurring due to insufficient holes [7].
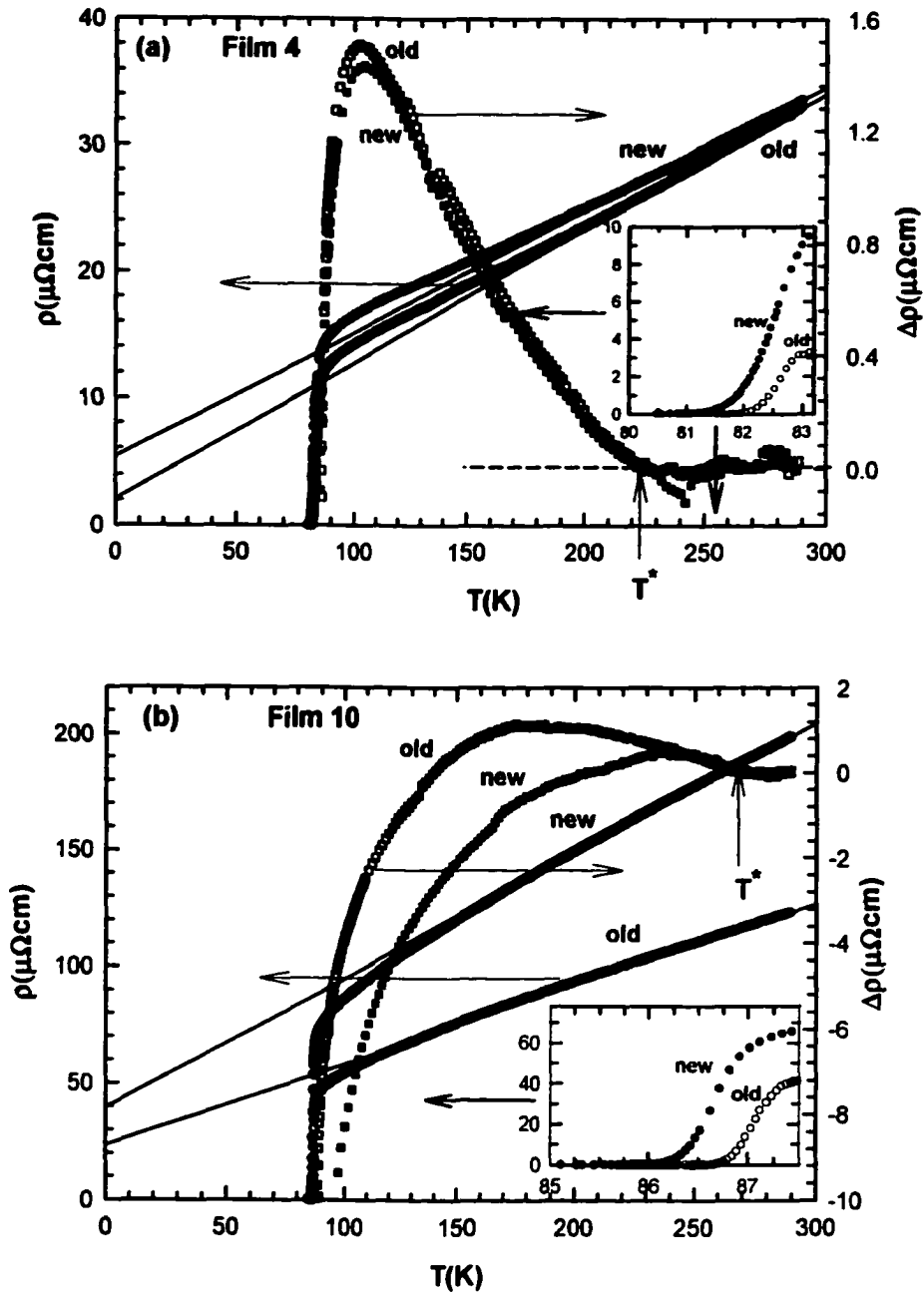
Figure 3.5: Comparison between the old and new measurements of the temperature dependence of the in-plane resistivity $\rho(T)$ measured in a zero magnetic field for two underdoped YBCO films 4 (a) and 10 (b) and the upward deviations, $\Delta\rho = \rho(T) - (a + bT)$, from the solid line fitted to the high temperature data. The insets show the old (open circles) and new (solid circles) resistive transition. Note the drop in T_c, the corresponding increase in resistivity, the increase in the y-intercept and the corresponding decrease in the upward deviation $\Delta\rho$ for the new measurement in comparison to those for the old one.

66

Since the residual resistivity $\rho(0)$ increases with a decreasing oxygen concentration, this could lead to the conclusion that $\rho(0)$ is directly related to the hole concentration [4] [see Figs. 3.4 and 3.5 and Table 3.2]. The upward deviation from the T-linear dependence $\Delta\rho(T)$ in the temperature region $T_1 < T < T^*$ can be fitted to an empirical power law of the form:

$$\Delta\rho(T) \propto \left(1 - \frac{T}{T^*}\right)^m \tag{3.1}$$

The results of fitting of $\Delta\rho(T)$ data using Eq.3.1 are shown in Fig.3.6 for films 3,4,7,9 and 11. Fig.3.6 shows the natural logarithm of $\Delta\rho/\rho(100K)$ as a function of the natural logarithm of $(1 - T/T^*)$. The fitting allowed us to determine the values of the power m from the slope of the lines fitted to the data. These values which range between 1.1 to 1.5 for different YBCO films, are in contrast to Bi-2223 values which range between 1.6 and 2.0 [7].

3.4 Summary and Conclusions

We have investigated the temperature dependence of the normal state resistivity $\rho(T)$ for a temperature range between T_c onset and 300 K in a zero magnetic field for thirteen YBCO films both underdoped and optimally doped of different T_c, thickness, and preparation techniques. For all films studied except one, $\rho(T)$ showed an upward deviation from the high temperature T-linear dependence below a characteristic temperature $T^* \sim 265\,K$ for optimally doped films $(T_c \sim 90\,K)$ and below $T^* \sim 210 - 240K$ for underdoped ones $(T_c \sim 80 - 86.5\,K)$. While $\rho(T)$ continues to decrease with a decreasing T as usual, the upward deviation continues to increase with a decreasing temperature down to another characteristic temperature T_1 close to T_c onset. This upward deviation from the T-linear dependence increases with an increasing oxygen content (optimally doped films shows the largest upward deviation). There is a direct relationship between the upward deviation and the corresponding y-intercept at T=0 K (residual resistivity) of the straight line fitted to the high tem-

67
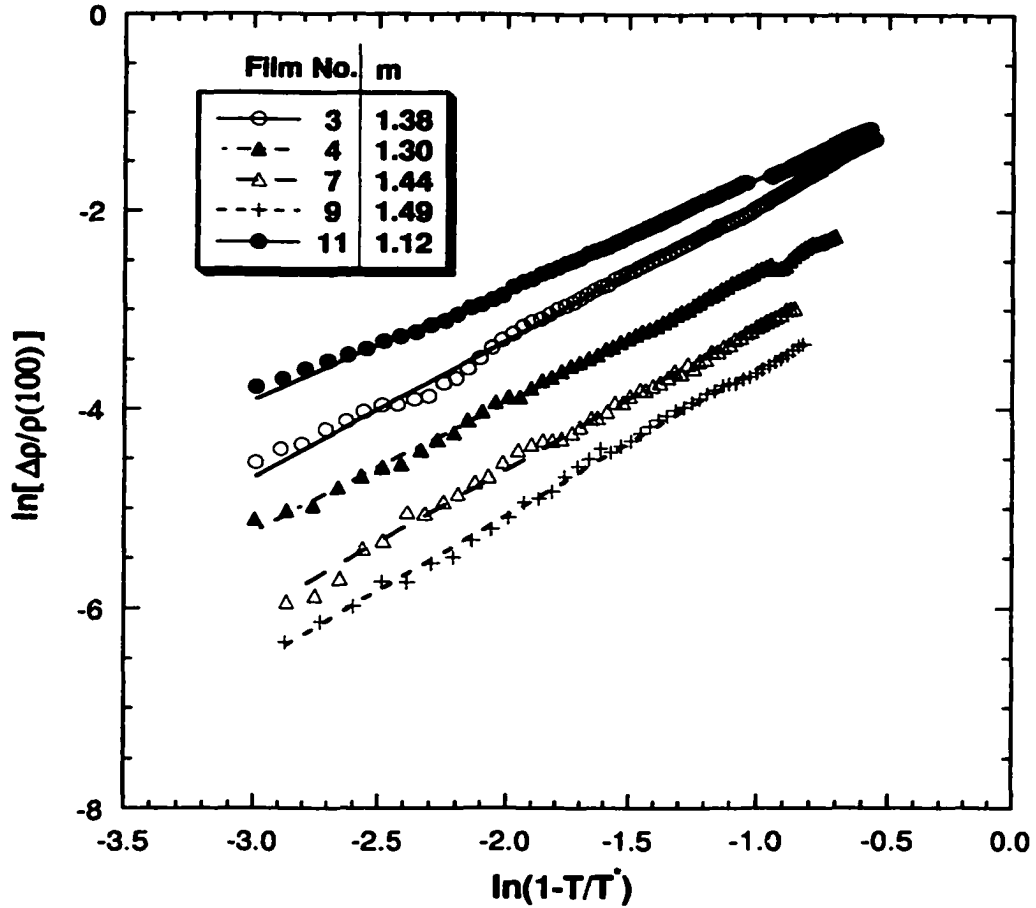
Figure 3.6: Logarithmic plots of $\Delta\rho/\rho(100K)$ versus $(1 - T/T^*)$ for films 3,4,7,9 and 11 for the temperature range between T_1 and T^* . The solid lines represent a fit of the function $\Delta\rho = (1 - T/T^*)^m$ to the experimental data. The slopes of the lines give the exponent m for different films (see the inset).

perature data of $\rho(T)$. Films with a large upward deviation show a *large negative* y-intercept, while those with small deviation show a small (close to zero) positive or negative y-intercept.

The question is why most YBCO thin films, both optimally doped and under-doped, show an upward deviation? This behavior has been observed in other YBCO thin films [13] and other HTSC like BSCCO (both 2212 and 2223), $La_{2-x}Sr_xCuO_4$, and even in YBCO single crystals [14, 15]. However, it has not received enough attention because it has been believed that this behavior is due to sample inhomogeneity. It is strongly believed that high quality optimally doped single crystals show a linear

68

behavior in $\rho(T)$, that extends over a wide range of temperatures between T_c onset and room temperature, and an almost zero residual resistivity (zero y-intercept at T=0 K). Moreover In general, a low resistivity, high T_c, sharp superconducting transition, and a perfect T-linear relation of $\rho(T)$ are associated with high-quality samples. In terms of this criteria, single crystals are considered better quality (defect free) than thin films or polycrystalline samples, and therefore considered as a representative of the intrinsic nature of the material. Recent results reported by Qadri et al. [14] suggest that this may not be true. With the use of high resolution x-ray diffraction, their results revealed a distribution in the c-axis lattice parameters, which was interpreted as an evidence of a distribution in oxygen content. This led them to conclude that structural defects exist even in single crystals with sharp superconducting transitions ($< 0.5K$). Assuming that random oxygen defects affect normal state transport properties in CuO_2 planes through scattering, the mean free path in the ab-planes must be related to the density of these defects (average distance between defects is approximately $a/\sqrt{\delta}$, where a is the lattice parameter and δ is the oxygen deficiency) [15]. The measurement of $\rho(T)$ for single crystals reported by [14, 15] showed an upward deviation from the high temperature T-linear relation similar to the one observed by our thin films. Our earlier investigations of $\rho(T)$ in ceramic polycrystalline YBCO samples (T_c is close to 91 K) revealed that $\rho(T)$ shows either a T-linear dependence between T_c onset and room temperature or an upward deviation. These experimental findings suggest that an upward deviation in $\rho(T)$ from the T-linear dependence may be related to the disorder which results from distribution of oxygen content in the sample.

69

Bibliography

[1] N. P. Ong, *Physical properties of high temperature superconductors* **II**, ed. by D. M. Ginsberg, World Scientific, Singapore 1994, P. 459.

[2] T. Ito, K. Takenaka, and S. Uchida , *Phys. Rev. Lett.* **70**, 3995 (1993).

[3] B. Wuyts, V. V. Moshchalkov, and Y. Bruynseraede, *Phys. Rev. B* **53**, 9418 (1996).

[4] George A. Levin and Khandker F. Quader, *Phys. Rev. B* **46**, 5872 (1992).

[5] M. Gurvitch and A. T. Fiory , *Phys. Rev. Lett.* **59**, 1337 (1987).

[6] S. Martin, A. T. Fiory, R. M. Fleming, L. F. Schneemeyer, and J. V. Waszczak , *Phys. Rev. B* **41**, 846 (1990).

[7] Weimin Chen, J. P. Franck, and J. Jung, *Phys. Rev. B* **60**, 3527 (1999).

[8] P. Dai, M. Yethiraj, H. A. Mook, T. B. Lindemer, and F. Dogan, *Phys. Rev. Lett.* **77**, 5425 (1987).

[9] Y. Nakamura and S. Uchida, *Phys. Rev. B* **46**, 5841 (1992).

[10] J. M. Tranquada and J. D. Axe, N. Ichikawa, Y. Nakamura, and S. Uchida, B. Nachumi, *Phys. Rev. B* **54**, 7489 (1996).

[11] J. Rossat-Mignod, L.P. Regnault, C. Vettier, P. Bourges, P. Burlet, J. Bossy, J. Henry, G. Lapertot, *Physica C* **185-189**, 86 (1991).

[12] J. M. Tranquada, P. M. Gehring, and G. Shirane, S. Shamoto and M. Sato, *Phys. Rev. B* **46**, 5561 (1992).

[13] U. Poppe, N. Klein, U. Dahne, H. Soltner, C. L. Jia, B. Kabius, K. Urban, A. Lubig, K. Schmidt, S. Hensen, S. Orbach, G. Muller, H. Piel, *J. Appl. Phys.* **71**, 5572 (1992).

[14] S. B. Qadri, M. S. Osofsky, V. M. Browning, E. F. Skelton, *Appl. Phys. Lett.* **68**, 2729 (1996).

[15] V. M. Browning, E. F. Skelton, M. S. Osofsky, S. B. Qadri, J. Z. Hu, L. W. Finger, P. Caubet, *Phys. Rev. B* **56**, 2860 (1997).

Chapter 4

Twin-Boundary Pinning in YBCO Thin Films

4.1 Introduction

The central question in all flux motion models is the nature of the effective pinning centers. Various defects have been suggested, including oxygen vacancy clusters, secondary phases, columnar defects produced by proton and heavy-ion irradiation, and twin boundaries (TB's). Among those defects TB's, a common naturally occurring type of c-axis correlated disorder, are considered one of the most important sources of vortex pinning in $YBa_2Cu_3O_{7-\delta}$ (YBCO). Twins are ubiquitous in superconducting YBCO. They normally form to accommodate strains arising from a crystallographic tetragonal to orthorhombic transitions as a result of oxygen vacancy ordering. Twins occur in two orthogonal families called "colonies". For YBCO, the coherent TB is lying within {110} directions, so there are two sets of twins lying on $\langle 110 \rangle$ and $\langle 1\bar{1}0 \rangle$ planes [1].

Experimental evidence for the role of TB's as effective pinning centers has been observed very early, just after discovery of high T_c materials. A sharp drop in resistivity as the magnetic field direction is rotated through the c-axis is normally considered to be a signature of this type of pinning in clean materials [2, 3, 4, 5]. Additional support

72

for the TB pinning came from a low-temperature neutron-diffraction measurements of heavily twinned YBCO [6]. A square pattern of Bragg peaks was strongly suggestive of pinning by two orthogonal families of twin planes for field parallel to the c-axis.

The effect of TB's on vortex dynamics has been investigated by many authors using different experimental techniques. Magnetic decoration experiments at low temperatures and low fields revealed a concentration of vortices along the TB planes [7, 8]. Magnetization hysteresis on twinned and untwinned crystals showed that TB's are effective pinning centers [9, 10]. Later, using a high resolution magneto-optical technique, it was possible to investigate the interaction of vortices with individual TB [11]. This study revealed that TB's do not act as channels for easy flux entry but they are strong barriers for transverse vortex motion. This results in a build-up of flux on the side of the TB facing the motion and consequently leads to a guided vortex motion parallel to the TB's in the region adjacent to it [11].

Investigations involving pinning by TB's take advantage of many useful features that are not available in any other kind of defects. These are: (1) The twin planes are naturally occurring in the system, which allows the use of fully oxygenated samples without the need to introduce additional artificial defects that may suppress T_c and increase oxygen deficiency; (2) samples can be cleaved to obtain parts with no or a few TB's, or TB's can be removed without altering the stoichiometry; (3) TB's pinning sites are observable optically which facilitates the alignment of field and current directions; and (4) TB's are extended planar objects, and therefore their effect as pinning centers can be seen through angular dependent measurements (resistive, magnetization and torque) [2]. The TB's planar nature and their existence in two different crystallographic directions ($\langle 110 \rangle$ and $\langle 1\bar{1}0 \rangle$), suggest that anisotropic pinning behavior for flux motion parallel and perpendicular to the TB's should be expected. A large effect of the TB's has been observed when the Lorentz force is directed perpendicular to them [12]. However, it has been shown by angular-dependent magnetoresistance measurements that pinning by TB's occurs even when the Lorentz force is directed parallel to them [12]. This was explained qualitatively in terms of

the existence of atomic-size defects and disorder within TB's [12]. Fleshler et al. [2] studied the relationship between TB pinning and direction of the Lorentz force in YBCO twinned single crystals near T_c using angular resistivity measurements in a moderate magnetic field. This was achieved by applying the current in the ab-planes either parallel, perpendicular, or at an angle of 45° with respect to TB's. Pinning by TB's manifests itself as a drop in the resistance when the magnetic field is oriented within a certain depinning angle relative to TB's near the c-axis. They found that the drop in resistivity, the depinning angle, and the zero-resistance temperature to be enhanced when the vortices move in a direction normal to TB's, indicating that the pinning barriers for this direction of flux motion are significantly larger. The depinning angle for rotations off the c-axis decreases with an increasing field and a decreasing temperature, whereas for rotations of field in the ab-planes it is nearly field independent.

The effect of TB's on motion of vortices has also been observed in the torque [13] and transport measurements of the critical current density J_c [14, 15]. Roas et al. [14] performed transport measurements of J_c for epitaxial thin films in a magnetic field with various orientations of the applied current with respect to TB's. Their results indicate that J_c does not depend on the direction of the Lorentz force with respect to TB's for $B \parallel$ c-axis. The authors have shown this for more than twenty samples, where the current paths were randomly oriented with respect to the a and b axis [14]. On the other hand, Safar et al. [15] carried out a transport resistive measurements on thick YBCO films at T=75 K and in field of 5.3 T in order to determine J_c. They performed the measurements for two different orientations of the applied current with respect to TB planes: one at 45° and the other is simultaneously parallel and perpendicular to TB's. Their results showed that J_c is a factor of two higher for the 45° orientation than that of the other one [15].

From the theoretical viewpoint, Blatter et al. [16] investigated the pinning properties of TB's in YBCO single crystals within the framework of the collective-pinning theory. They proposed that TB pinning can occur only for magnetic fields directed

74

within some critical angle ϕ_c relative to TB's. In the single-vortex pinning picture, this critical angle is determined by the tilt modulus and the pinning energy associated with the suppression of the order parameter in TB's. They showed that at angles $\phi < \phi_c$, the vortex lattice is accommodated to the lattice of twinning planes, resulting in a decrease in resistivity and a corresponding enhancement of the critical current density. Above the bulk depinning temperature T_p, the pinning properties of TB's are enhanced as compared to the bulk pinning [16]. Nelson and Vinokur [17] developed a theory of vortex pinning in high-T_c superconductors by correlated disorder in the form of TB's, grain boundaries, and columnar defects.

It is believed [2] that TB's pinning is strong enough to produce a minimum in $\rho(\phi)$ in single crystals, if the field is oriented within a certain depinning angle from the c-axis. In addition, the onset temperature of TB's pinning is marked by a shoulder observed in the low-temperature end of the magnetic field broadened resistive transition for **B** || c-axis for YBCO single crystals [2] and films [18]. However, Charalambous et al. [19] have found a shoulder in the temperature dependence of resistivity of twinned YBCO crystals for **B** $\perp$ c-axis and **J** || c-axis. This resistivity drop was interpreted as evidence for the first-order freezing transition into the Abrikosov flux lattice. In completely *twin-free* samples, a shoulder was also observed even for fields along the c-axis [17].

Our measurements of the angular dependence of resistivity performed on YBCO thin films of various T_c, J_c, thickness, and preparation techniques revealed that some films showed a minimum in $\rho(\phi)$ for fields oriented within a certain angle from the c-axis. The majority of these films did not show a sharp minimum but instead a smooth flat maximum as **B** is tilted closer to the c-axis, similar to that seen in typical untwinned YBCO crystals. However, those films which displayed a minimum in $\rho(\phi)$ for **B** close to the c-axis, did not show any characteristic shoulder in $\rho(T)$ measured in an applied magnetic field parallel to the c-axis in contrast to that reported in References [2, 18].

In this Chapter, we present detailed study of the angular dependence of resistivity

75

as a function of temperature and magnetic field for fifteen YBCO films of various T_c, J_c, thickness, substrates, and preparation techniques. We focus on the angular region of $\rho(\phi)$ with ϕ close to the c-axis where TB pinning is expected to be the most effective. Our results revealed that the angular width of the minimum (i.e the accommodation angle) for rotations off the c-axis decreases with an increasing field and an increasing temperature in accordance with previous reports [3]. The most striking result is that there is no correlation between the measured critical current density J_c in YBCO films and the presence of the minimum in $\rho(\phi)$. In fact, we have also found that the minimum in $\rho(\phi)$, for YBCO thin films studied, is present only in films which were deposited very slowly, thus allowing the growth of crystallographically well-defined and sharp TB's.

4.2 Results and discussion

Correlated disorder plays an important role in understanding the dynamics of vortex motion. One significant source of correlated disorder is twin boundaries. Potentially more important for applications are the columnar defects, produced by highly energetic heavy ions like lead, gold, uranium etc. The c-axis correlated disorder is manifested by a sharp drop in the angular dependence of resistivity $\rho(\phi)$ as the magnetic field **B** is aligned close to the c-axis (parallel to TB's or columnar defects) [2, 3, 4, 5, 20, 21]. In addition, columnar defects and TB's shift the irreversibility line to higher temperatures and increase the critical current density J_c at high temperatures and high fields due to a large increase in the pinning strength [15, 20, 21, 22].

In order to understand the effect of TB's as pinning centers in YBCO thin films, we have measured the angular dependence of resistivity $\rho(\phi)$ as a function of temperature and magnetic field for fifteen YBCO films of various T_c, J_c, preparation techniques, thickness and oxygen deficiency. Surprisingly, out of these fifteen films only three showed a minimum in $\rho(\phi)$ as the field is tilted close to the c-axis. The other films displayed no minimum but a round maximum similar to that observed in typical clean

76

Table 4.1: The normal and superconducting properties of YBCO films, ρ has been measured in the ab-planes, T_{c0} is the transition temperature at $\rho = 0$ and B=0, ΔT_c is the transition width at a zero field and t is the thickness of the film.

Film No.	substrate type	Deposition method	t (nm)	T_{c0} (K)	ΔT_c (K)	$\rho(100K)$ $(\mu\Omega cm)$	$\frac{\rho(300K)}{\rho(100K)}$
3	$SrTiO_3$	laser-ablation	230	89.5	1.2	74.9	3.55
4	Sapphire+CeO_2	laser-ablation	140	81.7	2.9	14.2	2.40
5	$SrTiO_3$	rf-magnetron	210	84.5	1.9	113.4	2.78
6	$Al_2O_3 + CeO_2$	rf-magnetron	330	84.6	2.5	259.4	2.86
7	$Al_2O_3 + CeO_2$	rf-magnetron	610	85.0	2.0	289.4	2.87

untwinned YBCO crystal [21]. The superconducting and normal state characteristics of the samples used in this Chapter are listed in Table 4.1.

In the following sections we discuss the effect of the critical current density, temperature and magnetic field on the minimum around $\phi = 0°$, and estimate TB pinning energy from the accommodation angle.

4.2.1 Dependence of TB pinning on J_c

Fig.4.1 shows the angular dependence of resistivity $\rho(\phi)$ as a function of temperature close to T_c, in a constant magnetic field for two selected YBCO films 5 and 7 which displayed a minimum in $\rho(\phi)$. For both films the field was rotated in a plane perpendicular to the current direction in order to maximize the Lorentz force effect. For the range of temperatures shown in Fig.4.1, the resistivity increases as the magnetic field is tilted away from the ab-planes ($\phi = \pm 90°$), eventually reaching a maximum at an angle ϕ_{TB} (which is temperature dependent), and then decreases as the field direction approaches the c-axis, reaching a minimum at $\phi = 0°$ ($\mathbf{B} \parallel$ c-axis).

As we pointed out earlier in the introduction, the minimum in $\rho(\phi)$ that occurs when the field is oriented within a certain angular width around the c-axis is
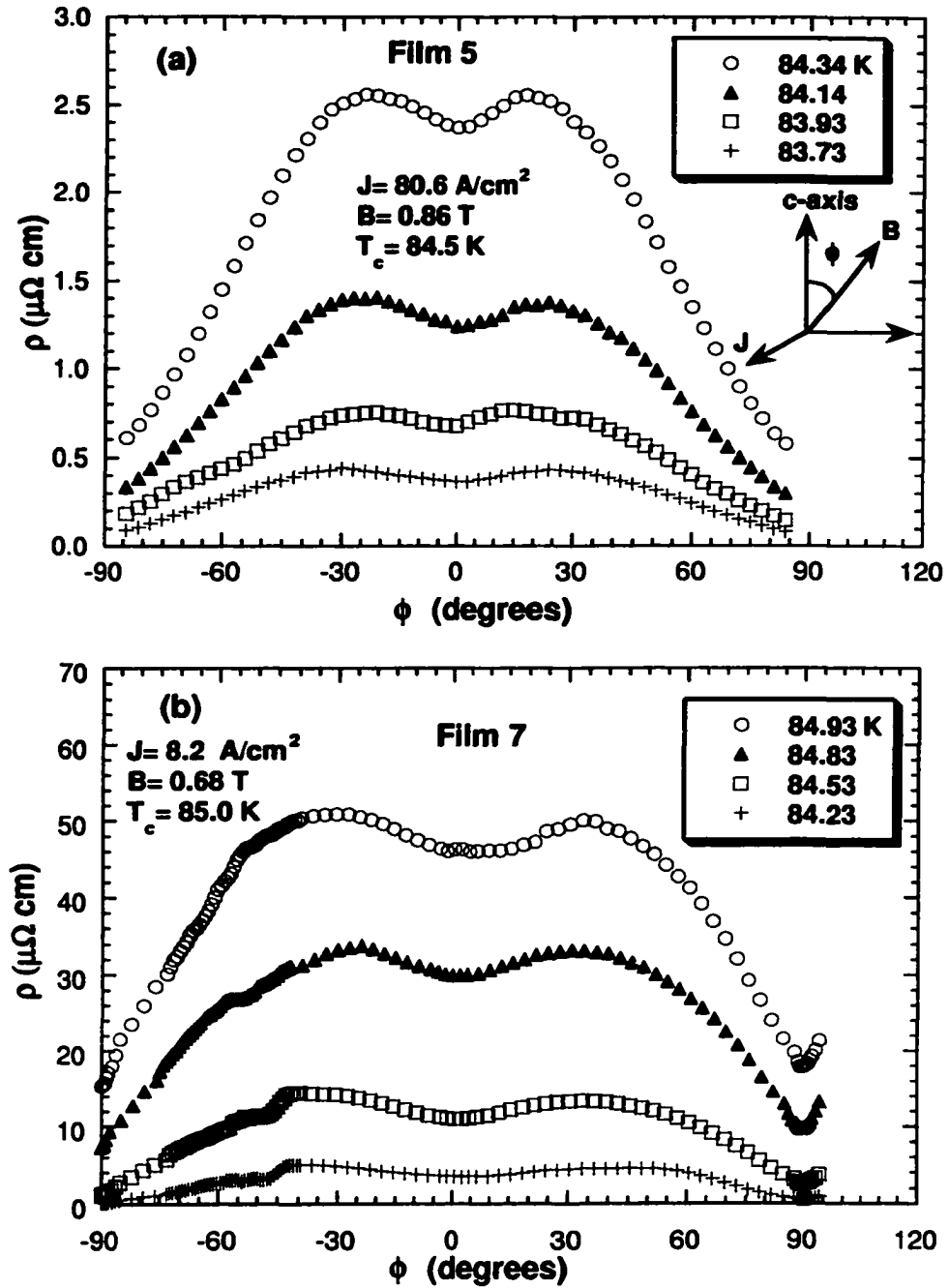
Figure 4.1: Angular dependence of resistivity $\rho(\phi)$ measured in a constant magnetic field at different temperatures close T_c for two YBCO films 5 (a) and 7 (b), which exhibits a minimum in $\rho(\phi)$ around $\phi = 0°$. The angle ϕ is measured with respect to the c-axis ($\phi = 0°$) and the field is rotated off the c-axis in the plane perpendicular to the applied current direction ($\mathbf{B} \perp \mathbf{J}$) [see the inset in (a)]. The minimum in $\rho(\phi)$ is due to the twin boundary pinning in both films. Note that $\rho(\phi)$ increases as $\mathbf{B}$ is rotated away from the ab-planes ($\phi = \pm90°$), reaching a maximum at a certain angle ϕ, and then decreases as the $\mathbf{B}$ approaches the c-axis, reaching a minimum at $\phi = 0°$ ($\mathbf{B} \parallel$ c-axis).

78

attributed to twin boundary pinning [2, 23]. Film 5 has a relatively high critical current density J_c at 77 K, while film 7 has a low J_c (see Table 4.2). Fig.4.2 presents $\rho(\phi)$ as a function of temperature close to T_c, at a constant magnetic field for two selected YBCO films 3 and 4 that did not show a minimum in $\rho(\phi)$ for B close to the c-axis. Film 3 has the highest J_c at 77 K compared to other films investigated, while film 4 has the lowest J_c (see Table 4.2). Note that the resistivity for films 3 and 4 of Fig.4.2 is the largest when the field is aligned parallel to the c-axis and has a minimum when the field is parallel to the ab-planes. This angular dependence of resistivity arises from the intrinsic anisotropy of YBCO. Films with large anisotropy exhibit a large difference between $\rho(0^o)$ and $\rho(90^o)$. It is worth noting here that the mass anisotropy ratio $\gamma = \sqrt{m_c/m_{ab}}$ was estimated to be 35 for film 3 and about 400 for film 4 (see the next Chapter).

In order to verify if there is any correlation between the minimum in $\rho(\phi)$ and the magnitude of J_c for different films, it is important to use J_c values measured at a fixed reduced temperature T/T_c very close to T_c where the measurement of $\rho(\phi)$ has been performed. For this purpose, J_c values measured at $T/T_c = 0.977$ were used. At high temperature of $T/T_c = 0.977$ thermal activation energy is high enough to overcome pinning by point defects and therefore any vortex pinning by point defects can be neglected. Thus only c-axis oriented defects (TB's, grain boundaries, columnar defects) are the source of effective pinning centers. TB's are planar defects and their effect should be visible even at high temperature as demonstrated by the minimum at $\phi = 0^o$. Comparing the values of J_c measured at $T/T_c = 0.977$ (see Table 4.2) for films 5, 6 and 7 (with a minimum) with those of films 3 and 4 (without a minimum), we could not establish any correlation between the presence of the minimum in $\rho(\phi)$ for field rotations close to the c-axis and the magnitude of J_c.

Temperature dependence of J_c was measured by a contactless magnetic method using a scanning Hall probe [24]. This method involves inducing a supercurrent in a disk- or a ring- shaped sample by applying an external magnetic field and subsequently switching it off . The measurement of J_c using a self-supporting supercurrent prevents

79
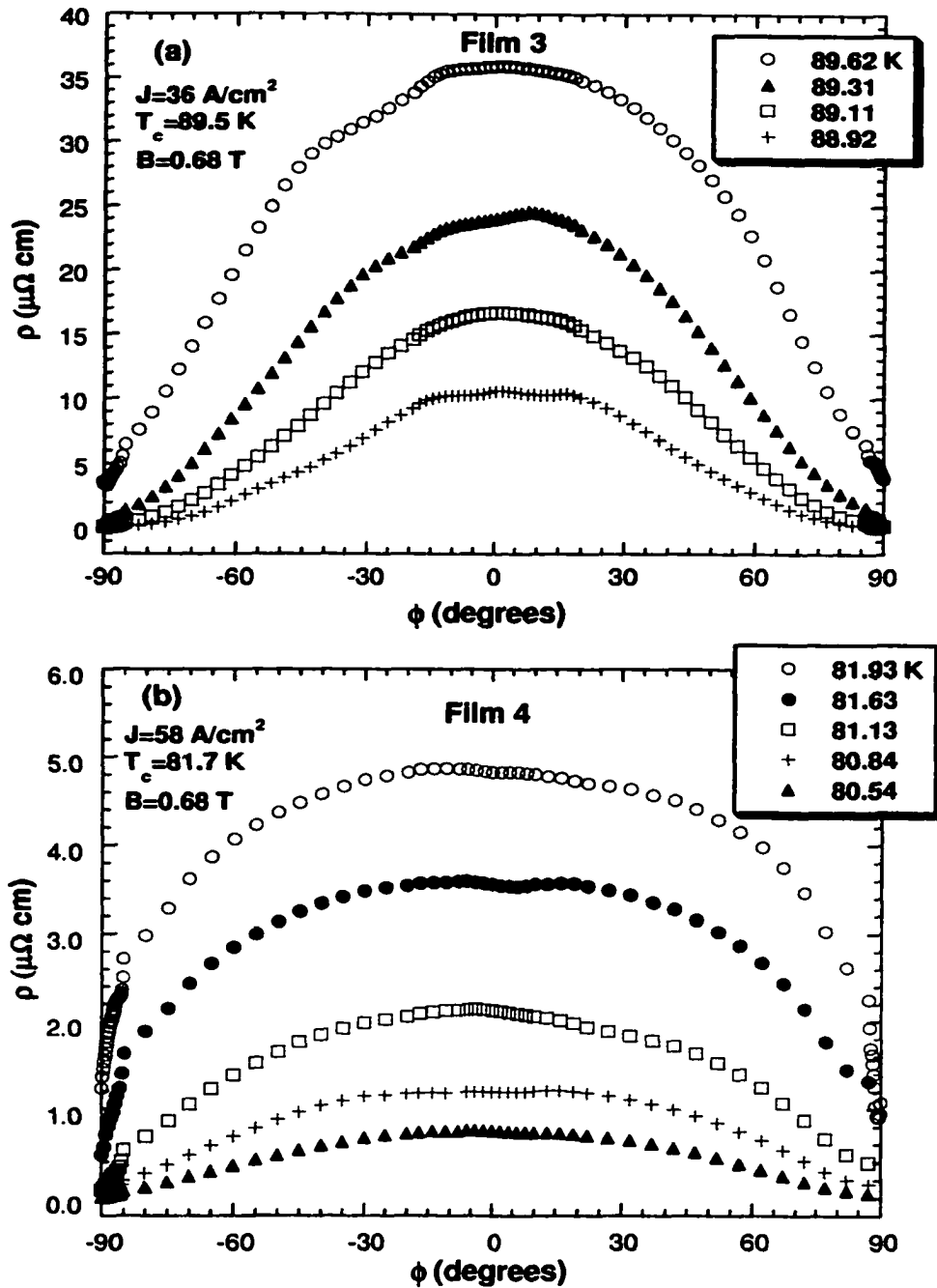
Figure 4.2: Angular dependence of resistivity $\rho(\phi)$ measured in a constant magnetic field at different temperatures close T_c for two YBCO films 3 (a) and 4 (b), which exhibits a broad maximum in $\rho(\phi)$ around $\phi = 0^o$. The angle ϕ is measured with respect to the c-axis and the field is rotated off the c-axis in the plane perpendicular to the applied current direction ($\mathbf{B} \perp \mathbf{J}$). Note that $\rho(\phi)$ for both films is the largest when $\mathbf{B} \parallel$ c-axis and has a minimum when $\mathbf{B} \parallel$ ab-planes. This angular dependence is a result of the intrinsic anisotropy of YBCO.

80

Table 4.2: Characteristics of the YBCO films: critical current density J_c measured at 77 K and at a reduced temperature $T/T_c = 0.977$, ϕ_{TB} is the TB's accommodation angle taken from Fig.4.4, and $[\rho(\phi_{TB}) - \rho(0°)]/\rho(\phi_{TB})$ is the normalized depth of the minimum in $\rho(\phi)$.

Film No.	minimum present	$J_c(77K)$ (A/cm^2)	$J_c(\frac{T}{T_c} = 0.977)$ (A/cm^2)	ϕ_{TB} (degrees)	$\frac{\rho(\phi_{TB})-\rho(0°)}{\rho(\phi_{TB})}$
3	no	2.36×10^6	7.28×10^4	N/A	N/A
4	no	8.10×10^4	1.62×10^4	N/A	N/A
5	yes	1.08×10^6	2.82×10^4	23.8	0.116
6	yes	1.13×10^5	1.59×10^4	28.8	0.134
7	yes	1.03×10^5	1.02×10^4	37.0	0.240

adding normal currents (which may flow through parts of the sample of very low resistance) to the measured value of J_c. Effects of normal currents on J_c especially very close to T_c can not be avoided in standard methods such as an I-V four probe method. According to our method of measuring J_c, the induced supercurrent is circulating in a closed loop in the ab-plane of the film. Therefore the effect of TB's pinning should be encountered especially at high temperatures close to T_c where the effect of point defect pinning is negligible.

Fig.4.4 shows the angular dependence of resistivity $\rho(\phi)$ at a fixed field and a reduced temperature T/T_c for three YBCO films very close to T_c. All three films display a minimum for angles near $\phi = 0°$. This minimum is characterized by a width and a depth which are temperature, field, and sample dependent. The accommodation angle (ϕ_{TB}) is defined as half of the angular width between the two resistivity maxima surrounding the minimum (see Fig.4.4). The accommodation angle represents the largest angular range for which TB pinning is effective. The normalized depth of the minimum defined as $[\rho(\phi_{TB}) - \rho(0°)]/\rho(\phi_{TB})$, is also temperature, field, and sample dependent. The accommodation angles ϕ_{TB}, calculated from Fig.4.4, for

81
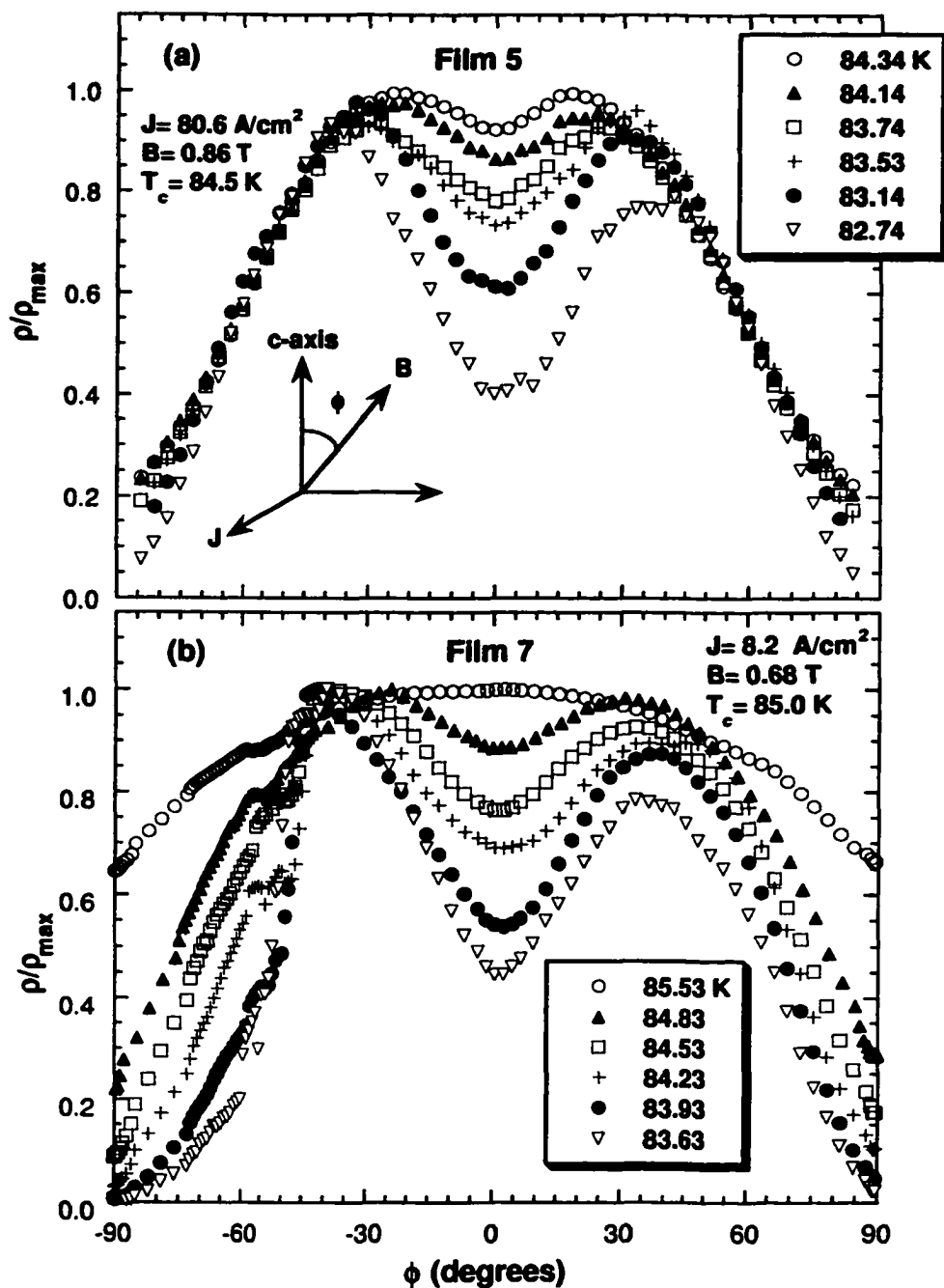
Figure 4.3: Normalized angular dependence of resistivity $\rho/\rho_{max} = \rho(\phi)/\rho(\phi_{TB})$ measured in a constant magnetic field at different temperatures close T_c for films 5 (a) and 7 (b). The field was rotated off the c-axis in a plane perpendicular to the current direction. Each normalized angular-dependent isotherm curve was produced by dividing $\rho(\phi)$ [shown in Fig.4.1] by its maximum value $\rho(\phi_{TB})$. Note that the depth of the minimum in $\rho(\phi)$ decreases as temperature is increased and eventually disappears completely close to T_c.

82

films 5, 6 and 7 are 23.8^o, 28.8^o and 37.0^o, respectively. The depths of the minimum $[\rho(\phi_{TB}) - \rho(0^o)]/\rho(\phi_{TB})$ for films 5, 6 and 7 are 0.116, 0.134, and 0.240 respectively. ϕ_{TB}, $[\rho(\phi_{TB}) - \rho(0^o)]/\rho(\phi_{TB})$ and J_c at $T/T_c = 0.977$ are listed in Table 4.2 for comparison. Note that film 5 has the highest J_c and film 7 has the lowest one. From Table 4.2, one can also see that ϕ_{TB} and $[\rho(\phi_{TB}) - \rho(0^o)]/\rho(\phi_{TB})$ increase with a decreasing J_c. This kind of behavior is not expected since the TB pinning should have the same effect on the magnitude of J_c and the minimum in $\rho(\phi)$. In other words, the width and the depth of the minimum should increase with an increasing J_c. This behavior can be explained by taking into account the direction of the applied current I relative to the TB.

YBCO films contain TB's along both $\langle 110 \rangle$ and $\langle 1\bar{1}0 \rangle$ directions and thus the Lorentz force that acts on the flux lines is directed at two angles relative to TB's directions simultaneously. The alignment of bridges (current direction) was randomly chosen for all films studied, which implies that the current could be directed parallel and perpendicular to TB or at an arbitrary angle with respect to the TB mosaic. A large effect of TB pinning is expected for directions of I at 45° from the mosaic of TB's but a smaller one when I is oriented parallel and perpendicular to TB's. Safar et al. [15] investigated the effect of TB on J_c in thick YBCO films. They observed that J_c was a factor of two higher when the current was directed at 45° from the mosaic of TB's in comparison to the case when I was directed parallel and perpendicular to TB's. Fleshler et al. [2] studied extensively the Lorentz-force dependence of TB pinning in YBCO single crystals close to T_c. They cut these crystals in order to obtain samples with only one TB orientation. Current was applied in the ab-planes at three different directions relative to TB's: parallel, perpendicular, and at 45°. The authors observed that TB's reduce the resistance more significantly and provide pinning over a wider angular range (ϕ_{TB} is larger and the minimum is deeper) when the Lorentz force is oriented perpendicular to TB planes (i.e I $\parallel$ TB's) for rotations off the c-axis. More explicitly, ϕ_{TB} for crystals with I $\parallel$ TB's is more than twice that for crystals with I $\perp$ TB's, and the ratio $[\rho(\phi_{TB})/\rho(0^o)]$ is two orders of magnitude
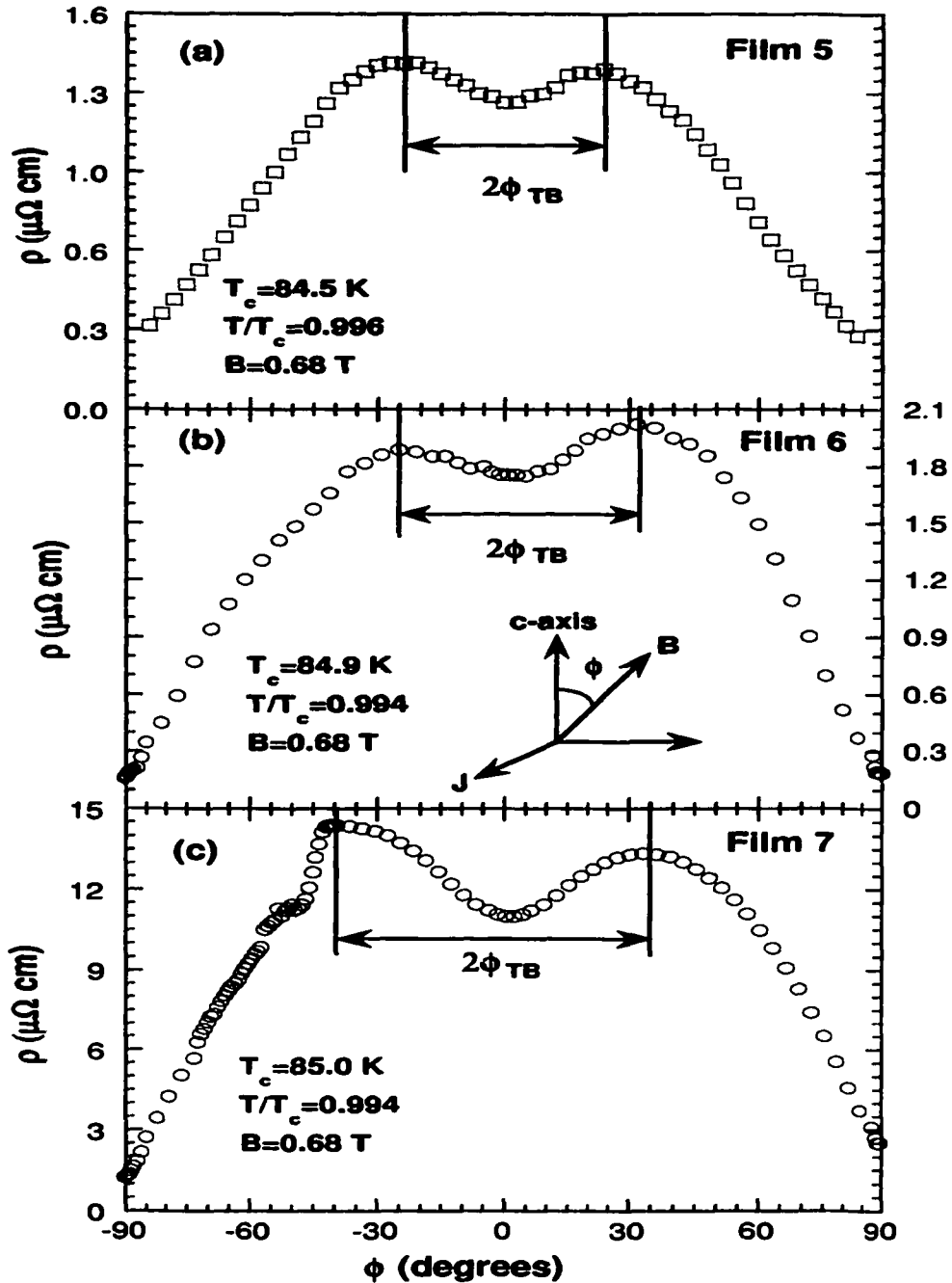
Figure 4.4: Angular dependence of resistivity $\rho(\phi)$ measured in a constat field and a constant reduced temperature T/T_c for three YBCO films 5 (a), 6 (b) and 7 (c) very close to T_c. All three films display a minimum for angles near $\phi = 0°$. The accommodation angle (ϕ_{TB}) is defined as the half of the angular width between the two resistivity maxima surrounding the minimum. The inset in (b) shows the experimental configuration for all three films where **B** is rotated off the c-axis with **B** $\perp$ **J**. Note the sample-dependent variation of ϕ_{TB}.

84

larger for crystals with I ∥ TB's than that for crystals with I ⊥ TB's. Note that the minimum at $\phi = 0°$ was always observed for all orientations of I relative to TB planes. These two experimental observations suggest that the orientation of I relative to TB's is important because it determines the Lorentz-force direction which governs the direction of flux-motion. The flux lines experience the maximum TB's pinning when it moves across the TB's and the minimum pinning when they move parallel to TB's. In our case, films 6 and 7 have comparable J_c values at $T/T_c = 0.977$ which are about two times less than that for film 5 (see Table 4.2). For the measurement of J_c, the issue of orientation of I is not important since in our contactless measurement the supercurrent is circulating in a closed loop (thus crossing all TB planes in a certain area). Films 6 and 7 are expected to have similar TB pinning strength and the difference between their respective minima depths and widths could be due to orientation of I at different angles relative to TB mosaic. For film 5, with the highest J_c and smallest ϕ_{TB} among all three films (see Table 4.2), the effect of TB's pinning could be minimized if the direction of I is parallel and perpendicular to TB planes. This is in fact consistent with the results of Safar [15] et al. discussed earlier, which showed a change of J_c by a factor of two due to different orientations of I relative to TB planes. This change is similar to the difference in J_c values between films 5 and 6 (see Table 4.2).

4.2.2 Onset of twin-boundary pinning

Fig.4.3(b) displays the normalized angular dependence of resistivity $\rho(\phi)/\rho(\phi_{TB})$ for an angular range between $-90°$ and $+90°$ for film 7 at a fixed field of 0.68 T measured at different temperatures very close to T_c. The field was rotated in a plane perpendicular to the current direction in order to maximize the Lorentz force effect. The drop in $\rho(\phi)$ relative to $\rho(\phi_{TB})$ due to TB's pinning is very large at low temperatures, about 55% at 83.63 K, for film 7 [see Fig.4.3(b)], but it decreases as temperature is increased and eventually disappears completely near 85.5 K. In order to identify the temperature at which the minimum disappears completely, $\rho(\phi)$ has been measured

for a finer temperature interval of 0.1 K. The results of this measurements for an angular range between -50° and $+50^o$ in a constant field of 0.68 T for film 7 is shown in Fig.4.5(a) for a temperature range between 84.83 K and 85.53 K. For film 7, effect of TB pinning is still detectable up to 85.43 K at which a very shallow minimum appears over the angular range between -30° and 35°. However at 85.53 K, the minimum in $\rho(\phi)$ for field tilts close to the c-axis completely disappears and instead a round maximum is observed. Thus the TB onset temperature (T_{TB}) below which TB causes a drop in the angular dependence of resistivity for B=0.68 T is $85.50 \pm 0.05K$.

Fleshler et al. reported a measurement of $\rho(\phi)$ and $\rho(T)$ as a function of temperature at a constant magnetic field on YBCO twinned crystals close to T_c. They have identified a shoulder in the temperature dependence of resistivity $\rho(T)$ that corresponds to a steep upturn in the derivative $d\rho/dT$ [see Fig.5 in Ref. [2]]. The authors have shown that the temperature at which the upturn in $d\rho/dT$ occurs corresponds to the onset temperature of the TB pinning T_{TB} [2]. Casaca et al. [18] also reported a similar observation of a characteristic shoulder in $\rho(T)$ for YBCO thin films in magnetic fields up 18 T. They identified this effect as a signature of the onset of TB pinning [18]. In order to verify whether our measurement shows a similar characteristic shoulder, the resistivity as a function of temperature at a constant field of 0.68 T (applied along the c-axis) has been measured over a temperature range between 83 and 96 K. The results of $\rho(T)$ and $d\rho/dT$ for film 7 are shown in Fig.4.5(b). This figure did not reveal any characteristic shoulder in $\rho(T)$ or any corresponding upturn in $d\rho/dT$ at the temperature which corresponds to the onset of TB pinning.

It is important to verify whether the resistivity curve $\rho(T)$ measured for **B** $\parallel$ c-axis and its derivative $d\rho/dT$ for films whose $\rho(\phi)$ has a minimum have any special character that distinguish them from those films whose $\rho(\phi)$ has a maximum for field alignments close to the c-axis. Fig.4.6(a) shows the normalized resistivity $\rho(\phi)/\rho(0^o)$ for film 3, with $T_c = 89.5K$, measured at different temperatures in a field of 0.68 T for **B** $\perp$ **J**. This film shows a maximum in $\rho(\phi)$ which excludes the possibility of any significant TB pinning at all temperatures and fields investigated [see Figures 4.2(a)

86
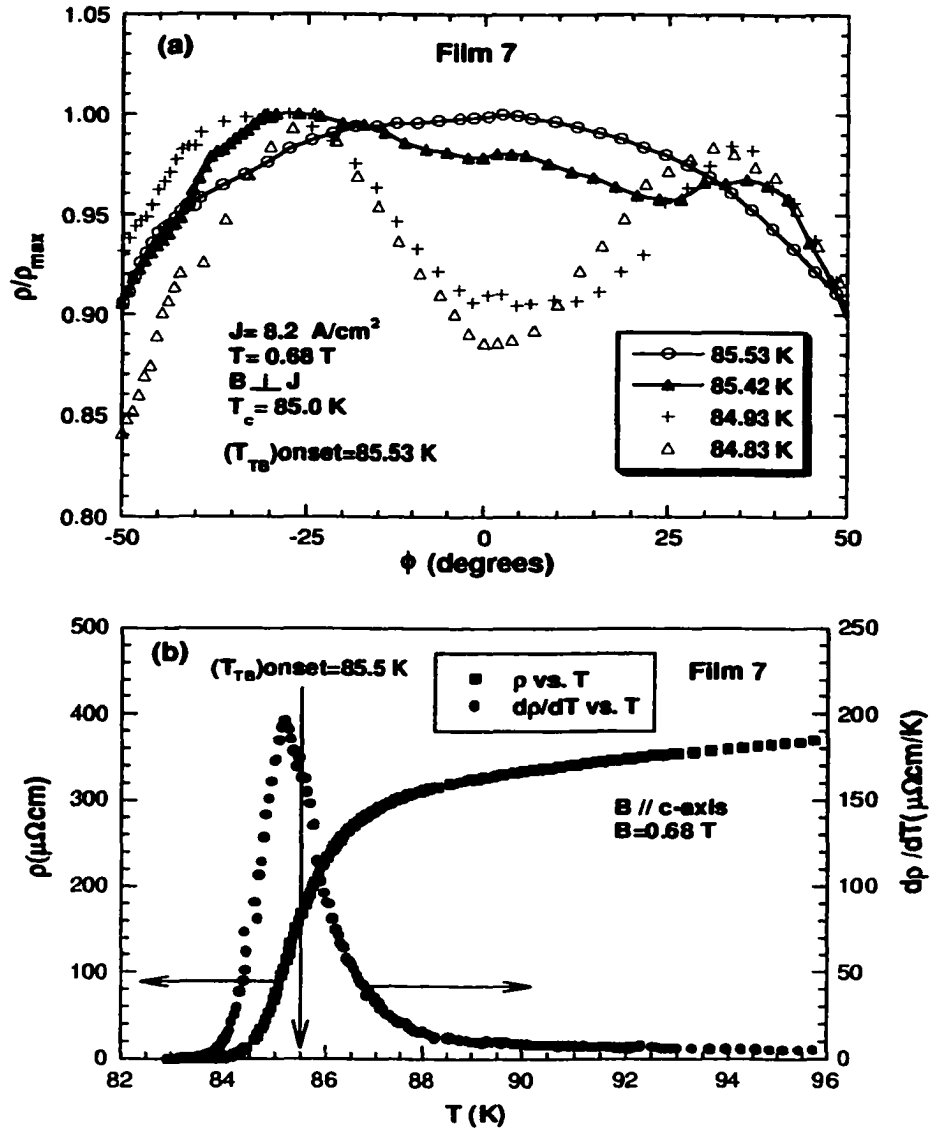
Figure 4.5: (a) Normalized angular dependence of resistivity $\rho/\rho_{max} = \rho(\phi)/\rho(\phi_{TB})$ measured at different temperatures close to T_c onset, and over a small angular range between $-50°$ and $+50°$ in a constant field for film 7 (with a minimum near $\phi = 0°$). The minimum (due to TB's pinning) in $\rho(\phi)$ can be seen up to 85.42 K, but it disappears completely at 85.53 K. (b) Resistivity and its temperature derivative $d\rho/dT$ measured as a function of temperature near the transition (between 83 and 96 K) in a constant field $\mathbf{B} \parallel$ c-axis. The temperature $T_{TB}=85.5$ K, at which the minimum in $\rho(\phi)$ disappears completely, marks the onset temperature of TB's pinning. Note that $d\rho/dT$ did not show any steep upturn or shoulder as observed in YBCO single crystals.

87

and 4.6(a)]. Fig.4.6(b) presents $\rho(T)$ measured in a field of 0.68 T (applied along the c-axis) and the derivative $d\rho/dT$ as a function of temperature between 87 and 96 K for film 3. Comparison of the data for film 7 [see Fig.4.5(b)] with those of film 3 [see Fig.4.6(b)], revealed no change in the shape of either $\rho(T)$ or $d\rho/dT$ curves between the two films. Therefore we conclude that the onset temperature of TB pinning in YBCO films is not correlated to a shoulder in $\rho(T)$ or a steep upturn in $d\rho/dT$ in contrast to that observed by Fleshler et al. [2] and Casaca et al.[18]. The magnitude of the applied magnetic field does not have any significant effect on the existence of such features in $\rho(T)$ or in $d\rho/dT$. These features were observed both in a low field of 1-3 T for single crystals [2] and in a high field of 14-18 T for thin films [18]. Our measurements performed in a low field ($B < 1T$), did not show any similar features.

The onset temperature of TB pinning for YBCO films occurs at temperatures above the middle of the transition (marked by the peak in $d\rho/dT$ [see Fig.4.5(b)] for **B** ∥ c-axis). For higher fields T_{TB} shifts to lower temperatures. This result is consistent with the results of Fleshler et al. for YBCO twinned crystals (see Fig.6 in Ref. [2]) and Casaca et al. for YBCO thin films (see Fig.2 in Ref. [18]).

It is important to indicate that a similar kind of shoulders in $\rho(T)$ have also been observed for different orientations of field in YBCO materials. Charalambous et al. [19] found a shoulder in $\rho(T)$ of twinned YBCO crystals, when the field was oriented perpendicular to the c-axis. This shoulder was interpreted as an evidence for first order freezing transition of flux into the Abrikosov lattice. However, in completely twin-free YBCO crystals, a shoulder in $\rho(T)$ was also observed even for fields aligned along the c-axis [17].

Polarized light microscope studies on YBCO films that showed a minimum in $\rho(\phi)$ at $\phi = 0^o$ (films 5,6, and 7) did not show any trace of twin boundaries even with use of the highest resolution available (1000 times magnification). This may imply that the spacing between these twin boundaries is very small, on a sub-micron level, to be seen using this magnification. Typical TB spacing in single crystals $0.2 - 15\mu m$ [2, 11] as determined by transmission electron and optical microscopies. For thin

88
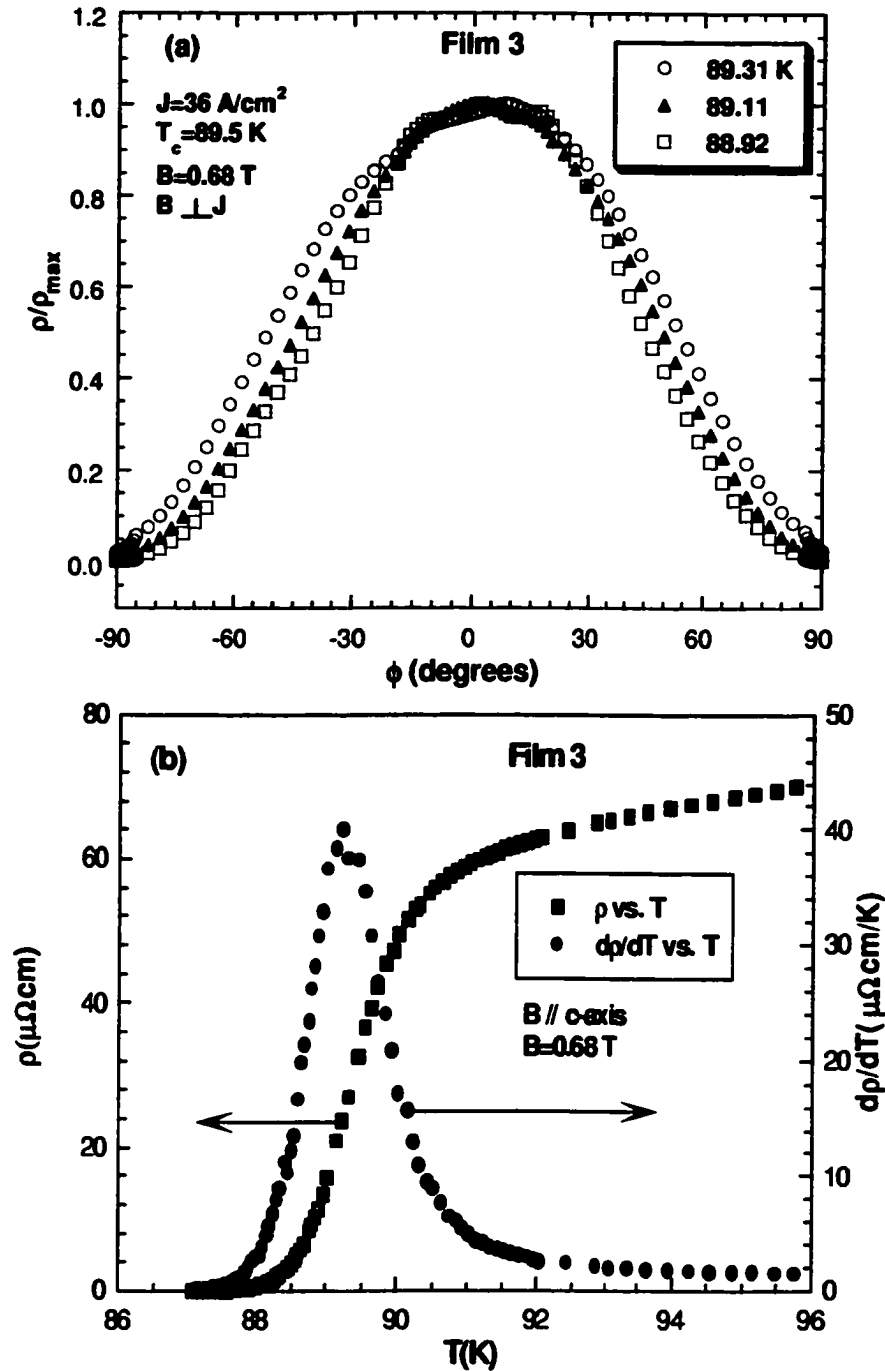
Figure 4.6: (a) Normalized angular dependence of resistivity $\rho/\rho_{max} = \rho(\phi)/\rho(0^o)$ measured for different temperatures close to T_c in a constant field for film 3 (with a maximum in $\rho(\phi)$ near $\phi = 0^o$). (b) Resistivity and its temperature derivative $d\rho/dT$ measured as a function of temperature near the transition (between 87 and 96 K) in a constant field $\mathbf{B} \parallel$ c-axis. Note that $d\rho/dT$ did not show any noticeable difference from that shown by film 7 (with a minimum in $\rho(\phi)$) [see Fig.4.5(b)].

89

films, transmission electron microscope studies by Safar et al. [15] indicated that films contain grains of typical size between 2 to 5 μm . These grains are seen to have many TB's with a typical separation of $0.2\mu m$. They also noticed that, most grains contain TB's running along a single direction (either along (110) or (11$\bar{1}$0)). There is a little correlation between the orientation of TB's in adjacent grains. As a result, the sample is composed of a dense distribution of small domains, extending over very few grains, of single TB orientation. This is in contrast to single crystals where large domains (hundreds of microns) of the same TB orientation is normally observed [2, 12]. These results suggest that the TB's in YBCO films exist within the grains and they are very small to be seen using an optical polarized light microscope which is in contrast to those of single crystals which can be seen easily using polarized light microscope. Therefore one has to use a transmission electron microscopy technique to see that.

4.2.3 Temperature and field dependence of TB pinning

The minimum in $\rho(\phi)$ around $\phi = 0^o$ is characterized by a width and a depth which are temperature, field, and sample dependent. The sample dependence has been discussed in the first section. In this section we focus on temperature and field dependence of TB minimum. The TB accommodation angle ϕ_{TB} is operationally defined as half of the angular width between the two resistivity maxima around the minimum [see Fig.4.4 and Fig.4.8].

Fig.4.1 shows the resistivity $\rho(\phi)$ as a function of temperature in a constant magnetic field for films 5 and 7 for $\mathbf{B} \perp \mathbf{J}$. The measurement were done for a range of temperatures very close to T_c. Since the variation in resistivity close to T_c is very large, it is difficult to see the effect of temperature changes on the minimum in $\rho(\phi)$. In order to see this effect more clearly, each angular-dependent resistivity isotherm was normalized to the maximum resistivity at $\phi = \phi_{TB}$. The results of this normalization for films 5 and 7 are shown in Fig.4.3 for a wider range of temperatures for each film. For both films, the width of the minimum (2 ϕ_{TB}) and the normalized

depth, defined as $[\rho(\phi_{TB}) - \rho(0^o)]/\rho(\phi_{TB})$, increase with a decreasing temperature. Fig.4.7(a) shows the accommodation angle ϕ_{TB}, calculated from Fig.4.3, as a function of the reduced temperature T/T_c at a constant field for films 5 and 7. The two films display a relatively different non-linear behavior, which may suggest a difference between their respective TB's pinning mechanisms. For both films ϕ_{TB} decreases with an increasing reduced temperature T/T_c.

Fig.4.7(b) shows the variation of the normalized depth, calculated from Fig.4.3, as a function of the reduced temperature T/T_c at a constant field for films 5 and 7. We defined the normalized depth as the difference between resistivities measured at $\phi = \phi_{TB}$ (maximum resistivity) and $\phi = 0^o$ (minimum resistivity for **B** || c-axis) normalized to $\rho(\phi_{TB})$: $\Delta\rho/\rho(\phi_{TB}) = [\rho(\phi_{TB}) - \rho(0^o)]/\rho(\phi_{TB})$. This ratio shows the fractional drop in $\rho(\phi)$ relative to $\rho(\phi_{TB})$. This depth measures the strength of the TB pinning. For both films, the normalized depth displays a linear behavior with T/T_c. $\Delta\rho/\rho(\phi_{TB})$ decreases with an increasing temperature. The two slopes are almost equal, -28.1 for film 7 and -27.2 for film 5. These large slopes imply that the TB pinning strength is increasing very fast with a decreasing temperature.

Measurements of TB accommodation angle in YBCO single crystals revealed a value of $\phi_{TB} = 24^o$ at a reduced temperature of $T/T_c = 0.950$ and a field of 1 T [2, 3]. For our YBCO films, TB accommodation angle reaches a value of $\phi_{TB} = 36^o$ at $T/T_c = 0.980$ and a field of 0.86 T for film 5 and a value of $\phi_{TB} = 44^o$ at $T/T_c = 0.980$ and a field of 0.68 T for film 7. These values are even larger at lower temperatures. Therefore TB pinning manifests itself over a much wider angular range in YBCO thin films in comparison to those observed in YBCO single crystals (24°) at lower temperatures $T/T_c = 0.950$, or in the torque measurements $(5 - 7^o)$ at 77 K [25]. Decoration experiments revealed that TB's affect the vortex configuration for field tilts up to 40° off the c-axis in a low magnetic field (10 G) and liquid helium temperatures [26].

Fig.4.8 shows the angular dependence of resistivity at fields of 0.59 T and 0.86 T and at 84.34 K for film 5 [Fig.4.8(a)] and at 84.43 K for film 7 [Fig.4.8(b)]. In
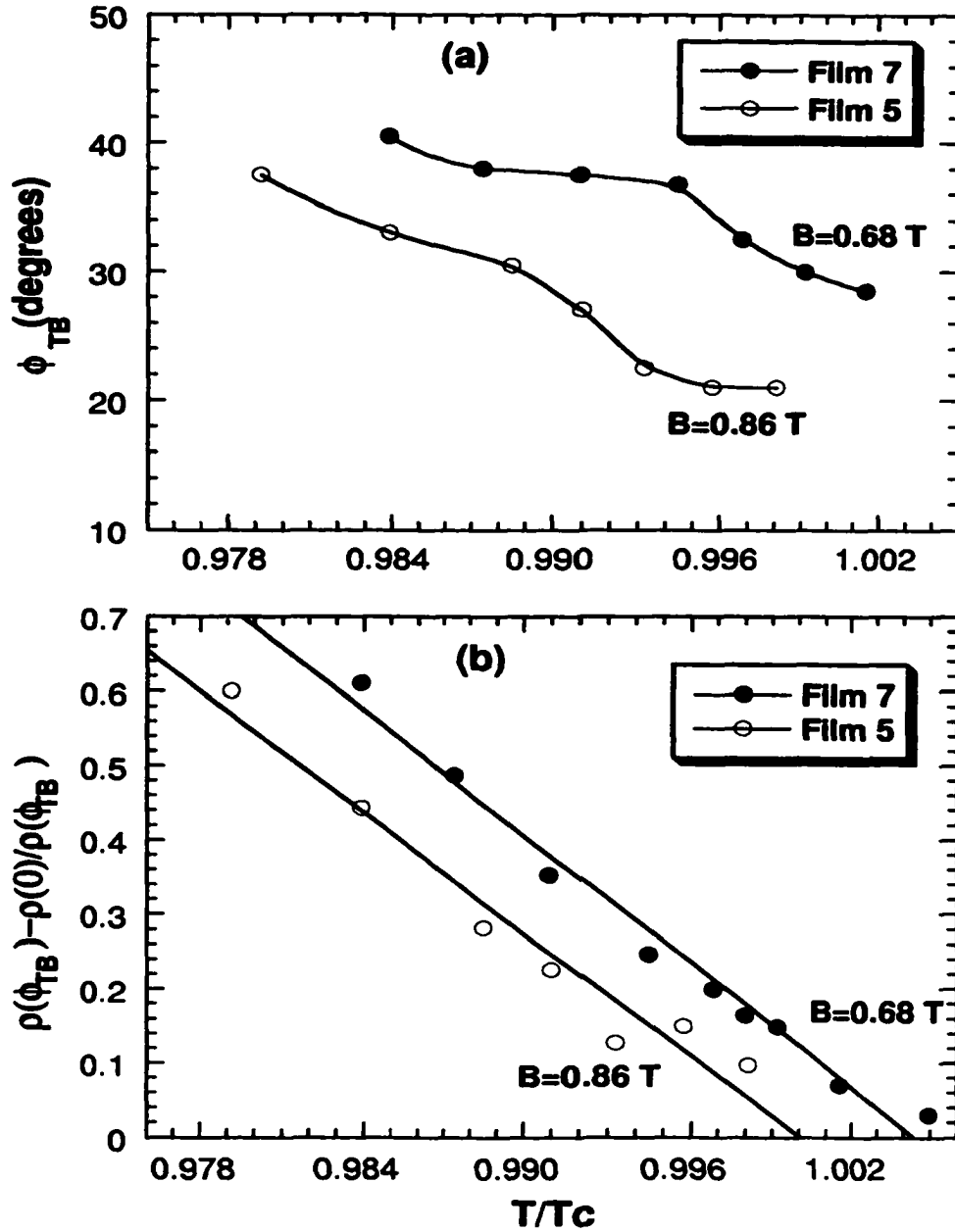
Figure 4.7: (a) The accommodation angle ϕ_{TB}, calculated from Fig.4.3, as a function of the reduced temperature T/T_c at a constant field for films 5 (open circles) and 7 (solid circles). ϕ_{TB} is defined as the half of the angular width between the two resistivity maxima surrounding the minimum in $\rho(\phi)$ [see Fig.4.4]. The solid lines are guides for the eye. (b) The normalized depth, calculated from Fig.4.3, as a function of the reduced temperature T/T_c at a constant field for films 5 (open circles) and 7 (solid circles). The normalized depth is defined as $\Delta\rho/\rho(\phi_{TB}) = [\rho(\phi_{TB}) - \rho(0^\circ)]/\rho(\phi_{TB})$. Note the linear decrease of $\Delta\rho/\rho(\phi_{TB})$ with temperature for both films. The solid lines are the linear fits to the experimental data.

92

order to see the effect of the field on the minimum clearly, each angular-dependent resistivity measured at a constant temperature and field has been normalized to the maximum resistivity at $\phi = \phi_{TB}$. The results of this normalization for film 5 is shown in Fig.4.8(c) for four different fields. The width of the minimum ($2\phi_{TB}$) and the normalized depth, $[\rho(\phi_{TB}) - \rho(0^o)]/\rho(\phi_{TB})$, increase with a decreasing field.

Fig.4.9(a) displays the field dependence of the accommodation angle, calculated from Fig.4.8, at a constant reduced temperature for films 5 and 7. The accommodation angle was found to decrease with an increasing field for both films.

Fig.4.9(b) shows the normalized depth $[\rho(\phi_{TB}) - \rho(0^o)]/\rho(\phi_{TB})$, calculated from Fig.4.8, as a function of magnetic field at a constant reduced temperature for films 5 and 7. For both films, the normalized depth was found to decrease smoothly with an increasing magnetic field over the entire range of fields investigated. The decrease in depth for film 7 is faster than that of film 5. The slopes of the linear parts for the field range between 0.5 to 0.9 T were -0.13/T and -0.64/T for films 5 and 7, respectively. This suggests that the TB pinning in film 5 could provide pinning for a larger range of magnetic fields (larger density of flux lines) compared to film 7 where the strength of TB pinning decreases much faster (five times faster) with an increasing field. In YBCO films the accommodation angle ϕ_{TB} decreases with an increasing field much faster in comparison to that for YBCO single crystals. For film 7, the slope of the linear part of the data in a field region between $0.45T$ and $0.9T$ is a about $-19.6^o/T$ [see Fig.4.9(a)] compared to $-1.6^o/T$ for single crystals [2], which is roughly an order of magnitude smaller than that for YBCO films. Paulius et al. reported a slope of $-16.7^o/T$ in untwinned YBCO single crystal irradiated with 1-GeV uranium ions [21].

4.2.4 Calculation of the pinning energy per unit length from the accommodation angle

It is possible to relate the observed angular dependence of resistivity to the microscopic pinning characteristics. This allows one to estimate the strength of the pinning

93
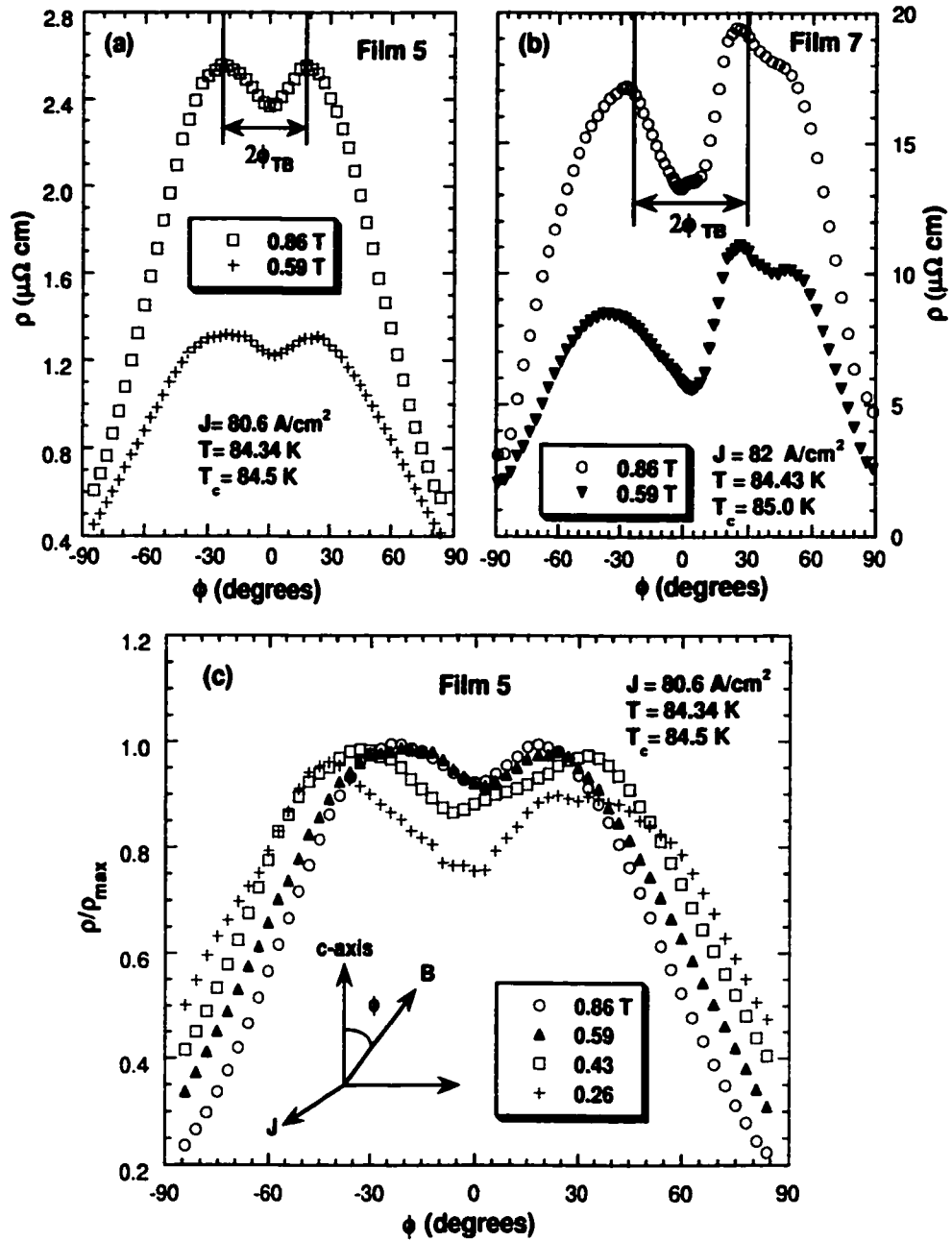
Figure 4.8: Angular dependence of resistivity $\rho(\phi)$ measured for fields of 0.59 T and 0.86 T at 84.34 K for film 5 (a) and at 84.43 K for film 7 (b). Note the difference between the width $(2\phi_{TB})$ and the depth $[\rho(\phi_{TB}) - \rho(0°)]/\rho(\phi_{TB})$ of the minimum between these films. (c) Normalized angular dependence of resistivity $\rho/\rho_{max} = \rho(\phi)/\rho(\phi_{TB})$ measured in four different fields at a constant temperature of 84.34 K for film 5. The width of the minimum ($2\phi_{TB}$) and the normalized depth, $[\rho(\phi_{TB}) - \rho(0°)]/\rho(\phi_{TB})$, are increasing with a decreasing field. The inset shows the experimental configuration where B is rotated off the c-axis and B $\perp$ J.

94
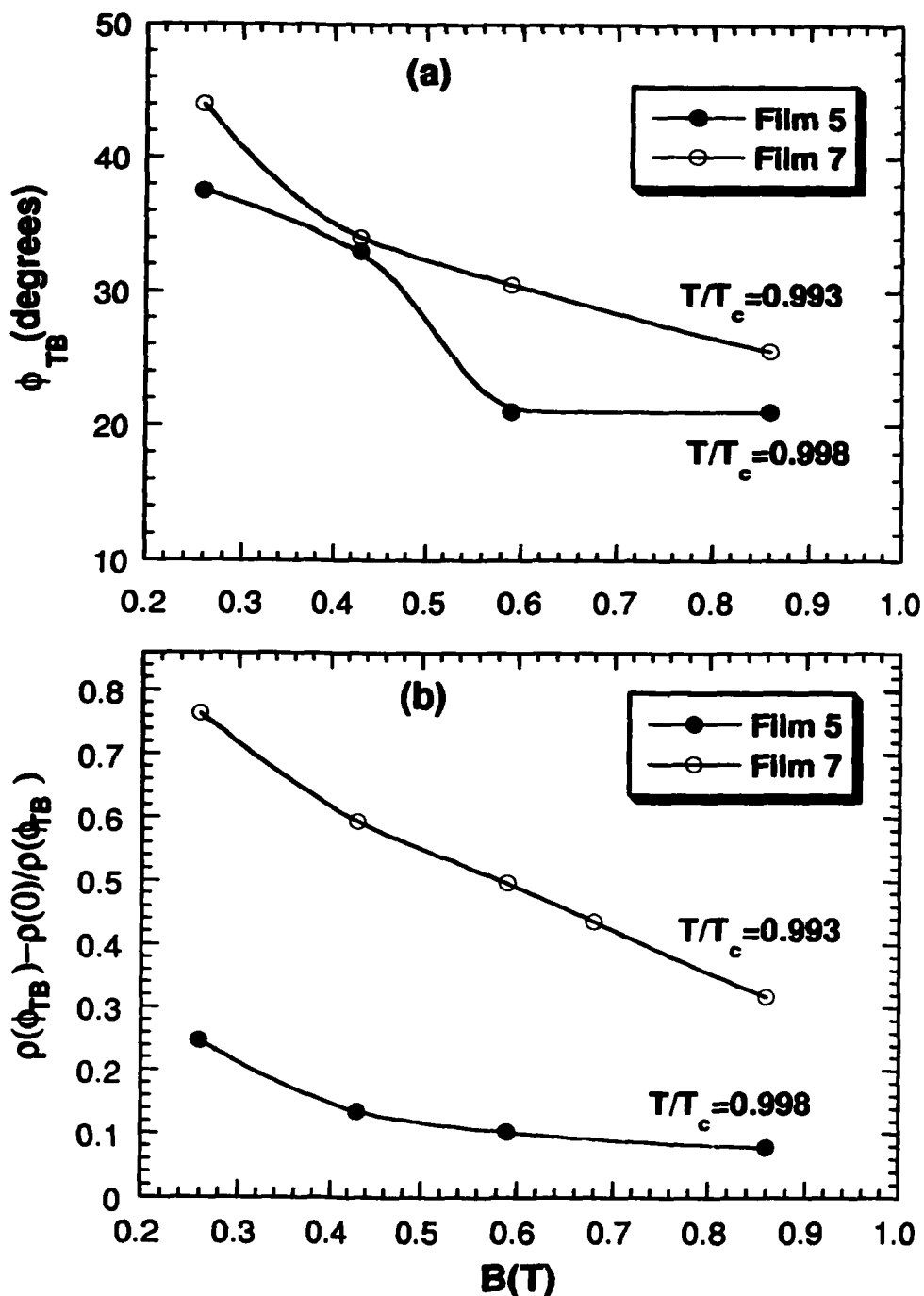
Figure 4.9: (a) The accommodation angle as a function of field, calculated from Fig.4.8, at a constant reduced temperature for films 5 (solid circles) and 7 (open circles). (b) The normalized depth $[\rho(\phi_{TB}) - \rho(0°)]/\rho(\phi_{TB})$, calculated from Fig.4.8, as a function of magnetic field at a constant reduced temperature for films 5 (solid circles) and 7 (open circles). Both the accommodation angle and the normalized depth decrease with an increasing field for both films. The solid lines are guides for the eye.

95

energy per unit length U_P from the depining angle. Sonin [27] studied pinning by twin boundary in terms of continuum electrodynamics for type II superconductors, which takes into account the elastic vortex-line tension, but neglects the shear rigidity of the vortex array. When the field is applied at angle ϕ with respect to the TB plane, the trapped vortex line in the TB consists of three regions: a trapped piece of length l_{tr} joined by two "healing" (non-trapped) regions traversing between neighboring TB's, as reported by Sonin [27]. At low temperatures, where the effect of thermal energies can be neglected, the depinning angle coincides with the accommodation angle. The accommodation angle is the angle at which the trapped length of the vortex line l_{tr} goes to zero [16]. The accommodation angle can be expressed as a function of the pinning energy per unit length of the linear correlated defect (TB)[21, 3] as

$$\tan \phi_{TB} = \sqrt{\frac{2U_P}{\epsilon_1}} \qquad (4.1)$$

where,

$$\epsilon_1 = \left(\frac{\Phi_0}{4\pi\lambda_c(T)}\right)^2 \ln\left[\frac{a_0}{\xi(T)}\right] \qquad (4.2)$$

is the linear tension of the vortex line in an anisotropic superconductor, $\Phi_0 = 2.07 \times 10^{-7} G\,cm^2$ is the flux quantum, $a_0 \sim (\Phi_0/B)^{1/2}$ is the distance between vortices, and $\lambda(T)$ and $\xi(T)$ are the temperature-dependent magnetic penetration depth and coherence length, respectively. Thermal fluctuations become important when $k_B T$ becomes of the order of the energy of the pinned vortex E_{pv}. At angles $\phi \leq \phi_{TB}$, where the characteristic trapped length l_{tr} is of the order of a_0/γ, $E_{pv} \sim U_p a_0/\gamma$. For $k_B T < U_p a_0/\gamma$, the depinning angle is very close to the accommodation angle. At higher temperatures when $k_B T > U_p a_0/\gamma$, the accommodation angle decreases due to thermal fluctuations and the pinning energy per unit length is given by [21, 3]

$$U_p = \epsilon_0 \left[\frac{2k_B T \tan \phi_{TB}}{\epsilon_0 a_0}\right]^{2/3} \qquad (4.3)$$

where k_B is the Boltzman constant and ϵ_0 is given by,

$$\epsilon_0 = \frac{\Phi_0^2}{(4\pi\lambda_{ab})^2} \qquad (4.4)$$

96

Using Eq.4.3 and the accommodation angles from Fig.4.7(a), one could estimate the pinning energy per unit length U_P as a function of temperature and at a constant field for films 5 and 7. In our calculations of U_P, we assumed a temperature-dependent penetration depth of the form $\lambda_{ab} = 1400\text{Å}/\sqrt{2(1 - T/T_{c0})}$ [21, 3]. Fig.4.10 shows the twin boundary pinning energy per unit length U_P (calculated from Eq.4.3) as a function of T/T_c for the same range of temperatures shown in Fig.4.7(a) for films 5 and 7. For both films, the TB pinning energy per unit length U_P was found to decrease smoothly with an increasing temperature over the entire range of temperatures investigated. For $T/T_c < 0.988$ these two films display almost the same behavior and have the same magnitude of U_P, however, for $T/T_c > 0.988$ the TB pinning energy of film 7 becomes larger than that of film 5 until they match again at T_c. The values that are obtained for films 5 and 7 are closely comparable to those obtained for twinned single crystals and about an order of magnitude smaller than that of irradiated crystals. Teresa et al. [3] reported a pinning energy of $U_P \approx 4 \times 10^7 \, K/cm$ at $T/T_c = 0.97$ and B=1 T, for YBCO twinned crystals. At the same temperature and field Paulius et al. [21] reported a value of $U_P \approx 2 \times 10^8 \, K/cm$ for irradiated untwinned YBCO single crystals. Twinned YBCO single crystal value is very close to our value of $U_P \approx 4.5 \times 10^7 \, K/cm$ at the same reduced temperature and a field of 0.86 T, while U_P of irradiated untwinned YBCO crystal is approximately five times larger than our U_P.

4.2.5 Mechanism of twin boundary pinning

The existence of a minimum in the angular dependence of resistivity for field alignments less than ϕ_{TB} off the TB's implies that vortices are pinned in the TB's over some part of their length. It has been shown experimentally [2] that the maximum effect of the TB pinning is achieved when the Lorentz force is normal to TB (i.e. applied current is parallel to TB's), since the large potential barriers associated with the planar interface of TB must be overcome. These barriers are due to strains associated with the interchange of the a and b axes across the twin plane and are present
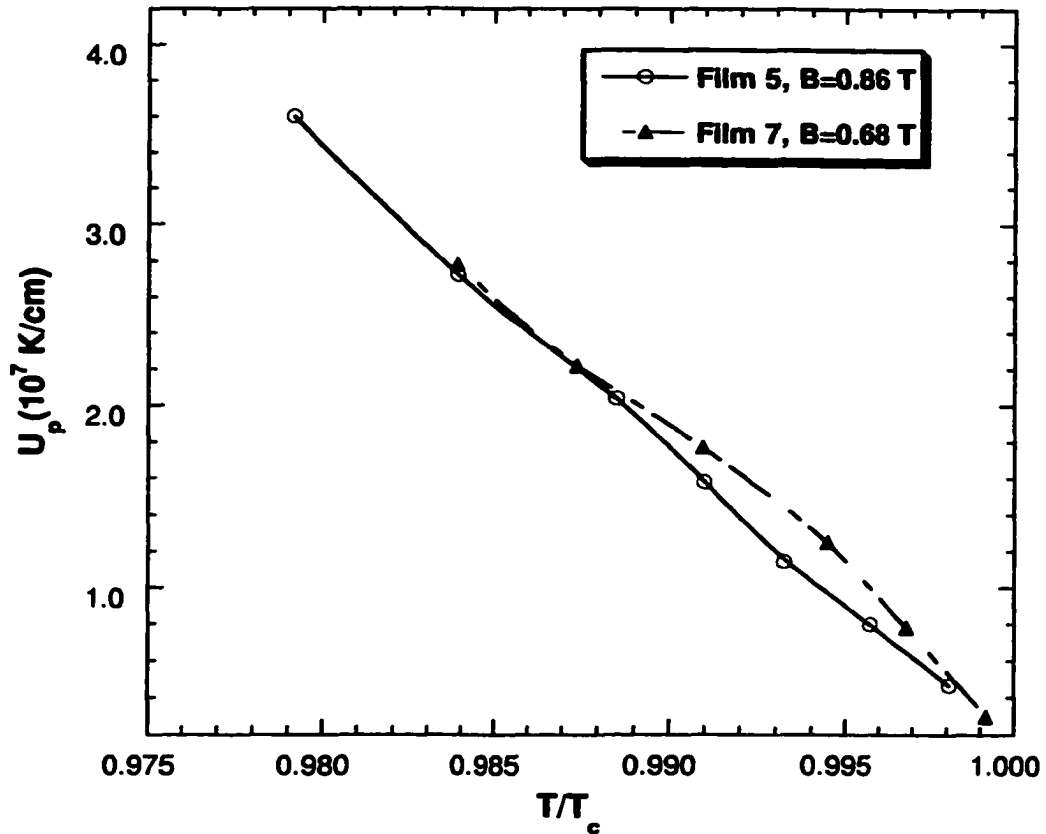
Figure 4.10:   Twin boundary pinning energy per unit length U_P (calculated from Eq.4.3 and the data in Fig.4.7(a) (see text) as a function of T/T_c at a constant magnetic field for films 5 (open circles) and 7 (solid triangles). The lines are guides for the eye.

even when TB's are free from atomic defects. The effect of TB pinning can also be seen when the Lorentz force is directed parallel to TB's. In this case the pinning is controlled by point-defects, which are likely to be enhanced in the TB's relative to the bulk.

The static configuration of a single vortex for a magnetic field oriented at an angle relative to TB's was considered in a model proposed by Blatter, Rhyner, and Vinokur [16]. The vortex configuration is determined by two competing energy contributions: the gain in energy due to pinning by TB's and the loss in elastic energy due to bending of the vortex line away from the internal field. When the magnetic field is parallel to the TB's, the vortex line is straight and pinned over its entire length

98

because of the low condensation energy of the TB's compared to the surrounding perfect superconductor. For a slight misalignment of the field relative to the TB's, the model assumes that the vortex line bends itself such that some segments $r(\phi)$ of the line remain in the TB's to take advantage of the reduced condensation energy. This results in a staircase vortex line, taking advantage of the pinning energy at each successive TB by following it for a finite length $r(\phi)$. As the magnetic field is rotated further away from the TB's, the elastic energy required to bend the line at each TB plane becomes greater, and the distance over which the vortex is pinned by the TB's decreases. The critical angle is defined as the angle at which $r(\phi)$ goes to zero and occurs when the loss in elastic energy equals the gain in the TB pinning energy $\Delta\epsilon$ which determines the critical angle $\phi_c = (2\Delta\epsilon/\epsilon_l)^{1/2}$, where ϵ_l is the tilt modulus of an isolated vortex [16, 2]. Above the critical angle, the cost of the elastic energy becomes so large that it is no longer energetically favorable for the vortex to bend itself and the vortex is then directed parallel to the internal field.

Using this staircase model, the strong dependence of the accommodation angle ϕ_{TB} on the magnetic field shown in Fig.4.9(a) can be explained qualitatively. In this model, the structure of the staircase pattern depends on the competition between the TB pinning energy (favoring alignment of the vortex line with the TB) and the elastic bending energy (favoring alignment of the vortex with the internal field). As the field increases, the elastic bending energy for a certain angular displacement from the TB also increases, while the TB pinning energy remains essentially constant. Since the accommodation angle ϕ_{TB} is the angle at which the two energies are equal, then the increase in field requires a reduction in the angle in order to reach this equality between the two energies. Thus, the pinning effect, and the accommodation angle ϕ_{TB}, are reduced with an increasing field.

4.3 Summary and Conclusions

We have investigated the angular dependence of resistivity $\rho(\phi)$ for the angular range $(-90^o \geq \phi \leq +90^o)$ close to T_c in YBCO thin films. We have found that only a few films exhibited a minimum in $\rho(\phi)$ near $\phi = 0^o$ (B $\parallel$ c-axis) which is typical of magnetic pinning at twin boundaries. Most of the YBCO films display a broad maximum around $\phi = 0^o$. Our results did not reveal any relationship between the magnitude of the critical current density and the existence of a minimum in $\rho(\phi)$ near $\phi = 0^o$. The width (ϕ_{TB}) and the depth of the minimum decreases with an increasing temperature and an increasing magnetic field.

The question is why the minimum in $\rho(\phi)$ due to TB's does not show up in all YBCO thin films since all of them are twinned. Our investigations of the minimum around $\phi = 0^o$ in the angular dependence of resistivity for field rotations off the c-axis, showed that this minimum is present only in films that were deposited very slowly, thus allowing the growth of crystallographically well-defined and sharp TB's. Films 5, 6, and 7, which showed a minimum, were grown using the rf-magnetron deposition techniques with sputtering time ranging from 14 to 18 hours while films 3 and 4, which did not show a minimum, were grown using laser-ablation technique with a short deposition time between 15 and 20 minutes. The absence of the minimum in $\rho(\phi)$ in those films (grown fast) suggests that thin film growth leads to disordered TB's [28] which are a weak flux pinning centers. In YBCO the twins nucleate during the tetragonal-to-orthorhombic phase transformation. The twin spacing and colony size are optimized to accommodate the strain in the local environment. Sarikaya and Stern [29] attributed the variations in twin spacing to variations in oxygen content and local changes in orthorhombicity. This suggests that slow growth of the film allows sufficient time for a smooth transition from a tetragonal phase to an orthorhombic phase, which produces well-defined sharp twin boundaries. Thus, this may provide a possibility of explaining why the minimum in $\rho(\phi)$ near $\phi = 0^o$ does not appear in YBCO films which are grown rapidly resulting in a formation of thick disordered and interfering TB's. In order to confirm this, one has to do a careful investigation of

100

both types of films (those with and without a minimum) using transmission electron microscope. Polarized light microscope studies on both types of films did not reveal any difference in the structure between the two types. Careful investigation using high magnification ratio up to 1000 times on films with a minimum did not show any trace of twin boundaries in these films. This may suggest that, unlike YBCO single crystals, the twin boundaries spacing is very small to be seen using optical devices (like the polarized light microscope). Scanning electron microscope studies of the surface of the thick films that showed a minimum, revealed the existence of granular structure with an average size of the grain of about $0.4\mu m$. We could not see any twinning within the grains themselves, which may suggest that the strong pinning could be due to the grain boundaries instead of twin boundaries. Other films (that showed a minimum around $\phi = 0^o$) showed an array of holes similar to that seen in an irradiated samples (columnar defects). These holes could be a source of strong pinning. An additional structural investigations are needed in order to reach a more conclusive decision about the nature of the pinning that causes this type of minimum near $\phi = 0^o$.

Bibliography

[1] T. Roy, T. E. Mitchell, Philos. Mag. A **63**, 225 (1991).

[2] S. Fleshler, Wai-Kwong Kwok, U. Welp, V. M. Vinokur, M. K. Smith, J. Downey, G. W. Crabtree , Phys. Rev. B **47**, 14448(1993).

[3] T. Puig, Z. Obradors, Phys. Rev. Lett. **84**, 1571 (2000).

[4] T. Puig, F. Galante, E. M. Gonzalez, J. L. Vicent, B. Martinez, X. Obradors , Phys. Rev. B **60**, 13099 (1999).

[5] G.W. Crabtree, W.K. Kwok, U. Welp, J. Downey, S. Fleshler, K.G. Vandervoort, Physica C **185-189**, 282 (1991).

[6] M. Yethiraj, H. A. Mook, G. D. Wignall, R. Cubitt, E. M. Forgan, D. M. Paul, T. Armstrong , Phys. Rev. Lett. **70**, 857 (1993).

[7] G.J. Dolan, G.V. Chandrashekhar, T.R. Dinger, C. Feild, F. Holtzberg , Phys. Rev. Lett. **62**, 827 (1989).

[8] P. L. Gammel, C. A. Duran, D. J. Bishop, V. G. Kogan, M. Ledvij, A. Yu. Simonov, J. P. Rice, D. M. Ginsberg , Phys. Rev. Lett. **69**, 3808 (1992).

[9] G. W. Crabtree, J. Z. Liu, A. Umezawa, W. K. Kwok, C. H. Sowers, S. K. Malik, B. W. Veal, D. J. Lam, M. B. Brodsky, J. W. Downey , Phys. Rev. B. **36**, 4021 (1987).

[10] J. Z. Liu, Y. X. Jia, R. N. Shelton, M. J. Fluss , Phys. Rev. Lett. **66**, 1354 (1991).

[11] V. K. Vlasko-Vlasov, L. A. Dorosinskii, A. A. Polyanskii, V. I. Nikitenko, U. Welp, B. W. Veal, G. W. Crabtree, Phys. Rev. Lett. **72**, 3246 (1994).

[12] W. K. Kwok, U. Welp, G. W. Crabtree, K. G. Vandervoort, R. Hulscher, J. Z. Liu , Phys. Rev. Lett. **64**, 966 (1990).

[13] B. Janossy, R. Hergt, L. Fruchter, Physica C **170**, 22 (1990).

[14] B. Roas, L. Schultz, G. SaemannIschenko, Phys. Rev. Lett. **64**, 479 (1990).

[15] H. Safar, S.R. Foltyn, Q. X. Jia, M.P. Maley, Philos. Mag. B **74**, 647 (1996).

[16] G. Blatter, J. Rhyner, V. M. Vinokur, Phys. Rev. B **43**, 7826 (1991).

[17] D. R. Nelson, V. M. Vinokur, Phys. Rev. B **48**, 13060 (1993).

[18] A. Casaca, G. Bonfait, M. Getta, M. Lenkens, G. Muller, Phys. Rev. B **56**, 5677 (1997).

[19] M. Charalambous, J. Chaussy, P. Lejay, Phys. Rev. B **45**, 5091 (1992).

[20] W. K. Kwok, L. M. Paulius, V. M. Vinokur, A. M. Petrean, R. M. Ronningen, G. W. Crabtree , Phys. Rev. Lett. **80**, 600 (1998).

[21] L. M. Paulius, J. A. Fendrich, W.-K. Kwok, A. E. Koshelev, V. M. Vinokur, G. W. Crabtree, B. G. Glagola , Phys. Rev. B **56**, 913 (1997).

[22] V. S. Bobrov, M. A. Lebyodkin, Physica C **178**, 411 (1991).

[23] F. Galante, E. Rodriguez, J. Fontcuberta, X. Obradors , Physica C **296**, 96 (1998).

[24] H. Darhmaoui, J. Jung, Phys. Rev. B **53**, 14621 (1996).

[25] R. Hergt, W. Andrä, W. Schüppel, Phys. Status Solidi A **122**, K51 (1990).

[26] I. V. Grigori'eva, L. A. Gurevich, L. Ya. Vinnikov , Physica C **195**, 327 (1992).

[27] Sonin, Phys. Rev. B **48**, 10487 (1993).

[28] M. Suenaga, private communications.

[29] M. Sarikaya, E. A. Stern, Phys. Rev. B **37**, 9373 (1988).

104

Chapter 5

Large Variation in Intrinsic Anisotropy of YBCO Thin Films

5.1 Introduction

Most of high-T_c layered cuprates, including Bi-based and highly oxygen-deficient $YBa_2Cu_3O_{7-\delta}$ ($\delta > 0.3$), are quasi-2D materials exhibiting weak interlayer coupling and large resistivity anisotropies ρ_c/ρ_{ab} ranging from 10^5 in $Bi_2Sr_2CaCu_2O_8$ to 10^3 in oxygen-deficient $YBa_2Cu_3O_{6.7}$ [1]. The anisotropy is defined as the ratio of the effective masses of the Cooper pair motion in the CuO_2 planes to that along the c-axis and expressed as $\gamma = \sqrt{\frac{m_c}{m_{ab}}} = \frac{\xi_{ab}}{\xi_c} = \frac{\lambda_c}{\lambda_{ab}}$, where ξ and λ are the temperature dependent coherence length and magnetic penetration depth, respectively. Estimations of γ have been made from extensive studies of the normal state resistivity, magnetic penetration depth, coherence length (through the upper critical field) and the torque measurements in the ab-planes and along the c-axis. These studies have shown that for $YBa_2Cu_3O_{7-\delta}$, γ increases with a decreasing oxygen doping from 7 for optimal doping ($\delta = 0.05$) up to about 30 for an extremely underdoped case ($\delta = 0.3$). On the other hand $Bi_2Sr_2CaCu_2O_8$ (BSCCO) exhibits a 2D anisotropy with γ as high as 140 [1]. This high anisotropy is generally accompanied by a "semiconducting-like" increase in the c-axis resistivity ρ_c near T_c, $[\rho_c \sim T^{-\alpha}(0 < \alpha < 2)]$.

Experimental evidence about the dimensionality of superconducting thin films is usually obtained from the angular dependence of the upper critical field H_{c_2}. Tinkham [2] was the first to point out that while the angular dependence of the H_{c_2} is a continuous differentiable function in 3D GL theory, $H_{c_2}(\theta)$ shows a "cusp-like" behavior with a discontinuous derivative in a 2D thin film limit. Naughton et al. [3] reported that $H_{c_2}(\theta)$ (with θ measured from the ab-planes) of $YBa_2Cu_3O_{6.9}$, shows a smooth behavior around $\theta = 0^o$ in accord with the 3D-GL theory. On the other hand, a 2D cusp-like $H_{c_2}(\theta)$ with a sharp peak at $\theta = 0^o$, has been observed in BSCCO [3]. Bauhofer et.al. [4] studied the angular dependence of H_{c_2} in YBCO as a function of oxygen deficiency. A 3D-like H_{c_2} has been observed in $YBa_2Cu_3O_{6.9}$ while a 2D cusp-like H_{c_2} has been seen in $YBa_2Cu_3O_{6.6}$. Anisotropy of the latter composition was found to be $\gamma = 40$ [4]. Difficulty with the measurement of H_{c_2} in high-T_c superconductors is that this field can not be accurately determined from the dependence of resistive transition on the magnetic field, due to thermally activated flux flow.

Anisotropy of the electronic properties can be viewed as a direct consequence of anisotropy of the crystallographic structure. The distance d between the CuO_2 bilayers for BSCCO (2212) (15.5Å) is much higher than that for YBCO(123) compound (11.7Å). Depending on the value of ξ_c with respect to d, layered superconductors can be described either by the 3D anisotropic GL effective-mass model or with the Lawrence-Doniach model for 2D superconducting layers weakly coupled by Josephson junctions [5]. For temperatures close to T_c, $\xi_c(T) = \xi_c(0)/\sqrt{1 - T/T_c}$ is large enough for superconductor to be described in terms of the 3D-GL model. However, a dimensional crossover from 3D to 2D behavior is expected to happen at temperatures for which ξ_c is less than the layer spacing d. According to the Lawrence-Doniach model, if a magnetic field is strictly parallel to the ab-planes, $H_{c2}^{\|ab}$ is predicted to diverge at a temperature T^* for which $\xi_c(T^*) = d/\sqrt{2}$. On the other hand, at lower temperatures the vortex core lies between the layers and if each layer is treated as a 2D superconductor of zero thickness, it will have an infinite critical field. The 3D-2D crossover temperature T^* can be calculated from the expression $\gamma^2(1 - T^*/T_c) = 2[\xi_{ab}(0)/d]^2$

106

[6]. For BSCCO with $\xi_{ab}(0) = 2.7 - 3.8\,nm$, $d = 1.2\,nm$ and $\gamma \sim 50 - 70$, one obtains $T^*/T_c = 0.996$. For YBCO with $\xi_{ab}(0) = 1.6 - 2.4\,nm$, $d = 1.2\,nm$ and $\gamma \sim 5$, one gets $T^*/T_c = 0.68$. This implies that YBCO behaves like a 3D superconductor at temperatures down to about 60 K, whereas for BSCCO a crossover to a 2D behavior occurs at temperatures less than 0.4 K below T_c.

When the coupling between the superconducting layers becomes very weak, description of a superconductor in terms of superconducting layers coupled by 2D Josephson junctions is more realistic than that given by the 3D-GL model. In a 2D description the order parameter is large in the CuO_2 planes, but almost vanishes between the layers. This leads to a breakdown of Abrikosov's Flux-Line-Lattice (FLL) model when a magnetic field is applied parallel to the ab-planes, which also implies that the formation of FLL is only related to the field component perpendicular to the layers [7].

Anisotropy reveals itself clearly in the dependence of resistivity on the angle between the ab-planes and the direction of an applied magnetic field **B**. For very highly anisotropic cuprates, with both field and current applied parallel to the ab-planes, the angular dependence of resistivity is independent of the angle between the direction of magnetic field **B** and the direction of applied current **J** [8]. This behavior contradicts the standard flux flow picture where dissipation stems from the Lorentz force which acts on the flux lines and therefore strongly depends on the angle between **B** and **J**. High anisotropy is also responsible for a sharp minimum in the angular dependence of resistivity $\rho(\theta)$ as the magnetic field is brought very close to the ab-planes ($\theta \simeq 0^o$). Moreover, the minimum at $\theta = 0^o$ is almost independent of the magnitude of the applied field. Since highly anisotropic superconductors behave like 2D ones, the resistivity is expected to depend only on the vertical component of the field (c-axis component) and therefore should scale with $B\sin\theta$. On the other hand, for less anisotropic cuprates, $\rho(\theta)$ depends on the angle between **B** and **J** and the difference between $\rho(0^o)$ (**B** ||ab-plane) and $\rho(90^o)$ (**B** ||c-axis) decreases with a decreasing anisotropy. For **B** close to the ab-planes, $\rho(\theta)$ has a flat behavior with no

sharp minimum. In this case, the angular dependent resistivity can be scaled using the anisotropic 3D-GL model.

Angular dependence of resistivity has been studied extensively by many groups [9, 10, 11, 12]. Iye et al. studied the resistivity of both YBCO and BSCCO thin films for magnetic field applied close to the ab-planes as a function of the angle between $\mathbf{B}$ and $\mathbf{J}$ (both in the ab-planes). Their results revealed that $\rho(\phi)$ depends on the angle ϕ between $\mathbf{B}$ and $\mathbf{J}$ for YBCO, but it is independent of ϕ for BSCCO [9]. Moreover, for YBCO they noticed that the dependence on ϕ diminishes and the minimum in $\rho(\theta)$ becomes sharper as the film thickness decreases, which indicates that YBCO approaches a 2D limit with a decreasing thickness [10]. For BSCCO they observed a very sharp minimum in $\rho(\theta)$ at $\theta = 0°$. $\rho(\theta)$ in BSCCO scales almost perfectly with $B \sin \theta$ except for very small angles $\theta < 1°$, which reflects finite dimensionality of the sample [9, 13, 14]. Kwok et al. [15] studied $\rho(\theta)$ for both twinned and untwinned single crystals of optimally doped YBCO. They reported an observation of a very sharp minimum (of width $\sim 0.5°$) in $\rho(\theta)$ that occurs only when the magnetic field direction is below a critical angle $\theta_c < 1°$ from the CuO_2 planes. This sharp minimum has been seen only for $\mathbf{B} \perp \mathbf{J}$ orientation while for $\mathbf{B} \parallel \mathbf{J}$ such an effect has not been observed. The resistivity for $\mathbf{B} \parallel \mathbf{J}$ is lower by one order of magnitude from that for $\mathbf{B} \perp \mathbf{J}$. They explained this sharp minimum in terms of a lock-in transition of vortices in the ab-planes due to a very strong intrinsic pinning.

The experiments described above suggest that the measurement of the angular dependence of resistivity could be used to obtain a quantitative estimation of the anisotropy factor γ in high-T_c materials through using the scaling laws. Comprehensive investigations of anisotropy in YBCO thin films or crystals of different T_c using scaling laws were not performed before. Most experimental studies of an optimally doped YBCO assume a constant value of the anisotropy factor $\gamma \sim 5 - 7$, which is underestimated in many cases.

We have used the measurements of angular dependence of resistivity and the scaling laws, to study anisotropy of fifteen different YBCO thin films (both optimally

doped and underdoped) of various thickness and preparation techniques. Our results revealed a large variation of the anisotropy factor from a 3D to a 2D-like in these films. The anisotropy does not depend on the transition temperature, thickness or critical current density.

5.2 Experimental results

Temperature dependence of resistivity $\rho(T)$ for four YBCO thin film samples (see Table 5.1) described in this Chapter has been measured in a zero magnetic field over a temperature range between $T_{c_0}(\rho = 0, \mathbf{B} = 0)$ and 300 K. $\rho(T)$ has been investigated for different orientations of the magnetic field with respect to the direction of current density $\mathbf{J}$ for a smaller range of temperatures between $T_{c_0}(\rho = 0, \mathbf{B})$ and 100 K. A semi-logarithmic plot of the temperature dependence of resistivity in zero magnetic field and a temperature range of T_{c_0}-100 K , for four YBCO films is shown in Fig.5.1(a). A plot of the normalized resistivity $\rho/\rho(100K)$ as a function of the normalized temperature T/T_c in a zero magnetic field is shown in Fig.5.1(b).

Fig.5.2(a) shows two possible orientations of the magnetic field $\mathbf{B}$ with respect to $\mathbf{J}$ and the ab-plane of the films, used in the experiments. The left figure illustrates the case where the field $\mathbf{B}$ is rotated in a plane which is parallel to the direction of $\mathbf{J}$, while the right one represents the case where $\mathbf{B}$ is rotated in a plane perpendicular to $\mathbf{J}$. We refer to the first configuration as $\mathbf{B} \parallel \mathbf{J}$ and the second one as $\mathbf{B} \perp \mathbf{J}$. Resistivity measurements for each YBCO film in a constant field were carried out for three different orientations of $\mathbf{B}$ relative to $\mathbf{J}$: $\mathbf{B} \parallel \mathbf{J}$ (with $\mathbf{B} \parallel$ ab-planes, i.e $\theta = 0^o$), $\mathbf{B} \perp \mathbf{J}$ (with $\mathbf{B} \parallel$ ab-planes, i.e $\theta = 0^o$) and $\mathbf{B} \parallel$ c-axis (with $\mathbf{B} \perp \mathbf{J}$, i.e $\theta = 90^o$). A semi-logarithmic plots of the resistivity as a function of temperature in a field of 0.68 T for these orientations as well as for $\mathbf{B}=0$, are shown in Figures 5.2 and 5.3.

Comparisons of $\rho(T)$ for four different YBCO films show that the difference between T_{c_0} for $\mathbf{B}=0$ and $\mathbf{B} \parallel$ c-axis: $\Delta T'_{c_0} = T_{c_0}(\mathbf{B} = 0) - T_{c_0}(\mathbf{B} \parallel \text{c-axis})$ increases from

109
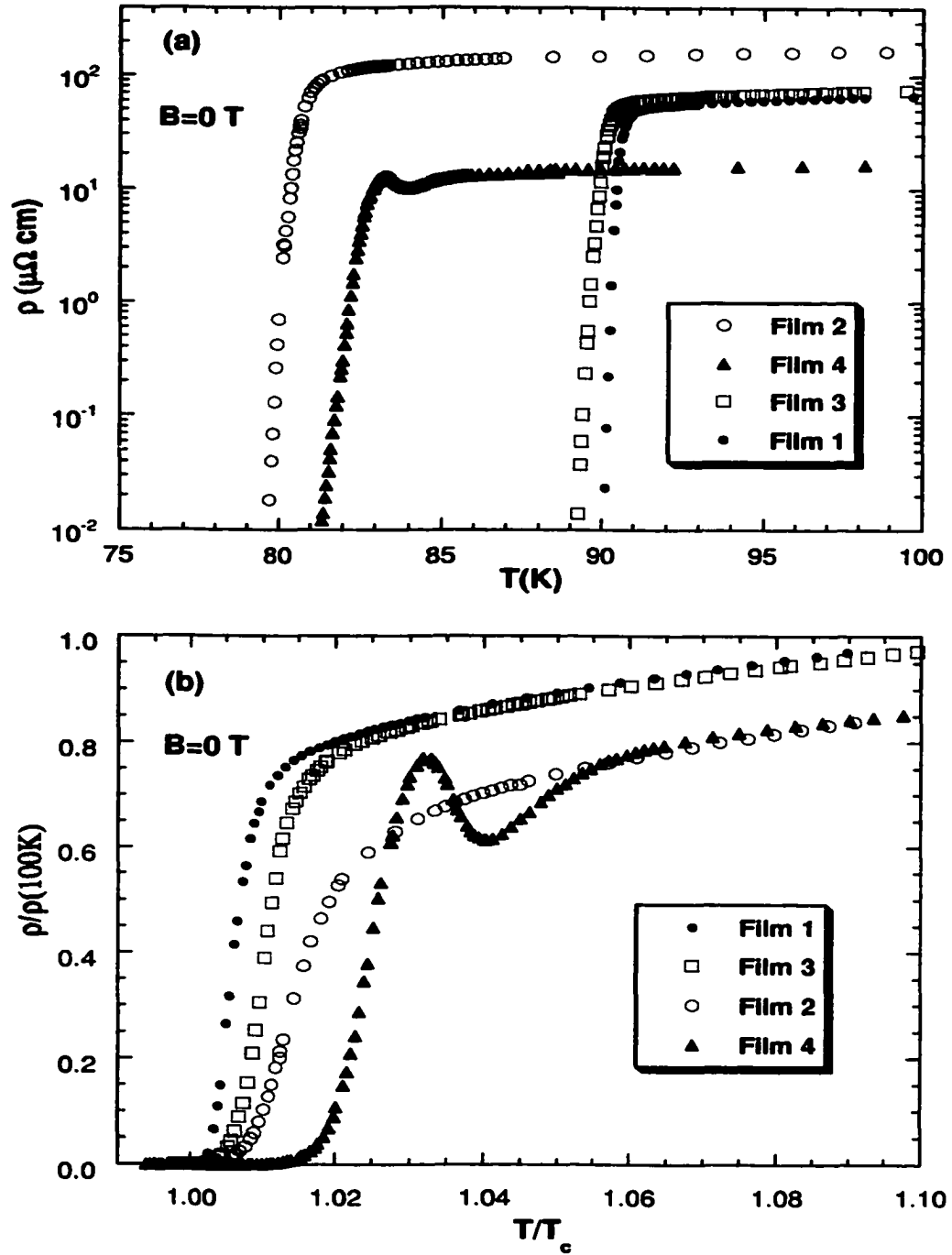
Figure 5.1: (a) A semi-log plot of the temperature dependence of resistivity for four YBCO thin films of different T_c (see Table 5.1) measured in a zero magnetic field. (b) the corresponding normalized resistivity $[\rho/\rho(100K)]$ as a function of the normalized temperature (T/T_c).

110
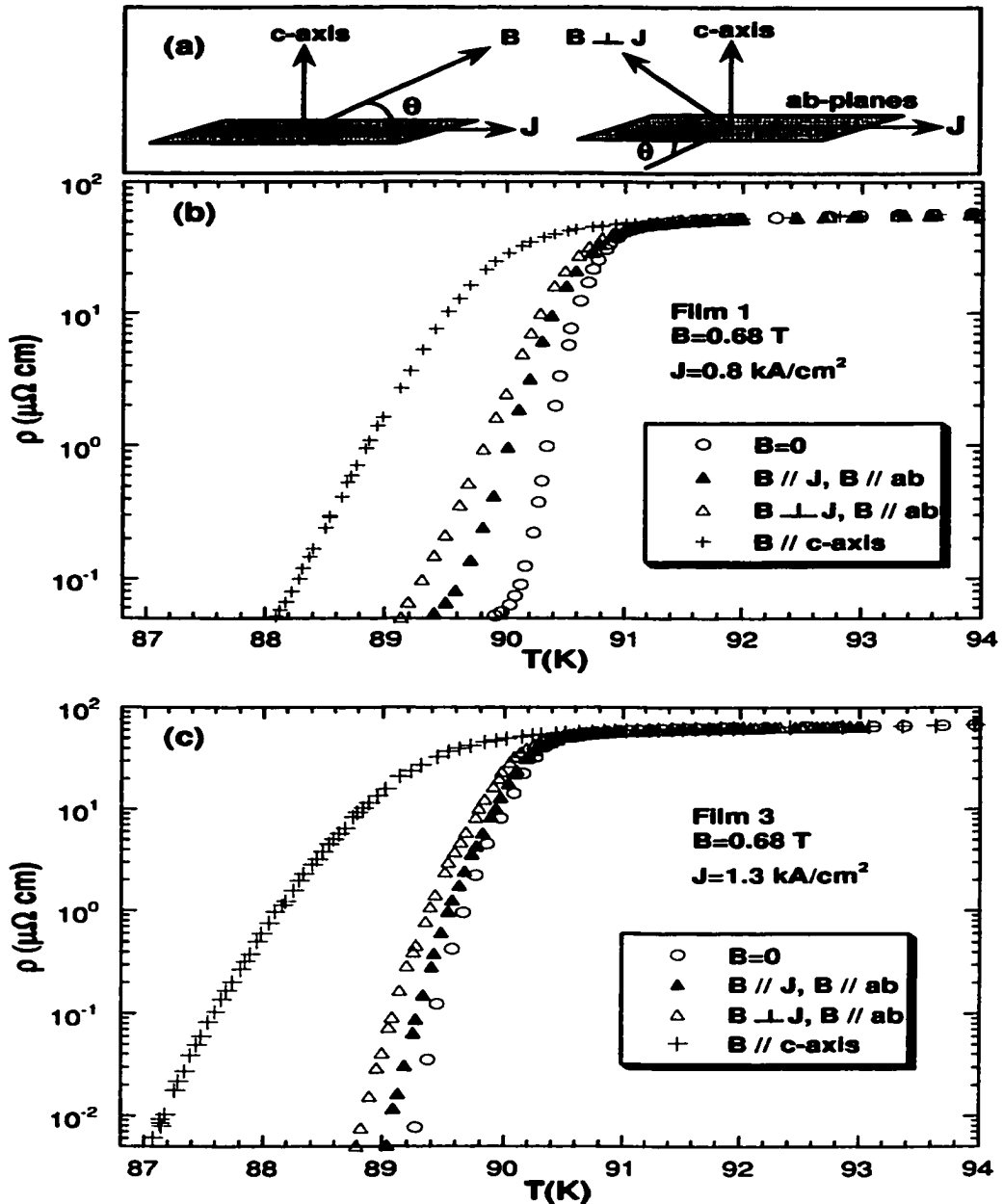
Figure 5.2: (a) Two configurations of **B** with respect **J** that were used during the measurements of the angular dependence of resistivity $\rho(\theta)$ in a magnetic field: **B** is rotated in a plane parallel to both **J** and the c-axis (left side), or **B** is rotated in a plane parallel to the c-axis but perpendicular to **J** (right side). A semi-log plots of the resistivity as a function of temperature measured in B=0 and B=0.68 T for film 1 (b) and film 3 (c). The measurements in B=0.68 T were carried out for three different orientations of **B** relative to **J** : **B** ∥ **J** (with **B** ∥ ab-planes, i.e $\theta = 0°$), **B** ⊥ **J** (with **B** ∥ ab-planes, i.e $\theta = 0°$) and **B** ∥ c-axis (with **B** ⊥ **J**, i.e $\theta = 90°$). Note that the shift in T_c between the (**B** ⊥ **J** ∥) ab-planes and **B** ∥ c-axis orientations for film 1 is about 1.0 K and that for film 3 is about 1.7 K.

111
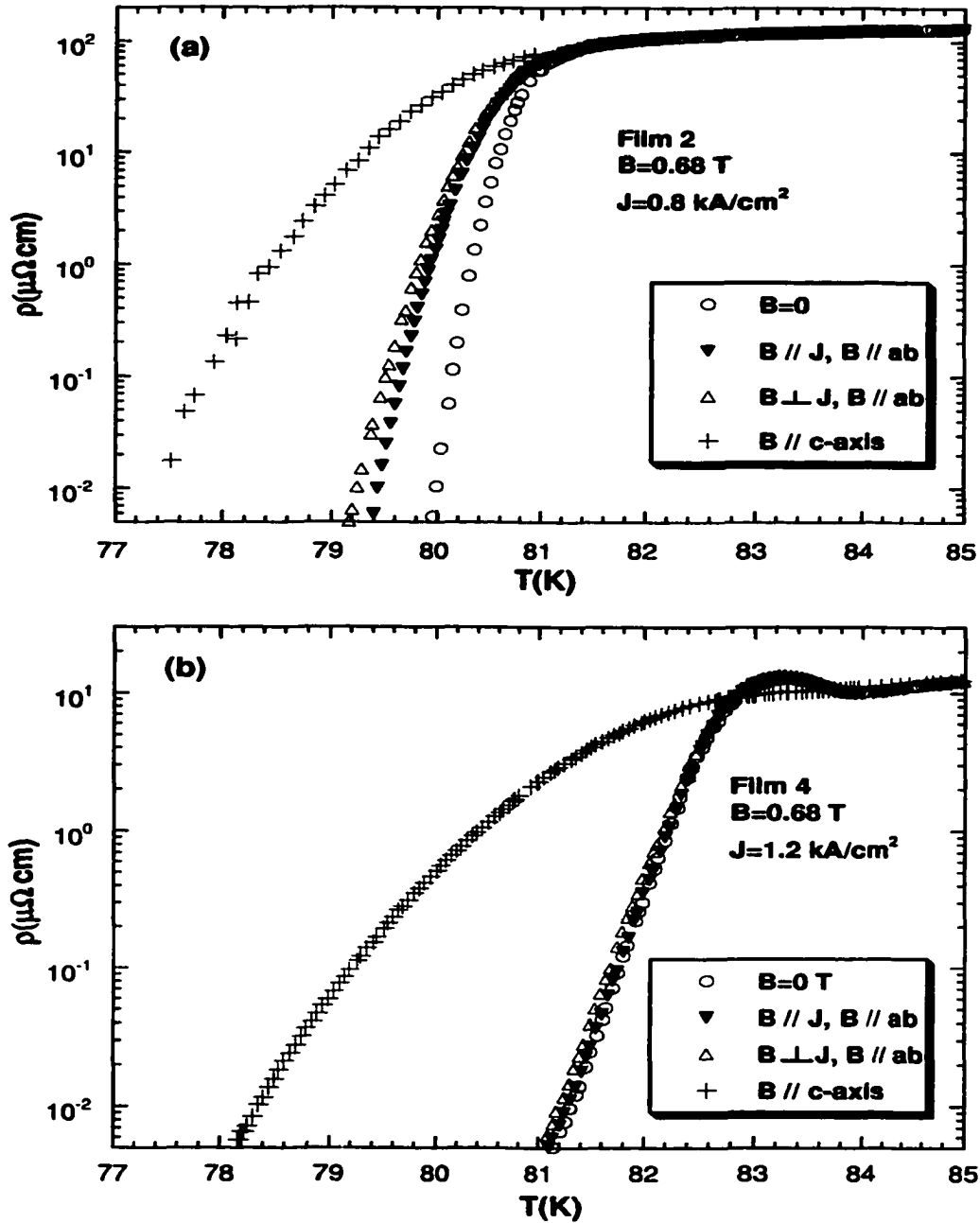
Figure 5.3: A semi-log plots of the resistivity as a function of temperature measured in B=0 and B=0.68 T for film 2 (a) and film 4 (b). The measurements in B= 0.68 T were carried out in three different orientations of **B** relative to **J** : **B** || **J** (with **B** || ab-planes, i.e $\theta = 0°$), **B** $\perp$ **J** (with **B** || ab-planes, i.e $\theta = 0°$) and **B** || c-axis (with **B** $\perp$ **J**, i.e $\theta = 90°$). Note that the shift in T_c between the (**B** $\perp$ **J** ||) ab-planes and **B** || c-axis orientations for film 2 is about 2.0 K and that for film 4 is about 3.0 K. Notice also the overlap of the data for film 4 for the three configurations: **B** || **J**, **B** $\perp$ **J**, and B=0 T.

112

about 2 K for optimally doped films 1 and 3 up to about 3 K for underdoped films 2 and 4. While $\Delta T'_{c0}$ increases with a decreasing T_{c0} ($B = 0$), there is no correlation between $\Delta T'_{c0}$ and J_c or $\rho(100K)$ (see Table 5.1). On the other hand, the difference between $T_{c0}(B = 0)$ and $T_{c0}[B \perp J$ with $B \parallel$ ab-planes] or between T_{c0} ($B = 0$) and $T_{c0}[B \parallel J$ with $B \parallel$ ab-planes] is sample dependent. There is no relationship between $\Delta T''_{c0} = T_{c0}(B = 0) - T_{c0}$ ($B \perp J$, $B \parallel$ ab-planes) and T_c, J_c or $\rho(100K)$ listed in Table 5.1. However, there is some correlation between $\Delta T''_{c0}$ and the magnitude of ρ measured with $B \parallel$ ab-planes close to T_{c0} at $T/T_{c0} = 0.99$.

Film 4 [see Fig.5.3(b)] shows a unique behavior of resistivity. Unlike all other films studied, for $B \parallel$ab-planes the resistivity of this film does not depend on the magnitude of the applied field or the angle between the field and the current directions for temperatures below 82.8 K. Moreover, there is a very large anisotropy in resistivity between $B \parallel$ ab-planes and $B \parallel$ c-axis. This film also exhibits a peak in $\rho(T)$ close to T_c onset. This peak disappears when B is oriented along the c-axis. This peak is not caused by the phase separation but by the resistivity induced phase-slip events (see next Chapter).

Angular dependence of resistivity $\rho(\theta)$ in a magnetic field at different temperatures, has been measured for both $B \parallel J$ and $B \perp J$ configurations for an angular range from -20° to $+20^o$. Fig.5.4 presents $\rho(\theta)$ for four YBCO samples in a magnetic field of 0.68 T (for $B \perp J$ orientation) at a constant reduced temperature $T/T_c = 0.990$. For all samples, $\rho(\theta)$ displays a minimum at $\theta = 0^o$. The width of this minimum is sample dependent. Film 4, which has the lowest resistivity at $\theta = 0^o$ among all films studied, shows the smallest width of the minimum, while film 1 which has the highest resistivity, shows a very broad minimum. There is no correlation between the width of the minimum and T_{c0}.

Figures 5.5 and 5.6 display the normalized resistivity $(\rho/\rho(10^o)_{B\perp J})$ as a function of θ for both $B \parallel J$ and $B \perp J$ configurations, at a fixed temperature and field for all four films. The data in Figures 5.5 and 5.6 revealed sample dependent variations of $\rho(\theta)$ when B is rotated from the ab-planes for both $B \parallel J$ and $B \perp J$ orientations.

113
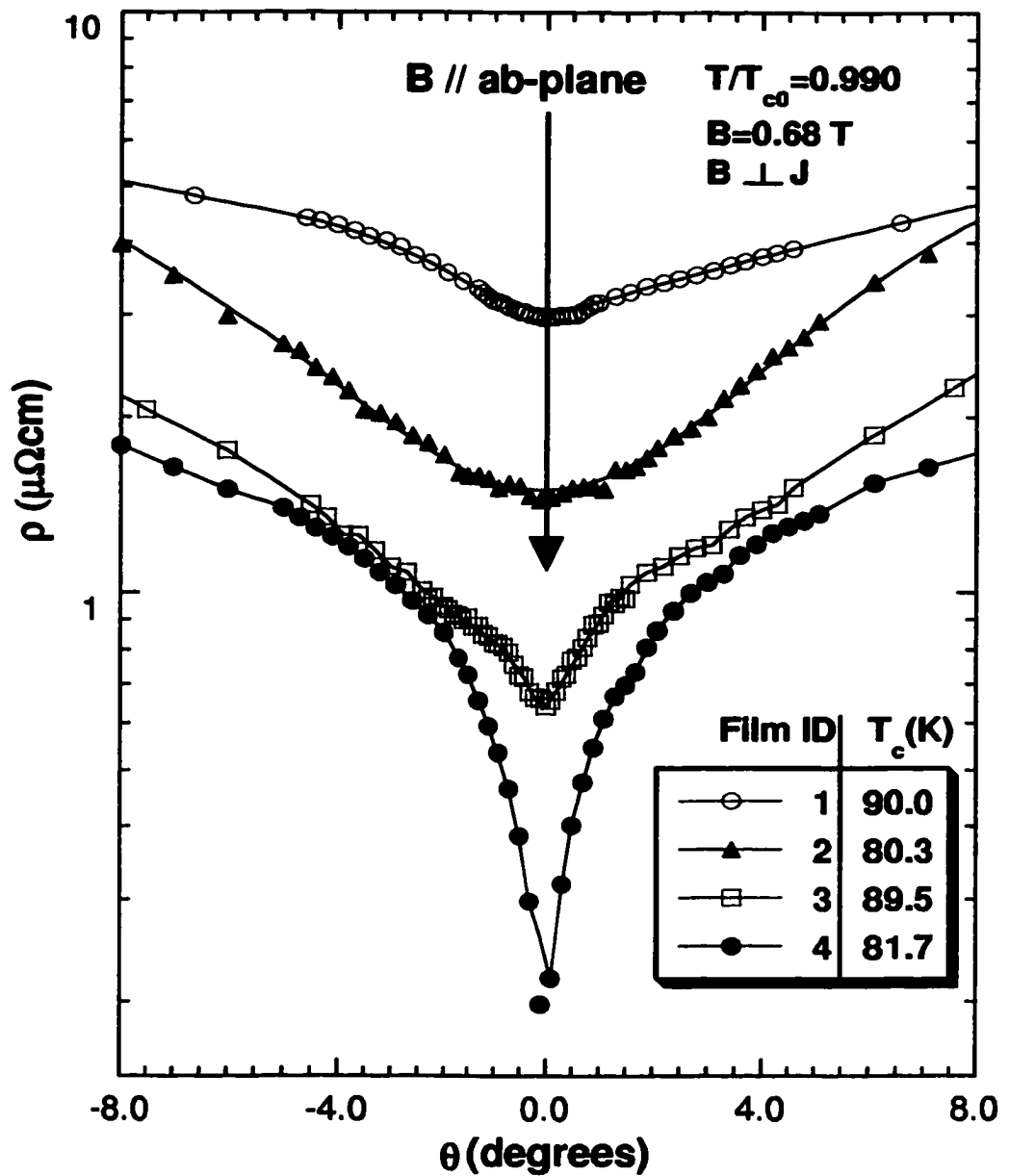
Figure 5.4: Angular dependence of resistivity $\rho(\theta)$ for θ between -8° and 8° for four YBCO thin films of different T_c , measured in an applied magnetic fields of 0.68 T for **B** $\perp$ **J** at a fixed reduced temperature $(T/T_{c0} = 0.990)$ for all films. The graph shows that the width of the minimum in $\rho(\theta)$ decreases with a decreasing resistivity, with the sharpest minimum (smallest width), for film 4, corresponding to the lowest resistivity. Note that there is no correlation between the width of the minimum and T_{c0}. The lines are guides for the eye.

114

Table 5.1: The normal and superconducting properties of YBCO films, J_c and ρ have been measured in the ab-planes, T_{c0} is the transition temperature at $\rho = 0$ and B=0, ΔT_c is the transition width and t is the film thickness.

Film No.	substrate type	t (nm)	T_{c0} (K)	ΔT_c (K)	$J_c(10K)$ $(\frac{MA}{cm^2})$	$J_c(77K)$ $(\frac{MA}{cm^2})$	$\rho(100K)$ $(\mu\Omega cm)$	$\frac{\rho(300K)}{\rho(100K)}$
1	$SrTiO_3$	210	90.0	1.0	24.0	2.21	68.3	3.4
3	$SrTiO_3$	230	89.5	1.2	24.1	2.36	74.9	3.5
4	Sapphire/CeO_2	140	81.7	2.9	5.23	0.08	14.2	2.4
2	$LaAlO_3$	310	80.3	2.0	10.4	0.20	169.7	2.7

$\rho(\theta)$ exhibits two types of minima near $\theta = 0^\circ$: the first one with a flat minimum shown by films 1 and 2 and the second one with a sharp minimum shown by films 3 and 4. The ratio $\frac{\rho(10^\circ)_{B\|J}}{\rho(10^\circ)_{B\perp J}}$ for all films is listed in Table 5.2. In general, this ratio is increasing with a decreasing width of the minimum from 0.25 for film 1 to 1.00 for film 4. The difference between $\rho_{B\perp J}$ and $\rho_{B\|J}$ decreases with a decreasing angle θ for all films except film 4 which does not show any significant difference between the two orientations.

Fig.5.7 shows resistivity versus the angle θ close to the ab-planes for film 4 for several temperatures near T_{c0} in a magnetic field of 0.68 T for $\mathbf{B} \perp \mathbf{J}$ orientation. An identical behavior of $\rho(\theta)$ has been observed for $\mathbf{B} \| \mathbf{J}$ orientation for this film. This figure shows a sharp drop in resistivity as the angle θ approaches zero. The width of the drop at FWHM (indicated in the graph as $2\theta_c$) decreases with an increasing temperature from 3.2° at T=81.23 K to 2.0° at T=81.63 K. The drop in resistivity defined as $\rho(0^\circ)/\rho(5^\circ)$ increases with an increasing temperature from about 8% at T=81.23 K to about 19% at T=81.63 K.

Basic normal and superconducting properties of the four films studied, i.e T_c, J_c, thickness, transition width etc. are listed in Table 5.1.

115
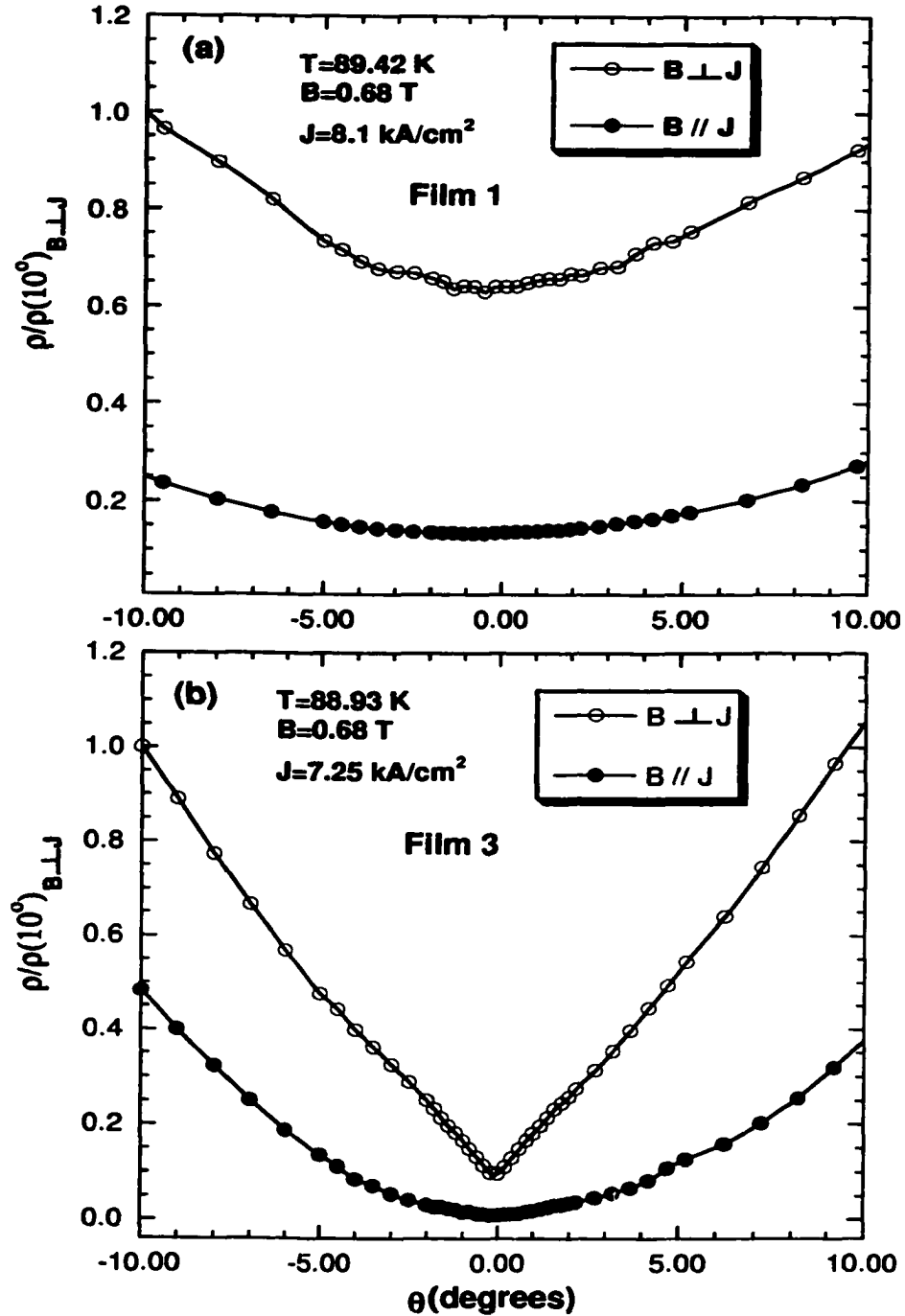
Figure 5.5: Normalized angular-dependent resistivity $[\rho/\rho(10^o)_{B\perp J}]$ as a function of θ for $\mathbf{B} \parallel \mathbf{J}$ and $\mathbf{B} \perp \mathbf{J}$ orientations, at a fixed reduced temperature $T/T_c = 0.994$ and in a field of 0.68 T for films 1 (a) and 3 (b). While film 1 displays a flat minimum in $\rho(\theta)$ and a small $\frac{\rho(10^o)_{B\parallel J}}{\rho(10^o)_{B\perp J}}$ ratio of 0.25, film 3 has a sharper minimum and a larger $\frac{\rho(10^o)_{B\parallel J}}{\rho(10^o)_{B\perp J}}$ ratio of 0.5. The lines are guides for the eye.

116
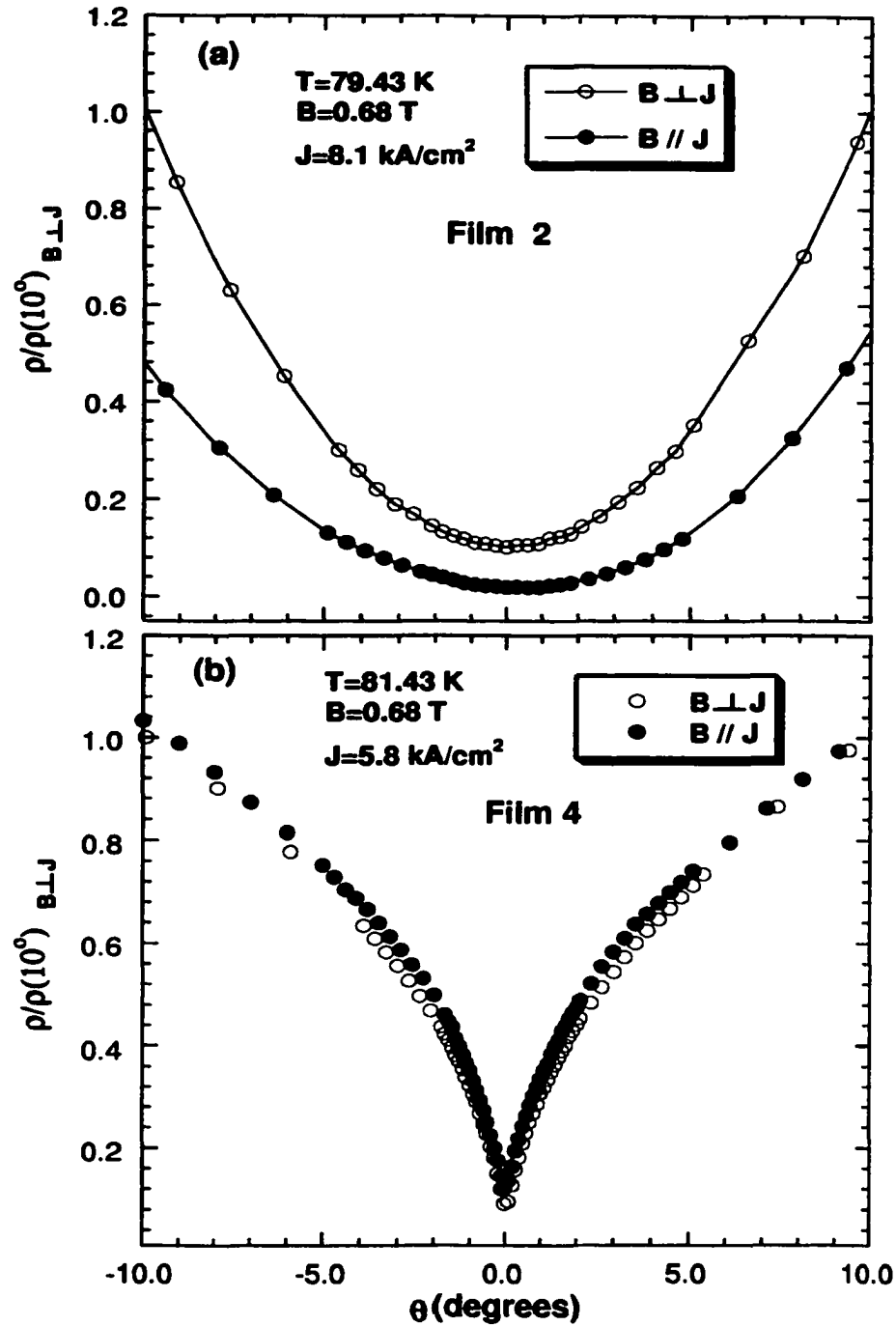
Figure 5.6: Normalized angular-dependent resistivity $[\rho/\rho(10°)_{B\perp J}]$ as a function of θ for $\mathbf{B} \parallel \mathbf{J}$ and $\mathbf{B} \perp \mathbf{J}$ orientations, at a fixed field of 0.68 T and a reduced temperature $T/T_c = 0.990$ for film 2 (a) and a reduced temperature $T/T_c = 0.996$ film 4 (b). Note the sharp minimum in $\rho(\theta)$ and the overlap of data of $\rho(\theta)$ for $\mathbf{B} \parallel \mathbf{J}$ and $\mathbf{B} \perp \mathbf{J}$ orientations for film 4. The ratio $\frac{\rho(10°)_{B\parallel J}}{\rho(10°)_{B\perp J}}$ is 0.5 for film 2, and 1.0 for film 4. The lines are guides for the eye.

117
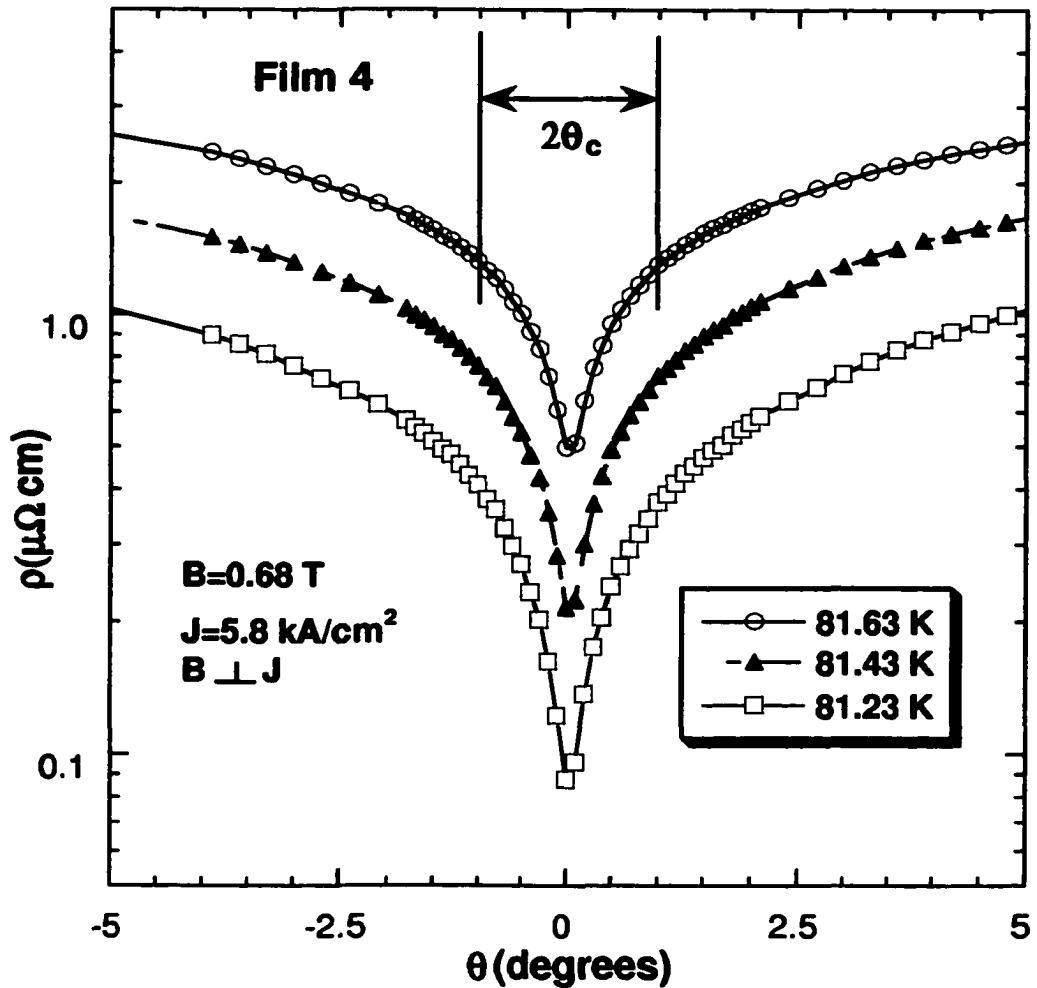
Figure 5.7: A semi-log plot of resistivity versus angle θ for film 4 for several temperatures near T_{c0} in a field of 0.68 T for $B \perp J$ orientation. An identical behavior of $\rho(\theta)$ has been observed for $B \parallel J$ orientation. $2\theta_c$ represents the width of the minimum at FWHM. This width decreases with an increasing temperature from 3.2^o at T=81.23 K to 2.0^o at T=81.63 K. The drop in resistivity defined as $\rho(0^o)/\rho(5^o)$ increases with an increasing temperature from about 8% at T=81.23 K up to about 19% at T=81.63 K.

118

5.3 Discussion

Anisotropy of YBCO films and crystals has been investigated extensively by various experimental methods including resistive [16, 17], magnetic [18] and torque [19] measurements. In general these investigations have given consistent results with values of the anisotropy factor γ ranging between 5 and 10 for pure YBCO close to an optimal doping. However a much higher values of γ have been reported for YBCO in the case of very thin films and highly oxygen deficient crystals. Iye et al. [10] reported a very large value of γ close to infinity for a very thin YBCO film of $10\,nm$ in thickness (T_c of this film was 81.5 K, which corresponds to $\delta = 0.13$). In this case, the film approaches a 2D limit and $\rho(\theta)$ scales well with the perpendicular component of the field: $B \sin \theta$. Bauhofer et al. [4], using resistive measurements to determine H_{c_2} as a function of the angle θ, reported a value of $\gamma = 40$ for highly underdoped YBCO crystals with $\delta = 0.4$ and $T_c = 60K$. Fu et al. [20] reported on measurements of magnetoresistance as a function of the angle θ in $YBCO/PrBa_2Cu_3O_7$ superlattices. $\rho(\theta)$ measured in different fields was scaled with a reduced field of the form: $B\sqrt{\sin^2 \theta + \gamma^{-2} \cos^2 \theta}$. For thick multilayer YBCO/PrBCO=1:3 superlattice a very good scaling was obtained with the perpendicular component of the field, which implies fully decoupled YBCO layers ($\gamma \sim \infty$). For a thinner superlattice YBCO/PrBCO=1:1, a finite anisotropy ($\gamma = 50$) had to be assumed in order to achieve a good scaling.

Our measurements of the angular dependence of resistivity in a magnetic field up to 1 T, performed on YBCO thin films revealed that in some cases an increase in the anisotropy is neither related to a decrease in thickness of the film nor to an increase in the oxygen deficiency δ. In the following sections we have calculated the anisotropy factors of these films using various methods.

119

5.3.1 Calculation of anisotropy from Bardeen–Stephen theory

In the flux flow regime, according to Bardeen-Stephen theory [21] the resistivity in a magnetic field can be expressed as

$$\rho = \rho_n \frac{H}{H_{c_2}},\tag{5.1}$$

where H_{c_2} is the upper critical field. For a field applied at an angle θ to the ab-planes, $H_{c_2}(\theta)$ is given by the anisotropic Ginzburg-Landau theory [22] as :

$$H_{c_2}(\theta) = H_{c_2}^{\parallel c}(\sin^2 \theta + \gamma^{-2} \cos^2 \theta)^{-1/2},\tag{5.2}$$

where γ is the anisotropy factor given by:

$$\gamma = \sqrt{\frac{m_c}{m_{ab}}} = \frac{H_{c_2}^{\parallel ab}(0)}{H_{c_2}^{\parallel c}(0)}\tag{5.3}$$

Here $H_{c_2}^{\parallel c}(0)$ and $H_{c_2}^{\parallel ab}(0)$ are the upper critical fields along the c-axis and in the ab-planes at zero temperature, respectively. Substituting Eq.(5.2) into Eq.(5.1) results in an expression for the angular dependence of resistivity:

$$\rho(\theta) = \rho(0^o)(\cos^2 \theta + \gamma^2 \sin^2 \theta)^{1/2},\tag{5.4}$$

where

$$\rho(0^o) = \rho_n \frac{H}{\gamma H_{c_2}^{\parallel c}}\tag{5.5}$$

is the resistivity at $\theta = 0^o$. Using Eq.(5.4), it is possible to obtain a quantitative value for the anisotropy factor γ by fitting the data of $\rho(\theta)$ at different fields to this equation. Fig.5.8 represents such a fit at different magnetic fields for films 1 and 3. The results of this fitting give a value of $\gamma = 7 - 8$ for film 1 (of $T_c = 90K$) and $\gamma = 32 - 35$ for film 3 (of $T_c = 89.5K$). Both films are very close to optimal doping and therefore they should have an anisotropy factor γ no larger than 7, according to many reports (see for example Ref. [23]). While γ values obtained from fitting for film 1 agree closely with these reports, film 3 has a much higher value of γ than the

120
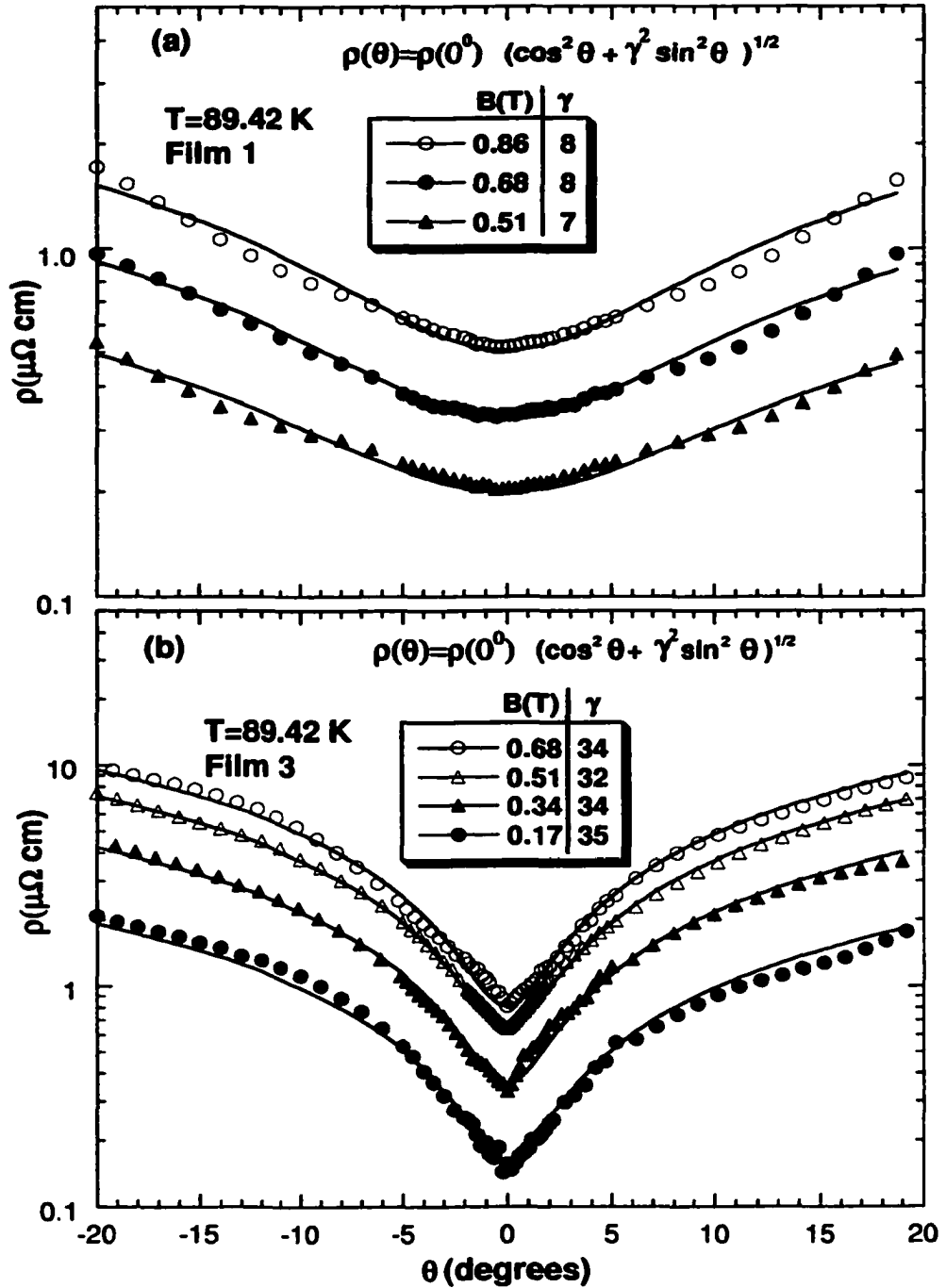
Figure 5.8: A semi-log plot of resistivity versus the angle θ measured for different applied magnetic fields at a temperature of 89.42 K for films 1 (a) 3 (b). The solid lines represent a fit to the equation $\rho(\theta) = \rho(0^{\circ})(\cos^2 \theta + \gamma^2 \sin^2 \theta)^{1/2}$ for $\rho(\theta)$ at different fields (see text). While film 1 displays a flat minimum at different fields (a), film 3 shows a sharp minimum with a width that decreases with an increasing magnetic field (b).

121

expected one. In fact, a value of $\gamma = 32 - 35$ obtained for film 3 is very close to $\gamma = 40$ reported by Bauhofer [4] for heavily underdoped YBCO crystals with $\delta = 0.4$.

Fitting using Eq.(5.4) has been performed as well for an underdoped film 2 (of $T_c \approx 80K$). The fitting results (not shown) is not as good as the one displayed in Fig.5.8 for higher T_c films. The obtained value of $\gamma = 25 - 29$ is higher than that expected for such an underdoped film. A value of $\gamma = 10$ has been reported for a YBCO sample with $T_c = 80K$ and $\delta = 0.13$ [1]. We could not achieve any reasonable fitting using Eq.(5.4) for film 4 which shows a sharp minimum in $\rho(\theta)$. Equation (5.4) describes the high angle (high resistivity) region in which flux flow is the dominant contribution to dissipation. For small angles, $H_{c_2}(\theta)$ becomes larger and the pinning potentials increases as well. With an increase of pinning, other dissipation mechanisms such as flux creep become more effective, and this may cause the resistivity to decrease faster with a decreasing θ than that given by Eq.(5.4). In systems with higher anisotropy like BSCCO (of $\gamma > 100$) and for field direction close to the ab-planes, the intrinsic pinning due to the layered structure becomes effective, and the extra pinning causes significant deviations from $\rho(\theta)$ given by Eq.(5.4) [24]. This implies that failure of Eq.(5.4) to fit the data of $\rho(\theta)$ for film 4 is probably caused by high anisotropy of this film. This high anisotropy is reflected by the sharp minimum [see Fig.5.6(b)], developed at angles close to the ab-planes, which is caused by a strong intrinsic pinning. We have therefore attempted to calculate γ for this film using different methods.

5.3.2 Effect of anisotropy on the temperature dependence of resistivity at different field orientations

Measurements of the resistivity in a magnetic field as a function of an angle θ can provide information about the anisotropy factor γ through Eq.(5.4). For $\theta = 90^o$ Eq.(5.4) becomes:

$$\gamma = \frac{\rho(90^o)}{\rho(0^o)} \tag{5.6}$$

Figures 5.2 and 5.3 show the temperature dependence of resistivity for films 1 and 3 and films 2 and 4, respectively. Resistivity was measured for four different configurations of the magnetic field; B=0, **B** ∥ **J** (with **B** ∥ ab-planes), **B** ⊥ **J** (with **B** ∥ ab-planes) and **B** ∥c-axis (with **J** ∥ ab-planes). Comparison of the data for films 1 and 3 of Fig.5.2, reveals that the difference in resistivity between **B** ∥ c-axis ($\rho(90^o)$) and **B** ⊥ **J** ∥ ab-planes ($\rho(0^o)$) for film 3 is larger than that for film 1. On the other hand, the difference in resistivity between **B** ⊥ **J** and **B** ∥ **J** configurations for film 3 is smaller than that for film 1. For **B** ∥ab-planes, the effect of the magnitude of the field on resistivity is small for film 3 compared to film 1. $\rho(T)$ for films 2 and 4 of Fig.5.3 shows clearly that the difference in resistivity between $\rho(90^o)$ and $\rho(0^o)$ for film 4 is much larger than that for film 2. In fact this difference is the largest among all fifteen films studied. Moreover, the data obtained for **B** ⊥ **J** and **B** ∥ **J** configurations for film 4 are almost identical and overlap with the resistivity measured in a zero field. This indicates that for this film when a magnetic field is applied parallel to the ab-planes, the magnitude of the field does not affect dissipation. Film 2 displays similar behavior to that of film 1 but with a smaller difference between the **B** ⊥ **J** and **B** ∥ **J** resistivities. The ratio $\rho(90^o)/\rho(0^o)_{B\perp J}$, which is equal to γ for the pure flux flow regime, is shown in Table 5.2 for all four YBCO films.

Variations of anisotropy between different samples could also be found by analyzing the difference in the angular dependence of resistivity between **B** ⊥ **J** and **B** ∥ **J** configurations. This difference decreases with an increasing anisotropy and disappears completely for highly anisotropic materials like BSCCO for fields applied close to the ab-planes. For very large anisotropy the vertical component of the applied field becomes the only factor that controls the dissipation and since this component is the same for both field orientations (i.e **B** ⊥ **J** and **B** ∥ **J**), there should not be any difference between the resistivities measured in these two cases. $\rho(\theta)$ for **B** ⊥ **J** and **B** ∥ **J** configurations for all films is shown in Fig.5.5 and Fig.5.6 at temperatures just below T_{c0} and in a field of 0.68 T. The difference between $\rho_{B\perp J}$ and $\rho_{B\parallel J}$ at $\theta = 10^o$ is the largest for film 1 ($\rho_{B\parallel J} = 0.25\rho_{B\perp J}$), is reduced by 50% ($\rho_{B\parallel J} = 0.50\rho_{B\perp J}$)

123

for films 2 and 3 and vanishes in the case of film 4 $(\rho_{B\|J} \simeq \rho_{B\perp J})$. This difference decreases further with a decreasing angle $|\theta|$ and reaches its minimum value at $\theta = 0^o$. Another anisotropy related feature which can be seen in Figures 5.5 and 5.6 is the sharpness of the minimum in $\rho(\theta)$. While films 1 and 2 display broad minima for $\mathbf{B} \perp \mathbf{J}$, as well as for $\mathbf{B} \parallel \mathbf{J}$, films 3 and 4 exhibit sharp minima (the sharpest in the case of film 4).

The three experimental observations discussed above: variations of the anisotropy in the resistivity $\rho(\theta)$ upon rotating the field $\mathbf{B}$ from the ab-planes to the c-axis (i.e variations of the ratio $\rho(90^o)/\rho(0^o)$), various dependencies of $\rho(\theta)$ on the angle between $\mathbf{B}$ and $\mathbf{J}$ (i.e from a large to an almost vanishing dependence), and the film-dependent changes in the sharpness (width) of the minimum in $\rho(\theta)$, suggest a corresponding variation in the intrinsic anisotropy (represented by γ) in these films. Several groups have studied variation of these properties and the corresponding anisotropy in different HTSC materials, but no detailed investigations of variation of anisotropy in different YBCO films were reported. Iye et al. [9, 10, 11, 13, 14] reported the measurements of $\rho(\theta)$ in thin films of BSCCO(2212) and YBCO(123) at temperatures between T_c to 15 K below T_c. When both $\mathbf{B}$ and $\mathbf{J}$ are oriented along the ab-planes, ρ does not change with the variation of the angle between $\mathbf{B}$ and $\mathbf{J}$ for BSCCO but it does for YBCO [13]. The minimum in $\rho(\theta)$ for BSCCO becomes very sharp for angles θ very close to the ab-planes ($\theta < 2^o$), whereas this minimum is much broader for YBCO [10, 8]. They also observed that the difference between ρ for $\mathbf{B} \parallel$ c-axis and ρ for $\mathbf{B} \parallel$ ab-planes is very large for samples with large anisotropy like BSCCO [$\rho(90^o) \gg \rho(0^o)$] but this difference decreases with a decreasing anisotropy [10]. These observations are in agreement with our observations for YBCO films. Therefore we could conclude that film 1 has the smallest anisotropy and its $\gamma \sim 7$ value is very close to those previously reported but film 4 has the largest anisotropy (2D-like) which is comparable to that of BSCCO. Films 2 and 3 have an intermediate anisotropy, larger than film 1 but smaller than film 4.

A decrease of the difference in $\rho(\theta)$ between $\mathbf{B} \perp \mathbf{J}$ and $\mathbf{B} \parallel \mathbf{J}$ orientations and an

increase in the sharpness (decrease in the width) of the minimum close to $\theta = 0^o$ is a result of a strong intrinsic pinning due to the layered structure in highly anisotropic superconductors. Materials with large anisotropy display a behavior which is very close to a 2D limit. Flux lines penetrating a weakly coupled layered superconductor at an angle θ may be viewed as a stack of 2D pancakes vortices. In this 2D limit, the pancake vortices in adjacent layers are completely decoupled and their density is directly related to the vertical component of the applied field ($B \sin \theta$). The independence of $\rho(\theta)$ on the orientation of the magnetic field with respect to current (identical behavior of $\rho(\theta)$ for $\mathbf{B} \perp \mathbf{J}$ and $\mathbf{B} \parallel \mathbf{J}$ configurations) for film 4, shown in Fig.5.6(b), can be attributed to the fact that the contribution to $\rho(\theta)$ due to the motion of Josephson vortices (strings) for $\mathbf{B} \perp \mathbf{J}$ configuration is negligible. This happens because of a very strong intrinsic pinning which locks them between the planes and therefore prevents their expected motion (due to Lorentz force) along the c-axis. For both $\mathbf{B} \perp \mathbf{J}$ and $\mathbf{B} \parallel \mathbf{J}$ orientations, components of $\mathbf{B}$ perpendicular to the ab-planes are identical, and this results in an identical Lorentz force acting on pancake vortices, giving rise to an identical electric field $\mathbf{E} \parallel \mathbf{J}$. For film 1 [see Fig.5.5(a)], which has a small anisotropy, the large difference in $\rho(\theta)$ between $\mathbf{B} \perp \mathbf{J}$ and $\mathbf{B} \parallel \mathbf{J}$ configurations could be attributed to additional contribution, due to the motion of Josephson strings for $\mathbf{B} \perp \mathbf{J}$, since intrinsic pinning there is much weaker. For the other two films 2 and 4, which have intermediate anisotropies, larger intrinsic pinning reduces the contribution due to the motion of Josephson strings and consequently reduces the difference between $\rho(\theta)$ for $\mathbf{B} \perp \mathbf{J}$ and $\mathbf{B} \parallel \mathbf{J}$ configurations.

125

Table 5.2: Comparison of anisotropies obtained by different methods for YBCO films. γ_f is obtained by fitting $\rho(\theta)$ with Eq.(5.4), γ_s is the corresponding value obtained using scaling, and T^* is the 2D-3D crossover temperature.

Film No.	$\frac{\rho(90^\circ)}{\rho(0^\circ)_{B \perp J}}$	$\frac{\rho(10^\circ)_{B \parallel J}}{\rho(10^\circ)_{B \perp J}}$	γ_f	γ_s	T_c (K)	T^* (K)
1	11	0.25	7-8	8	90.0	73.8
2	12	0.48	25-29	17	80.3	76.7
3	59	0.48	32-35	35	89.5	88.6
4	227	1.00	N/A	400	81.7	81.69

5.3.3 Calculation of anisotropy using scaling of $\rho(\theta)$ at different fields

It has been proposed by Kes et al.[7] that in a layered superconductor with a very weak coupling between the layers, only the field component perpendicular to the layers is relevant for the analysis of transport and magnetic properties. These properties therefore should scale with the perpendicular component of the field. This has been proven by Raffy et al. [5] by scaling the angular dependence of resistivity of BSCCO thin films with $B \sin \theta$. However this scaling is not valid when the angle θ is smaller than a certain critical value ($\theta_{cr} \sim 1^\circ$), which is a consequence of a finite dimensionality of these compounds (not a perfect 2D). Blatter et al. [25] developed a theoretical model which allows one to translate various superconducting properties from isotropic to anisotropic ones. According to Blatter et al., the angular dependence of resistivity in a magnetic field at an arbitrary angle θ can be scaled with a reduced field given by:

$$B_{red} = B(\gamma^{-2} \cos^2 \theta + \sin^2 \theta)^{1/2} \tag{5.7}$$

This equation adds a weighted parallel component to the perpendicular component of the field. This relation is reduced to $B \sin \theta$ for a perfect 2D case where $\gamma \approx \infty$. Using this reduced field as a scaling parameter, Iye et al. [26] were able to obtain

126

a good scaling of $\rho(\theta)$ in BSCCO thin films, using an anisotropy factor of $\gamma = 200$. This value substantially exceeds previous estimates which gave $\gamma = 55$ [27] or $\gamma = 120$ [28]. Iye et al. attempted also to scale the same data using $\gamma = \infty$ (i.e using $B \sin \theta$ as a scaling parameter) but below $B \sin \theta \sim 0.1\,T$ they could not obtain good scaling (significant deviations can be seen on a log-log scale).

Using Eq.(5.7) as a scaling parameter we were able to obtain very good scaling for $\rho(\theta)$ measured at different fields for films 1,2 and 3. The scaling behavior of the angular dependence of resistivity as a function of magnetic field at a constant temperature is shown in Fig.5.9 (for films 1 and 3) and Fig.5.10 (for films 2 and 4). The insets in these Figures show $\rho(\theta)$ as a function of magnetic field for $\mathbf{B} \parallel \mathbf{J}$ orientation. These measurements were performed at high temperatures very close to T_c (T/T_c ranges from 0.994 to 0.998) to ensure that thermal activation is high enough to neglect any effects of vortex pinning and to ensure a 3D behavior of vortices [29]. All the scaled data for different fields can be plotted on a single curve, as shown in Figures 5.9 and 5.10 for films 1,2 and 3. In order to investigate scaling in the vicinity of $\theta = 0^o$ and in the low field region, where some deviations are expected, the data were plotted on a logarithmic scale [see Figures 5.9 and 5.10(a)].

Even on this scale one could not observe any significant deviations from the single curve for all three films investigated. Values of the anisotropy factor γ obtained from this scaling are close to those obtained by fitting the same data to Eq.(5.4) (see Table 5.2). Only for film 1 (of $T_c = 90K$) the obtained value of $\gamma = 7 - 8$ is consistent with that reported for optimally doped YBCO [23]. On the other hand, film 3 (of $T_c = 89.5K$) whose oxygen content is also very close to optimal doping has a relatively high anisotropy which is in fact comparable to that of a highly oxygen deficient YBCO of $\delta = 0.4$, $T_c \sim 60K$ and $\gamma = 40$ [4]. Film 2, an underdoped one with $T_c = 80K$, shows a larger than expected anisotropy, but still smaller than that of film 3. This implies that in some cases the anisotropy is independent of T_c. This appears to contradict the fact that anisotropy is increasing with a decreasing T_c due to an increasing oxygen deficiency. For film 4 (which exhibits a sharp minimum in

127
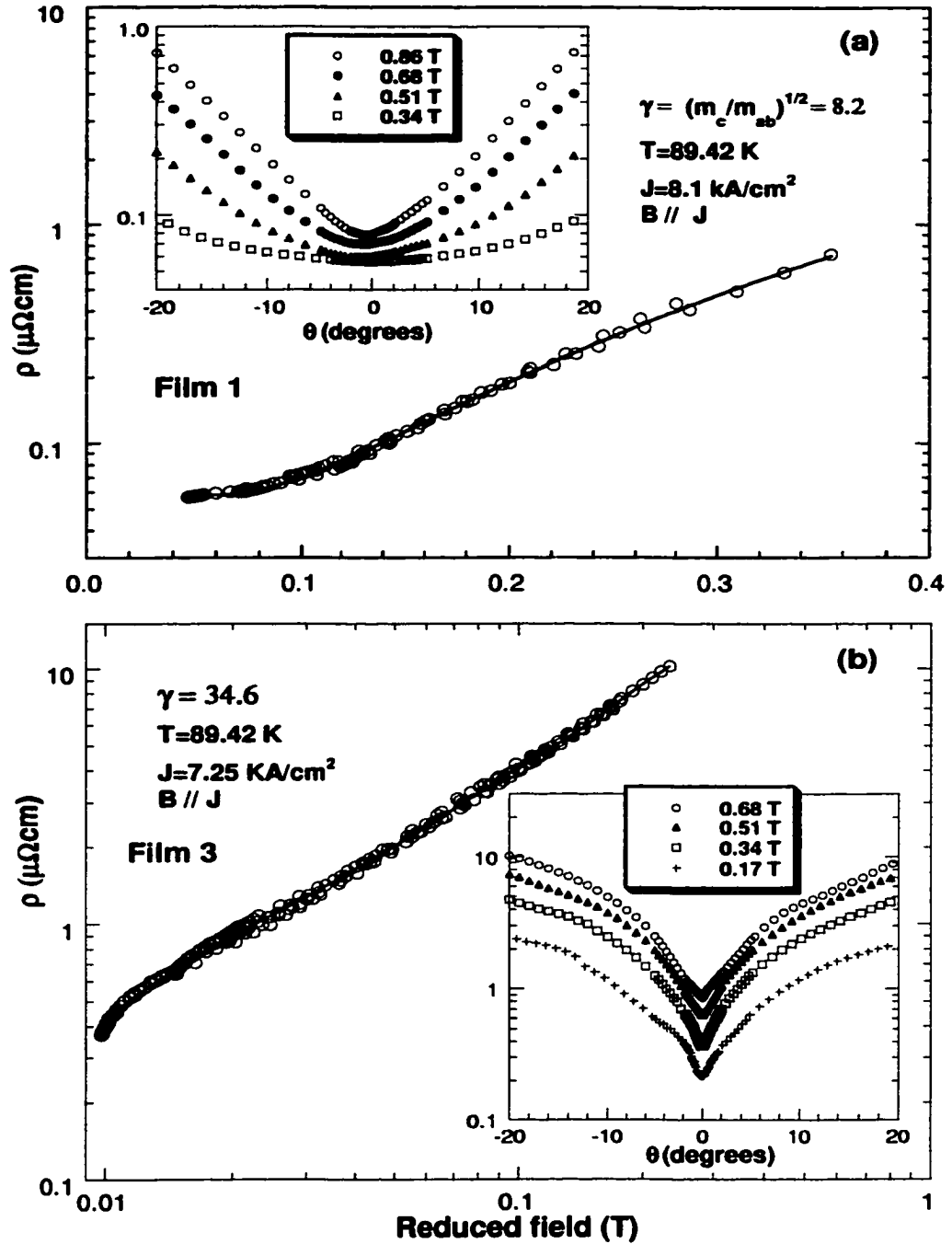
Figure 5.9: $\rho(\theta)$ measured in different fields for $\mathbf{B} \parallel \mathbf{J}$ orientation at T=89.42 K, as a function of the reduced field $B(\gamma^{-2} \cos^2 \theta + \sin^2 \theta)^{1/2}$ for films 1(a) and 3(b) (see text). The insets show a semi-log plot of resistivity $\rho(\theta)$, before scaling, for different magnetic fields $\mathbf{B}$ at T=89.42 K. The scaling gives a γ=8.2 for film 1 and 34.6 for film 3. The lines are guide to the eye.

128
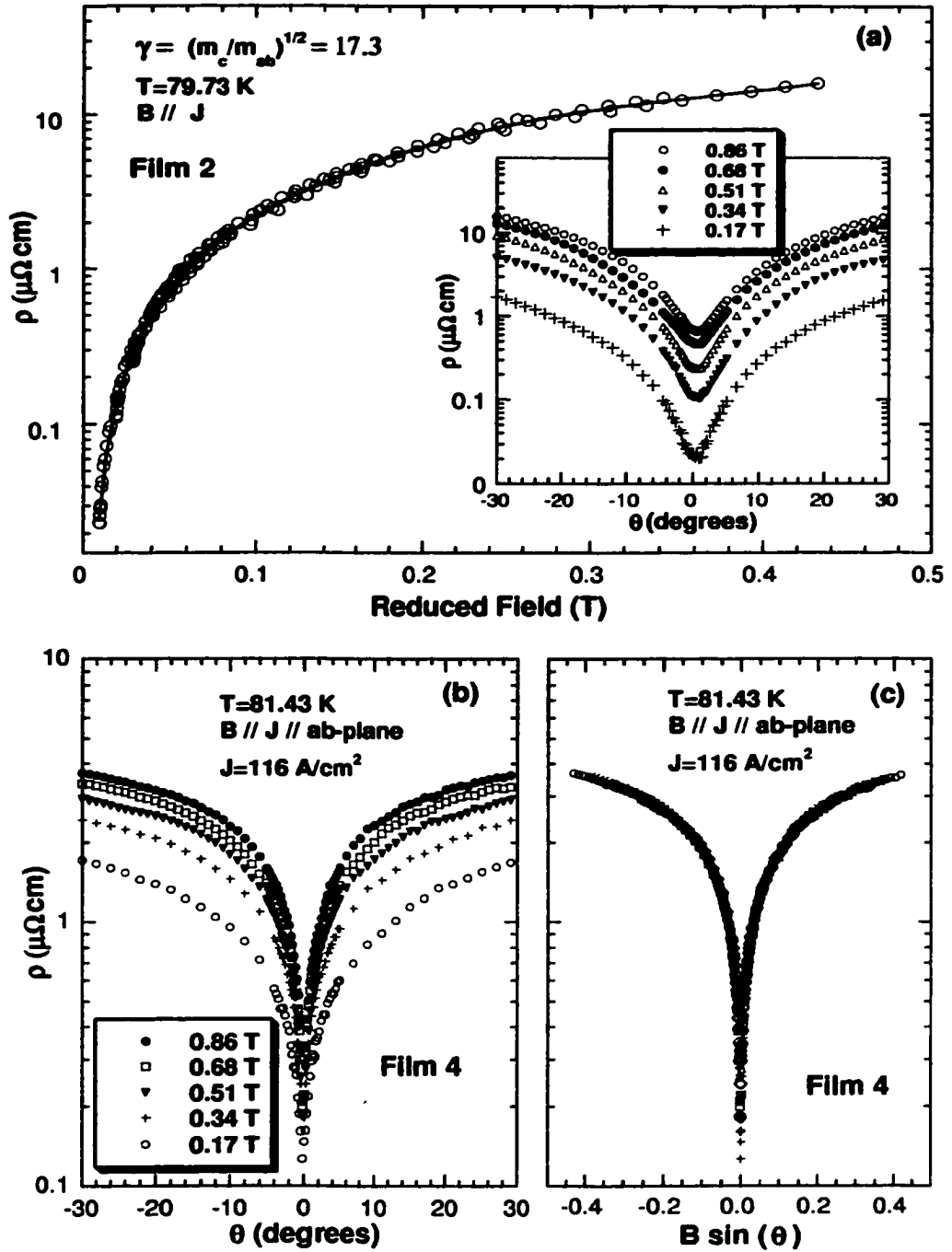
Figure 5.10: (a) A semi-log plot of $\rho(\theta)$, measured in different fields for $\mathbf{B} \parallel \mathbf{J}$ orientation (at T=79.73 K), as a function of the reduced field $B(\gamma^{-2}\cos^2\theta + \sin^2\theta)^{1/2}$ for film 2 (see text). The inset shows a semi-log plot of resistivity $\rho(\theta)$, before scaling, for different magnetic fields $\mathbf{B}$ at T=79.73 K. (b) A semi-log plot of resistivity $\rho(\theta)$ for different magnetic fields $\mathbf{B}$ for $\mathbf{B} \parallel \mathbf{J}$ orientation, for film 4 at T=81.43 K.(c) the corresponding scaling behavior, of $\rho(\theta)$ in (b), as a function of the c-axis component of the field $B\sin\theta$. The lines are guides for the eye.

129

$\rho(\theta)$ [see Fig.5.10(b)]) we were unable to get any reasonably good scaling with the reduced field of Eq.(5.7) up to a value of $\gamma = 50$. However very good scaling has been obtained using $B \sin \theta$ as a scaling parameter. Such a scaling makes all data points from different fields to collapse onto a single curve [see Fig.5.10(c)], indicating that the 2D model could be successfully applied to some YBCO films. This type of scaling works quite well in a linear plot and even in a semi-log plot [see Fig.5.10(c)]. However, these plots can not differentiate between the real 2D-limit and the 3D anisotropic effective mass model with large value of γ, especially at very small angles and fields. In order to resolve this problem and investigate more carefully this scaling at very small angles ($\theta \sim 0^o$), the data for film 4 were replotted on a log-log scale in Fig.5.11(a) with $\gamma \approx \infty$ (which implies the use of the perpendicular component of the field as a scaling parameter). In this log-log plot, scaling is very good only down to $B \sin \theta \approx 0.003T$, but below that value slight deviations become apparent. The best scaling for these data was achieved using a 3D anisotropy of Eq.(5.7) with $\gamma = 400$ [see Fig.5.11(b)].

X-ray diffraction (XRD) data of film 4 showed a typical patterns of stoichiometric c-axis oriented YBCO films [Fig.5.12(a)]. The data did not reveal any observable secondary impure phases. The lines are strong and sharp [the half width of the (005) line is 0.26^o which is consistent with an epitaxial layer. The only CeO_2 line present is the (200) line. This indicates a single orientation of the CeO_2 layer. Film 4 has a good microwave surface resistance at 32 GHz. The XRD data for this film has $2\theta = 22.82^o$ for the (003) line. This gives a c-axis spacing of 3.90 Å, which implies a somewhat lower oxygen composition of about 6.8 [30]. For comparison purposes, the XRD data for film 12, of higher T_c=85.4K than film 4 (see Table 2.2), is also shown in data Fig.5.12(b). The XRD patterns of film 12 is very much similar to that of film 4. Film 12 had a very good surface resistance at 32 GHz. There is a slight shift of the (003) peak for film 12 compared to film 4 $2\theta = 22.86^o$. This gives a c-axis spacing of 3.89 Å, which corresponds to an oxygen composition of about 6.9. The other difference between the XRD data of the two films is that the YBCO peaks for film 4 are smaller

130
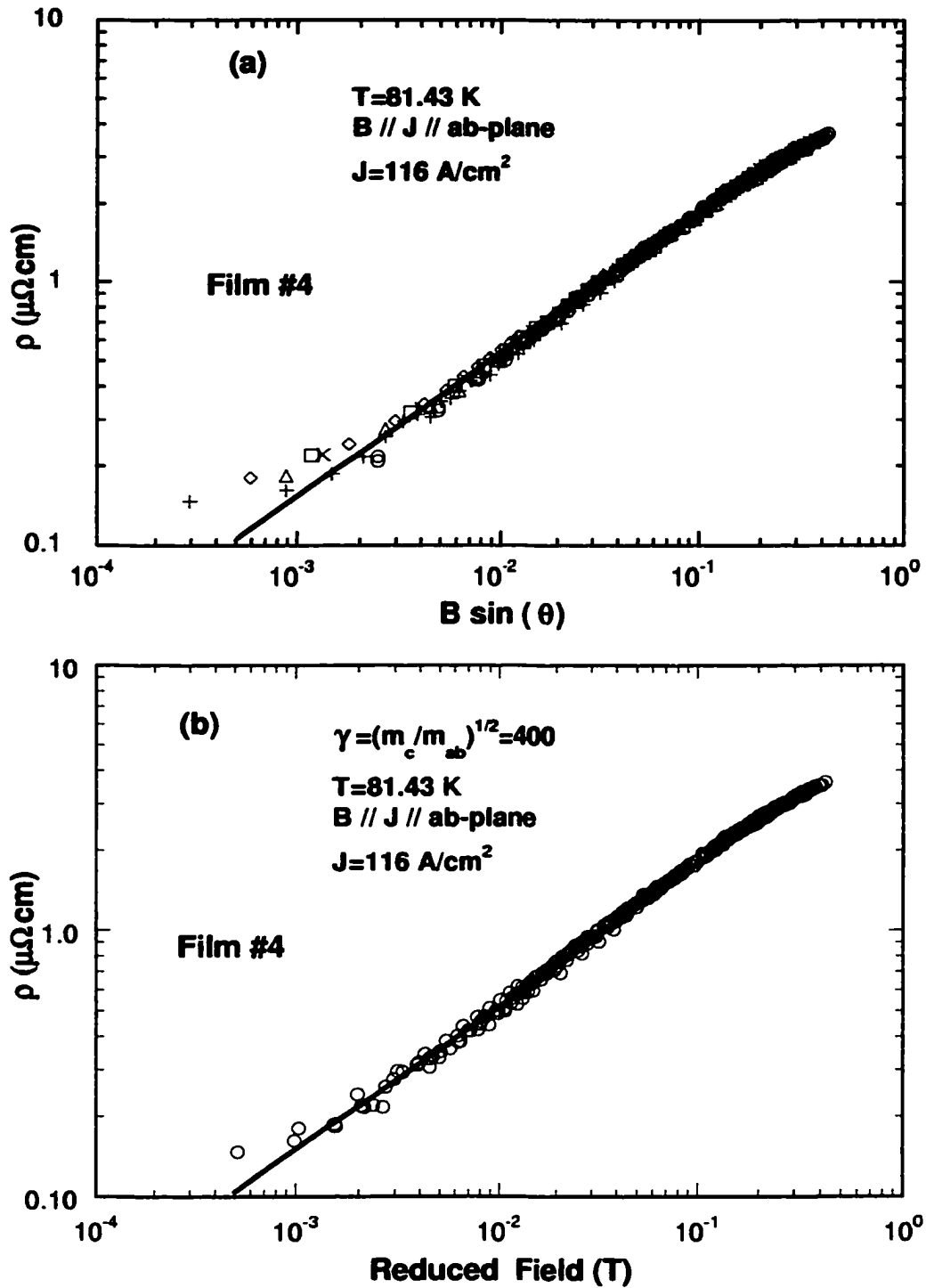
Figure 5.11: (a) Replot of Fig.5.10(c) on a log-log scale (positive angles only). Note the deviation from the scaling curve at low angles and fields for $B\sin\theta < 0.003T$. (b) A repolt of Fig.5.11(b) (on a log-log scale), as a function of the reduced field $B(\gamma^{-2}\cos^2\theta + \sin^2\theta)^{1/2}$ for film 4. The scaling gives a finite value of $\gamma = 400$ for film 4. The lines are guide for the eye.

131

than that for film 12, probably because the YBCO film 4 is thinner than film 12 (see Table 2.2).

The results of scaling of $\rho(\theta)$ indicate that the intrinsic anisotropy of various YBCO(123) films does not depend on T_c, thickness, critical current density and preparation techniques and can be substantially larger than previously believed and reported, approaching that of BSCCO in some cases. On the other hand, even for films with very high γ values, like film 4, scaling behavior is distinctly different from that for the 2D-limit model, indicating a finite interlayer coupling. Sometimes, finite mosaic spread of the sample and/or insufficient angular resolution of the used experimental technique could lead to an underestimation of anisotropy in YBCO films.

5.3.4 Lock-in transition

In highly anisotropic materials, like Bi and Tl based HTSC, the most favorable magnetic flux lattice structure consists of Abrikosov vortices (pancakes) along the c-axis and Josephson vortices parallel to the layers. For a magnetic field applied in the ab-planes, the vortex cores prefer to lie between the layers, and at a certain angle with respect to the ab-planes, a tilted vortex forms kinks connected by segments parallel to the layers [31, 32]. Feinberg and Villard [33] predicted that when a magnetic field direction is at a certain angle $\theta < \theta_c$ very close to the layers, these kinks become unstable and vortices prefer to run strictly parallel to the layers with their cores remaining locked-in between the layers. This process is called the "lock-in transition" and implies a " transverse Meissner effect" with the field component perpendicular to layers being zero. Theoretical predictions have provided different values for the lock-in transition angle θ_l (measured from the ab-planes): $4 - 71^o$ [33], $0.1 - 1^o$ [34] for YBCO and 21° [33] for BSCCO(2212).

There have been many reports of experimental evidence for a lock-in transition in HTSC. It was believed that torque measurements for fields near the ab-planes direction would bring clear and direct evidence for this transition. Farrell et al. [23] reported an anomaly in the angular dependence of the magnetic torque for YBCO at

132
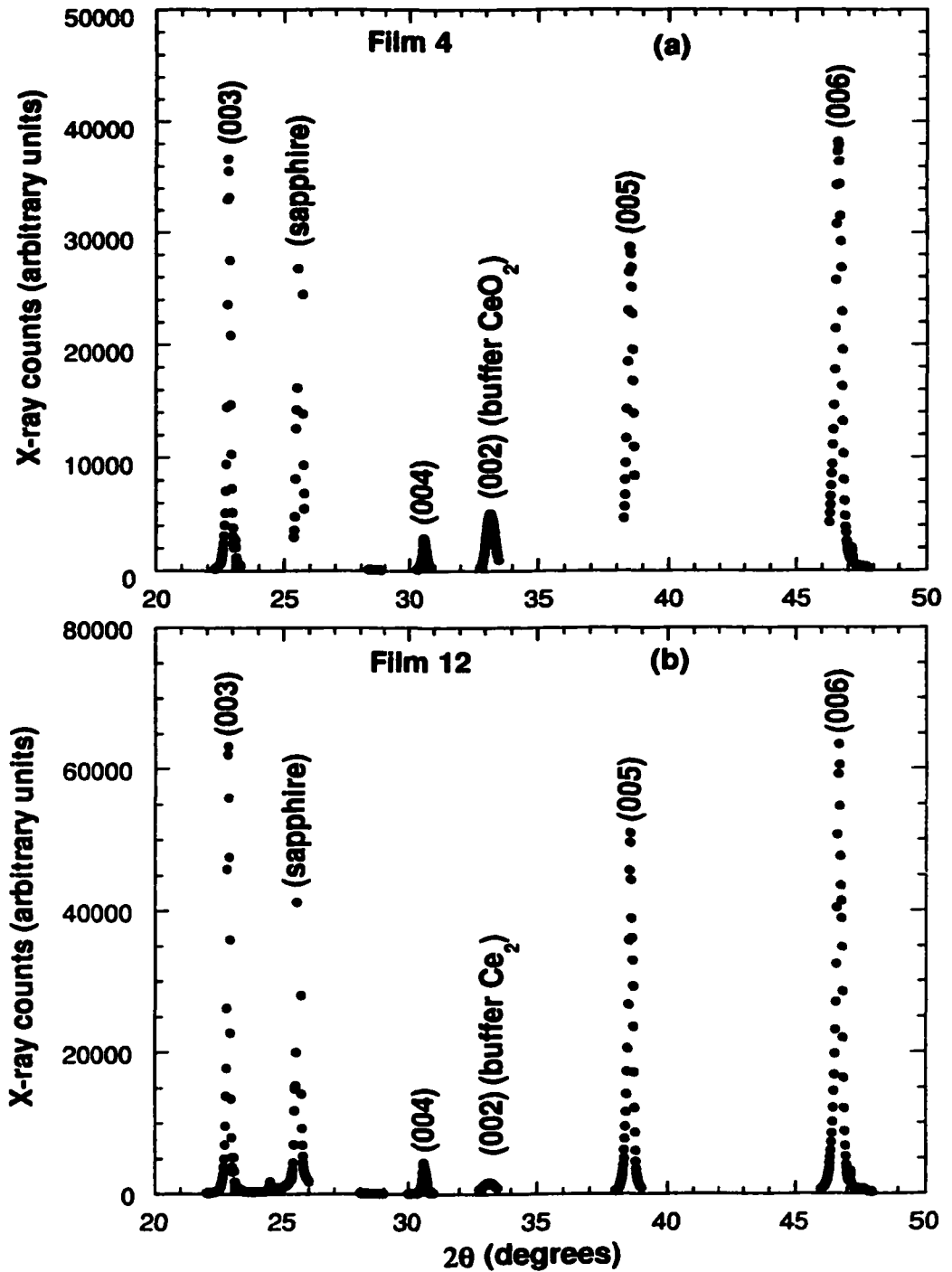
Figure 5.12: x-ray diffraction spectrum using Cu Kα radiation of an average wavelength of 1.54186 Åfor c-axis oriented YBCO films 4 (a) and 12 (b) which were grown on a sapphire substrate covered with CeO_2 buffer layer about 20 nm thick. The YBCO c-axis lines are indexed.

133

80 K. Janossy et al. [35] showed that magnetization for Tl(2212) near the ab-planes is independent of temperature and applied field, which suggests that vortices are locked parallel to the planes. An experimental evidence for a lock-in transition was also obtained from magnetization measurements in the low field region for BSCCO(2212) [36].

Experimental investigation of the lock-in transition is difficult for several reasons. In low magnetic fields, flux penetration is diminished by pinning and surface barriers, so that magnetization and torque [37] are dominated by a strong diamagnetic contribution due to screening currents. In high fields, the lock-in transition takes place at angles θ very close to the planes ($\theta < 0.5^{o}$) and can be detected only using an extremely high angular resolution method [15]. Moreover, at high temperatures thermal fluctuations may make this effect undetectable [36].

Kwok et al. [15] reported the observation of a strong intrinsic pinning represented by a sharp drop in the angular dependence of resistivity $\rho(\theta)$ in YBCO single crystals for fields very close to the ab-planes, and at temperatures very close to T_c. This drop in resistivity was seen only when the field was rotated in a plane perpendicular to the current and parallel to the c-axis. The authors argued that this sharp minimum in $\rho(\theta)$ could be attributed to a lock-in transition of the vortex lines due to a strong intrinsic pinning.

From the theoretical point view, the lock-in transition phenomena have been investigated for different ranges of fields by Feinberg and Villard [33], however they have not accounted for the effects of demagnetizing factor (sample geometry), which is of great importance. This problem has been studied carefully by Feinberg and Ettouhami [31]. They analyzed this effect both in the quasi-2D regime of Lawrence-Doniach (LD) model for $T \ll T^{*}$, where $\xi_c(T) < d$, (T^{*} is the 3D-2D crossover temperature and d is the interlayer distance) and in the quasi-3D anisotropic regime of the GL model for $T > T^{*}$, where the core of the vortex extends over more than one interlayer spacing. According to their analysis, the angle θ_l at which the lock-in

134

transition occurs for the quasi-2D regime is given by

$$H \sin \theta_l = \frac{\phi_0}{4\pi\lambda_{ab}^2} \left[\ln \frac{min(\lambda_{ab}, \gamma d)}{\xi_{ab}} + \alpha_{2D} \right], \qquad T \ll T^*, \qquad (5.8)$$

and for the quasi-3D regime is given by

$$H \sin \theta_l = \frac{\phi_0}{\pi\lambda_{ab}^2} \sqrt{\frac{2\alpha_1(\ln\gamma + \alpha_0)}{\pi}}, \qquad T > T^*, \qquad (5.9)$$

where λ_{ab} and ξ_{ab} are the penetration depth and the coherence length parallel to the ab-planes, respectively, α_{2D} denotes the core energy of a single 2D vortex, α_0 is a constant, and α_1 is defined as

$$\alpha_1(T) = 0.285 \left(\frac{d}{\xi_{ab}(T)} \right)^2 = 0.57\frac{t}{t^*}, \qquad (5.10)$$

with $t = 1 - T/T_c$ and $t^* = 1 - T^*/T_c$.

We have tried to use the above equations to calculate the lock-in transition angle θ_l for YBCO films studied. In order to do that, one has to find first the crossover temperature T^* for each film. Roughly speaking, one could take $\xi_{ab}(0) \approx 20\mathring{A}$ as a representative average value for YBCO ($\xi_{ab}(0)$ ranges between 16-24Å[1]). Using $\gamma = \xi_{ab}(0)/\xi_c(0)$, we have calculated $\xi_c(0)$ for all films using the estimated values of γ_s obtained from the scaling procedure listed in Table 5.2. For films 1, 2, 3 and 4, $\xi_c(0) = 2.4, 1.2, 0.58$ and $0.05\mathring{A}$ respectively. Taking the interlayer distance d=8 Å, we have estimated the crossover temperature T^* by setting (see Ref. [6])

$$\xi_c(T^*) = \frac{d}{\sqrt{2}} = \frac{\xi_c(0)}{\sqrt{1 - T^*/T_c}} \qquad (5.11)$$

The estimated values of T^* are listed in Table 5.2. According to these values, the temperature range over which the measurements of $\rho(\theta)$ were performed is above T^* for all films except film 4. Therefore films 1, 2 and 3 follow the 3D regime, and film 4, which exhibits a crossover from 3D to 2D regime at temperatures less than 10 mK below T_c (because of very high anisotropy), follow a 2D regime. Calculations of the lock-in transition angle using Eqs.(5.8) and (5.9) were performed only for films 3 and 4, since these two films show a sharp drop in resistivity for **B** very close to the

135

ab-planes. Films 1 and 2 have a flat minimum in $\rho(\theta)$ at small angles and therefore they are unlikely to exhibit any lock-in transitions [see Figures 5.5 and 5.6]. Film 4 shows a very sharp minimum in $\rho(\theta)$ with a width of the minimum about 2°. At $T = 81.43K < T^* = 81.69K$ this film is in a 2D regime, therefore one could use Eq.(5.8) to find θ_l. Assuming $\gamma = 400$, $\lambda_{ab}(t) = 1600t^{-1/2}\text{Å}$, $\xi_{ab}(0) = 20\text{Å}$ and $\alpha_{2D} = 0.75$ [31], $H\sin\theta_l$ in Gausses is given by

$$H\sin\theta_l = 375\,t \qquad (5.12)$$

For T=81.43 and H=6800 G, the critical angle (θ_l) is equal to 0.010^o. The calculated critical angle θ_l is the angle between the internal magnetic field H_i and the ab-planes, while the measured angle θ_{lm} for the lock-in transition is the angle between the external applied field H_a and the ab-planes. H_a is related to H_i by [15, 31, 33]

$$H_a = \mathbf{n}B + (1 - \mathbf{n})H_i \qquad (5.13)$$

For $\theta < \theta_{lm}$, $B_x \cong H_{ix}$, $B_z = 0$ and $H_{az} = (1 - n_z)H_{iz}$, where B_x is the horizontal component of the field (parallel to the ab-planes), H_{az} is the vertical component of the applied field (parallel to the c-axis) and n_z is the demagnetization factor. For very small θ one could write $\theta_{lm} = (1 - n_z)\,\theta_l$ [15].

For a film of thickness s and width w, $(1 - n_z) = \pi s/2w$. For film 4, s=144 nm and $w = 60\mu m$, and the lock-in transition occurs at $\theta_{lm} = 0.00004^o$. This value is much smaller than the measured width of $2^o/2 = 1^o$. This very small value is impossible to observe in our experimental system with an angular resolution of 0.045^o. For film 3, which shows a wider minimum than film 4, the measurement were done at a temperature of 88.93 K which is higher than the estimated crossover temperature $T^* = 88.6K$. Therefore, at this temperature film 3 is in a 3D regime and one should use Eq.(5.9) to calculate θ_l. Assuming $\gamma = 35$, $\lambda_{ab}(t) = 1600\,t^{-1/2}\text{Å}$, $T^* = 88.6K$, and $\alpha_0 = 2.13$ [31], $H\sin\theta_l$ in Gausses is given by

$$H\sin\theta_l = 3686\,t^{3/2} \qquad (5.14)$$

For T=88.93K and H=6800 G, $\theta_l = 0.016^o$. Using the demagnetization expression $(1 - n_z) = \pi s/2w$ with s=230nm and $w = 60\mu m$, the lock-in transition for film 3

136

should occur at $\theta_{lm} = 0.0001^\circ$, which is also much smaller than the observed width of $4^\circ/2 = 2^\circ$. From these calculations, the width of the minimum $(2\theta_l)$ is decreasing with an increasing anisotropy factor γ, giving a sharper minimum in $\rho(\theta)$ for larger γ. Our measurements agree with this; the observed FWHM of the minimum in $\rho(\theta)$ of film 3 (2°) is almost double that of film 4 (1°).

We conclude that the observed sharp drop in resistivities of films 3 and 4 as θ approaches zero is not due to the lock-in transition. The lock-in transition is very difficult to observe in thin films using transport measurements because of a very small $(1 - n_z)$ factor [31, 33, 34].

Feinberg and Ettouhami [31] provided an expression for the kink energy E_K in a 3D regime $(T > T^*)$ given by

$$E_K = 4d \left(\frac{\phi_0}{4\pi\lambda_{ab}} \right)^2 \sqrt{\frac{\alpha_1(\ln\gamma + \alpha_0)}{\pi}} \qquad (5.15)$$

Quantitatively, for optimally doped YBCO with $\gamma = 7$, $\lambda_{ab}(t) = 1600\, t^{-1/2}\text{Å}$ and $T^* = 80K$, one finds the following temperature dependence of E_K (in degrees Kelvin)

$$E_K = 7.9 \times 10^3\, t^{3/2} \qquad (5.16)$$

Therefore even at t=0.1 (T=80 K), E_K is of the order of a hundred degrees K, so one could expect many kinks to be thermally created. This makes the lock-in transition difficult to observe using transport measurements [31]. To our knowledge, the only experimental observation of a lock-in transition in YBCO using transport measurements was reported by Kwok et al. [15] who observed (very close to T_c) a sharp drop in resistivity, which however does not fall down to zero at $\theta = 0^\circ$. The authors analyzed their experimental findings for the lock-in angle using theoretical predictions of Feinberg and Villard [33] and Blatter et al. [38]. They argued that since the relative change in resistivity is considerably less than unity, then even at $\theta = 0^\circ$ there is a considerable number of thermally activated kinks which implies that the kink energy $E_K \geq T$ [15]. Based on this assumption and using $E_K = \sqrt{\alpha}\,\eta[\phi_0^2 d/(4\pi\lambda_{ab})^2]\ln(\kappa\gamma)$, they obtained a value of 3 for the constant $\sqrt{\alpha}\,\eta$ which

137

was used to find $\theta_{lm} \sim 0.21^o$ close to the measured one of 0.3^o. According to Feinberg and Ettouhami [31] the calculated value of θ_{lm} could be overestimated due to an overestimation of E_K itself. Using the experimental conditions of Ref.[15] T= 89.71 K and T_c=90.31, the kinks energy E_K given by Eq.(5.15) is $E_K \approx 4.3K$ which is much smaller than $E_K = T = 89.7K$. On the other hand, using Eq.(5.9) one could estimate the lock-in transition angle θ_l in this case. For T=89.71 K and H=1T, $\theta_l \sim 0.004^o$. Taking into account the demagnetization factor n_z, $(1 - n_z) = 0.09$ for the YBCO crystal, $\theta_{lm} \sim 0.00034^o$ which is surprisingly about four orders of magnitude smaller than $\theta_{lm} \sim 0.21^o$ reported in Ref.[15].

5.4 Summary and conclusions

The measurements of the angular dependence of resistivity $\rho(\theta)$ in a magnetic field **B** close to the angle $\theta = 0^o$ (**B** $\parallel$ ab-planes) were performed for several underdoped and optimally doped YBCO thin films of T_c between 80 and 90 K using two different configurations of **B** versus **J** i.e **B** $\parallel$ **J** and **B** $\perp$ **J**. These measurements revealed sample-dependent variations in the shape of the minimum around $\theta = 0^o$, from a flat to a very sharp behavior. The results of scaling of $\rho(\theta)$ with the reduced field $B(\gamma^{-2}\cos^2\theta + \sin^2\theta)^{1/2}$ allowed us determine the value of the anisotropy factor γ which varies between 7 and 400, and is independent of T_c, film thickness, or critical current density.

The question is what is the reason behind this large variation in γ for YBCO films close to an optimal doping. X-ray diffraction (XRD) data of the film with high $\gamma \sim 400$ showed a typical patterns of stoichiometric c-axis oriented YBCO with no difference in the structure compared to other films of moderate anisotropy. The data did not reveal any observable secondary impure phases. High resolution electron microscopy studies of YBCO crystals by Etheridge [39] revealed a weak diffuse scattering in electron diffraction pattern of $YBa_2Cu_3O_{6+x}$ ($x > 0.9$) which arise from static displacements of atoms from their periodic lattice sites. The local atomic displacements partition

138

the copper-oxygen planes into cells with dimension comparable to coherence length in the ab-planes (about 2nm). These studies have suggested that the ab-planes buckle into the network of slightly misaligned cells in a struggle to relieve internal stresses. One source of internal stress is a mismatch between "natural" (sometimes called prototypical) lattice constants of the copper-oxygen planes and the chain-oxygen and barium-oxygen planes. It is therefore very likely that the coupling between the ab-plane layers in YBCO and thus the anisotropy factor γ could be affected by the "buckling" process in the copper-oxygen planes. The "buckling" is very sensitive to a local disorder in oxygen concentration. This could explain the large variations in γ in YBCO films close to an optimal doping.

Halbritter [40] discussed anisotropy in YBCO and argued that high anisotropy in this material could be attributed to weak-link effects. Defects can either create insulating or conducting behavior depending on the position of the defects and orientation of the current. For example, defects may enhance the small conductivity $\sigma^{\perp}$ perpendicular to the planes, whereas defects reduce the strong conductivity $\sigma^{\parallel}$ along the planes. This implies that defects make cuprate superconductors more isotropic. Due to layered structure defects are often organized in planes, of reduced conductivity, which are named "weak links". Their grain boundary resistances $(R_{gb}^{\parallel} \geq 10^{-7} - 10^{-9}\Omega cm^2)$ are several orders of magnitude larger than the metallic resistance, indicating that weak-links are insulating. Weak links contain localized states that carry current across by resonant tunneling. For YBCO such states are due to oxygenation in the Cu chains. By pair weakening the localized states have a lowered energy gap and by resonant tunneling the defects reduce the perpendicular resistivity $\rho^{\perp}$ drastically. For YBCO this yields an intrinsic anisotropy of 5×10^5 [40] which suggests that weak-link effects could result in a very large anisotropy.

National Laboratory. This research has been funded by a grant from the Natural Sciences and Engineering Research Council of Canada (NSERC).

140

Bibliography

[1] S. L. Cooper and K. E. Gray, *Physical properties of high temperature supercon-ductors* **IV**, ed. by D. M. Ginsberg, World Scientific, Singapore 1994, P. 61.

[2] M. Tinkham, *Phys. Rev.* **129**, 2413 (1964).

[3] M.J. Naughton, R.C. Yu, P.K. Davies, J.E. Fischer, R.V. Chamberlin, Z.Z. Wang, T.W. Jing, N.P. Ong, P.M. Chaikin, *Phys. Rev. B* **38**, 9280 (1988).

[4] W. Bauhofer, W. Biberacher, B. Gegenheimer, W. Joss, R. K. Kremer, Hj. Mat-tausch, A. Muller, A. Simon , *Phys. Rev. Lett.* **63**, 2520 (1989).

[5] H. Raffy, S. Labdi, O. Laborde, P. Monceau, *Phys. Rev. Lett.* **66**, 2515 (1991).

[6] M. Tinkham, *Introduction to Superconductivity*, McGraw-Hill, New York,(1996).

[7] P. H. Kes, J. Aarts, V. M. Vinokur and C. J. van der Beek, *Phys. Rev. Lett.* **64**, 1063 (1990).

[8] Y. Iye, S. Nakamura, T. Tamegai, T. Terashima, K. Yamamoto, Y. Bando , *Physica C* **166**, 62 (1990).

[9] Y. Iye, A. Fukushima, T. Tamegai, T. Terashima and Y. Bando, *Physica C* **185**, 297 (1991).

[10] Y. Iye, T. Terashima and Y. Bando, *Physica C* **184**, 362 (1991).

[11] Y. Iye, A. Watanabe, S. Nakamura, T. Tamegai, T. Terashima, K. Yamamoto, Y. Bando, *Physica C* **167**, 278 (1990).

141

[12] D. H. Kim, D. J. Miller, J. C. Smith, R. A. Holoboff, J. H. Kang, J. Talvacchio , *Phys. Rev. B* **44**, 7607 (1991).

[13] Y. Iye, S. Nakamura, T. Tamegai , *Physica C* **159**, 433 (1989).

[14] Y. Iye, T. Tamegai and S. Nakamura, *Physica C* **174**, 227 (1991).

[15] W. K. Kwok, U. Welp, V. M. Vinokur, S. Fleshler, J. Downey, G. W. Crabtree , *Phys. Rev. Lett.* **67**, 390 (1991).

[16] Y. Iye, T. Tamegai, H. Takeya and H. Takei, *Jpn. J. Appl. Phys.* **26**, L1057 (1987).

[17] T. K. Worthington, W. J. Gallagher, T. R. Dinger, *Phys. Rev. Lett.* **59**, 1160 (1987).

[18] U. Welp, W. K. Kwok, G. W.Crabtree, K. G. Vandervoort, J. Z. Liu , *Phys. Rev. Lett.* **62**, 1908 (1989).

[19] D. E. Farrell, C. M. Williams and S. A. Wolf, N. P. Bansal, V. G. Kogan , *Phys. Rev. Lett.* **61**, 2805 (1988).

[20] C. M. Fu, V. V. Moshchalkov, W. Boon, K. Temst, Y. Bruynseraede, G. Jakob, T. Hahn, H. Adrian, *Physica C* **205**, 111 (1993).

[21] J. Bardeen and M. J. Stephen, *Phys. Rev. A* **140**, 1197 (1965).

[22] V. L. Ginzburg and L. D. Landau, *Zh. Eksperim. i. Teor. Fiz.* **20**, 1064 (1950).

[23] D. E. Farrell, J. P. Rice, D. M. Ginsberg, J. Z. Liu , *Phys. Rev. Lett.* **64**, 1573 (1990).

[24] J.N. Li, K. Kadowaki, Z. Koziol and J.J. Franse, *Physica C* **185-189**, 1875 (1991).

[25] G. Blatter, V. Geshkenbein, and A. Larkin, *Phys. Rev. Lett.* **68**, 875 (1992).

[26] Y. Iye, I. Oguro, T. Tamegai, W. R. Datars, N. Motohira, K. Kitazawa, *Physica C* **199**, 154 (1992).

[27] D. E. Farrell, S. Bonham, J. Foster, Y. C. Chang, P. Z. Jiang, K. G. Vandervoort, D. J. Lam, V. G. Kogan , *Phys. Rev. Lett.* **63**, 782 (1989).

[28] K. Okuda, S. Kawamata, S. Noguchi, N. Itoh, K. Kadowaki , *J. Phys. Soc. Jpn.* **60**, 3226 (1991).

[29] G. Blatter, V. Feigel'man, V. Geshkeibein, A. Larkin, and V. Vinokur, *Rev. Mod. Phys.* **66**, 1125 (1994).

[30] M. W. Denhoff and J. P. McCaffrey, *J. Appl. Phys.* **70**, 3986 (1991).

[31] D. Feinberg, and A.M. Ettouhami, *Int. J. Mod. Phys.* **7**, 2085 (1993).

[32] M. Amirfeiz, M. R. Cimberle, C. Ferdeghini, E. Giannini, G. Grassano, D. Marre, M. Putti, A. S. Siri , *Physica C*,**288**, 37 (1996).

[33] D. Feinberg and V. Villard, *Phys. Rev. Lett.* **65**, 919 (1990).

[34] S.S. Maslov, and V. L. Pokrovsky, *Europhys. Lett.* **14**, 591 (1991).

[35] B. Janossy, A. de Graaf, P. H. Kes, V. N. Kopylov, T. G. Togonidze , *Physica C* **246**, 277 (1995).

[36] S. Kolesnik, T. Skoskiewicz, J. Igalson, Z. Tarnawki, *Phys. Rev. B* **54**, 13319 (1996).

[37] L. Fruchter,and I.A. Campbell, *Phys. Rev. B* **40**, 5158 (1989).

[38] G. Blatter, J. Rhyner, V. M. Vinokur, *Phys. Rev. B* **43**, 7826 (1991).

[39] J. Etheridge, *Philos. Mag.* **A73**, 643 (1996).

[40] J. Halbritter, *Phys. Rev. B* **48**, 9735 (1993).

Chapter 6

Giant Phase Slip Dissipation in YBCO Thin Film

6.1 Introduction

[1] One of the most fascinating properties of high-T_c layered cuprates is their anisotropy, especially high in bismuth and thallium based materials, which results from the weak interlayer coupling. This coupling influences the vortex dynamics, which is different than that observed in conventional or less anisotropic materials (3D-like YBCO). For a magnetic field applied at an angle with respect to the layers, this weak coupling changes the effective dimensionality of the vortex lines to 2D ("pancake" vortices), allows formation of Josephson vortices and vortex loops in the insulating regions between the CuO_2 bilayers, and causes very strong intrinsic pinning for the motion of Josephson vortices along the c-axis [1].

It is believed that for a tilted magnetic field ($H_{c_1} < H < H_{c_2}$), applied at an angle θ relative to the CuO_2 layers of a superconductor, the vortex lattice breaks up into a staircase structure. In weakly coupled layered materials, this can be considered as a combined lattice of Abrikosov point vortices (pancakes) in the planes, connected by Josephson strings locked in the space between the planes [2]. In highly anisotropic

---

[1] A version of this Chapter has been submitted for publication to *Phys. Rev. Lett.*

cuprates this staircase provides a possible explanation for the in-plane resistivity, that is independent of the relative angle between the current density **J** and the magnetic field **H** , both in the ab-planes. Since the staircase always has a component of **H** perpendicular to **J**, there will be a Lorentz force on it, which results in an electric field **E** || **J**. As the angle θ is reduced, the number of pancake vortices decreases with a decreasing $\sin\theta$ and at the same time, intrinsic pinning of the Josephson strings between the planes prevents direct string hopping parallel to c-axis except perhaps at very high applied transport currents [3, 4]. This implies that in this case dissipation is directly related to pancake motion and in the absence of thermal excitations, it depends only on the c-axis component of the magnetic field ($H\sin\theta$). This dependence has been revealed by many measurements performed over a wide range of angle θ and magnetic field **H**. Therefore this is believed to control the dissipation in Bi and Tl-based superconductors [3, 4].

If the magnetic field is tilted very close to the ab-plane, additional features could be observed. At $\theta = 0$, one expects that for a very clean sample and a sufficiently high anisotropy ($\gamma = \sqrt{\frac{m_c}{m_{ab}}} > 100$), no pancake vortices are present (since the c-axis component of **H** is zero). For a quasi-2D superconductor a lock-in transition has been predicted [6, 7]. It implies that if the field H is applied at an angle θ less than a certain critical angle θ_c the flux lines prefer to run strictly parallel to the ab-planes and remain locked-in between the layers. The lock-in transition is expected to cause a distinct change in torque, a sharp drop in the flux-motion resistance (a minimum in resistivity $\rho(\theta)$) and a corresponding rise in the critical currents, all within some critical angle θ_c very close to the CuO_2 planes. Sharp drop in the flux motion resistivity has been observed in moderately anisotropic materials like YBCO crystals [8]. A change in torque related to a lock-in transition has been reported in higher anisotropy materials like BSCCO and TBCCO [9, 10, 11].

Moreover, for the same parallel configuration (H parallel to the ab-planes), unexpected features have been observed in highly anisotropic layered superconductors. A peak at H || ab-planes has been seen in the angular dependence of resistivity

145

$\rho(\theta)$ of films and single crystals of BSCCO, TBCCO and organic superconductors. Aukkaravittaryapun et al [12] investigated the angular dependence of resistivity in BSCCO whiskers. They observed unusual angular dependence in the ohmic flux flow regime (at low currents and for temperatures close to T_c at zero resistivity). For magnetic field close to the ab-plane, they found two resistivity minima with a central maximum , a three minima and two maxima or a single minimum with shoulders, depending on temperature. Scaling of resistivity with field revealed that these features depend only on the magnitude of the field component perpendicular to the layers ($H \sin \theta$). Their results were explained using a model of a transition between a very mobile vortex gas and vortex solid phases [13]. Chaparala et al [14] reported that when a magnetic field is brought close to the layers [in Tl-2212, Bi-2212, Tl-1223 or $(BEDT - TTF)_2 Cu(NCS)_2$ single crystals], an anomalous rise was observed in the in-plane resistivity with a large maximum centered at $\theta = 0$, superimposed on a small background resistivity minimum over a relatively narrow angular range of approximately 1^0. The authors argued that this maximum corresponds to a local minimum in the critical current density at a zero angle. This extraordinary dissipation was attributed to the motion of noninteracting thermally excited vortex-antivortex pairs in the planes at low vortex densities. The authors concluded that the quasi-2D nature and the high anisotropy ($\gamma > 100$) in the materials they studied, are solely responsible for the increase in dissipation at an applied field H $\parallel$ ab-planes. They stated that this could explain why this resistivity maximum has never been reported in moderately anisotropic superconductors like YBCO.

However in a 2D-like YBCO thin film of $T_c \simeq 81$, similar effects have been observed. We report on the first experimental evidence for an extraordinary dissipation peak in the angular dependence of resistivity of YBCO. For temperatures very close to T_c onset, as the magnetic field is brought parallel to the CuO_2 layers, we have observed an increase in the in-plane resistivity with a peak centered at $\theta = 0$. The width of this peak decreases with an increasing magnitude of the field. Temperature dependence of the in-plane resistivity revealed the corresponding peak at tempera-

146

tures just below the onset T_c. The peak in $\rho(T)$ disappears when the magnetic field direction is rotated from the ab-planes towards the c-axis. The magnitude of this peak is also reduced by an increasing applied current. Similar features have been observed in highly anisotropic $Nd_{1.85}Ce_{0.15}CuO_4$ and $Pr_{1.85}Ce_{0.15}CuO_4$ crystals by Crusellas et al. [15] and in BSCCO(2212) crystals by Han et al. [16]. The authors argued that these features are due to a quasireentrant superconducting behavior in these systems. In thin wires of conventional superconductors like aluminium (Al) [17, 18, 19], the temperature dependence of resistivity has been found to exhibit a peak below T_c onset, which decreases with an increasing applied current. The peak in $\rho(T)$ of Al wires has been attributed to the phase-slip induced dissipation according to the Langer-Ambegaokar (LA) theory [20].

Our results obtained on a 2D-like YBCO film imply that the major contribution to the resistive peak comes from the phase-slip events. Since the LA theory is valid only for one-dimensional superconducting wires, this observation suggests a filamentary flow of the current in this system.

6.2 Experimental procedure

6.2.1 Sample Preparation

We have studied an epitaxial c-axis oriented YBCO thin film (140 nm thick) grown on a (100) oriented sapphire substrate (with CeO_2 buffer layer) using laser ablation technique. The sample exhibits a vanishing zero-field resistivity at $T_c = 81.7K$ and has a transition width of about 3.4 K, and room temperature resistivity $\rho_{300K} = 34.2\mu\Omega cm$ $\left(\frac{\rho_{300K}}{\rho_{100K}} = 2.4\right)$. This film has a relatively high critical current density J_c of $5.2 \times 10^6 A/cm^2$ at 10 K. Critical current measurements versus temperature were performed using a scanning Hall probe technique [21] and a disk-shaped sample. J_c was estimated from the magnitude of the remanent magnetization at the saturation level using the Biot-Savart law.

Initially the film was patterned with a metal mask, using conventional photolithog-

raphy and wet etching, to form of a disk of an 8.5 mm in diameter. After the measurement of the temperature dependence of the critical current density (J_c), the film was patterned into a form of a $60\mu m$ wide and 6.4 mm long strip with six measurement probes. Large area contacts on the film were deposited by silver-sputtering in order to minimize Joule heating effects. Copper leads were attached to silver contacts using mechanically pressed indium. A typical distance between voltage probes was 0.4 mm.

6.2.2 Measurement Procedure

We performed the measurements of the resistivity as a function of the angle θ between the ab-plane of the film and the direction of the magnetic field H. These angular studies were done over a temperature range within the superconducting transition [between $T_{c0}(R = 0)$ and T_c onset], as a function of the magnitude of the magnetic field and applied current density. The angular measurements were carried out by rotating a copper sample holder about its vertical axis in a horizontal magnetic field up to 1 Tesla generated by a copper-wound coil magnet.

The angular rotation was driven by a computer-controlled, backlash-free, stepping motor and a 100 to 1 gear reducer combination. The reading of the angle was accurately monitored by an 8000-line optical encoder attached to the sample holder. The angular resolution of the system is 0.045^o as determined by the optical encoder. The film was mounted on the sample holder with the c-axis perpendicular to the holder's vertical rotating axis, which allowed us to change the magnetic field direction in a plane parallel to the c-axis.

Resistivity was measured using a standard DC four-probe method. The current was applied to the sample in the form of short pulses (of duration less than 200 ms) in both directions, in order to eliminate the background noise and charge accumulation as well as to reduce Joule heating. The voltage was measured using a Keithley 2182 Nanovoltmeter in synchronization with a Keithley 236 Current Source, where the nanovoltmeter was used as the triggering unit. The nanovoltmeter was operated in a Delta mode. This mode allowed the measurement and the calculation of the

148

voltage for the DC current-reversal technique to eliminate the effects of thermal emf's in the leads. Each Delta reading was calculated from two voltage measurements of the sample for two opposite directions of the current. Since the measurements were done in the superconducting transition region where the change in resistivity with temperature was the steepest, a precise temperature control was an essential experimental requirement. Temperature was monitored by a carbon-glass resistance thermometer and an inductanceless heater and controlled to better than $\pm 10mK$ for each single angular sweep. This was achieved by rotating the sample very slowly in the magnetic field in order to reduce variations in the emf in the heater which could disturb the temperature reading. The term "resistivity" is used in this paper to denote the quantity E/J (where E is the electric field and J is the transport current density), and it does not imply an ohmic response.

All measurements were carried out with the transport current **J** parallel to the ab-planes. However, each measurement was performed for two different orientations of the magnetic field with respect to the current. In the first one, the field was rotated in a plane perpendicular to the current direction while in the other one the field was rotated in a plane parallel to the current and the c-axis directions [see Fig.6.1(a)]. All measurements were done in a field cooling (FC) regime, with the magnetic field applied to the sample at a temperature above the T_c(onset), followed by slow cooling down to the required temperature of measurement.

6.3   Experimental results

6.3.1   Temperature dependence of resistivity

The temperature dependence of resistivity ρ has been measured over a temperature range of 78-300K in a zero magnetic field. For a smaller range, (78-90 K) between $T_{c0}(R = 0)$ and T_c(onset), ρ has been investigated for different orientations of the magnetic field with respect to the direction of the current density **J**. Fig.6.1(a) shows two possible orientations of the magnetic field **B** with respect to **J** and the ab-plane

149

of the film. The left figure illustrates the case where the field $\mathbf{B}$ is rotated in a plane which is parallel to the direction of $\mathbf{J}$ while the right one represents the case where $\mathbf{B}$ is rotated in a plane perpendicular to $\mathbf{J}$. We refer to the first configuration as $\mathbf{B} \parallel \mathbf{J}$ and the second one as $\mathbf{B} \perp \mathbf{J}$. Fig.6.1(b) shows the temperature dependence of resistivity for a temperature range of 78-87 K for B=0 T and 0.68 T. The resistivity measurements in the field were carried out for three different orientations: $\mathbf{B} \parallel \mathbf{J}$ ($\theta = 0$), $\mathbf{B} \perp \mathbf{J}$ with $\mathbf{B}$ parallel to the ab-plane ($\theta = 0$), and with $\mathbf{B}$ parallel to the c-axis. In Fig.6.1(b) two temperature regions are identified: region I represents the range of temperatures over which the angular dependence of resistivity ρ as a function of θ [$\rho(\theta)$] shows a minimum for both $\mathbf{B} \parallel \mathbf{J}$ and $\mathbf{B} \perp \mathbf{J}$ while region II represents the range of temperatures over which $\rho(\theta)$ and $\rho(T)$ displays a maximum for the same configurations. It is important to notice that for $\mathbf{B}$ parallel to the ab-planes, in region I, $\rho(T)$ is independent of the magnitude of $\mathbf{B}$ and the relative angle between $\mathbf{B}$ and $\mathbf{J}$. On the other hand in region II, $\rho(T)$ is independent of $\mathbf{B}$ only for $\mathbf{B} \parallel \mathbf{J}$. The peak in $\rho(T)$ in this region for $\mathbf{B} \perp \mathbf{J}$ is higher than that observed for $\mathbf{B} \parallel \mathbf{J}$. This peak is completely suppressed for $\mathbf{B} \parallel$ c-axis case. The maximum resistivity in the peak is higher than the onset resistivity. The resistivity between the onset temperature and the room temperature exhibit a linear temperature dependence.

6.3.2 Angular dependence of resistivity: Effect of temperature and magnetic field

The angular dependence of resistivity $\rho(\theta)$ in a constant magnetic field for different temperatures in region I, has been measured for both $\mathbf{B} \parallel \mathbf{J}$ and $\mathbf{B} \perp \mathbf{J}$ for the angular range from -20° to $+20^\circ$. Fig.6.2(a) shows $\rho(\theta)$ as a function of temperature from 81.43 K to 82.23 K in a magnetic field of 0.68 T. $\rho(\theta)$ displays a sharp minimum at $\theta = 0$ and it increases with temperature. $\rho(\theta)$ is the same for both $\mathbf{B} \parallel \mathbf{J}$ and $\mathbf{B} \perp \mathbf{J}$. The very small differences in $\rho(\theta)$ could be attributed to small temperature fluctuations. The width of this minimum [defined as half width at half minimum

150
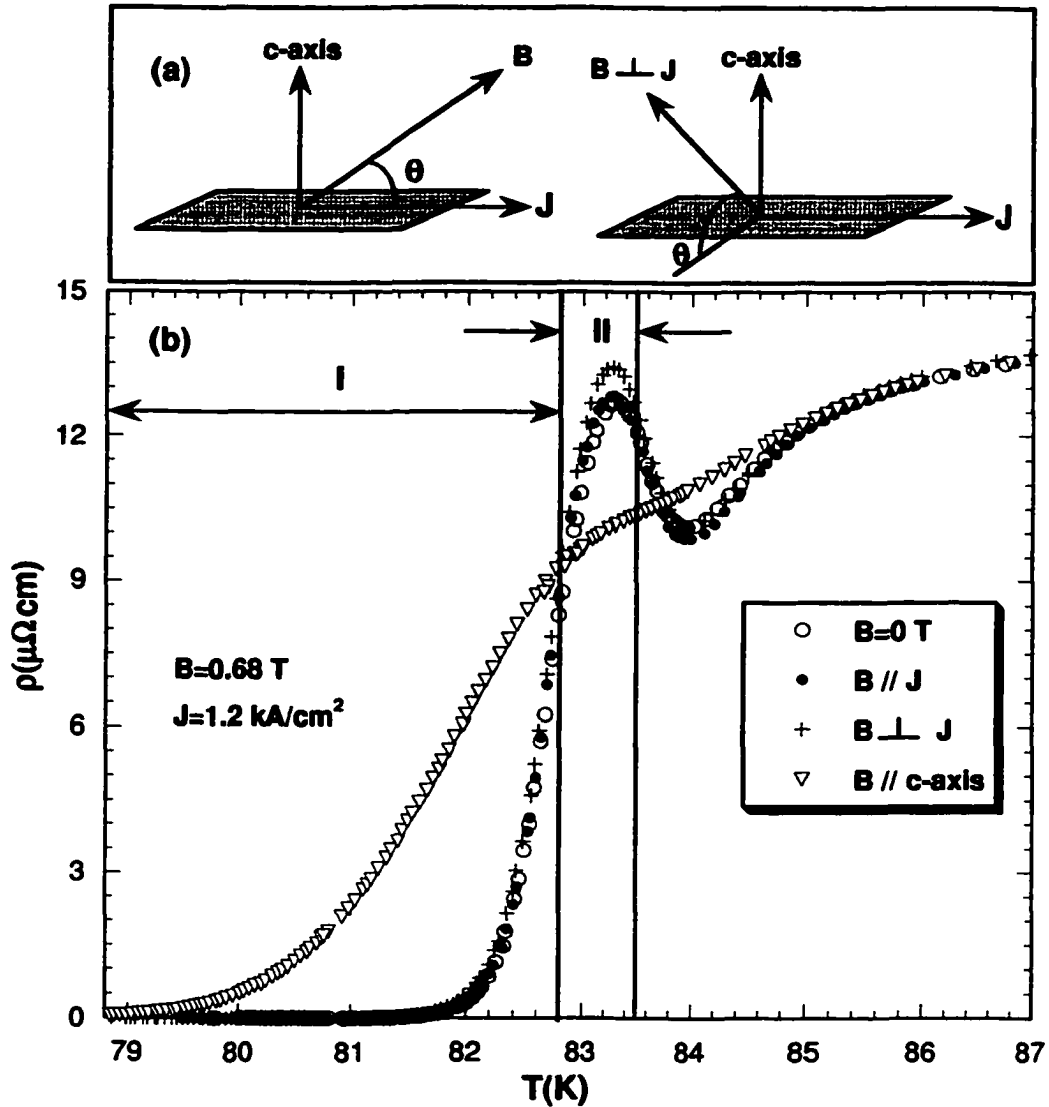
Figure 6.1: (a) Two configurations of **B** with respect **J** that were used during the measurements of the angular dependence of resistivity $\rho(\theta)$ in a magnetic field: **B** is rotated in a plane parallel to both **J** and the c-axis (left side), or **B** is rotated in a plane parallel to the c-axis but perpendicular to **J** (right side). (b) Temperature dependence of resistivity for YBCO thin film measured in a field of 0.68 T at different orientations and in a zero field. Region I denotes a temperature range over which $\rho(\theta)$ displays a minimum at $\theta = 0^{\circ}$ (**B** parallel to the ab-planes) [see Figs.6.2(a) and 6.3(a)]. Region II denotes a temperature range over which $\rho(\theta)$ displays a maximum at $\theta = 0^{\circ}$ [see Fig.6.3(b)]. A minimum in $\rho(\theta)$ at $\theta = 0^{\circ}$ was again observed for the temperature range of 83.5-84.0 K. For **B** parallel to the ab-planes, a maximum in $\rho(T)$ at T=83.25 K was observed. It is independent of the magnitude of **B** for **B** ∥ **J**. For **B** ⊥ **J** this maximum increases with **B**. Note the absence of the maximum when **B** is oriented along the c-axis.

151

(HWHM)], decreases with an increasing temperature. The widths at 81.43 K and 82.23 K are 1.54^o and 1.07^o, respectively. On the other hand, the depth of the minimum, defined as $(\rho(5^o) - \rho(0^o))$, increases with an increasing temperature. The depths of the minimum at 81.43 K and 82.23 K are 1.49 $\mu\Omega cm$ and 2.24 $\mu\Omega cm$, respectively.

Fig.6.2(b) shows the angular dependence of resistivity at a constant temperature of T=81.43 K, as a function of magnetic field. We measured this dependence for both **B** $\parallel$ **J** and **B** $\perp$ **J** configurations. The data for these two configurations are identical. The minimum in resistivity at $\theta = 0^o$ is independent of the magnitude of **B**. HWHM decreases from HWHM=2.3^o at B=0.17 T down to HWHM=2.0^o at B=0.86 T. The depth of the minimum increases with the field.

Fig.6.3(a) shows $\rho(\theta)$ as a function of temperature between 82.52 K and 82.93 K in a magnetic field of 0.68 T. At a temperature of approximately 82.82 K, which corresponds to the border line between region I and II in Fig.6.1(b), there is a crossover from a minimum in $\rho(\theta)$ to a peak in $\rho(\theta)$. This peak grows with an increasing temperature reaching a maximum value at 83.23 K [see Fig.6.3(b)]. While the minimum in $\rho(\theta)$ is independent of the orientation of B with respect to J [**B** $\perp$ **J** and **B** $\parallel$ **J**, see Fig.6.2(a)], the peak in $\rho(\theta)$ depends on these orientations [$\rho(\theta)_{B \perp J} > \rho(\theta)_{B \parallel J}$].

The peak height plotted as a function of temperature is shown in Fig.6.4(a). This behavior is approximately parabolic with a maximum at 83.25 K.

In order to compare the peak in $\rho(\theta)$ at $\theta = 0^o$ with that at $\theta = 90^o$, we measured $\rho(\theta)$ over an angular range between -30° and 210° [see Fig.6.4(b)]. Clearly, ρ for **B** $\parallel$ ab-plane is much higher than that for **B** $\parallel$ c-axis. Moreover $\rho(\theta)$ reaches its minimum at $\theta = 36^o$ for all fields.

The peak in $\rho(\theta)$ was measured as a function of magnetic field for both **B** $\perp$ **J** and **B** $\parallel$ **J** configurations [see Fig.6.5]. For fields between zero and 0.5 T, the peak increases with field but the magnitude of the peak saturates at higher fields. In Fig.6.5(a) for **B** $\perp$ **J** configuration, one can distinguish two different dissipation regimes: the first one for $| \theta | > 1.5^o$ where $\rho(\theta)$ decreases with an increasing field,

152
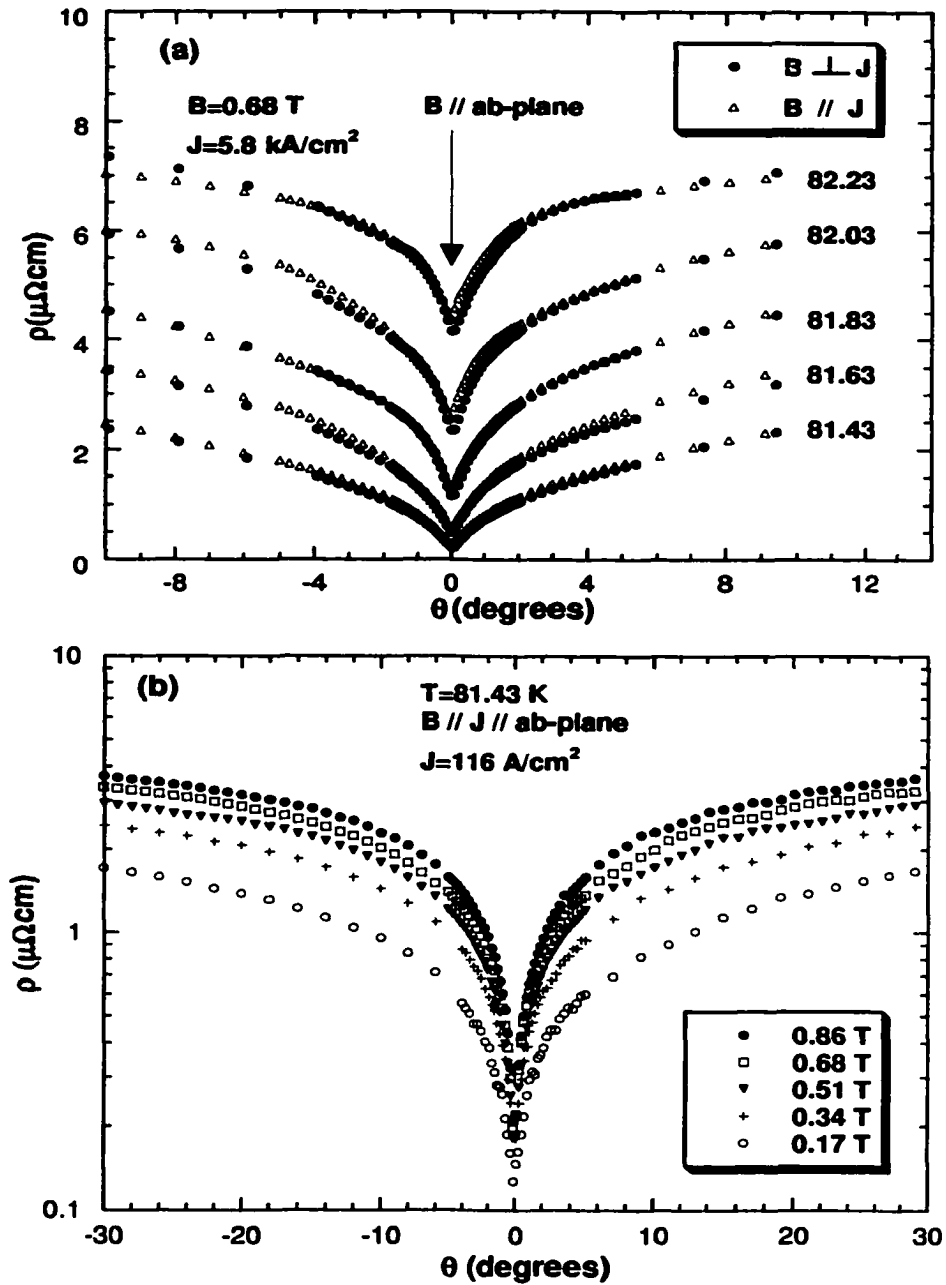
Figure 6.2: (a) Angular dependence of resistivity for YBCO film, at different temperatures between 81.43K and 82.23K in a field of 0.68 T for both $B \parallel J$ and $B \perp J$ configurations, which reveals a minimum in $\rho(\theta)$ at $\theta = 0^\circ$ (B parallel to the ab-planes). Identical behavior of $\rho(\theta)$ can be observed for both field orientations with respect to J ($B \parallel J$ and $B \perp J$). (b) The corresponding angular dependence of ρ measured as a function of the magnitude of B at a temperature of 81.43 K for the $B \parallel J$ orientation. An identical behavior has been observed for $B \perp J$ orientation.

153
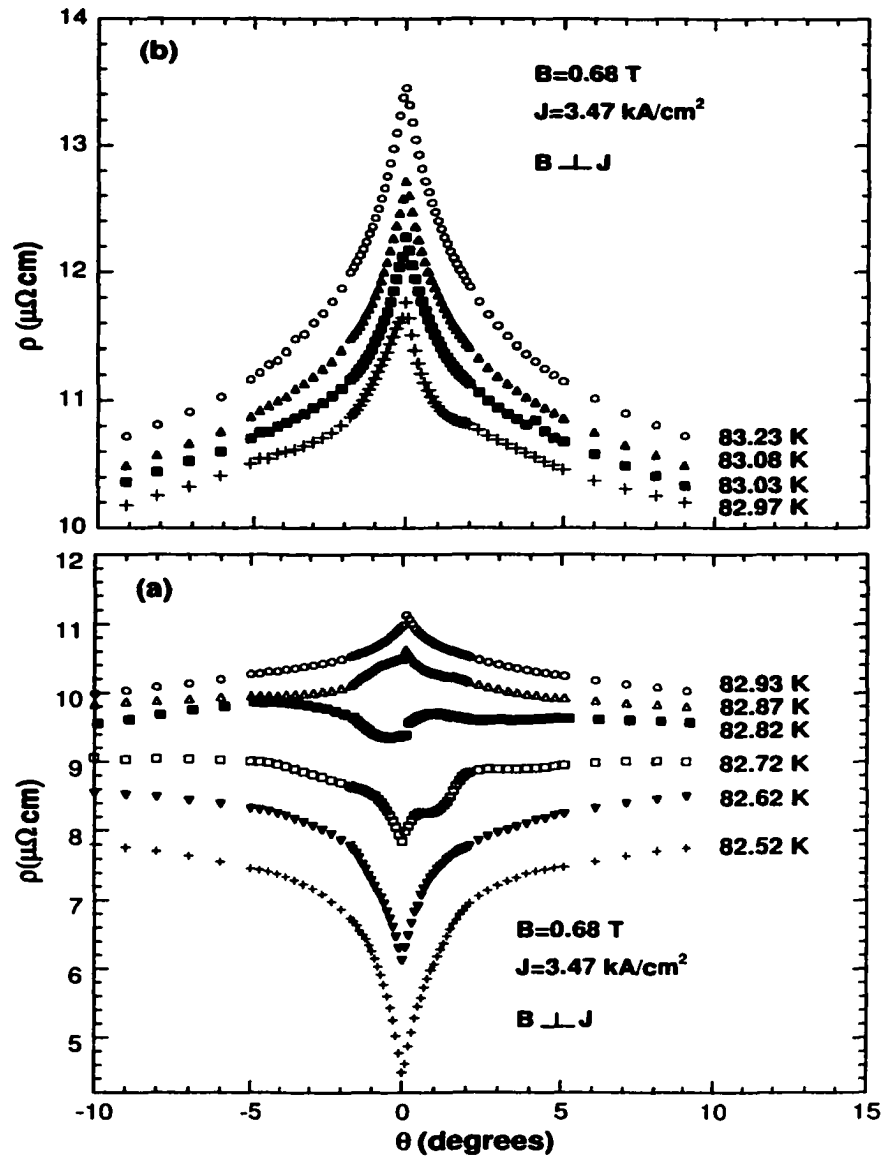
Figure 6.3: Angular dependence of resistivity in a field of 0.68 T, measured as a function of temperature from 82.52 K up to 83.23 K. Note the change of $\rho(\theta)$ at $\theta = 0°$ from a minimum at low temperatures $(T < 82.82K)$(a) to a maximum at higher temperatures (b).

154
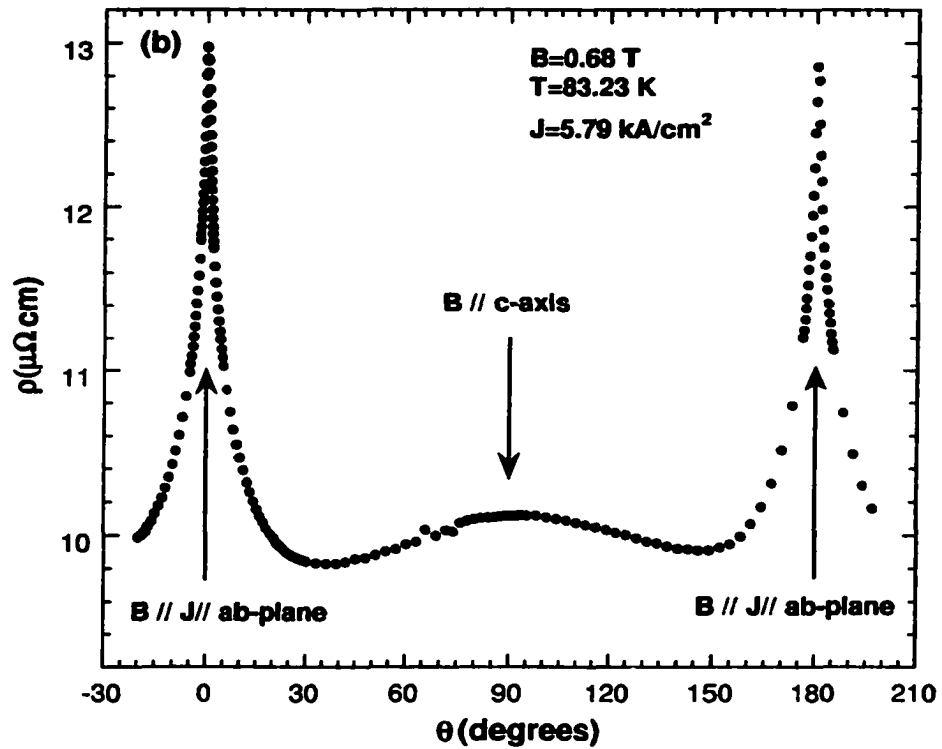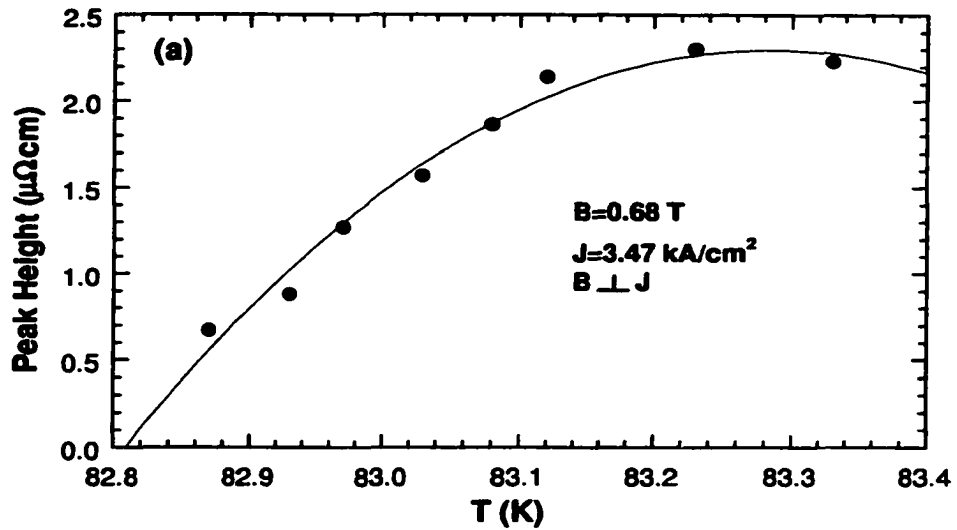
Figure 6.4: (a) Temperature dependence of the peak height, defined as $\Delta\rho = \rho(0^o) - \rho(5^o)$, in $\rho(\theta)$ seen in Fig.6.3. (b) Angular dependence of resistivity $\rho(\theta)$ in a field of 0.68 T, measured over an angular range between -30° and 210° at a temperature of 83.23 K. Note the resistive peaks at $\theta = 0^o$ and $\theta = 180^o$ (**B** parallel to the ab-planes) which are about 30% higher than the maximum at $\theta = 90^o$ (**B** parallel to the c-axis).

155

while the other for smaller angles ($|\ \theta\ | < 1^o$) where $\rho(\theta)$ increases with an increasing field. For the **B** $\|$ **J** case [Fig.6.5(b)], $\rho(\theta)$ for $|\ \theta\ | > 0.3^o$ is dominated by the first regime [$\rho(\theta)$ decreases with an increasing **B**]. For small angles ($|\ \theta\ | < 0.3^o$), $\rho(\theta)$ is almost independent of the field.

Fig.6.6(a) compares the peaks in $\rho(\theta)$ for the **B** $\|$ **J** and **B** $\perp$ J at 0.68 T and 83.13 K. $\rho(\theta)$ for **B** $\perp$ **J** is larger than that for **B** $\|$ **J** for the whole range of angles measured, but the difference between the two curves is decreasing with a decreasing angle $|\ \theta\ |$. Peak height, defined as $\rho(0^o) - \rho(5^o)$, increases logarithmically with the field **B** [see Fig.6.6(b)], while the peak width (half width at half maximum HWHM) decreases logarithmically with an increasing **B** [Fig.6.6(c)]. The peak height is larger for **B** $\|$ **J** case in comparison to that for **B** $\perp$ **J**, however the peak width for **B** $\|$ **J** is smaller than that for **B** $\perp$ **J**.

6.3.3 Angular dependence of resistivity: Effect of the applied current

The angular dependence of resistivity was measured also as a function of the applied current density at a constant temperature and field. Fig.6.7(a) presents the results for the peak in $\rho(\theta)$ for a wide range of applied current density J (from 0.9 to 69.4 kA/cm^2) at a field of 0.68 T and a temperature of 83.03 K. As expected, for angles $|\ \theta\ | > 2^o$, $\rho(\theta)$ increases non-linearly with an increasing J, but for small angles $|\ \theta\ | < 1^o$ the opposite happens. In the region, where $|\ \theta\ | < 1^o$, starting at small current density ($J \leq 11.6 kA/cm^2$) the peak initially decreases with an increasing current, but for J larger than $23.1 kA/cm^2$, a minimum in $\rho(\theta)$ develops. This behavior is essentially the same for both **B** $\|$ **J** and **B** $\perp$ **J** configurations. At temperatures lower than 82.80 K, $\rho(\theta)$ exhibits a minimum for both **B** $\|$ **J** and **B** $\perp$ **J** [see Figures 6.2(a) and 6.3(a)]. Effect of the current on this minimum is different from that observed for the peak at higher temperatures. The minimum in $\rho(\theta)$ is completely suppressed at very large applied currents ($J \geq 57.9 kA/cm^2$). At very small J, less than $0.2 kA/cm^2$, the minimum is independent of J.

156
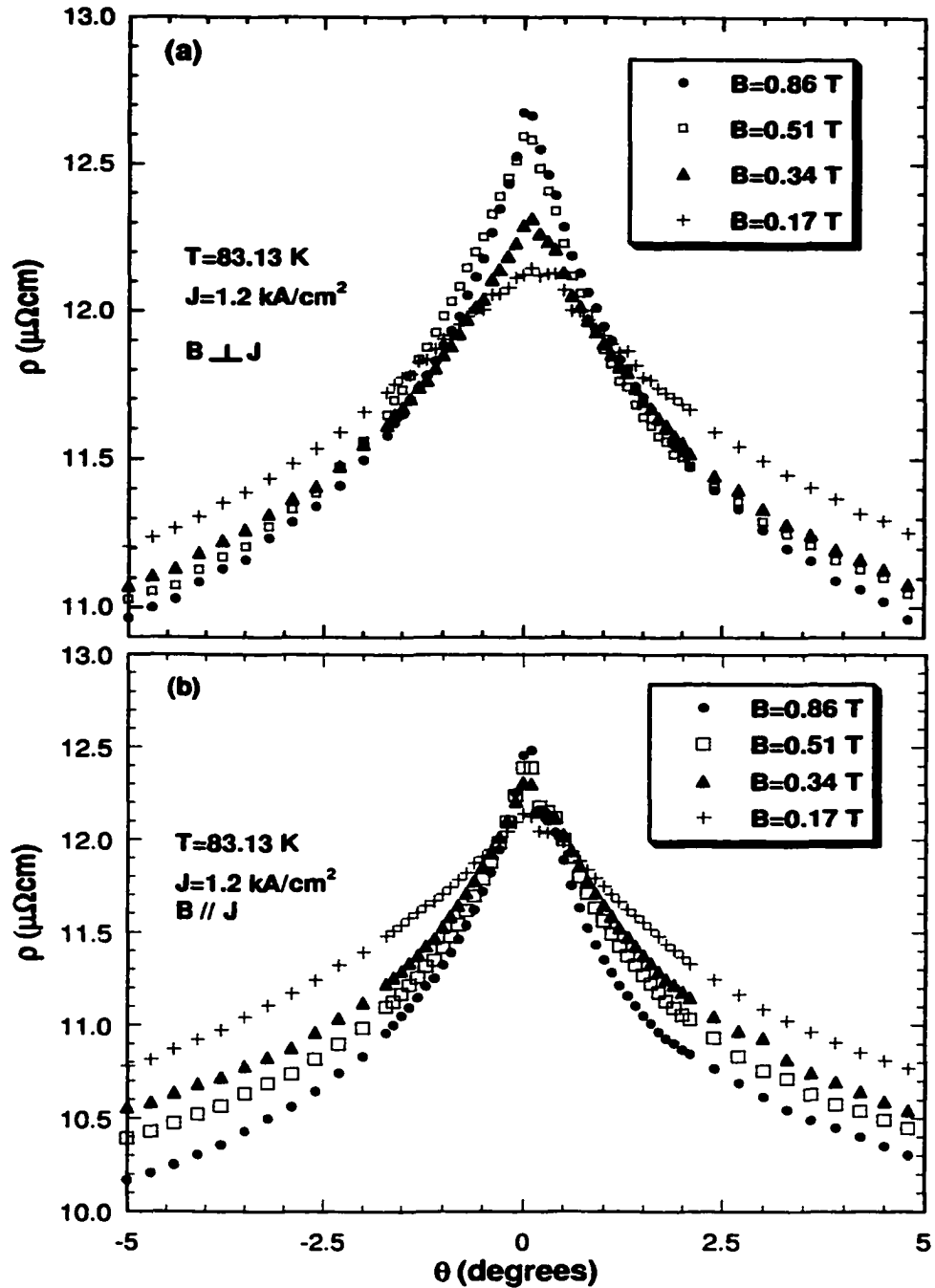
Figure 6.5: Angular dependence of resistivity $\rho(\theta)$ for θ between -5° and 5°, measured for different applied magnetic fields at a fixed temperature of 83.13 K. (a) the data for $\mathbf{B} \perp \mathbf{J}$ orientation where $\rho(\theta)$ increases with an increasing $\mathbf{B}$ for $\mid \theta \mid < 1^{o}$ but decreases with an increasing $\mathbf{B}$ for $\mid \theta \mid > 1^{o}$. (b) the data for $\mathbf{B} \parallel \mathbf{J}$ orientations; ρ at $\theta = 0^{o}$ is almost independent of $\mathbf{B}$. Note the decrease of $\rho(\theta)$ with an increasing $\mathbf{B}$ for $\mid \theta \mid > 0.5^{o}$.

157
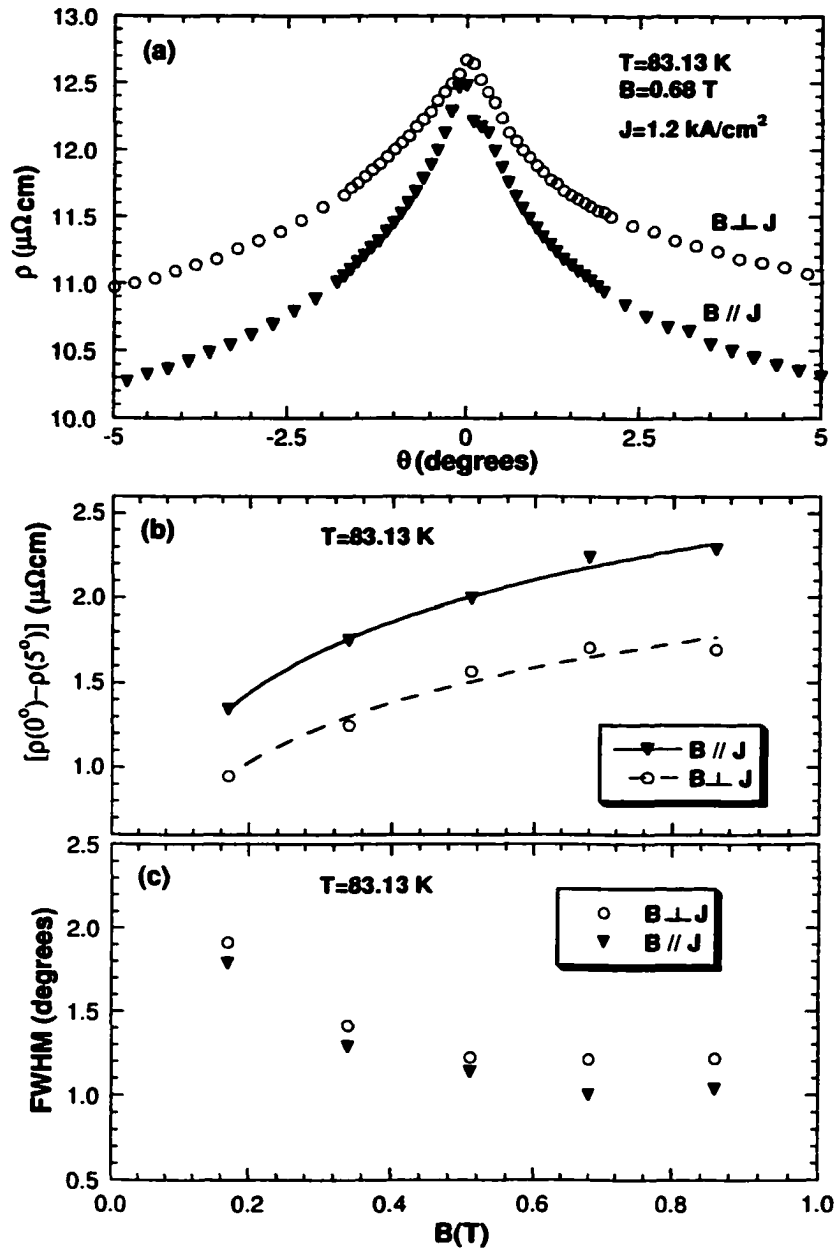
Figure 6.6: (a) Comparison of $\rho(\theta)$ measured for $\mathbf{B} \perp \mathbf{J}$ and $\mathbf{B} \parallel \mathbf{J}$ orientations in a field of 0.68 T at a temperature of 83.13 K. Note that for $\mathbf{B} \parallel \mathbf{J}$ orientation $\rho(\theta)$ decreases faster with an increasing $| \theta |$ than that for $\mathbf{B} \perp \mathbf{J}$. Comparison of the peak height $\Delta\rho = \rho(0^o) - \rho(5^o)$ (b) and the peak width (FWHM) (c) measured as a function of B for $\mathbf{B} \perp \mathbf{J}$ and $\mathbf{B} \parallel \mathbf{J}$ orientations at a temperature of 83.13 K.

158
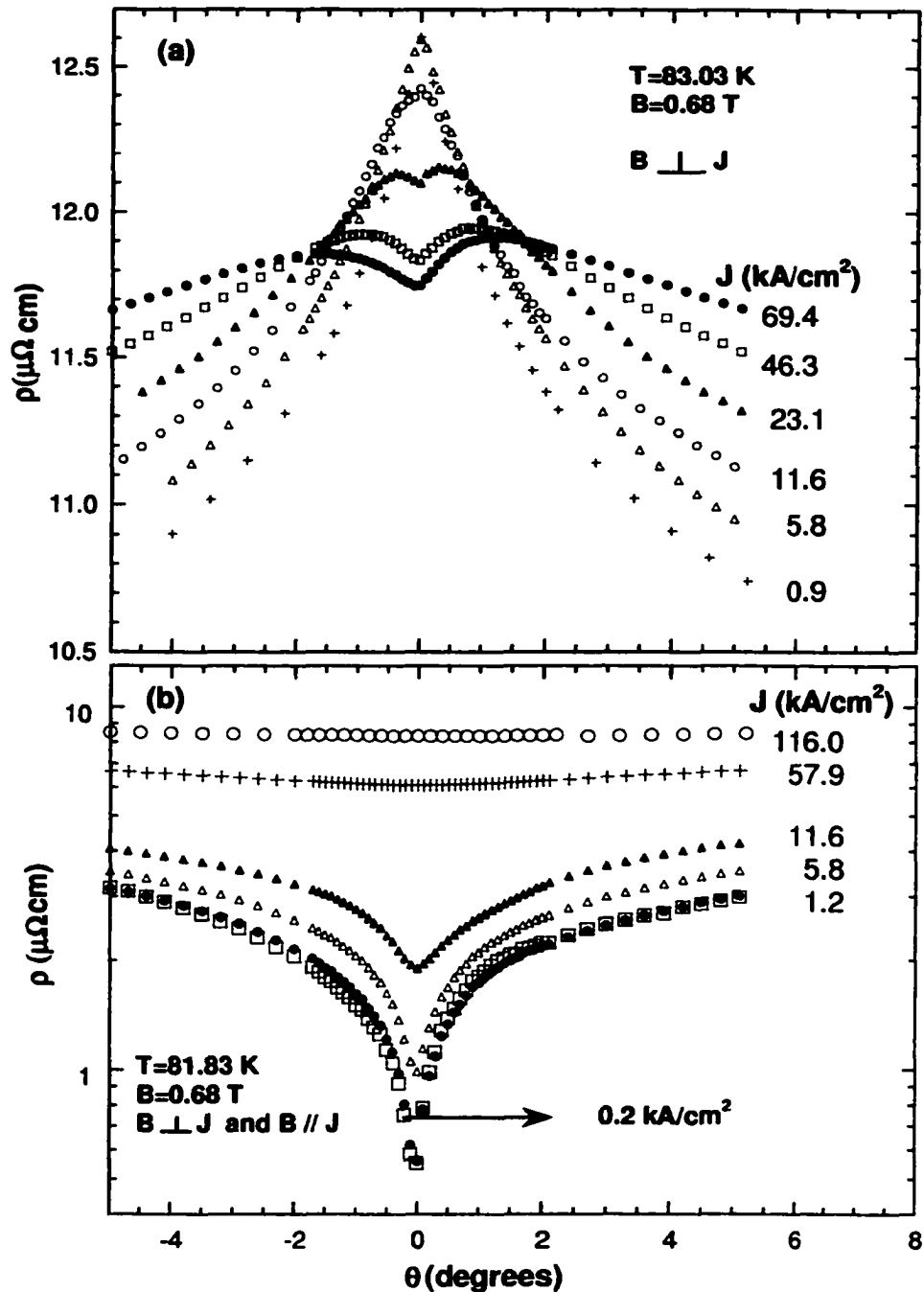
Figure 6.7: (a) Angular dependence of resistivity $\rho(\theta)$ measured as a function of an applied current density J over an angular range of -5° and 5° (for B=0.68 T and T=83.03 K) . Note that the maximum observed at $\theta = 0^{o}$ at low J is gradually converted to a minimum when J is increased. (b) The corresponding behavior of $\rho(\theta)$ as a function of J measured at a lower temperature of 81.83 K. Note that the minimum at $\theta = 0^{o}$ observed at low J, disappears gradually when J is increased.

159

Temperature dependence of resistivity was measured as a function of current density at a fixed field for $\mathbf{B} \parallel \mathbf{J}$. Fig.6.8(a) shows $\rho(T)$ for three selective applied current densities J (from 0.1 to 57.9 kA/cm^2) at a field of 0.68 T. For the range of temperatures over which $\rho(T)$ displays a peak [region II in Fig.6.1(b)], $\rho(T)$ decreases with an increasing current. At all other temperatures, $\rho(T)$ increases with an increasing current as expected. The inset in Fig.6.8(a) shows the resistivity as a function of current at a fixed temperature of 83.19 K and a field of 0.68 T for $\mathbf{B} \parallel \mathbf{J}$. At temperatures less than 82.8 K, just below the peak in $\rho(T)$, $\rho(\theta)$ exhibits a minimum at $\theta = 0^o$ [see Fig.6.3(a)]. The question was, what is the shape of $\rho(\theta)$ around $\theta = 0^o$ above the peak in $\rho(T)$, at temperatures between 83.4 K and T_c (onset), where $\rho(T)$ increases with J. Fig.6.8(b) displays $\rho(\theta)$ as a function of temperature between 83.03 K and 83.83 K in a magnetic field of 0.68 T for $\mathbf{B} \perp \mathbf{J}$. $\rho(\theta)$ displays a peak for the range of temperatures between 82.87 K to 83.35 K similar to that shown in Fig.6.3(b), but at higher temperatures $(T > 83.4K)$ a minimum in $\rho(\theta)$ starts to develop over a narrow angular range of $\mid \theta \mid< 1^o$ while still the peak persists for angles $\mid \theta \mid> 1^o$. However at higher temperatures $(83.65K < T < 84.0K)$, the peak disappears completely and instead a sharper minimum appears similar to those shown in Fig.6.2(a). The inset of Fig.6.8(b) is a re-plot of the minimum at two temperatures 83.63 and 83.83 K using a smaller vertical scale to show the sharpness of the minimum.

6.4 Discussion

6.4.1 Investigations of Anisotropy

Almost all careful experimental investigations of the angular dependence of resistivity $\rho(\theta)$ of $YBa_2Cu_3O_{7-\delta}$ (YBCO) thin films in a magnetic field parallel to the ab-planes revealed a clear difference between $\rho(\theta)$ for $\mathbf{B} \parallel \mathbf{J}$ and $\mathbf{B} \perp \mathbf{J}$ configurations [3, 4, 22, 23]. The only exception from this behavior is the case of very thin films ($\sim 10nm$), with T_c=80.5 K and $\delta = 0.13$ [4], where the film approaches the 2D limit and the results for the two configurations $\mathbf{B} \parallel \mathbf{J}$ and $\mathbf{B} \perp \mathbf{J}$ are identical. The

160
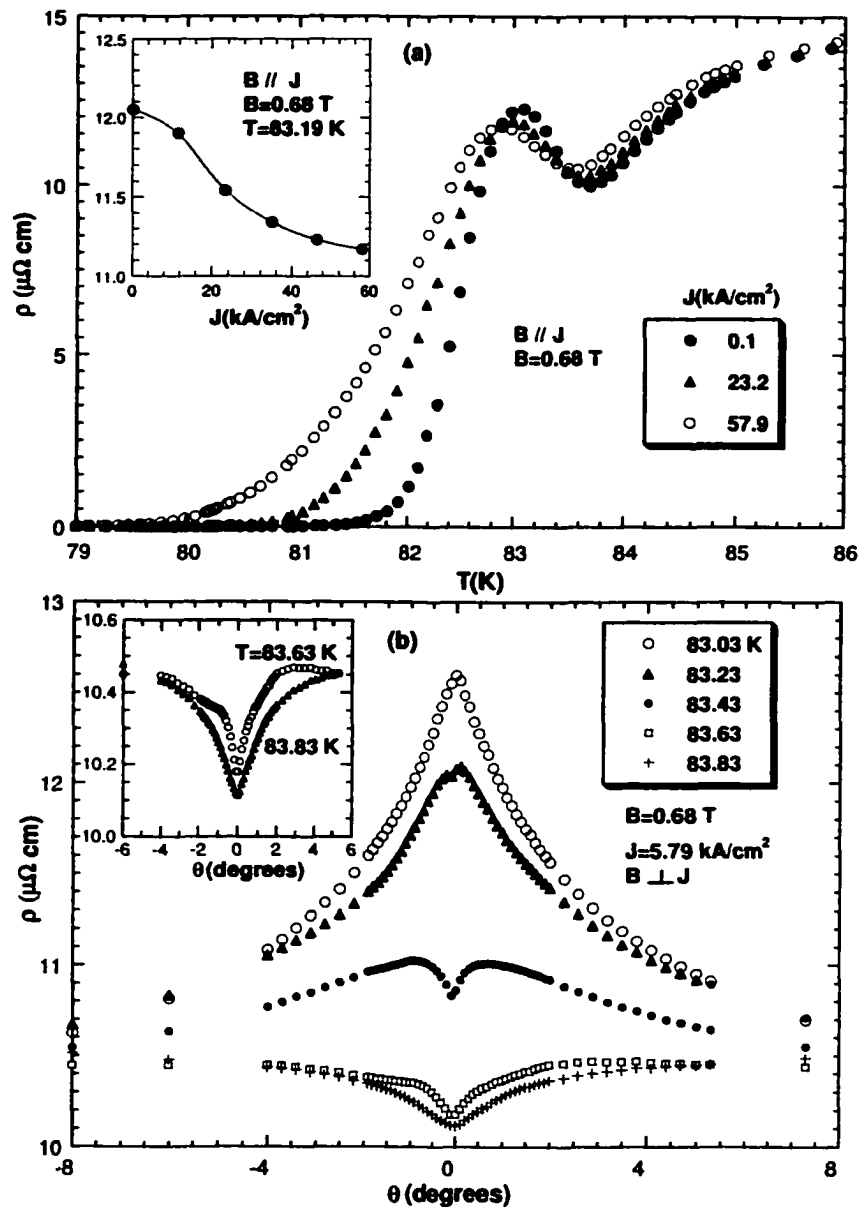
Figure 6.8: Temperature dependence of resistivity $\rho(T)$ measured as a function of an applied current density J for **B** ∥ **J** orientations in a field of 0.68 T. At a temperature of 83.19 K a maximum in $\rho(T)$ is seen. The resistivity at the maximum decreases with an increasing J (see the inset). (b) Angular dependence of resistivity $\rho(\theta)$ measured at different temperatures higher than 83.03 K over an angular range of −5° and 5° (in a field of 0.68 T). When the temperature is increased towards T_c onset, the maximum at $\theta = 0°$ is converted to a minimum. The minima at temperatures of 83.63 K and 83.83 K are shown on an expanded vertical scale in the inset.

161

difference between $\rho(\theta)$ for $\mathbf{B} \parallel \mathbf{J}$ and $\mathbf{B} \perp \mathbf{J}$ indicates smaller anisotropy. In general YBCO behaves like 3D and in fact is believed to be the least anisotropic among all high-T_c cuprates. In general, the anisotropy factor γ in YBCO increases with an increasing oxygen deficiency factor δ. The results of our experiments contradict this general behavior. They revealed that some YBCO films, of thickness much larger than 10 nm (namely between 140 and 300 nm) and of $T_c = 82K$ or 90 K , do not follow the general dependence of γ on δ and in fact exhibit a higher anisotropy (a 2D like at small δ i.e $\gamma = 35$ for YBCO with $T_c \sim 90K$ and $\gamma > 100$ (see Chapter 5) for YBCO with $T_c \sim 82K$). The following experimental observations on a selected YBCO film support this argument. Temperature dependence of resistivity [Fig.6.1(b)] for temperatures less than 82.8 K (region I), shows the overlapping data for $\mathbf{B} \parallel \mathbf{J}$, $\mathbf{B} \perp \mathbf{J}$ and $\mathbf{B}{=}0$ ($\mathbf{B} \parallel$ab-planes). In other words, $\rho(T)$ is independent of the magnitude of $\mathbf{B}$ and the angle between $\mathbf{B}$ and $\mathbf{J}$ which means that the dissipation is mainly controlled by the component of $\mathbf{B}$ perpendicular to the ab-planes ($\mathbf{B}_\perp = \mathbf{B}\sin\theta$), and $\rho(\theta)$ scales with $\mathbf{B}\sin\theta$. This type of dissipation is a result of 2D-like anisotropy. Observation of the minimum in $\rho(\theta)$ [Fig.6.2(b)], measured at different temperatures, which is independent of the relative orientation of $\mathbf{B}$ with respect to $\mathbf{J}$ indicates a large anisotropy (which approaches the 2D limit) like that observed for BSCCO system [24]. $\rho(\theta)$ measured at different applied currents densities [see Fig.6.7(b)], is also independent of $\mathbf{B} \parallel \mathbf{J}$ and $\mathbf{B} \perp \mathbf{J}$ orientations, and very similar to that observed in BSCCO [24]. For materials with small anisotropy, the difference in $\rho(\theta)$ between $\mathbf{B} \parallel \mathbf{J}$ and $\mathbf{B} \perp \mathbf{J}$ is expected to increase with an increasing current which we do not observe here.

Large anisotropy is responsible for the fact that $\rho(\theta)$, plotted in Fig.6.2(b) for different fields $\mathbf{B}$, is independent of $\mathbf{B} \parallel \mathbf{J}$ and $\mathbf{B} \perp \mathbf{J}$ orientations. This figure enabled us to obtain a quantitative estimate of the anisotropy of the sample using scaling. The anisotropy factor γ of YBCO, for a 3D case, can be calculated using the anisotropic Ginzburg-Landau (GL) model (known as the effective mass model). The effective mass anisotropy factor $\gamma = \sqrt{\frac{m_c}{m_{ab}}} = \frac{\xi_{ab}}{\xi_c}$ is about 5 [25, 26, 28] for fully

162

oxygenated YBCO (overdoped case , $\delta = 0$). Factor γ in YBCO increases with an increasing oxygen deficiency, as the CuO chain layer becomes more insulating. For YBCO of $T_c \approx 80K$, similar to the YBCO film we studied, γ is about 16 [29] while for low T_c YBCO ($\approx 60K$), γ is as high as 40 [29]. However, no scaling of $\rho(\theta)$ with a reduced field defined as $B\sqrt{\gamma^{-2}\cos^2\theta + \sin^2\theta}$, according to the GL model, has been achieved for $\gamma = 16$ [Fig.6.9(a)] for our film. A better scaling (especially at low angles θ) has been obtained using $\gamma = 40$, the largest reported for YBCO, [see Fig.6.9(b)]. Surprisingly an excellent scaling has been obtained using $B\sin\theta$ as the scaling parameter instead of $B\sqrt{\gamma^{-2}\cos^2\theta + \sin^2\theta}$. Such scaling makes all data points from different fields to collapse onto a single curve, which shows that the 2D model works quite well for the YBCO sample under study [see Fig.6.9(c)]. Therefore this film appears to be very highly anisotropic with a value of γ similar to that of BSCCO ($\gamma > 100$). The anisotropy of this sample approaches the 2D limit, which means that the magnetic field lines penetrating the film at an angle θ to the planes, consist of strongly pinned Josephson strings between the layers, connected by "pancake vortices" in the layers. The former contributes very little to the dissipation.

It has been argued [14] that a transport current applied along the ab-planes could make a detour across the layers (parallel to c-axis) due to stacking faults and other inhomogeneities that may be present in the ab-planes. For a highly anisotropic HTCS this interlayer current could produce an additional dissipation. In our measurement we excluded this possibility using the following arguments:

1. There is a significant difference between the peak in $\rho(T)$ [see region II in Fig.6.1(b)] measured for **B** $\parallel$ **J** and **B** $\perp$ **J** configurations [the peak of $\rho(T)_{B\perp J} >$ the peak of $\rho(T)_{B\parallel J}$]. If one assumes that **J** flows along the c-axis, one should not observe any difference between the peaks in $\rho(T)$ for these two configurations since the Lorentz force acting on the c-axis flux lines in both configurations is identical.

2. It has been shown that for BSSCO [27] when the current and magnetic field are both applied parallel to the c-axis, a maximum (peak) occurs in $\rho(T)$, even

163
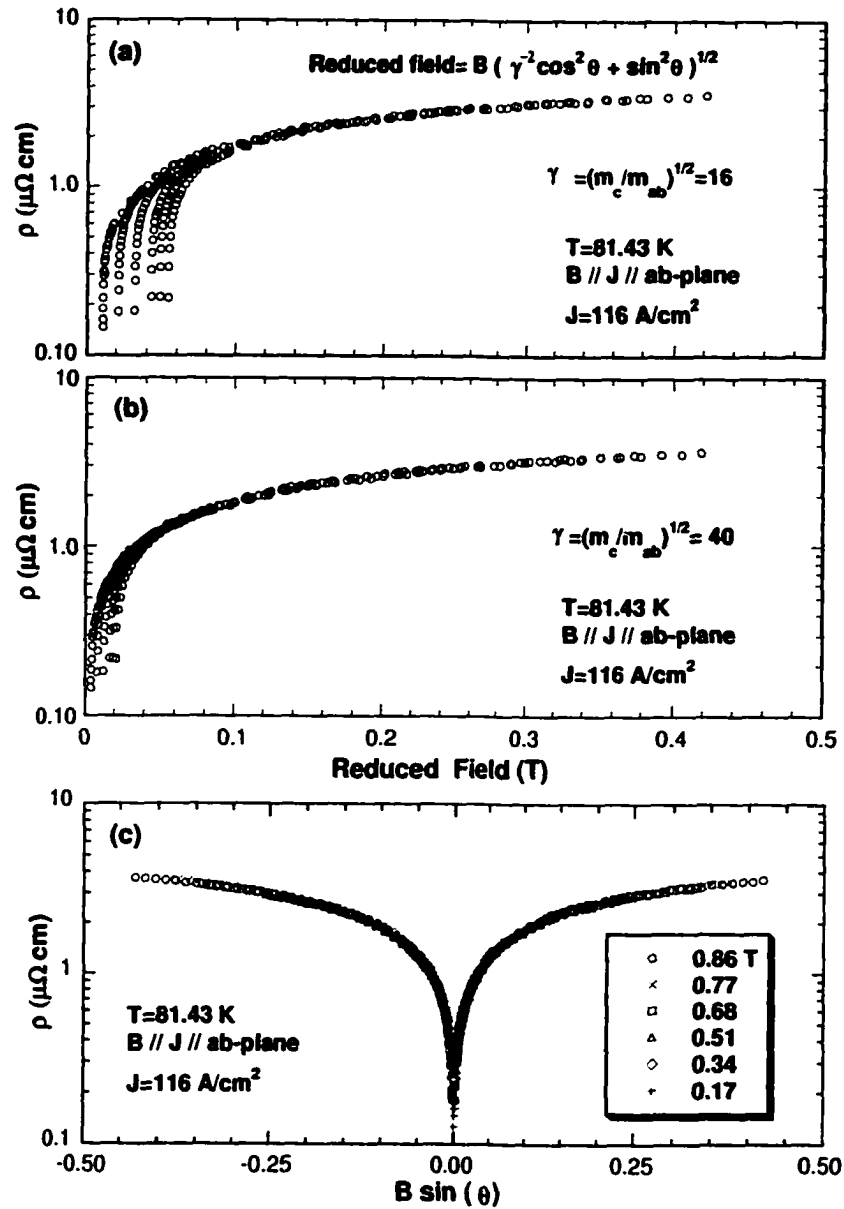
Figure 6.9: Scaling of $\rho(\theta)$, measured for different fields for the **B** $\parallel$ **J** orientation (at a temperature of 81.43 K), as a function of the reduced field $B(\gamma^{-2}\cos^2\theta + \sin^2\theta)^{1/2}$ for $\gamma = 16$ (a) and $\gamma = 40$ (b). (c) the corresponding scaling behavior of $\rho(\theta)$ as a function of the c-axis component of the field $B\sin\theta$.

164

at zero field, due to the competition between the semiconducting c-axis normal resistance and the Josephson interplanar coupling. Such a peak grows with the magnetic field. Therefore if one assumes a current flowing along the c-axis then the peak, that was observed in $\rho(T)$ for YBCO, should increase with an increasing c-axis field which is contrary to what we observed. In 2D-YBCO case a small magnetic field (500 G) applied parallel to the c-axis suppresses this peak completely [see Fig.6.2(b)].

6.4.2 Peak at $\theta = 0^o$ in the angular dependence of the resistivity

As mentioned in the introduction, observation of a dissipation peak in the angular dependence of resistivity at $\theta = 0^o$ in highly anisotropic HTSC single crystals has been reported by two groups under different experimental conditions [12, 14]. Aukkaravittayapun et al. [12] carried out a measurement of the angular dependence of resistivity on a single crystal BSCCO whiskers. For temperatures very close to T_c and small applied magnetic fields up to 0.1 T perpendicular to the current direction ($\mathbf{B} \perp \mathbf{J}$), they observed a peak centered at $\theta = 0^o$, which is completely suppressed at higher fields. In their case, $\rho(\theta)$ for different applied fields scales with the c-axis component of the magnetic field ($B \sin \theta$) for a range of temperatures between 67 and 70 K. The authors explained these results using the models of Brandt et al. [30] and Blatter and Geshkenbein [13]. According to Brandt et al. thermal fluctuations produce a long range Van der Waals interactions between flux lines. Blatter and Geshkenbein predicted transitions from a dilute vortex gas phase to an intermediate liquid vortex phase or to a solid vortex phase as a function of the strength of these interactions. According to Aukkaravittayapun the peak at $\theta = 0^o$ originates from an enhancement of vortex mobility in the vortex gas phase close to T_c. At higher fields, the peak is suppressed due to a transition to the vortex solid phase. However, sharpening of the peak (decrease in the peak width) at fields higher than 0.1 T has not been explained by these models.

Detailed results of effect of the applied magnetic field and current on $\rho(\theta)$ for TBCCO (2212 and 1223) and BSCCO (2212) single crystals has been provided by Chaparala et al. [14]. For TBCCO (2212) at temperature of 90 K ($T/T_c = 0.86$) and for a field applied at an angle θ to the ab-planes (**B** $\perp$ **J**), their data show a sharp peak in the in-plane resistivity $\rho(\theta)$ at $\theta = 0^o$. For magnetic fields below 2 T, the peak height increases with the current and the field while the peak width (HWHM) increases with the current, but decreases with the field. On the other hand for fields larger than 2 T, the peak height decreases with both the field and the current. They also observed a decrease in the magnitude of the peak in $\rho(\theta)$ at $\theta = 0^o$ upon change of orientation of **B** from **B** $\perp$ **J** to **B** $\parallel$ **J**. Examination of Fig.2 in Ref. [14] shows that for small angles (very close to the ab-planes), the peak in $\rho(\theta)$ increases in magnitude with an increasing magnetic field but at the same time its width decreases. This means that there is a crossover from a regime at small θ where $\rho(\theta)$ increases with field to a one at larger θ where $\rho(\theta)$ decreases with the field. The authors proposed a tentative model based on thermal activation of vortex-antivortex pairs. Thermal fluctuations of Josephson strings as the angle θ approaches zero leads to a random nucleation of vortex-antivortex pairs out of the segments of the Josephson strings. Since the dissipation voltage is proportional to the product of the vortex density and the vortex mean velocity then the deficit in the density of the vortices due to a reduction of the angle θ should be overcome by an enhancement of the vortex velocity. This could explain an increase in the dissipation as the angle θ is reduced. According to this model an increasing applied current increases the velocity of the vortices and subsequently increases the dissipation.

Our results on YBCO film and the results of the above references (Refs [12, 14]) suggest that the presence of the peak in $\rho(\theta)$ at $\theta = 0^o$ is associated with high anisotropy of the samples studied ($\gamma > 100$).

A decrease in the width of the peak (FWHM) with an increasing magnetic field, observed in all these experiments, means that above a certain angle θ_c, resistivity decreases with an increasing field. This suggests that a standard dissipation mechanism

166

based on magnetic flux flow is not a major contributor to $\rho(\theta)$ at angles larger than θ_c.

Angular dependence of resistivity over a wide range of angles $0 - 180^o$ for a 2D-YBCO film [Fig.6.4(b)] reveals that $\rho(0^o)$ is approximately 30% larger than $\rho(90^o)$. This behavior was not observed in references [12, 14] where $\rho(0^o)$ is smaller than $\rho(90^o)$. In general, for a 2D system with a weakly coupled CuO_2 layers one expects a maximum resistive dissipation when a magnetic field is aligned along the c-axis due to the motion of a large number of pancake vortices. Therefore large resistivity at $\theta = 0^o$ implies dissipation mechanism different from that due to flux flow.

This is supported by an additional observation of a peak at a temperature of 83.3 K in the temperature dependence of resistivity for our YBCO film [see Fig.6.1(b)] whose magnitude is approximately 10% larger than the resistivity at T_c onset (85.1 K). This peak in $\rho(T)$ decreases with an increasing applied current and increasing c-axis component of an applied field. A similar phenomenon in the temperature dependence of resistivity $\rho(T)$ near T_c has been observed in conventional superconductors [17, 18, 19]. For example Moshchalkov et al [19] reported observation of a peak in $\rho(T)$ for Al strips of width much smaller than the Ginzburg-Landau coherence length and magnetic penetration depth. The peak is about $10 - 20\%$ higher than the normal state resistance determined from the plateau in $\rho(T)$ above T_c onset and is suppressed by an increasing transport current. This resistance anomaly has been explained in terms of thermally activated phase slips of the superconducting order parameter in quasi-one-dimensional wires according to the models of Langer-Ambegaokar (LA) [20] and McCumber-Halperin (MH) [31].

6.4.3 Phase slip model

The basic idea of the phase slip model comes from the fact that the conservation of a supercurrent J_s (neglecting the normal current) requires that $J_s(x) \propto |\psi(x)|^2 v_s(x)$ be constant. If the order parameter is defined as $\psi(x) = |\psi(x)| e^{i\phi(x)}$, where $\phi(x)$ is

167

the phase, then

$$| \psi(x) |^2 \frac{d\phi(x)}{dx} = const \propto I \tag{6.1}$$

A phase slip corresponding to a substantial increase of $\frac{d\phi(x)}{dx}$ in Eq. (6.1) should therefore be associated by a proper decrease of $| \psi(x) |^2$, which induces an intrinsic resistance in the superconducting state. For a 1D thin wire with a transverse dimension $d \ll \xi$ (the GL temperature dependent coherence length) and $d \ll \lambda$ (the magnetic penetration depth), so that magnetic energies can be neglected compared to kinetic energies, the (LA-MH) theory predicts that the resistance in the superconducting state is mainly determined by thermally activated phase slips events. These phase slips cause the magnitude of the order parameter to vanish briefly at some points along the wire. The free energy barrier (difference in free energy between the normal and superconducting states) associated with this process is

$$\Delta F_0 = \frac{8\sqrt{2}}{3}[A\xi(T)H_c^2(T)/8\pi] \tag{6.2}$$

where A is the cross sectional area of the wire and $H_c(T)$ is the thermodynamic critical field.

In the absence of the current, phase slips by $\pm 2\pi$ are equally likely, and this results in a fluctuating noise voltage with zero net dc component. If a constant voltage V is applied, the phase difference $\Delta\phi$ will increase steadily at a rate of $2eV/h$ but instantaneously snaps back by 2π whenever each phase slip occurs. This will cause the current to build up to a steady-state value at which the phase jumps of $\Delta\phi = -2\pi$ outnumber the phase jumps $\Delta\phi = +2\pi$ by an amount of $2eV/h$ per second according to Josephson relation. So the net result of the current in the wire is to make the phase jumps more probable in one direction than the other. The different jump rates arise from a difference δF in the energy barrier for jumps in two directions and this difference stems from the electric work $\int IVdt$ done in the process. For a phase slip of 2π, the energy difference is [32].

$$\delta F = \Delta F_+ - \Delta F_- = \frac{h}{2e}I_s = \phi_0 I_s \tag{6.3}$$

168

Where $\phi_0 = \frac{h}{2e}$ is the superconducting flux quantum. $\delta F = \phi_0 I$ should be larger than the thermal energy $k_B T$ (where k_B is the Boltzmann constant), which defines the characteristic current $I_1 = \frac{k_B T}{\phi_0}$, above which most phase slips go in the driven direction and the resistance is nonlinear [31]. I_1 sets a lower limit on the applied current I_s. The upper limit is set by the critical current I_c which is the mean-field critical current given by

$$I_c = \pi \sqrt{\frac{2}{3}} \frac{\Delta F_0}{\phi_0} \tag{6.4}$$

and

$$I_1 = \frac{k_B T}{\phi_0} < I_s < I_c \tag{6.5}$$

The average voltage V_s arising from the phase slip events is determined by the number of these events in the sample $[N(T) = L/\xi(T)$, where L is the length of the wire], a characteristic time $\tau(T)$, Boltzmann factor $\exp(-\Delta F_0(T)/k_B T)$, and the factor $\sinh(I_s \phi_0 / 2 k_B T)$ derived from the difference δF in the energy barrier for $+2\pi$ and -2π phase jumps

$$V_s = 2\phi_0 \Omega(I_s, T) \exp\left[-\frac{\Delta F(T)}{k_B T}\right] \sinh\left(\frac{I_s}{2 I_1}\right) \tag{6.6}$$

where

$$\Delta F(T) = \Delta F_0(T) + \left(\frac{2}{3}\right)^{1/2} \frac{I_s^2 k_B T}{3\pi I_1 I_c} \tag{6.7}$$

and $\Omega(I_s, T)$ is an attempt frequency which can be approximated as

$$\Omega(I_s, T) = \frac{N(T)}{\tau(T)} \sqrt{\frac{\Delta F_0}{k_B T}} (1 - \frac{2I_s}{3I_c})^{15/4} \tag{6.8}$$

It is very important to emphasize the fact that the energy being supplied during the occurrence of these phase slips at a rate of IV, is dissipated as heat rather than converted into kinetic energy of supercurrent, which would otherwise soon exceed the condensation energy [32]. The theory predicts that the total resistance of a macroscopic superconductor close to T_c can be calculated by assuming that the supercurrent I_s and the normal current I_n are running in parallel: $R^{-1} = R_s^{-1} + R_n^{-1}$. However, using this assumption it is not possible to obtain a total resistance R higher than R_n.

Moshchalkov et al. [19] suggested that for Al wires with width $w \ll \xi$, the currents I_s and I_n can not run in parallel for any specific time t_0 because the coexistence of the two currents in parallel leads to a huge increase in energy due to variation of the modulus of the order parameter on a very short length scale $w \ll \xi$. Therefore they proposed that in quasi-1D superconducting wires the instantaneous currents $I_s(t_0)$ and $I_n(t_0)$ can only flow *in series* and, assuming that Kirchhoff laws are still valid, $I_s(t_0) = I_n(t_0)$ and $R = R_s + R_n$ where $R_s = V_s/I_s$ and V_s is given by Eq. (6.6).

6.4.4 Phase slip dissipation in YBCO

Our explanation of the experimental results obtained on YBCO film is based mostly on the (LA-MH) phase slip model.

We suggest that the peaks in both $\rho(T)$ and $\rho(\theta)$ are mainly due to phase slip events with a small contribution due to flux motion. Fig.6.1(b) shows the resistivity peak, which is present only for magnetic field applied parallel to the ab-planes. This peak is completely suppressed when a field larger than 500 G is applied along the c-axis. For $\mathbf{B} \parallel$ c-axis case the field also broadens the transition (reduce zero-resistance T_c) while for $\mathbf{B} \parallel$ ab-plane, the field does not broaden the transition and T_{c_0} remains almost unchanged. Fig.6.5 reveals that for both $\mathbf{B} \parallel \mathbf{J}$ and $\mathbf{B} \perp \mathbf{J}$, $\rho(\theta)$ decreases with the field for angles θ larger than a certain critical angle θ_c. These two observations can be explained in terms of the phase slip model. Since the YBCO film under study behaves like a 2D system, only the c-axis component of the magnetic field contributes to any dissipation mechanism. The magnetic field dependence does not appear explicitly in Eq.(6.6) of the phase-slip model, however its effect on the phase-slip voltage appears through the dependence of I_c on the field, $I_c \propto \frac{1}{B \sin \theta}$. Increasing the c-axis component of $\mathbf{B}$, which can be done by increasing the angle θ and/or the magnitude of the field, reduces the critical current I_c. This in turn results in a reduction of the phase slip events and the voltage V_s. Observation of the phase-slip resistivity is confined to a range of the applied current I_s between I_1 and I_c [see Eq.(6.5)]. According to the theory I_s per 1D current channel has to be larger than

170

$I_1 = k_B T/\phi_0$, which is $0.56\mu A$ in our case. If I_s is too close to I_c, the phase-slip events are less likely to occur. Therefore reducing I_c while keeping I_s fixed leads to a reduction of the phase-slip events and consequently the voltage V_s. In other words, an increasing magnetic field reduces the phase slip resistivity through reducing the critical current I_c. The phase slip model depends only on the magnitude of $\mathbf{B}$ but not on the relative orientation of $\mathbf{B}$ with respect to $\mathbf{J}$.

Fig.6.7(a) and Fig.6.8(a) show that the peaks in both $\rho(\theta)$ and $\rho(T)$ decrease with an increasing current. This behavior provides further support to the phase-slip origin of these peaks. According to Eq.(6.6) of the phase-slip voltage, V_s decreases with an increasing I_s, since a decrease of the prefactor $\Omega(I_s, T)$ is faster than an increase in the $\sinh(\frac{I_s}{2I_1})$ factor. Appearance of a minimum in $\rho(\theta)$ at high applied currents $(J \geq 23kA/cm^2)$ can be explained by the fact that the applied current I_s approaches the critical current value I_c, leading to a large reduction of the phase-slip events. In this case the dissipation is governed by the flux flow and therefore one expects to observe a decrease in $\rho(\theta)$ as θ decreases (with minimum centered at $\theta = 0^o$). On the other hand, for fixed (even small) applied current and at temperatures above the peak in $\rho(T)$ ($83.4K < T < 84.0K$) a minimum in $\rho(\theta)$ has been also observed [see Fig.6.8(b)]. This can be explained by the fact that the decrease of I_c with an increasing temperature reduces the phase-slip events . In short, we can say that phase-slip events can be reduced either by increasing the applied current at fixed temperature or by increasing the temperature at fixed current.

The phase-slip model predicts a very sharp resistance peak, very close to the onset T_c, with a temperature width of a few mK. On the other hand, this model is valid for quasi one-dimensional wires of diameter smaller than the coherence length and the penetration depth . The peak in $\rho(T)$ measured in zero magnetic field for YBCO film [see Fig.6.1(b)] is very broad (of width about 1.1 K) compared to the that predicted by the model. YBCO is composed of well-separated cells, of c-axis lattice constant of $11.7\mathring{A}$, containing two closely-spaced CuO_2 plane layers. Therefore, the 2D-YBCO film, approximately $1400\mathring{A}$ thick, contains about 240 CuO_2 bi-layers. Because of

171

high anisotropy of the film, these layers are weakly coupled and behave like a stack of very thin independent superconducting sheets. Slight underdoping of the film with $T_c \simeq 82K$ could result in a variation of the transition temperature between the different layers. One can therefore assume that each layer produces a very sharp phase-slip peak of a few mK in width and the broad peak observed in this film is in fact the result of an overlap of a large number of sharp peaks (Gaussain distribution). Rough calculations revealed that the typical peak width is about 5 mK which would result in a total width of about 1 K, as observed.

6.4.5 Effect of flux flow

It should be noted that since Figures 6.1(b) and 6.6(a) show a difference between ρ for the **B** $\parallel$ **J** and **B** $\perp$ **J** orientations, there is another dissipation mechanism that depends on the angle between **B** and **J**. In order to understand the origin of this dissipation we plotted in Fig.6.10 the difference in $\rho(\theta)$ between **B** $\perp$ **J** and **B** $\parallel$ **J** orientations, $\Delta\rho(\theta) = \rho(\theta)_{B\perp J} - \rho(\theta)_{B\parallel J}$, as a function of angle θ. These results reveal that $\Delta\rho(\theta)$ decreases with a decreasing angle θ and displays a minimum at $\theta = 0^o$ which is similar to that observed at low temperatures close to T_{c_0} [see Fig.6.2(a)]. This behavior implies that flux flow contributes to the dissipation.

In the absence of phase slip events one expects to see a decrease in $\rho(\theta)$ as θ is decreased down to $\theta = 0^o$ because of the reduction of the c-axis component of the field. Therefore we can say that this flux flow dissipation is governed by the motion of Josephson strings since the difference $\Delta\rho(\theta)$ between the **B** $\perp$ **J** and **B** $\parallel$ **J**, shown in Fig.6.10, is proportional to the motion of these strings. For **B** $\parallel$ **J** and angles $\theta < \theta_c$, the peak in $\rho(\theta)$ at $\theta = 0^o$ is almost independent of the magnitude of the applied field. The contribution due to the motion of Josephson strings is almost zero in this case. On the other hand for **B** $\perp$ **J**, an increase in the peak height [see Fig.6.1(b)and Fig.6.5(a)] compared to that for **B** $\parallel$ **J** can be attributed to the motion of Josephson strings along the c-axis. This motion can be facilitated by thermal activation of vortex-antivortex pairs at low flux density and the Lorentz force along the c-axis. For

172
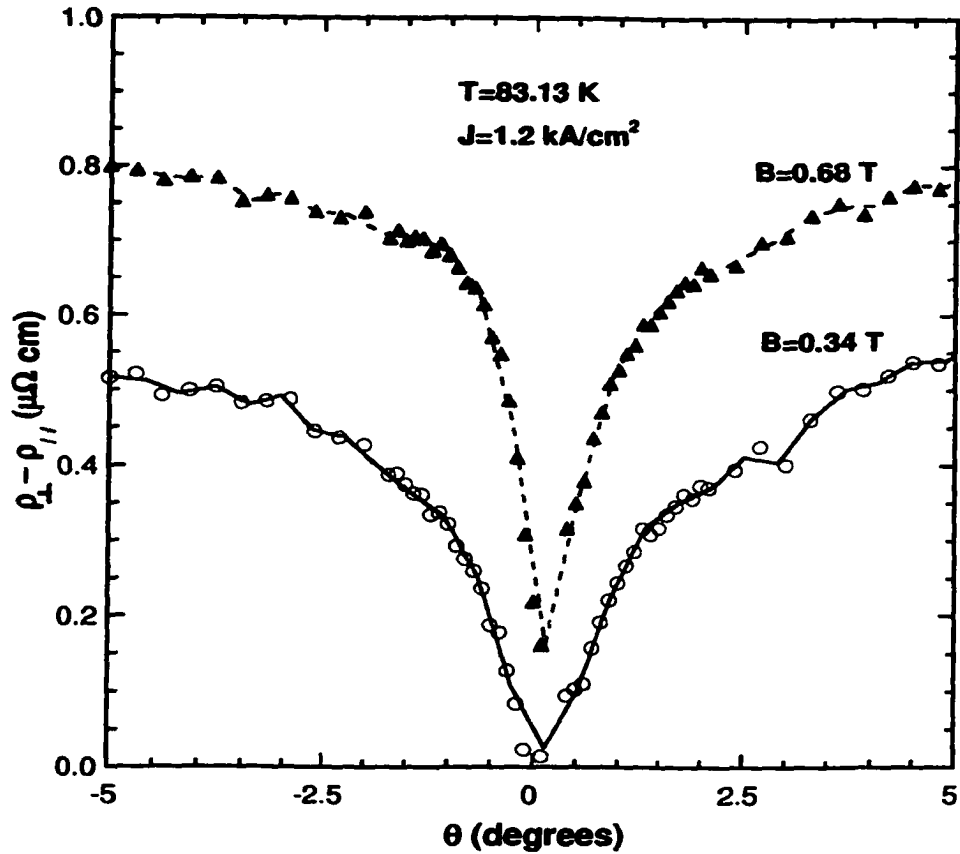
Figure 6.10: The difference between the maxima in $\rho(\theta)$ measured for B $\perp$ J and B $\parallel$ J orientations as a function of the angle θ. This difference $\rho_\perp - \rho_\parallel$ was calculated from Fig.6.6(a) for B=0.68 T. The dashed line is just a guide for the eye.

B $\perp$ J, the peak increases with an increasing field due to an increase of the Lorentz force. An increase of $\Delta\rho(\theta)$ in Fig.6.10 with an increasing angle θ can be attributed to a decrease in the length of the Josephson strings which leads to a reduced pinning of these short segments.

6.5 Summary and conclusions

Results of the measurements of resistivity ρ in a 2D-YBCO film, as a function of the angle θ between the ab-planes and the direction of the applied magnetic field revealed a resistive maximum in $\rho(\theta)$ at $\theta = 0^o$ over a narrow temperature range

below T_c onset. The width of this maximum decreases with an increasing magnetic field. A corresponding maximum has been observed in the temperature dependence of resistivity at temperatures just below T_c onset. The resistivity of the maximum is higher than the normal state resistivity at T_c onset. The maximum in $\rho(T)$ is independent of the magnitude of magnetic field applied along the ab-planes for the **B** $\parallel$ **J** configuration. However, the resistivity at the maximum is dramatically reduced when the magnetic field direction is rotated from the ab-planes towards the c-axis. The maxima in $\rho(T)$ and $\rho(\theta)$ at $\theta = 0°$ also decrease with an increasing applied current.

The data imply that the resistive peaks in $\rho(T)$ and $\rho(\theta)$ originate from the phase-slip voltage in accordance with theories of Langer-Ambegaokar and McCumber-Halperin [20, 31]. However these theories apply to one-dimensional wires of diameter less than $\xi(T)$ and $\lambda(T)$. Therefore, observation of phase-slip induced resistive peaks in a 2D-like YBCO film of $T_c \simeq 82K$, suggests that the current must flow in narrow filamentary paths of width $w < \xi(T)$ within the 2D CuO_2 sheets. This is likely to happen since this underdoped sample has a broad superconducting transition width. According to Moshchalkov et al. [19], who studied the phase-slip induced resistivity peak below the onset T_c in Al wires, the fact that the resistivity $\rho(T)$ in the phase-slip peak is higher than the normal state resistivity at the T_c onset, implies that the supercurrent and the normal current flow in series during the phase-slip events. Accordingly, in the case of YBCO film, filamentary structures in the 2D CuO_2 sheets could enhance the phase-slip resistivity.

The final question is why the phase-slip resistivity has not been continuously observed in 2D-like HTSC in general. This could be partly governed by the magnitude of the current applied to the sample during the measurements of resistivity. As mentioned in the discussion, observation of the phase-slip resistivity is limited to a narrow range of the applied current I_s ($k_B T/\phi_0 < I_s < I_c$). If I_s is either too close to $k_B T/\phi_0$ or to I_c, the phase-slip events are less likely to occur. Recent STM work by Howald et al. [33] and Pan et al. [34] on BSCCO(2212) cuprates revealed a nanodomain struc-

174

ture in the ab-planes. This in fact supports a filamentary (percolative) mechanisms of the flow of the current in these 2D materials.

Bibliography

[1] S. L. Cooper and K. E. Gray, *Physical properties of high temperature supercon-ductors* IV, ed. by D. M. Ginsberg, World Scientific, Singapore 1994, P. 61.

[2] A. Buzdin and D. Feinberg, *Phys. Lett. A* **165**, 281 (1992).

[3] Y. Iye, A. Fukushima, T. Tamegai, T. Terashima and Y. Bando, *Physica C* **185**, 297 (1991).

[4] Y. Iye, T. Terashima and Y. Bando, *Physica C* **184**, 362 (1991).

[5] Y. Iye, T. Tamegai and S. Nakamura, *Physica C* **174**, 227 (1991).

[6] M. Tachiki and S. Takahashi, *Solid State Commun.* **70**, 291 (1989).

[7] D. Feinberg and V. Villard, *Phys. Rev. Lett.* **65**, 919 (1990).

[8] W. K. Kwok, U. Welp, V. M. Vinokur, S. Fleshler, J. Downey, G. W. Crabtree, *Phys. Rev. Lett.* **67**, 390 (1991).

[9] K. Kadowaki and T. Mochiko, *Physica B* **194-196**, 2239 (1994).

[10] D. E. Farrell, J. P. Rice, D. M. Ginsberg, J. Z. Liu, *Phys. Rev. Lett.* **64**, 1573 (1990).

[11] P. Mansky, P.M. Chaikin and R.C. Haddon, *Phys. Rev. Lett.* **70**, 1323 (1993).

[12] S. Aukkaravittayapun, P. J. King, Yu. I. Latyshev, R. M. Bowley , *Physica C* **277**, 196 (1997).

[13] G. Blatter and V. Geshkenbein, *Phys. Rev. Lett.* **77**, 4958 (1996).

[14] M. Chaparala, O. H. Chung, Z. F. Ren, M. While, P. Coppens, J. H. Wang, A. P. Hope, M. J. Naughton , *Phys. Rev. B* **53**, 5818 (1996).

[15] M. A. Crusellas, J. Fontcuberta and S. Pinol, *Phys. Rev. B* **46**, 14089 (1992)

[16] S. H. Han, Y. Zhao, G. D. Gu, G. J. Russell, N. Koshizuka, *Advances in Superconductivity*,**8**, (1996), 109-112, Proc. of the 8th International Symposium on Superconductivity (ISS '95),Oct.30-Nov.2, 1995, Hamamatsu.

[17] M. Park, M.S. Isaacson, J.M. Parpia, *Phys. Rev. Lett.* **75**, 3740 (1995).

[18] Y.K. Kwong, K. Lin, P.J. Hakonen, M.S. Issacson, J. M. Parpia, *Phys. Rev. B* **44**, 462 (1991).

[19] V. V. Moshchalkov, L. Gielen, G. Neuttiens, C. Van Haesendonck, Y. Bruynseraede , *Phys. Rev. B* **49**, 15412 (1994).

[20] J.S. Langer and V. Ambegaokar, *Phys. Rev.* **164**, 498 (1967).

[21] H. Darhmaoui and J. Jung, *Phys. Rev. B* **53**, 14621 (1996).

[22] Y. Iye, A. Watanabe, S. Nakamura, T. Tamegai, T. Terashima, K. Yamamoto, Y. Bando, *Physica C* **167**, 278 (1990)

[23] D. H. Kim, D. J. Miller, J. C. Smith, R. A. Holoboff, J. H. Kang, J. Talvacchio, *Phys. Rev. B* **44**, 7607 (1991).

[24] Y. Iye, S. Nakamura, T. Tamegai , *Physica C* **159**, 433 (1989)

[25] Y. Iye, T. Tamegai, T. Sakakibara, T. Goto, N. Miura, H. Takeya and H. Takei, *Physica C* **153-155**, 26 (1988)

[26] D. E. Farrell, S. Bonham, J. Foster, Y. C. Chang, P. Z. Jiang, K. G. Vandervoort, D. J. Lam, V. G. Kogan , *Phys. Rev. Lett.* **63**, 782 (1989).

[27] G. Briceno, M.F. Crommie, A. Zettl, *Phys. Rev. Lett.* **66**, 2164 (1991).

[28] U. Welp, W. K. Kwok, G. W.Crabtree, K. G. Vandervoort, J. Z. Liu, *Phys. Rev. Lett.* **62**, 1908 (1989).

[29] T. Ito, H. Takagi, S. Ishibashi, T. Ido, S. Uchida, *Nature* **350**, 596 (1991).

[30] E. H. Brandt R. G. Mints, I.B. Snapiro, *Phys. Rev. Lett.* **76**, 827 (1996).

[31] D.E. McCumber and B.I. Halperin, *Phys. Rev. B* **1**, 1054 (1970).

[32] M. Tinkham,*Introduction to Superconductivity*, McGraw-Hill, New York,(1996).

[33] C. Howald, P. Fournier, and A. Kapitulink, *Cond.-mat. preprint 0101251* (January 2001).

[34] S. H. Pan, J.P. ÓNeal, R.L. Badzery, C. Chamon, H. Ding, J.R. Engelbrecht, Z. Wang, H. Eisaki, S. Uchida, A.K. Gupta, K. W. Ng, E.W. Hudson, K.M. Lang, and J. D. Davis, *Cond.-mat. preprint 0107347* (July 2001).

Chapter 7

Summary and Conclusions

The research in this thesis was focused on the angular dependence of resistivity $\rho(\theta)$, with θ the angle between the ab-planes and the applied magnetic field, measurements on YBCO thin films. These measurements were also used to study some intrinsic properties of this compound like anisotropy. This research can be divided into four major parts:

1. Deviation of the normal state resistivity from the linear behavior.

2. Strong pinning effects in $\rho(\theta)$ for field orientations close to c-axis ($\theta = 90^\circ$).

3. Large variation of intrinsic anisotropy factor γ.

4. Phase-slip resistivity peaks near T_c.

We have investigated systematically the angular dependence of resistivity $\rho(\theta)$, where θ is the angle between the magnetic field and the ab-planes, and the temperature dependence of resistivity $\rho(T)$ over a temperature range between T_{c0} and T_c-onset within the superconducting transition in an applied magnetic field **B** up to 1 T in a series of $YBa_2Cu_3O_{7-\delta}$ (YBCO) thin films both optimally doped and underdoped of different T_c, critical current density J_c, film thickness, and preparation techniques. The angular dependence of ρ was measured using a high resolution angle-

179

control system with the angular position of the sample accurately monitored by an optical encoder.

studies of the temperature dependence of the normal state resistivity $\rho(T)$ revealed an upward deviation in $\rho(T)$ from the high temperature T-linear dependence below a certain characteristic temperature T^*. This upward deviation increases with a decreasing temperature, eventually reaches a maximum at another characteristic temperature T_1. Our results showed that the upward deviation increases with an increasing oxygen content (optimally doped films show the largest upward deviation and the highest T^*). There is a direct relationship between the upward deviation and the corresponding y-intercept at T=0 K (residual resistivity) of the straight line fitted to the high temperature data of $\rho(T)$. Films with a large upward deviation show a *large negative* y-intercept, while those with small deviation show a small (close to zero) positive or negative y-intercept. Upward deviation of $\rho(T)$ from the T-linear dependence has been observed in YBCO single crystals and ceramic samples. For YBCO single crystals, high resolution x-ray diffraction [1] revealed a distribution in the c-axis lattice parameters, which can be interpreted as an evidence of a distribution in oxygen content. This lead to the conclusion that structural defects exist even in single crystals with sharp superconducting transitions ($< 0.5K$). We could not reach to a solid ground of what is causing the upward deviation in YBCO, but the experimental findings (for thin films and single crystals) suggest that an upward deviation in $\rho(T)$ from the T-linear dependence may be related to the disorder which results from distribution of oxygen content in the sample.

We have investigated systematically the angular dependence of resistivity $\rho(\theta)$ for a wide range of angles ($0^o \leq \theta \leq 180^o$) for about fifteen YBCO thin films near T_c. The results revealed three distinct behaviors for different films:

1. Three film showed a *broad minimum* near $\theta = 0^o$ and $\theta = 180^o$ ($B \parallel$ ab-planes), but *a sharp minimum* near $\theta = 90^o$ ($B \parallel$ c-axis).

2. Two films showed a *sharp minimum* near $\theta = 0^o$ and $\theta = 180^o$ ($B \parallel$ ab-planes) with a *broad maximum* near $\theta = 90^o$ ($B \parallel$ c-axis).

180

3. The majority of films a broad minimum near $\theta = 0^o$ and $\theta = 180^o$ ($B \parallel$ ab-planes) and a broad maximum near $\theta = 90^o$ ($B \parallel$ c-axis).

These three distinct behaviors can be related to the intrinsic properties of YBCO thin films. The first behavior, which was shown only by three films, is normally attributed to strong pinning by twin boundaries since all YBCO films are twinned. This behavior is also typical to all twinned YBCO single crystals. The presence of a minimum in $\rho(\theta)$ for **B** $\parallel$ c-axis is not related to the magnitude of J_c. The width and the depth of the minimum decreases with an increasing temperature and an increasing magnetic field. Our investigations showed that this minimum is present only in films that were deposited very slowly, thus allowing the growth of crystallographically well-defined and sharp TB's. The absence of the minimum in $\rho(\theta)$ in the films which were grown fast suggests that thin film growth leads to disordered twin boundaries [2] which are a weak flux pinning centers. Polarized light microscope studies on both types of films (with and without minimum) did not reveal any difference in the structure between the two types. Careful investigation using high magnification ratio up to 1000 times on films with a minimum did not show any trace of twin boundaries in these films. This may suggest that, unlike YBCO single crystals, the twin boundaries spacing is very small to be seen using optical devices (like the polarized light microscope). Scanning electron microscope studies of the surface of the thick films that showed a minimum, revealed the existence of granular structure with an average size of the grain of about $0.4\mu m$. We could not see any twinning within the grains themselves, which may suggest that the strong pinning could be due to the grain boundaries instead of twin boundaries. Other films (that showed a minimum around $\phi = 0^o$) showed an array of holes similar to that seen in an irradiated samples (columnar defects). These holes could be a source of strong pinning.

The measurement of $\rho(\theta)$ for field orientations close to $\theta = 0^o$ (**B** $\parallel$ ab-planes) for both **B** $\parallel$ **J** and **B** $\perp$ **J** (where **J** is the current density) revealed a sample dependent variations in the shape and width of the minimum at $\theta = 0^o$, from a flat to a very sharp behavior. The width and sharpness of this minimum is related to

181

the intrinsic anisotropy of YBCO. The results of scaling of $\rho(\theta)$ with the reduced field $B(\gamma^{-2}\cos^2\theta + \sin^2\theta)^{1/2}$ allowed a quantitative determination of the value of the intrinsic anisotropy factor γ which varies between 7 and 400, and is independent of T_c, film thickness, or the critical current density J_c. The sharper the minimum in $\rho(\theta)$ at $\theta = 0^o$ the larger is the anisotropy factor γ. For the highly anisotropic film with $\gamma \sim 400$, $\rho(\theta)$ showed an identical behavior for $\mathbf{B} \parallel \mathbf{J}$ and $\mathbf{B} \perp \mathbf{J}$. This behavior is identical to that shown by BSCCO and other highly anisotropic HTSC. This very high anisotropy in YBCO, which is known to be a moderately anisotropic material with $\gamma \sim 7$, is unexpected and therefore is revolutionary and needs more careful investigations. However, X-ray diffraction (XRD) data of the film with high $\gamma \sim 400$ showed a typical patterns of stoichiometric c-axis oriented YBCO with no difference in the structure compared to other films of moderate anisotropy. High resolution electron microscopy studies of YBCO crystals by Etheridge [3] revealed a weak diffuse scattering in electron diffraction pattern of $YBa_2Cu_3O_{6+x}$ ($x > 0.9$) which arise from static displacements of atoms from their periodic lattice sites. These studies have suggested that the ab-planes buckle into the network of slightly misaligned cells in a struggle to relieve internal stresses. One source of internal stress is a mismatch between "natural" (sometimes called prototypical) lattice constants of the copper-oxygen planes and the chain-oxygen and barium-oxygen planes. It is therefore very likely that the coupling between the ab-plane layers in YBCO and thus the anisotropy factor γ could be affected by the "buckling" process in the copper-oxygen planes. The "buckling" is very sensitive to a local disorder in oxygen concentration. This could explain the large variations in γ in YBCO films close to an optimal doping. On the other hand, Halbritter [4] discussed anisotropy in YBCO and argued that high anisotropy in this material could be attributed to weak-link effects. Weak links contain localized states that carry current across by resonant tunneling. For YBCO such states are due to oxygenation in the Cu chains. By pair weakening the localized states have a lowered energy gap and by resonant tunneling the defects reduce the perpendicular resistivity $\rho^\perp$ drastically. For YBCO this yields an intrinsic anisotropy

of 5×10^5 [40] which suggests that weak-link effects could result in a very large anisotropy.

Very large anisotropy in HTSC could lead to an unusual effects in the temperature and angular [5] dependence of resistivity. The last part of this thesis was devoted to the discussion of the effect of high anisotropy on the behavior of resistivity close to T_c. For a 2D-like highly anisotropic ($\gamma \sim 400$) film, the measurements of resistivity revealed a maximum in $\rho(\theta)$ around $\theta = 0^o$ over a narrow temperature range below T_c-onset. The width of this maximum decreases with an increasing magnetic field. A corresponding maximum has been observed in $\rho(T)$ at temperatures just below T_c onset. The resistivity of the maximum is higher than the normal state resistivity at T_c onset. The maximum in $\rho(T)$ is almost independent of the magnitude of magnetic field applied along the ab-planes for the **B $\parallel$ J** configuration. However, the resistivity at the maximum is dramatically reduced when **B** is rotated from the ab-planes towards the c-axis. The resistive peaks in $\rho(T)$ and $\rho(\theta)$ at $\theta = 0^o$ also decrease with an increasing applied current. The data imply that the resistive peaks in $\rho(T)$ and $\rho(\theta)$ originate from the thermally activated phase-slip voltage according to theories of Langer-Ambegaokar and McCumber-Halperin [6, 7]. The phase-slip resistivity peaks have been observed previously in many low T_c [10, 11, 12] and high T_c [8, 9, 5] materials. However these theories apply to one-dimensional wires of diameter less than $\xi(T)$ and $\lambda(T)$. Therefore, observation of phase-slip induced resistive peaks in a 2D-like YBCO film of $T_c \simeq 82K$, suggests that the current must flow in narrow filamentary paths of width $w < \xi(T)$ within the 2D CuO_2 sheets. This is likely to happen since this underdoped film has a broad superconducting transition width. Someone may ask why the phase-slip resistivity has not always been observed in any 2D-like HTSC in general. This could be partly governed by the magnitude of the current applied to the sample during the measurements of resistivity. According to the theory of Langer-Ambegaokar and McCumber-Halperin [6, 7], observation of the phase-slip resistivity is limited to a narrow range of the applied current I_s ($k_B T/\phi_0 <$ $I_s < I_c$). If I_s is either too close to $k_B T/\phi_0$ or to I_c, the phase-slip events are less

183

likely to occur.

In brief summary, I can say that careful study of a large number of samples of different characteristics (like different T_c, thickness, critical current density, preparation technique, etc.) leads to a better understanding of the superconducting properties of the material and may lead sometimes to a discovery of new unexpected phenomena. It is still too early and very difficult to talk about the general properties of YBCO on the basis of measurements done on few samples.

Bibliography

[1] S. B. Qadri, M. S. Osofsky, V. M. Browning, E. F. Skelton, *Appl. Phys. Lett.* **68**, 2729 (1996).

[2] M. Suenaga, private communications.

[3] J. Etheridge, *Philos. Mag.* **A73**, 643 (1996).

[4] J. Halbritter, *Phys. Rev. B* **48**, 9735 (1993).

[5] M. Chaparala, O. H. Chung, Z. F. Ren, M. While, P. Coppens, J. H. Wang, A. P. Hope, M. J. Naughton , *Phys. Rev. B* **53**, 5818 (1996).

[6] J.S. Langer and V. Ambegaokar, *Phys. Rev.* **164**, 498 (1967).

[7] D.E. McCumber and B.I. Halperin, *Phys. Rev. B* **1**, 1054 (1970).

[8] M. A. Crusellas, J. Fontcuberta and S. Pinol, *Phys. Rev. B* **46**, 14089 (1992)

[9] S. H. Han, Y. Zhao, G. D. Gu, G. J. Russell, N. Koshizuka, *Advances in Superconductivity*,8, (1996), 109-112, Proc. of the 8th International Symposium on Superconductivity (ISS '95),Oct.30-Nov.2, 1995, Hamamatsu.

[10] M. Park, M.S. Isaacson, J.M. Parpia, *Phys. Rev. Lett.* **75**, 3740 (1995).

[11] Y.K. Kwong, K. Lin, P.J. Hakonen, M.S. Issacson, J. M. Parpia, *Phys. Rev. B* **44**, 462 (1991).

[12] V. V. Moshchalkov, L. Gielen, G. Neuttiens, C. Van Haesendonck, Y. Bruynseraede , *Phys. Rev. B* **49**, 15412 (1994).

185